AUBURN

SAMUEL GINN
COLLEGE OF ENGINEERING

Research Report

SIMPLIFIED AND STANDARDIZED SEISMIC DESIGN AND DETAILING FOR ALABAMA BRIDGES

Submitted to

The Alabama Department of Transportation

Prepared by

Justin D. Marshall, Ph.D., P.E.
Joseph Broderick
Hongyang Wu

JANUARY 2019

Highway Research Center
Harbert Engineering Center
Auburn, Alabama 36849

www.eng.auburn.edu/research/centers/hrc.html

1. Report No. ALDOT 930-916	**2. Government Accession No.**	**Chapter 3. Recipient Catalog No.**
4 Title and Subtitle Simplified and Standardized Seismic Design and Detailing for Alabama Bridges		**5 Report Date** January 2019 **6 Performing Organization Code**
7. Author(s) Justin D. Marshall, Joseph Broderick, Hongyang Wu		**8 Performing** ALDOT 930-916
9 Performing Organization Name and Address Highway Research Center Department of Civil Engineering 238 Harbert Engineering Center Auburn, AL 36849		**10 Work Unit No. (TRAIS)** **11 Contract or Grant No.**
12 Sponsoring Agency Name and Address Alabama Department of Transportation 1409 Coliseum Boulevard Montgomery, Alabama 36130-3050		**13 Type of Report and Period Covered** Technical Report **14 Sponsoring Agency Code**
15 Supplementary Notes		

16 Abstract

Simplification and standardization of the seismic design processes for typical Alabama bridges has been investigated and developed in this research. A number of design tools have been developed to reduce the analysis complexity and time demands on bridge designers. These tools can be used to simplify and standardize the seismic design process due to the fact that the hazard in Alabama ranges from minimal to moderate. The parametric studies and research completed in the project has developed guidelines and simplified design methods for determining the fundamental period of vibration, displacement ductility for short columns, ductile detailing requirements for columns, substructure-to-superstructure connections and end diaphragm design for steel girder bridges.

17 Key Words Seismic bridge design, structural dynamic, ductile structural detailing		**18 Distribution Statement** No restrictions. This document is available to the public through the National Technical Information Service, Springfield, Virginia 22161	
19 Security Classification (of this report) Unclassified	**20 Security Classification (of this page)** Unclassified	**21 No. of pages** 208	**22 Price**

FORM DOT F 1700.7 (8-72)

Research Report

ALDOT Research Project #930-916

SIMPLIFIED AND STANDARDIZED SEISMIC DESIGN AND DETAILING FOR ALABAMA BRIDGES

Submitted to

The Alabama Department of Transportation

Prepared by

Justin D. Marshall
Joseph Broderick
Hongyang Wu

Highway Research Center

and

Department of Civil Engineering

at Auburn University

JANUARY 2019

DISCLAIMERS

The contents of this report reflect the views of the authors, who are responsible for the facts and the accuracy of the data presented herein. The contents do not necessarily reflect the official views or policies of Auburn University or the Federal Highway Administration. This report does not constitute a standard, specification, or regulation.

NOT INTENDED FOR CONSTRUCTION, BIDDING, OR PERMIT PURPOSES

Justin D. Marshall, Ph.D., P.E.
Research Supervisor

ACKNOWLEDGEMENTS

The authors would like to acknowledge all those who have participated in this project either as part of the team or the ALDOT Bridge Bureau personnel who provided input throughout the process.

Abstract

Bridge seismic design is a nationwide requirement. The magnitude of the hazard varies significantly around the United States. In Alabama the hazard varies from nearly non-existent to moderate. In the northern part of the state the seismic hazard exceeds the limitation which puts it into Seismic Design Category (SDC) B or in very poor soil conditions SDC C. For Seismic Design Category A (the lowest), a specified lateral force is applied to the structure based on the dead load reaction and no additional analysis or detailing is required. However, once the hazard meets or exceeds SDC B, additional design, analysis and detailing is required. While seismic design of standard bridges does not require explicit dynamic analysis, significant effort is required to approximate the system dynamic properties to develop equivalent static design loads. Seismic analysis and design requirements include determining an approximate fundamental period of vibration, the ductility demand and capacity of plastic hinges (also called the fuse element) and capacity-based force demands for non-fuse elements.

Simplification and standardization tools and equations were developed to aid Alabama bridge designers. A parametric study was completed to generate a series of regression-based equations to calculate the fundamental period of vibration in both the longitudinal and transverse direction of typical, simple span bridges using the basic geometric characteristics of the bridge. Nonlinear solid finite element analyses were utilized to generate displacement capacity equations which can be used for bridge columns shorter than is applicable to the current equations. Standard detail drawings were developed to identify the critical detailing requirements for ductile reinforced concrete columns as well as the connection to adjacent elements (i.e. drilled shaft, pile cap, or bent cap). Design of the superstructure-to-substructure connection between the girder and bent cap was investigated to determine the required support length and provide a design method resulting in sufficient connection capacity for both steel and prestressed bridge girders. Steel end diaphragm design was also analyzed to ensure that that sufficient capacity would be available using current configurations without significant changes to design or analysis methods.
The result of the development of these tools and guidelines will simplify seismic design of bridges in the moderate hazard of Alabama.

Table of Contents

List of Tables

List of Figures

Chapter 1 Introduction

1.1 Overview

Bridge seismic design is a nationwide requirement. The magnitude of the hazard varies significantly around the United States. In Alabama the hazard varies from nearly non-existent to moderate. In the northern part of the state the seismic hazard exceeds the limitation which puts it into Seismic Design Category (SDC) B or in very poor soil conditions SDC C. For Seismic Design Category A (the lowest), a specified lateral force is applied to the structure based on the dead load reaction and no additional analysis or detailing is required. However, once the hazard meets or exceeds SDC B, additional design, analysis and detailing is required. While seismic design of standard bridges does not require dynamic analysis, significant effort is required to approximate the system dynamic properties to develop equivalent static design loads. Seismic design includes determining an approximate fundamental period of vibration, ductility capacity of plastic hinges (also called the fuse element) and capacity design of the non-fuse elements. Previous research by the PI has investigated the severity, variability and impact of the seismic hazard in Alabama and developed a series of case study designs and construction details related to prestressed concrete girder bridges. These case studies have been developed into a design procedure based on the LRFD Guide Specification for Seismic Design of Bridges (AASHTO 2008) as part of the transition to LRFD bridge design (AASHTO 2012). The end goal of the prior research was to develop methodologies and resources to assist designers with the transition both to LRFD and the updated seismic provisions. The prior research on seismic design methods and details was successful but has identified additional challenges including:

- Significant time resources and modeling requirements beyond typical design

- Fundamental knowledge of structural dynamics and nonlinear behavior of structures for bridge designers
- Multiple new construction details which cause significant construction challenges

1.2 Problem Statement

To overcome these challenges and barriers the proposed work will create a simplified and standardized design procedure and construction details which will greatly reduce the required resources needed for seismic design and construction of effected bridges in Alabama. This will require a series of parametric studies looking at the dynamic properties and ductility capacity of typical Alabama bridges. The studies will focus on creating standardized designs over the hazard range in Alabama. The work will also refine and develop seismic details which are constructible, reliable and economical. Some of these construction details have been developed and evaluated previously (prestressed concrete girder to bent cap connections and column hinge detailing) while others have not been (steel girder bridges).

The motivation to simplify and standardize seismic design results from the current status of bridge construction. Material costs have become a much smaller portion of total construction price while labor and lane downtime are now driving construction costs and impacts. This paradigm requires a different way of looking at design. Simplification and standardization are the trend that will limit additional design time for seismic loads, accelerate construction schedules, reduce construction changes and errors, and improve performance over the life of bridges.

One of the key aspects of this project will be review of the proposed work by Alabama Department of Transportation (ALDOT) Bridge Bureau personnel. This will ensure that the final recommended outcomes and products meet the needs of the bridge design community and the construction industry so the barricades to implementation will be minimized.

1.3 Research Objectives

This proposed work has a number of objectives that will lessen the impact of seismic requirements on designers while improving constructability of new details which mitigates traffic downtime and construction errors. Simplification and standardization are possible due to the moderate hazard range present in Alabama. However to achieve simplification and standardization over this range requires a series of tasks and parametric studies. The goal is to determine the necessary ranges and to find the balance between the continuum and the bins of values that can be used in a simplified design process. The task objectives of the proposed work include:

1) Create a standardized Seismic Design Category (SDC) map and table for Alabama. The information needed for seismic design includes the geographic location, the soil type and the spectral acceleration.
2) Develop a method to approximate fundamental periods for typical Alabama bridge structures based on span, width, column height, column diameter, girder material and foundation type through a parametric study.
3) Determine the ductility capacity for the range of reinforced concrete bridge bents based on number, height and diameter of columns and foundation type through a parametric study.
4) Develop standard seismic detailing requirements including end diaphragms and superstructure-to-substructure connections for steel girder bridges.
5) Refine existing details to define practical, constructible standard reinforcing details for reinforced concrete columns and the transition to pile caps, drilled shafts and bent caps.
6) Demonstrate the standardized seismic design process through multiple case studies.
7) Integrate the proposed simplified design method and details into practice through a training workshop.

1.4 Research Scope

The scope of this study is to develop standard design procedures and construction details which apply to typical Alabama bridges that fall into SDC B and C. The developed procedures and details will minimize the resources needed to complete seismic design and detailing for bridges

where it is required. It will also clearly delineate the limits of where the standard details will apply. The range of bridges that will be involved in the study consists of the typical steel and prestressed concrete girder bridges. The range of span and column heights was determined in conjunction with ALDOT to find the range where the standardization can be effectively applied. While the moderate hazard in Alabama can be reasonably standardized there are specific cases where this standardization is not feasible. Some examples include very poor soil conditions, steel girders with high horizontal curvature, large skew and non-standard bridge construction (i.e. truss bridges, cable stayed, etc.). In addition to the development, a training workshop or series of workshops will be provided to demonstrate to the bridge design and construction community how the tools and details will be implemented.

1.5 Organization of Report

This report is divided into 9 chapters. Chapter 1 is an introductory chapter providing the motivation for the research project, objectives and a summary of the research performed. Chapter 2 provides both graphical and numerical information summarizing the seismic hazard in Alabama based on the county and the geotechnical site class to make the Seismic Design Category determination for Alabama bridges simple. Chapter 3 presents the parametric study and the results that were used to develop simplified equations to determine the fundamental period of vibration in the longitudinal and transverse directions for simple span bridges up to five spans based on standard ALDOT bridge parameters. Chapters 4 provides equations that can be used to determine the displacement capacity of columns that do not meet the geometric criteria of the equations in the Guide Specification. Chapter 5 presents drawings illustrating the requirements for ductile detailing of bridge columns in the plastic hinge zone as well as the connections of those columns to the foundations and bent caps. Chapter 6 provides recommendations for calculation of support length for simple span bridges without any modification to the substructure-to-superstructure

connection for prestressed concrete bridge girders. Chapter 7 outlines a design procedure for steel girder bridges beam-to-ca connection which includes a shear block to provide shear capacity in the transverse direction. Chapter 8 evaluates the effectiveness of existing design and analysis methods for end diaphragms in steel girder bridge and provides recommendations to meet current code provisions. The summary, conclusions and recommendations for the research report are provided in Chapter 9.

Chapter 2 Alabama Seismic Hazard

2.1 Introduction

The first step in seismic design of structures is to determine the seismic hazard of the site. This is currently accomplished by using contour maps within the AASHTO Guide Specifications (2011) or by using an online tool on the USGS website to determine the Seismic Design Category (SDC). However, in order to streamline the design process, maps of Alabama were created that delineate the SDC by each county. By creating visual maps, the designer can more quickly determine whether any seismic detailing is needed. Seismic detailing is needed in any location that has a one-second design spectral acceleration (S_{D1}) of 0.10g or more (AASHTO, 2011). While this procedure will simplify the approach to determining the hazard, conservatism is built into the procedure, and thus it may provide a seismic hazard that is more stringent than if a more precise procedure was followed.

2.2 Hazard Determination

The first step in determining the seismic hazard for Alabama is determining the Site Class of the construction site. There are multiple ways to determine the soil conditions at a site, with the most common way being to conduct a Standard Penetration Test (SPT) to count the number of blows (N_i) required to penetrate a layer of soil, and the most accurate way being to conduct a Shear Wave Velocity Test. The SPT is a simplified way to estimate the shear wave velocity of a soil. After this test is completed, Equation 2.1 is used to calculate the average standard penetration blow count (N). Based on this value and Table 3.4.2.1-1 in the AASHTO Guide Specifications (2011), the Site Class is determined. One limitation of this test is that it can only be applicable to Site Classes C-F. To be able to use the seismic hazard in a Site Class of A or B, the Shear Wave Velocity test must be used. One note to make is that although the Site Classes can be identified

all the way to Site Class F, Site Class F is uncommon and must be specifically tested which resulted in a hazard map not being developed for this Site Class.

$$N = \frac{\sum_{i=1}^{n} d_i}{\sum_{i=1}^{n} \frac{d_i}{N_i}} \qquad \text{Equation 2-1}$$

Where N = Average standard penetration blow count

n = total number of distinctive soil layers in the upper 100 ft of the site profile

i = any one of the layers between 1 and n

d_i = thickness of *i*th soil layer

N_i = Uncorrected blow count of *i*th soil layer

After determining the site class, the United States Geological Survey (USGS) seismic hazard batch-mode tool was used to determine the SDC. To create the seismic hazard maps, the USGS tool was used to obtain the hazard at six different locations in each county around the perimeter of the county (United States Geological Survey, 2018). Google maps were used to find the coordinates of these six locations, and the coordinates were input into the USGS tool (GOOGLE, 2018). The tool outputs numerous variables, but the most important variables obtained were the peak ground acceleration (A_s), the short period (0.2 s) design spectral acceleration (S_{DS}), the one second period design spectral acceleration (S_{D1}), and the SDC. The values for every point and every county were listed in an accessible database for future design. Each county was labeled based on the worst case SDC from the six coordinates. An online tool provided by mapchart.net was used to create the maps (Mapchart, 2018).

2.3 Hazard Maps

The hazard maps are presented in Figures 2-1 to Figure 2-4. It is clear from the maps that as the Site Class is increased, the SDC is also increased. Another pattern that is clear is the more northern or western the location, the higher the hazard. This pattern originates from the fact that

the New Madrid seismic zone is located to the north-west of Alabama and the East Tennessee Seismic Zone is located to the north-east of the state.

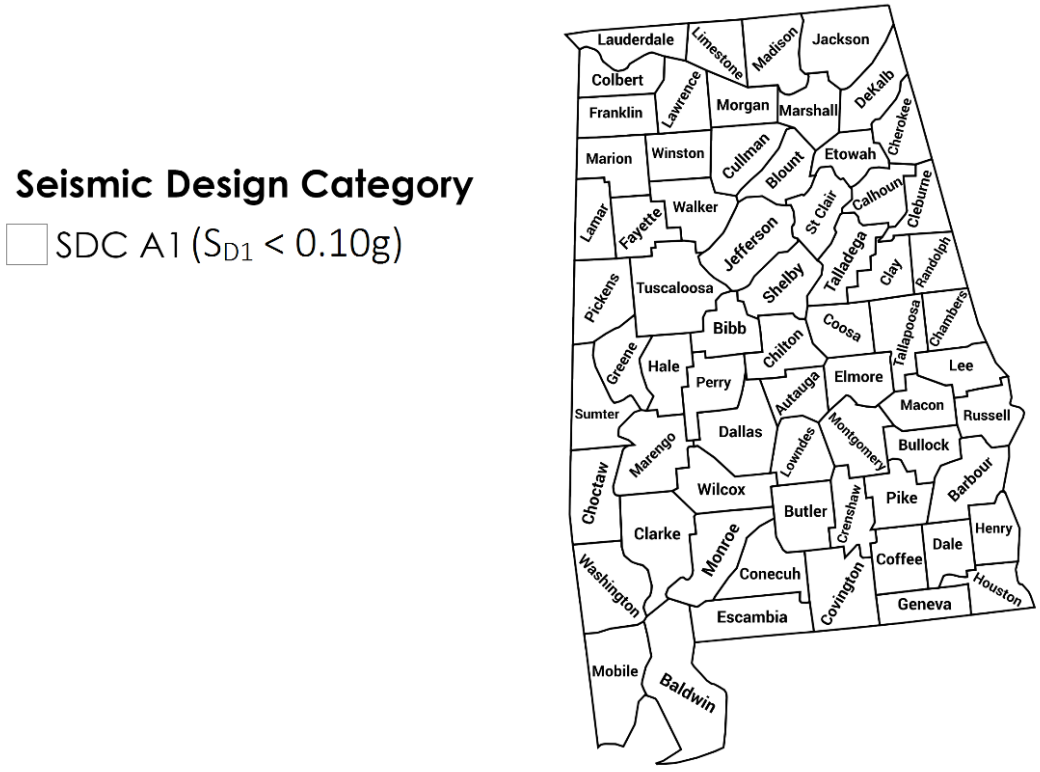

Figure 2-1 Seismic Hazard Map for Site Classes A and B

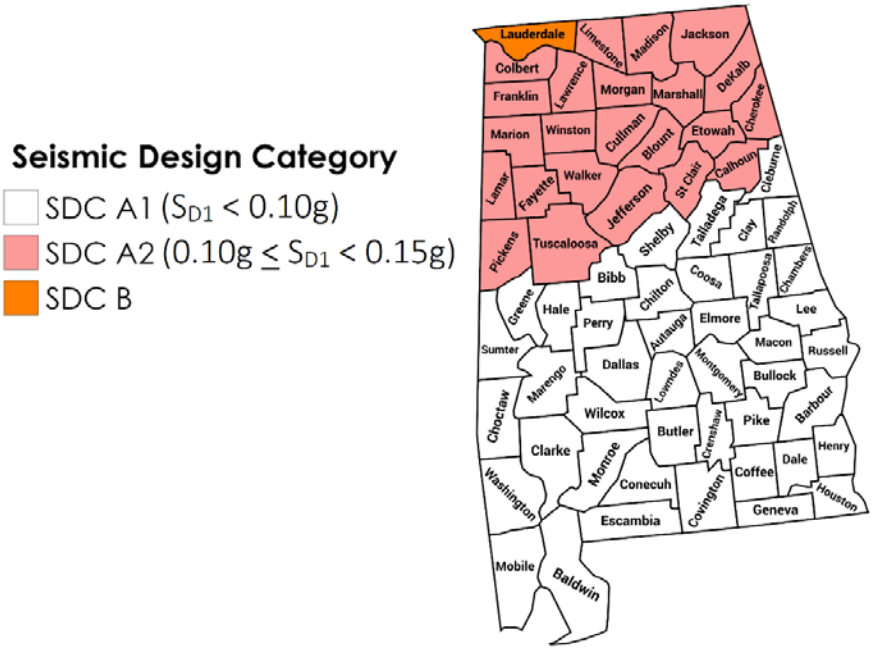

Figure 2-2 Seismic Hazard Map for Site Class C

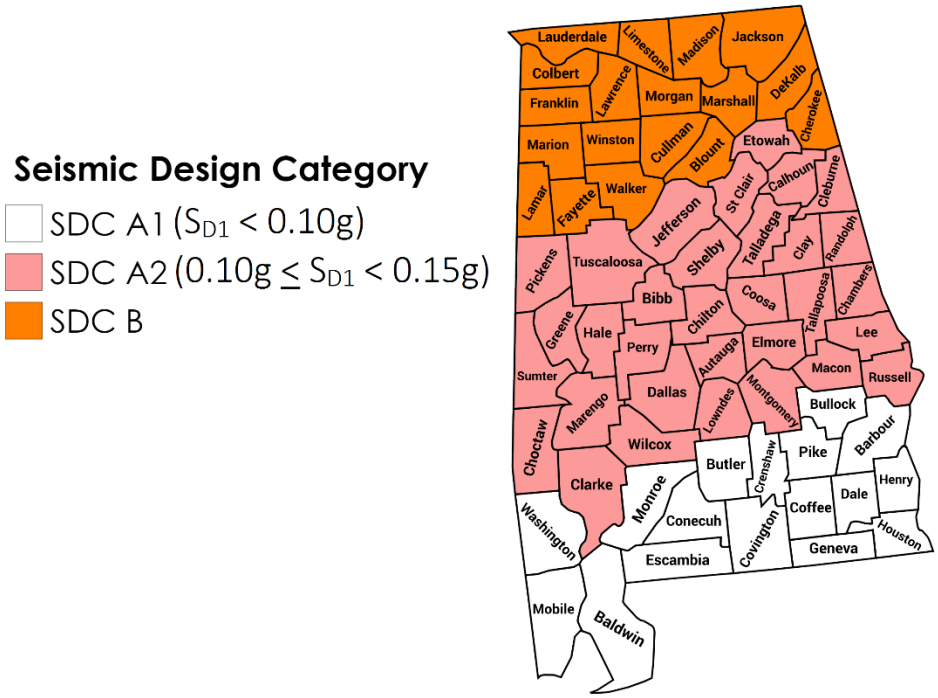

Figure 2-3 Seismic Hazard Map for Site Class D

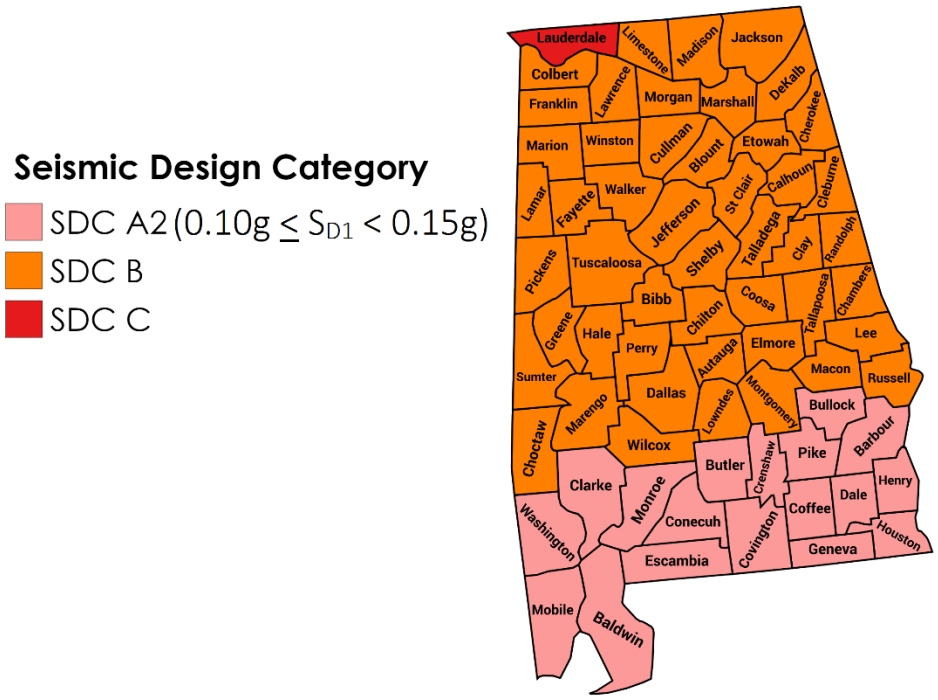

Figure 2-4 Seismic Hazard Map for Site Class E

2.4 Summary

This chapter established the procedure for determining the seismic hazard for a specific site and developed simplified hazard maps and a numerical database for each county and Site Class in Alabama. Engineers can use these maps and the ground motion values associated with each county to make their design process more expedient. Because this procedure is simplified, there is a certain amount of conservatism built in with it. The designer must balance the project's need for simplicity with its need for accuracy.

Chapter 3 Method to Approximate Fundamental Period of Vibration

3.1 Introduction

It is well known that the fundamental period of vibration of bridges has a significant impact on seismic demands. During the past decades, modal analysis has been considered as an efficient way to evaluate the dynamic properties of bridges in the frequency domain. Significant effort for the applications of modal analysis have been done according to recent research efforts (Maia & Silva, 1997; Juang, 1994; Ewins, 2000). In bridge engineering, modal analysis uses the mass, stiffness and damping matrix of the bridges to find the different periods of vibration and corresponding vibration modes by calculating the eigenvalues and eigenvectors. These fundamental periods of vibration are very important in bridge seismic design to determine the seismic demands on the structure. The design spectrum for Huntsville for Site Class D soil condition is shown in Figure 3-1. The Spectral Acceleration (Sa), which is directly related to the force demands, is based on the fundamental period of vibration (horizontal axis). It can be seen in the figure that a significant difference in demand exists based on the fundamental period. Standard bridges typically have fundamental periods in the transverse direction between 0.5s and 1.0 s so assuming the highest acceleration (i.e. the constant acceleration region) would be overly conservative. Several procedures to determine the period are provided in the AASHTO documents but all of them require modeling of the entire bridge and an understanding of structural dynamics.

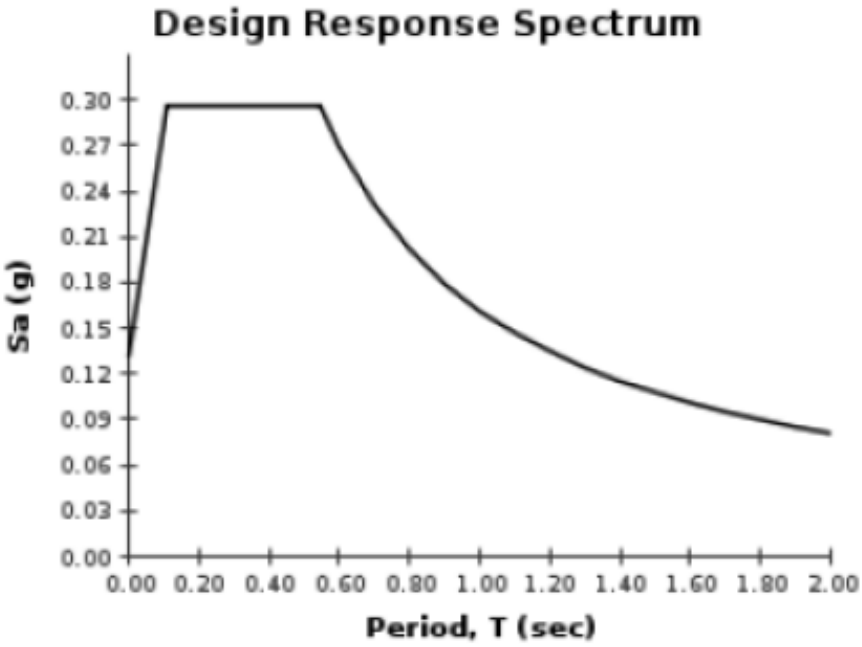

Figure 3-1 Design Response Spectrum for Huntsville, AL – Site Class D

A parametric study was designed and completed to create regression-based equations which are based on the important characteristics including span length, number of spans, girder type, column diameter, column height and foundation stiffness, etc. In this study, the bridge fundamental period was calculated by using CSIBRIDGE V15 (CSI., 2011). The study will be initiated with the bridges that have been used in past seismic research which cover the typical variation in bridge properties (Kane, 2013; Panzer, 2013; Law, 2013). Other highway bridges will also be modelled to fill other parametric study gaps. Regression analysis was performed to create regression equations which allow engineers use the primary bridge properties to calculate the fundamental period without any dynamic modeling.

3.2 Bridge Modelling

A three-dimensional (3D) model of the structural system is required to be built in CSIBRIDGE to capture the modal analysis response of the entire highway bridge system. According to the modal analysis results, different modes of vibration are highly correlated with bridge geometry characteristics which will directly affect the modal participating mass ratios in x, y and z

directions. The modes with large modal participating mass ratio will significantly affect the dynamic response of the bridge which need to be represented through the 3D model. In highway bridge modelling, different components can be distributed into two different groups. One is the linear elastic component group and the other one is the nonlinear component group. The first group consists of the bridge components which will remain elastic during the earthquake while the second group consists of the bridge components which will have nonlinear behavior due to nonlinear material stress-strain relations and geometric nonlinearities which represent the P-Δ effects in the structure inducing stability problems under large displacements which means equilibriums needs to be calculated under the deformed configuration. Table 3-1 summarizes the recommended group for different components of standard highway bridges when generating bridge numerical models (Aviram, Mackie, & Stojadinović, 2008). Based on Table 3.1, if the bridge components designed by the highway bridge design engineer fall into the linear elastic group, the corresponding components should be modeled as linear elastic elements instead of nonlinear elements since the accuracy and reliability of the analysis result will still be considered as reasonable. In addition, if the bridge components fall into the nonlinear group, they are supposed to be modelled as nonlinear element to capture the essential behaviors during the bridge dynamic analysis. However, for the highway bridge modal analysis, only linear elastic properties of bridge components should be considered to capture the bridge fundamental period. Therefore, in this study, the bridge components which are in the first group remained linear elastic while those which are in the second group will not be modeled or will be modeled using simplified elastic properties. For instance, the plastic hinge zone of columns was not modelled and all the degrees of freedom of the abutments were considered as fixed. The different modeling methodologies for different components will be explained later in the chapter.

Table 3-1 Recommended Group for Component Modelling (Aviram, Mackie, & Stojadinović, 2008)

Component	Linear-Elastic	Nonlinear
Superstructure	X	
Column–plastic hinge zone		X
Column–outside	X	
Cap beam	X	
Abutment–transverse		X
Abutment–longitudinal		X
Abutment–overturning		X
Abutment–gap		X
Expansion joints		X
Foundation springs	X	
Soil-structure interaction	X	

3.2.1 Superstructure Modelling

The superstructure of highway bridges includes the bridge deck and bridge girders. They were initially modelled by using information which was provided by ALDOT. All the spans in this study were simple spans. Figure 3-2 shows the cross section of the superstructure for the standard highway bridge. In this study, all the bridge cross sections in the parametric study later had a similar configuration. The deck width is 43 ft with a 7-inch concrete deck which is supported by 5 typical bridge girders. The distance between these bridge girders is 9.5 ft. There are six different bridge girders which can be selected by designers during standard highway bridge design including Type I, Type II, Type III, BT-54, BT-63 and BT-72 standard prestressed concrete girders. The preliminary selection of the bridge girders was directly related with the bridge span length. Table 3-2 shows the recommended girder selection based on the highway bridge span length. The concrete haunch thickness is always 2 inches in this study. All this geometric information about the highway bridge superstructure can be represented by inputting the correct parameter values in CSIBRIDGE. The parameters which need to be specified in the CSIBRIDGE model include the

total span length, girder spacing, concrete haunch thickness and slab thickness. The two guardrails are not modelled in this study as part of the bridge stiffness.

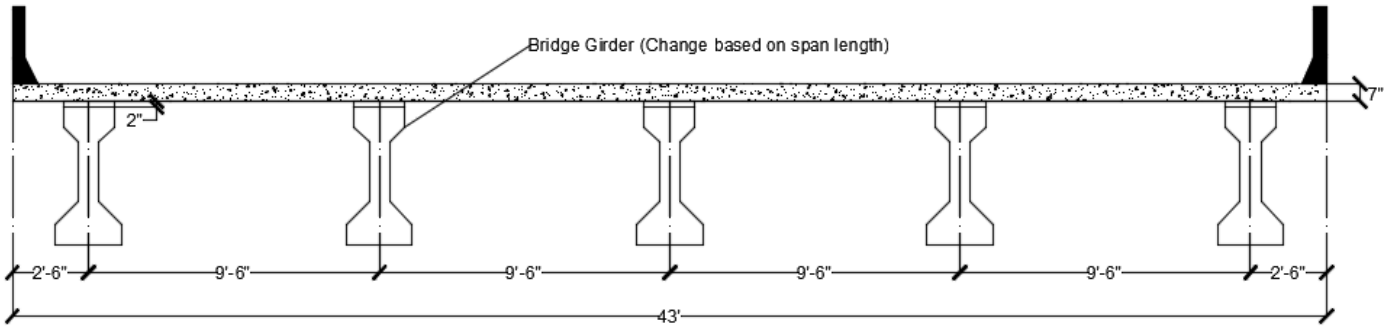

Figure 3-2 Cross Section of the Typical Superstructure of Highway Bridge

Table 3-2 Recommended Girder Selection based on Bridge Span Length

Girder Type	Maximum Span Length	Height(ft)	Distance to Filet(ft)
Type I	45ft	2.3	0.50
Type II	60ft	3	0.50
Type III	85ft	3.75	0.67
BT-54	100ft	4.5	1.75
BT-63	125ft	5.25	1.75
BT-72	140ft	6	1.75

The bridge deck was modelled by using shell elements. The shell element is a 2D element which can be assigned to carry plate bending, shear and membrane loading. Two types of shell element are commonly used in the finite element modelling. One is the quadrilateral shape and the other one is the triangular shape. In this study, the quadrilateral shape was chosen to mesh the concrete bridge deck. The preferred maximum submesh size for a bridge deck in CSIBRIDGE is 4 ft. Figure 3-3 shows one shell element which represents part of the concrete deck in the bridge model. The bridge deck in this study was made of 4,000 psi concrete which was defined by two parameters, Young's modulus and Poisson's ratio. The Young's modulus in this study is 3,605 ksi and the Poisson's ratio is 0.2.

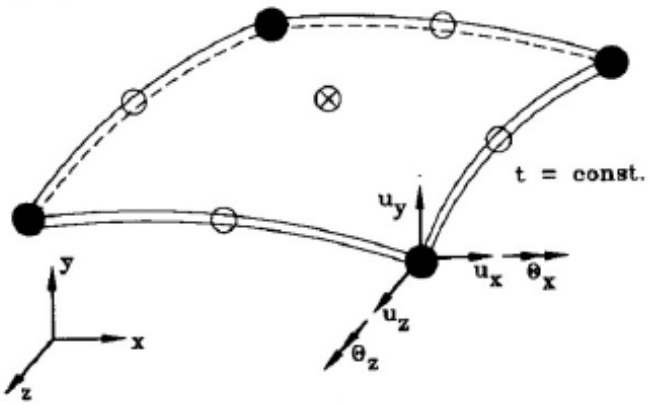

Figure 3-3 Shell Element in the Bridge Model (Caltrans, BRIDGE DESIGN PRACTICE, 2015)

All the bridge girders were modeled by using linear-elastic beam elements which are slender members carrying force and moment. There are two nodes for each beam element with six degrees of freedom at each node including three translation degrees of freedom and three rotational degrees of freedom. The bridge girders in this study were constructed with 6,500 psi concrete which was also defined by two parameters, Young's modulus and Poisson's ratio. The Young's modulus in this study is 4,595 ksi and the Poisson's ratio is 0.2. The properties of the beam element for the typical "I" bridge girder cross sections can be defined by using the section designer in CSIBRIDGE. Then the values of the cross-section area (A), torsional constant (J), moments of inertia (I_{22} and I_{33}), shear areas (A_{v2} and A_{v3}), elastic and plastic section modulus (S_{22}, S_{33}, Z_{22}, and Z_{33}), and radius of gyration (r_{22} and r_{33}) in the vertical and transverse directions will be calculated automatically. The elevation (node/element position) of the bridge components in the superstructure of the finite element highway bridge model were defined according to the physical highway bridge model. Figure 3-4 shows the comparison between the position of the bridge components in the finite element model and the physical model.

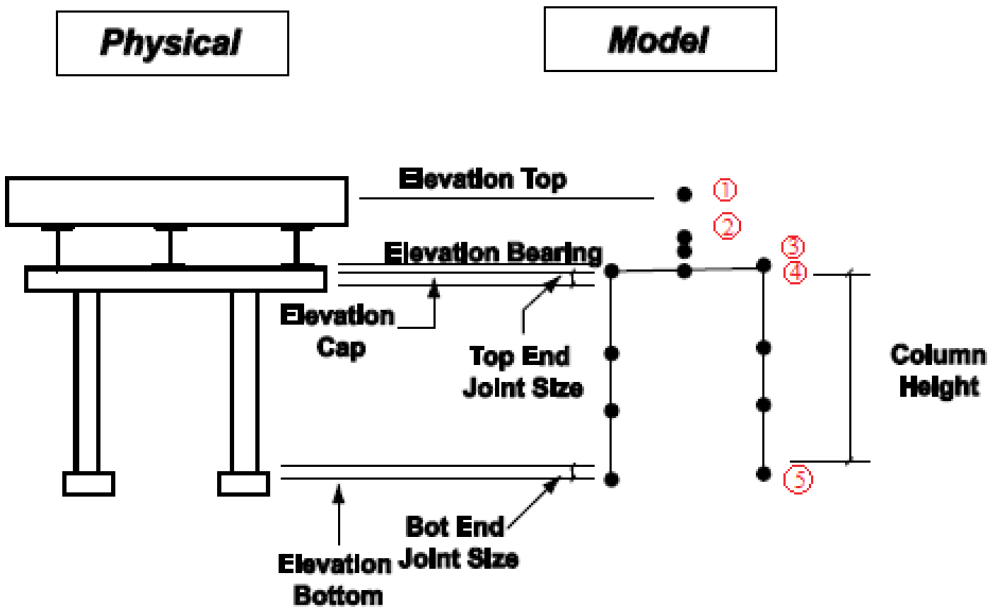

Figure 3-4 Comparison between Position of Bridge Components in the Finite Element Model and Physical Model (Caltrans, BRIDGE DESIGN PRACTICE, 2015)

Position 1 represents the position of bridge concrete deck which is at the same height level with the middle point of deck thickness in the physical model. Position 2 represents the position of the concrete girder which is at the same height level with the neutral axis of the concrete girder in the physical model. Rigid constraints were applied between the nodes in the position 1 and those in the position 2. Position 3 represents the position of the top of the bearing pad in this study. Rigid link elements were applied between the nodes in position 2 and 3. Position 4 represents the position of the cap beam which is at the same height level with the middle point of the cap beam depth in the physical model. The link elements which contain the properties of the bearing system which will be explained in this chapter were created between the nodes in position 3 and 4. Position 5 represents the bottom fixity points of the bridge piers. Foundation springs will be added to these nodes to represent the soil and foundation system. Figure 3-5 shows the extruded view of the highway bridge superstructure in CSIBRIDGE.

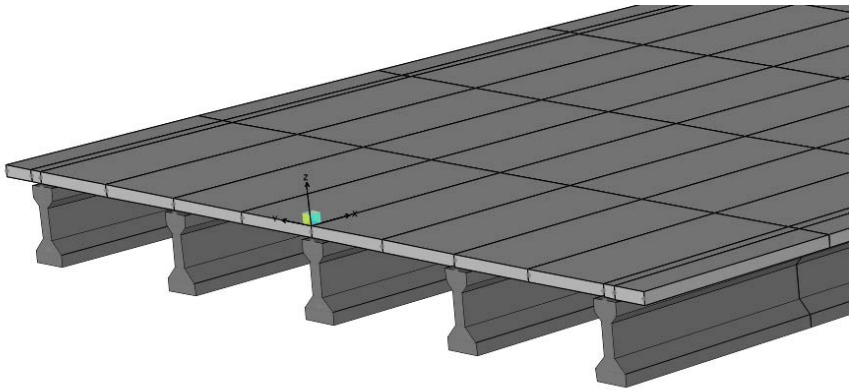

Figure 3-5 Extruded View of Highway Bridge Superstructure in CSIBRIDGE

3.2.2 Substructure Modelling

The highway bridge substructure includes the bridge cap beam, bridge pier and foundation spring. Figure 3-6 shows the elevation view of the substructure with multiple pier bents. The nonlinear joint between the cap beam and column and the column hinge are not included in this study for the modal analysis.

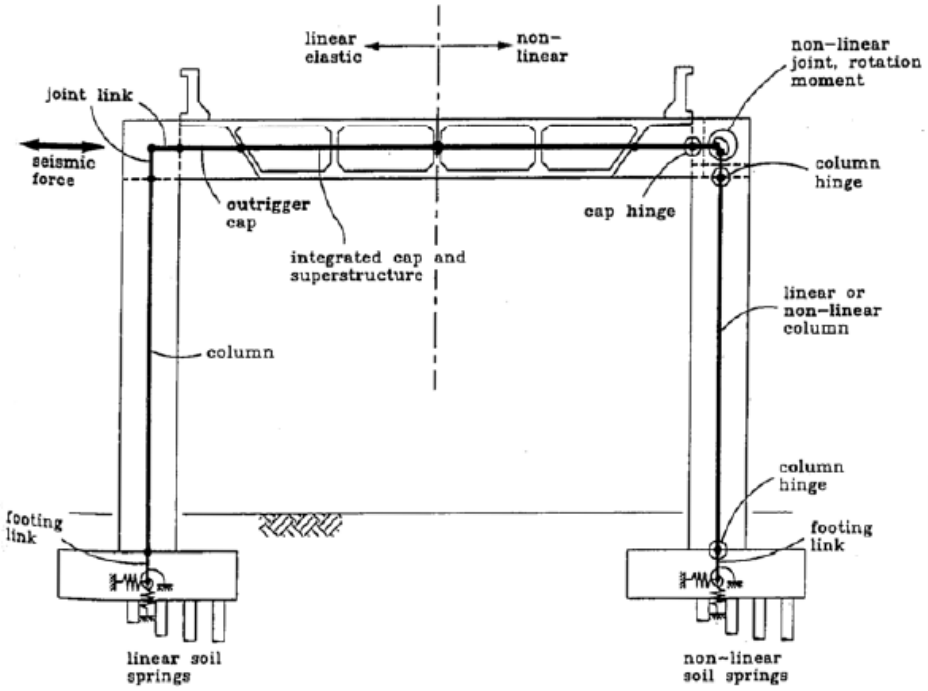

Figure 3-6 Multiple Column Bent Model (Priestley, Seible, & Calvi, 1996)

The cap beam is a concrete beam which supports bridge girders transfers load to the columns which can form a frame system to help to resist the lateral loads or displacements which were applied primarily in the transverse direction of the bridge. The cap beams were modelled as linear elastic beam elements with a solid rectangular cross section. In this study, all the cap beam cross sections were the same in the parametric study since the effect of cap beam size is not significant to the bridge period. The depth of cap beam is 7 ft while the width is 6 ft in the parametric study. The cap beam in this study was made of 4,000 psi concrete which is the same as the bridge deck concrete.

According to Panzer (2013), the bottom of the bridge column will be defined at the level of base fixity while the top of the column will be defined at the middle of the cap beam. Linear elastic three-dimensional beam elements were used to model the column and part of the drilled shaft or piles which were above the base fixity point. In the parametric study, the diameter of bridge shafts or piles were same as the bridge columns. The bridge column in this study was made of 4,000 psi concrete. Only circular columns with four different diameters including 4 ft, 4.5 ft, 5 ft and 5.5 ft were used in the parametric study. The column plastic hinge zone was not modelled in the bridge modal analysis. Figure 3-7 indicates the location of the column top and bottom points in the CSIBRIDGE model.

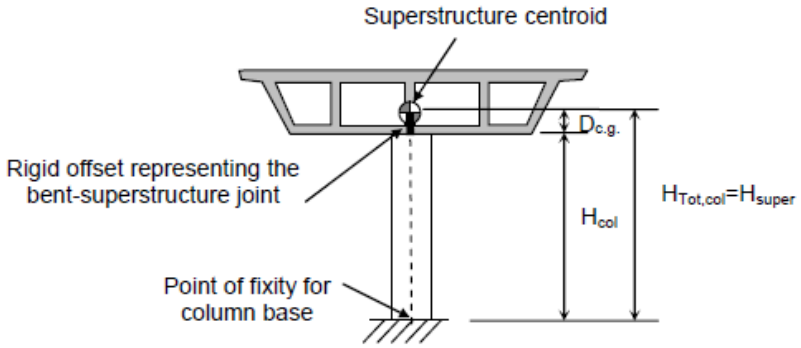

Figure 3-7 Location of column top and bottom nodes in the Bridge Model

Foundation springs at the bottom of the column (point of fixity for columns) was also considered in this study. There are six degrees of freedom for a foundation system including axial and bilateral translation and rotation about each of the three axes. The stiffness of these six degrees of freedom were based on the condition of bridge foundation itself and the corresponding soil which need to be defined in CSIBRIDGE. It can be appropriate to assume some DOF are fixed which means they do not need to be evaluated, such as axial translation or torsional rotation. A couple of static pushover analysis have been done to determine the stiffness of the foundation system at the bottom of columns by using FB-MultiPier (Kane, 2013). Figure 3-8 shows the direct modelling in FB-MultiPier and the simplified modelling of a foundation system in CSIBRIDGE, respectively. Based on Figure 3.8, the pile head was assumed to be fixed within the foundation cap which means they were modeled together. The system damping is not considered in this study. A stiffness range for the foundation system was created for the parametric study based on the result of Kane's research.

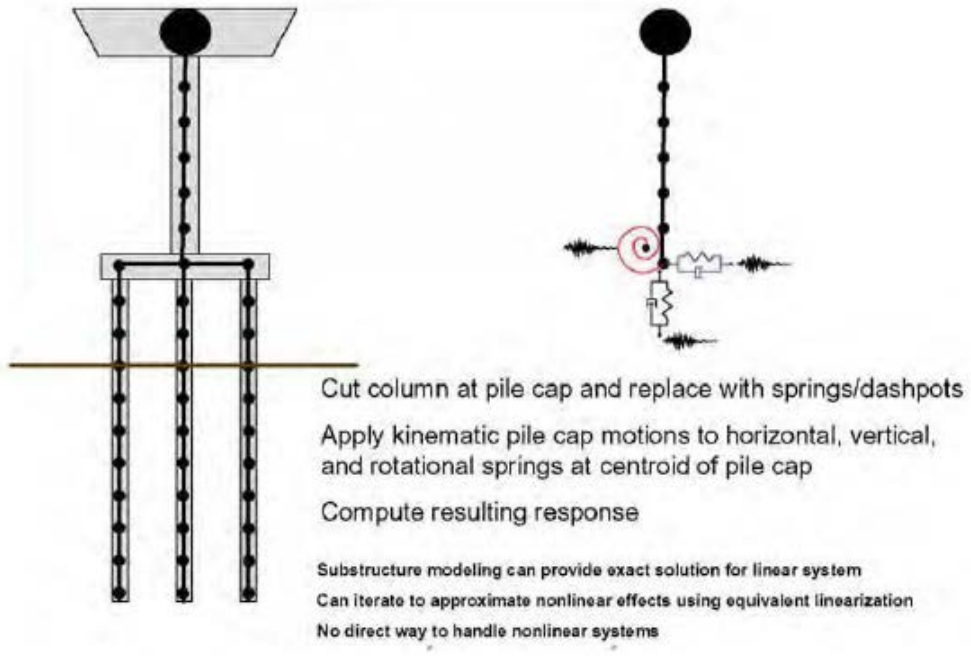

Figure 3-8 Foundation Substructure Model (Kavazanjian, 2011)

Abutment refers to one of the substructure components which resists the earth pressure and vertical loading at the end of the bridge. In addition, abutments can also resist the bridge inertial loads developed from strong ground motions. In design practice, abutment walls are usually designed as free-standing retaining walls based on the theories of active and passive earth pressure. However, these theories of earth pressure might be invalid during the earthquakes when the bridge inertial load is larger than the anticipated passive earth pressure (Martin & Lam, 1986). In addition, the behavior of abutments was found to have significant influence on the entire bridge system, especially, for highway bridges which have short spans with relatively high superstructure stiffness (Kotsoglu & Pantazopoulou, 2006). In this study, the abutments were assumed to be fixed on the ground with a large square cross section which represents the big mass of bridge abutment. The dimension of the cross section of the abutment in this study was 8 ft by 8ft. The length of the abutment was 43 ft which was same with the width of bridge deck in this study.

3.2.3 Connection Modelling

Connection behavior between the superstructure and substructure was also considered in this analysis. For the highway bridges in this study, they all contain a girder-to-elastomeric bearing pad connections at the end of each span. Figure 3-9 shows the detail of this type of bridge connection. Each of these bearing pads is made from layers of elastomeric material interspersed with thin steel plates (steel shims). These shims act to reduce bulging of the elastomeric material when subjected to vertical loads by limiting the thickness of each individual layer of elastomeric material (Panzer, 2013). The stiffness of elastomeric bridge bearings laterally can be determined according to Equation 3.1.

$$K_{bearing} = \frac{G*A}{t} \qquad \text{Equation 3.1}$$

Where

$K_{bearing}$= Shear stiffness of elastomeric bearing pad (lb/in)

G= Shear modulus of elastomeric bearing pad (psi)

A= Surface area of elastomeric bearing pad (in^2)

t= Thickness of elastomeric bearing pad material (in)

The dimensions of each bearing pad are directly related with the span length. The shear modulus (G) of 135 psi was selected from values found in a Caltrans design memo (Caltrans, 1994).

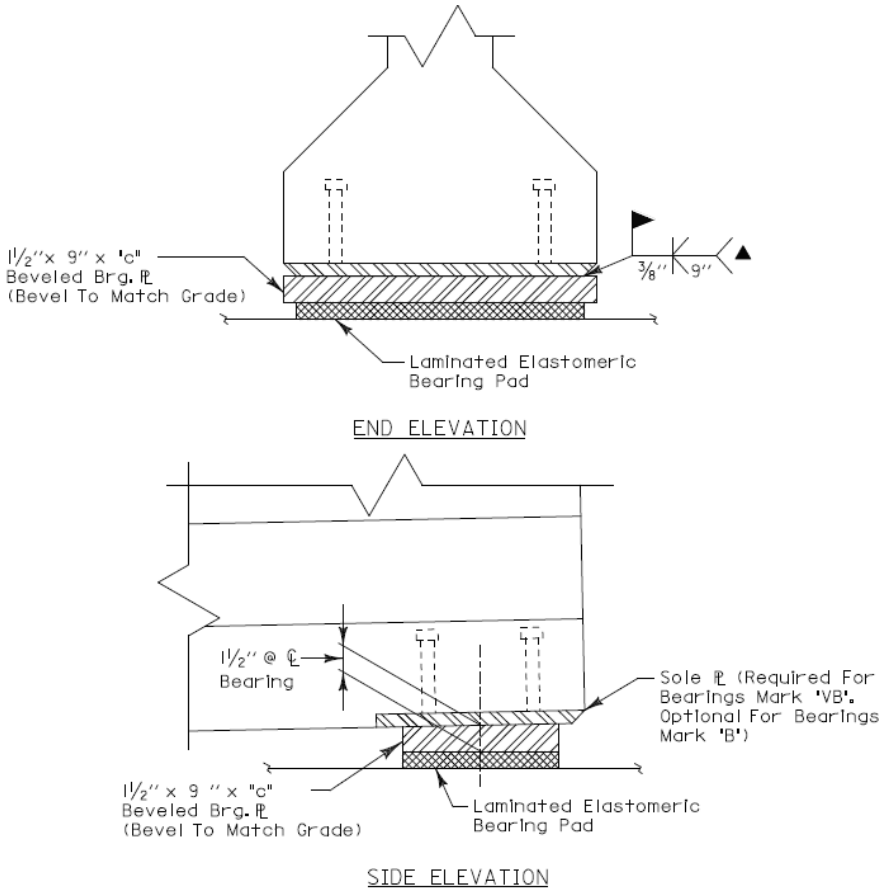

Figure 3-9 Detail of Elastomeric Bearing Pad (ALDOT, 2012)

All the bridge models were subjected to the loading in the longitudinal direction (direction of travel) and the transverse direction (perpendicular to direction of travel). The connection that resists motion in the longitudinal direction consists solely of a bearing pad, but both bearing pad

and a clip angles with anchor bolts resists motion in the lateral direction. Figure 3-10 shows the detail of a typical ALDOT connection. The clip angle system consists of steel clip angles fastened to the girder via threaded inserts and fastened to either abutments or bent caps via anchor bolts. For this analysis it is assumed that the small threaded inserts that transfer longitudinal or tensile forces from the girder to the clip angle are not sufficiently embedded within the girder to provide any real resistance. This configuration results in a single-level longitudinal connection system. However, the anchor bolt provides the clip angles with sufficient stiffness to resist transverse forces when the movement is towards the angle (Panzer, 2013). The shear capacity of an anchor bolt was defined by Equation 3.2, assuming adequate embedment was provided for the bolt. In this study, the elastic stiffness of the clip angle system was calculated by using the anchor bolt shear capacity divided by an overall displacement which is equal to 0.5 inches. A link element was created in the bridge model to represent the stiffness of the connection. Table 3-3 shows the detail of the stiffness of the connection in CSIBRIDGE. U2 and U3 represent the stiffness of the clip angle connection in the longitudinal and transverse directions, respectively.

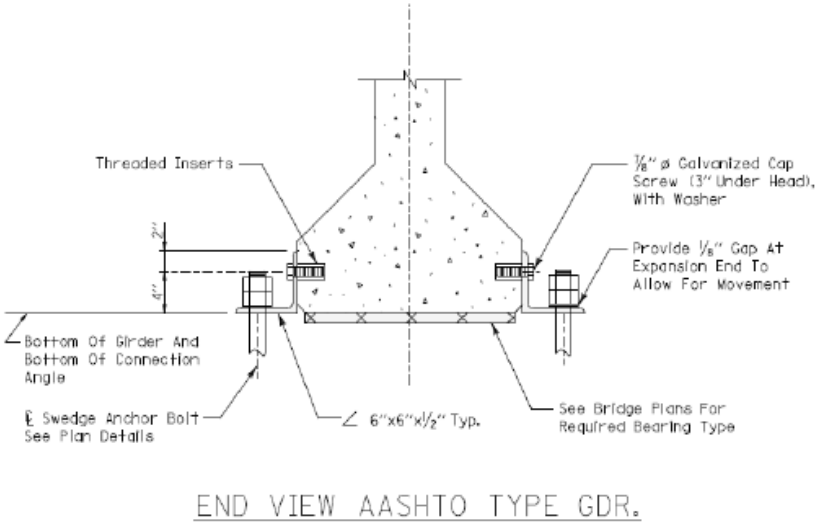

Figure 3-10 Clip Angle Connection Detail

$$V_n = 0.6 * Fu * A \qquad \text{Equation 3.2}$$

Where

V_n= Shear capacity of anchor bolt (kips)

Fu= Yield stress of anchor bolt (ksi)

A= Cross section area of anchor bolt (in^2)

Table 3-3 Detail of Stiffness of Bridge Connection in the CSIBRIDGE

Girder Type	Maximum Span Length	Height (ft)	Distance to Fillet (ft)	Bolt Diameter (in)	Bearing Pad Dimension			U2 (kip/ft)	U3 (kip/ft)
					Thickness (in)	Length (in)	Width (in)		
Type I	45ft	2.3	0.50	1	1.5	14.5	10	1344.12	156.60
				1.25				2012.10	
				1.5				2828.52	
				1.75				3793.39	
Type II	60ft	3	0.50	1	1.5	16.5	10	1365.72	178.20
				1.25				2033.70	
				1.5				2850.12	
				1.75				3814.99	
Type III	85ft	3.75	0.67	1	1.5	20.5	10	1408.92	221.40
				1.25				2076.90	
				1.5				2893.32	
				1.75				3858.19	
BT-54	100ft	4.5	1.75	1	2.5	24.5	10	1346.28	158.76
				1.25				2014.26	
				1.5				2830.68	
				1.75				3795.55	
BT-63	125ft	5.25	1.75	1	2.5	24.5	10	1346.28	158.76
				1.25				2014.26	
				1.5				2830.68	
				1.75				3795.55	
BT-72	140ft	6	1.75	1	2.5	24.5	10	1346.28	158.76
				1.25				2014.26	
				1.5				2830.68	
				1.75				3795.55	

3.3 Fundamental Period Selection

After modelling the highway bridge in CSIBRIDGE with all the parameters, the modal analysis was done by CSIBRIDGE. The fundamental period in the longitudinal direction and transverse direction were chosen based on the table of modal participating mass ratios from CSIBRIDGE. Table 3-4 shows an example table of modal participating mass ratios from CSIBRIDGE.

Table 3-4 Modal Participating Mass Ratio for an Example Bridge

Mode	Period (sec)	UX	UY	SumUX	SumUY
1	0.5937	0.6436	0.0000	0.6436	0.0000
2	0.4325	0.0005	0.0000	0.6441	0.0000
3	0.4132	0.1494	0.0000	0.7936	0.0000
4	0.2773	0.0000	0.5718	0.7936	0.5718
5	0.2743	0.0196	0.0000	0.8131	0.5718
6	0.1977	0.0000	0.1163	0.8131	0.6881
7	0.1624	0.0000	0.1570	0.8131	0.8451
8	0.1561	0.0000	0.0074	0.8131	0.8526
9	0.1489	0.0000	0.0029	0.8131	0.8555
10	0.1455	0.0126	0.0000	0.8257	0.8555
11	0.1378	0.0000	0.0227	0.8257	0.8782
12	0.1367	0.0000	0.0003	0.8257	0.8785

Based on Table 3-4, UX represents the mass participating ratio in the bridge longitudinal direction while UY represents the mass participating ratio in bridge transverse direction. Meanwhile, SumUX represents the accumulated mass participating ratio in the bridge longitudinal direction while SumUY represents the accumulated mass participating ratio in the bridge transverse direction. In this study, if a period had a mass participating ratio larger than 0.7, it would be selected as the fundamental period in the corresponding direction. However, if there is no period which had a mass participating ratio larger than 0.7, the first period which had an accumulated mass participating ratio larger than 0.7 was recorded as well to compare with the

result based on the single-mode spectral method according to the AASHTO guide specification (AASHTO, 2011). To calculate the fundamental period through the single-mode spectral method, one can follow the following procedures. First, calculate the static displacement $V_s(x)$ due to an assumed uniform loading p_0 which is arbitrarily set equal to 1.0 (kip/ft) as shown in Figure 3-11.

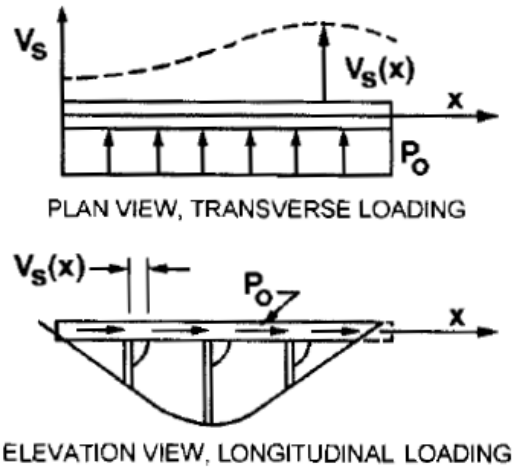

Figure 3-11 Bridge Deck Subjected to Assumed Transverse and Longitudinal Loading (AASHTO, 2011)

The static displacement $V_s(x)$ along with the bridge length in this study had been captured using CSIBRIDGE. Figures 3-12 and 3-13 show an example static displacement in the longitudinal direction and transverse direction, respectively.

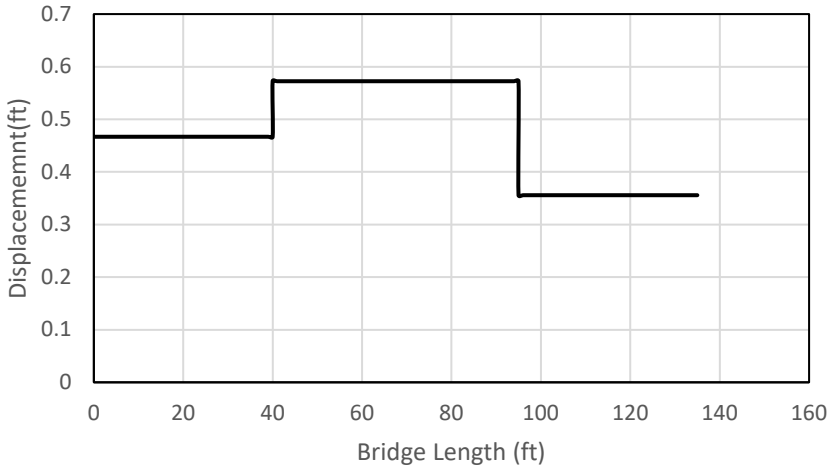

Figure 3-12 Static Displacement along the Bridge Length in the Longitudinal Direction

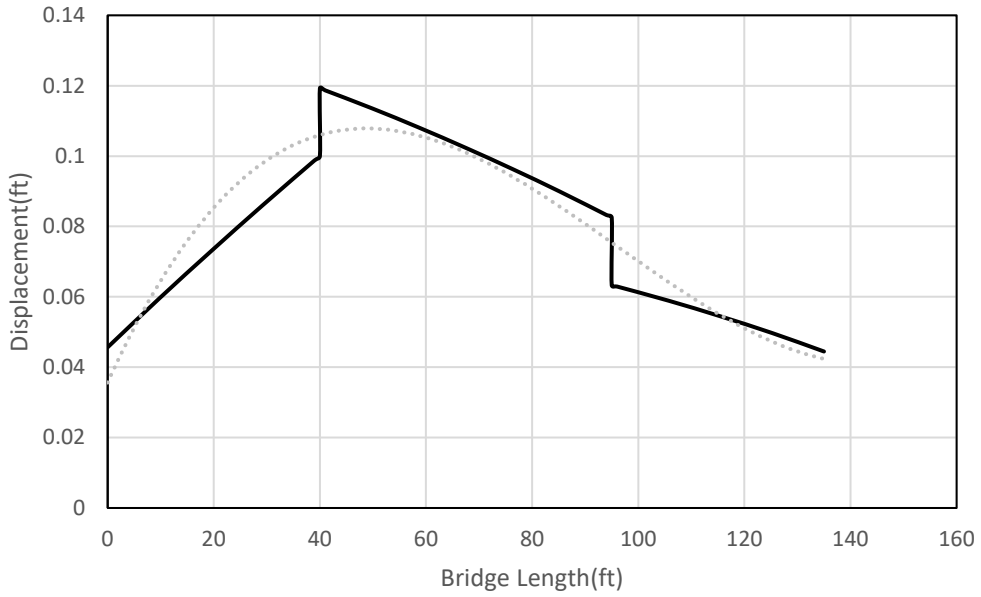

Figure 3-13 Static Displacement along the Bridge Length in the Transverse Direction

Then, two factors including α and γ need to be calculated based on the static displacement, $V_s(x)$. The two equations to calculate these two factors were shown in Equations 3.3 and 3.4. The computed factor α and γ have units of ft^2 and $kip * ft^2$, respectively. The bridge fundamental period by using single-mode spectral method can be calculated through Equation 3.5. If the bridge fundamental period based on single-mode spectral method is larger than the first period which has accumulated mass participating ratio larger than 0.7, the period based on the single-mode spectral method would be selected to be the fundamental period in the corresponding direction.

$$\alpha = \int V_s(x)dx \qquad \text{Equation 3.3}$$

$$\gamma = \int w(x)V_s^2(x)dx \qquad \text{Equation 3.4}$$

$$T_m = 2\pi\sqrt{\frac{\gamma}{p_0 g \alpha}} \qquad \text{Equation 3.5}$$

Where

p_0= Uniform loading p_0 which arbitrarily set equal to 1.0 (kip/ft)

$V_s(x)$= Deformation corresponding to uniform loading p_0(ft)

$w(x)$= Nominal unfactored dead load along the bridge length (kip/ft)

g= Acceleration of gravity (32.2ft/sec^2)

3.4 Parametric Study of Bridge Fundamental Period

The goal of this chapter is to approximate the fundamental period of vibration for standard highway bridges based on a number of characteristics without dynamic analysis methods or complete bridge models. Only prestressed concrete bridges were included in the parametric study in this project since the variability of steel plate girder. The steel plate girders were needed to be designed based on the load condition while the prestressed concrete girders can be directly related with span length. Therefore, the steel bridges would not be included in the parametric study. The primary variables investigated in this study will be the span length, pier height, pier diameter, number of piers, anchor bolt diameter, foundation translational stiffness parallel to bridge, foundation translational stiffness perpendicular to bridge, foundation rotational stiffness parallel to bridge and foundation rotational stiffness perpendicular to bridge. Three hundred seventy-five bridge models were built in CSIBRIDGE with different combinations of all these variables. The fundamental periods of vibration of the bridge in the longitudinal and transverse directions based on the methods and analysis discussed in section 3.3 were recorded for the parametric study. A regression analysis based on the parametric study database was performed to establish equations to predict the bridge fundamental period according to the bridge geometric properties. The first step in the process is to identify the range of all the variables in the regression analysis that need to be defined. The ranges of all the variables in this project were recommended by Alabama Department of Transportation based on the exist bridges in the state of Alabama.

3.4.1 Range of Variables in the Regression Analysis

All the span lengths in this study were between 35 ft and 140 ft. Based on Table 3.3, the properties of the bridge girder and bearing pad were directly related with the bridge span length. In addition, all the bridges were balanced in this study since this project was focusing on the standard highway bridge. Figure 3-14 shows the different span length combinations of the bridges in this study. The spans with same letter in a given configuration have the same span length.

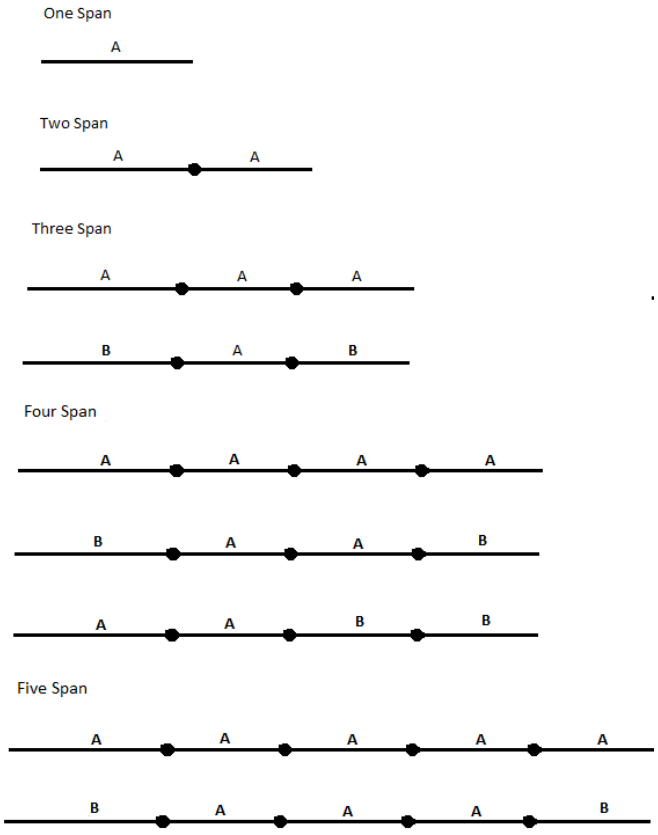

Figure 3-14 Different Balanced Span Length Combinations of Bridges

There are five variables belonging to the category of span length which are shown below.

Span_1= Span length of first span of bridge from left end (ft)

Span_2= Span length of second span of bridge from left end (ft)

Span_3= Span length of third span of bridge from left end (ft)

Span_4= Span length of fourth span of bridge from left end (ft)

Span_5= Span length of fifth span of bridge from left end (ft)

The effect of bridge piers on the fundamental period of highway bridges is significant. Therefore, three geometric properties were included in this parametric study, including pier height, pier diameter and number of piers. All the piers in this study are circular bridge piers with the range of pier heights between 5 ft and 55 ft. There are four variables belonging to the category of pier height as shown below. All the piers under the same cap beam have the same height.

Pierheight_1= Height of piers between first span and second span from left end (ft)

Pierheight_2= Height of piers between second span and third span from left end (ft)

Pierheight_3= Height of piers between third span and fourth span from left end (ft)

Pierheight_4= Height of piers between fourth span and fifth span from left end (ft)

There are four pier diameters included in this parametric study as shown in Table 3-5. “Pier diameter label” will be used in this study.

Table 3-5 Detail of Pier Diameter

Pier diameter label	Pier diameter(ft)
1	4
2	4.5
3	5
4	5.5

There are four variables belong to the category of pier diameter corresponding to the pier height which are shown below. All the piers under the same cap beam would have the same diameter.

Pierdia_1= Diameter of piers between first span and second span from left end (ft)

Pierdia_2= Diameter of piers between second span and third span from left end (ft)

Pierdia_3= Diameter of piers between third span and fourth span from left end (ft)

Pierdia_4= Diameter of piers between fourth span and fifth span from left end (ft)

Two different conditions of the number of piers under one cap beam were considered in this study as shown in Table 3-6. Either two or three piers would be modelled under the same cap beam. “Pier number label” will be used in this study.

Table 3-6 Detail of Pier Number

Pier number label	Number of Columns
1	2
2	3

There is only one variable belonging to the category of pier number which is shown in Table 3.6.

Pier_num= Number of piers under the same cap beam

Anchor bolt diameter was also considered in this study. There are four bolt diameters included in this parametric study as shown in Table 3-7. “Bolt label” will be used in this study.

Table 3-7 Detail of Anchor Bolt

Bolt label	Bolt diameter(in)
1	1
2	1.25
3	1.5
4	1.75

There is only one variable belonging to the category of bolt diameter which is shown in Table 3-7. All the anchor bolts in the same bridge model would have the same diameter.

Bolt= Diameter of anchor bolt for the bridge model (in)

The effect of the foundation and the corresponding soil condition on the fundamental period of vibration of the highway bridge is significant. Therefore, foundation springs in four degrees of freedom were included in this parametric study, including the foundation translational stiffness parallel to the bridge, the foundation translational stiffness perpendicular to the bridge, foundation rotational stiffness parallel to the bridge and foundation rotational stiffness perpendicular to the bridge. The range of the stiffness of the foundation springs for this parametric study were selected accord to Kane (2013). Static pushover analysis of the foundation system for five bridges in Alabama had been done to capture the stiffness of foundation systems which represent the stiffness of foundation springs in CSIBRIDGE. Figure 3-15 shows the location and the site condition of those five bridges. The red dots represent the bridges with drilled shaft foundations while the red H represents the bridges with driven H-pile foundations. Table 3-8 shows the results of the static pushover analysis from Kane's report.

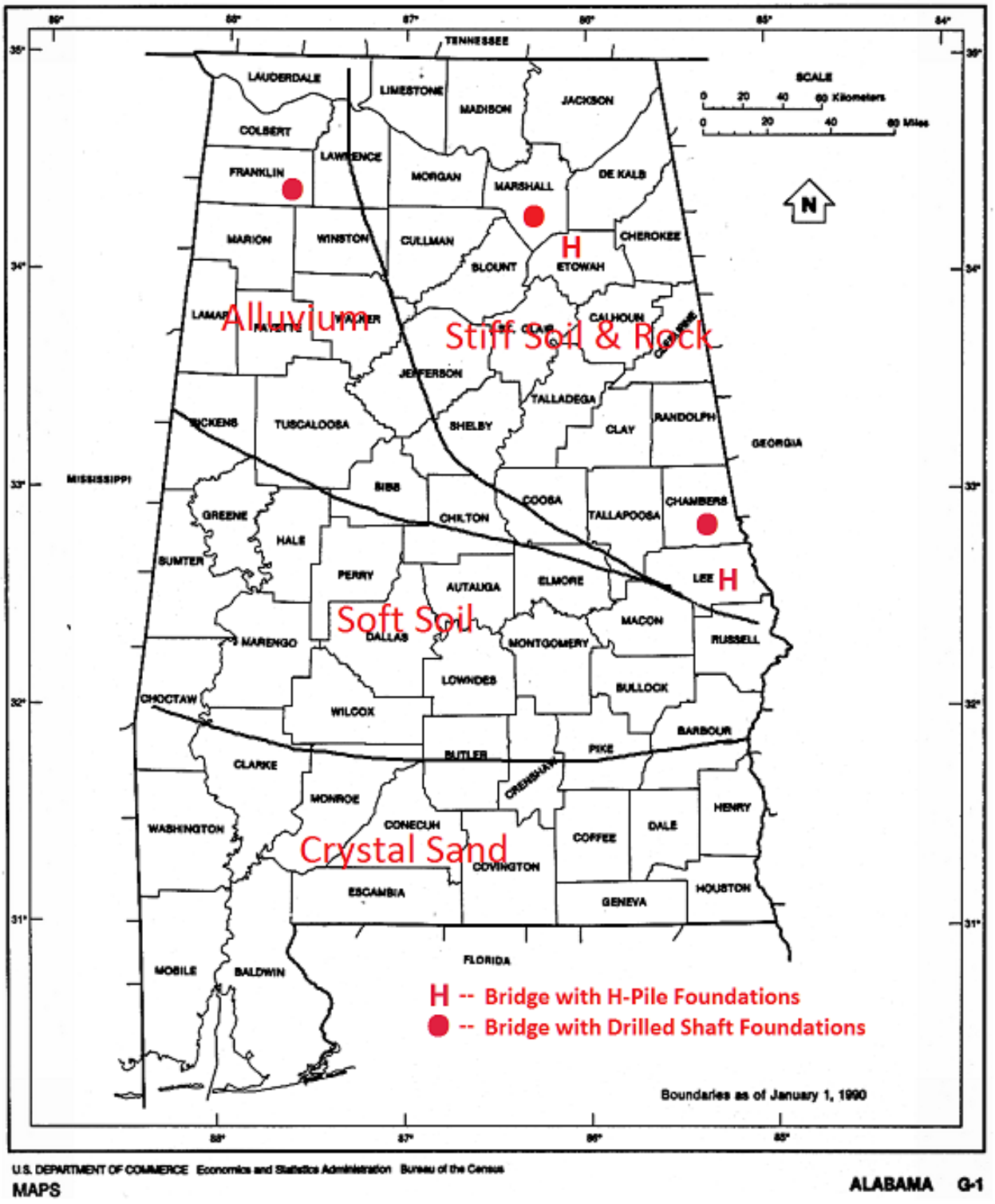

Figure 3-15 Map of Alabama Counties with Bridge Location and Soil Condition (Kane, 2013)

Table 3-8 Stiffness of Foundation System for five Bridges

Bridge Location	U2(kip/ft)	U3(kip/ft)	R2(kip-ft/rad)	R3(kip-ft/rad)
Lee County	15,241	9,708	335,075	472,973
Franklin County	2,173	2,173	1,362,683	1,362,683
Chambers County	8,234	6,263	263,627	516,528
Etowah County	66,168	66,168	7,500	7,500
Marshall County	36,240	36,240	2,676,158	2,676,158

A wide range of stiffness of the foundation system was created to represent most situations of standard highway bridges in Alabama. The range of foundation translation stiffness is between 1,000 kip/ft and 100,000 kip/ft while the range of foundation rotational stiffness is between 5,000 kip-ft/rad and 3,500,000 kip-ft/rad in this study. There are four variables belong to the category of foundation spring which are shown below.

Soil_U2= Foundation translational stiffness parallel to bridge (kip/ft)

Soil_U3= Foundation translation stiffness perpendicular to bridge (kip/ft)

Soil_R2= Foundation rotational stiffness parallel to bridge (kip-ft/rad)

Soil_R3= Foundation rotational stiffness perpendicular to bridge (kip-ft/rad)

Based on Figure 3.15, the bridge in Marshall County is a highway bridge with a drilled shaft foundation system in the stiff soil zone of Alabama. Figure 3-16 shows the cross section of the drilled shaft of this bridge.

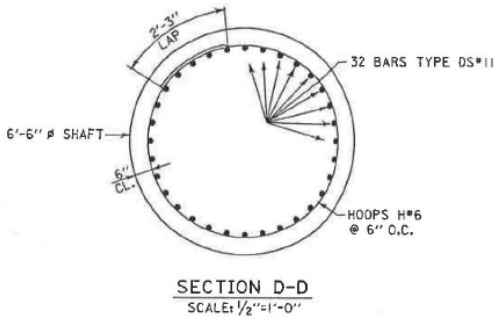

Figure 3-16 Cross Section of Drill Shaft of Highway Bridge in Marshall County

Based on Figure 3-16, the diameter of drill shaft of the highway bridge in the Marshall county is 6.5 ft which is the upper limitation for the standard highway bridge in Alabama. In addition, Marshall county is located within the stiff soil & rock zone of Alabama. Therefore, it is reasonable to assume that the foundation rotational stiffness perpendicular to bridge of this bridge which is 2,676,158 kip-ft/rad is close to the upper boundary for the standard highway bridge on the standard site. In this study, 3,500,000 kip-ft/rad was chosen to be upper boundary of the bridge foundation system which will be used in the regression analysis later.

3.4.2 Results of Regression Analysis

After defining the range of variables in the parametric study, regression analyses were performed for the one-span, two-span, three-span, four-span and five-span bridges based on the parametric study database. Table 3-9 shows the period where the design spectrum transitions from constant acceleration to constant velocity (Ts) in the design response spectrum for the corresponding county in Alabama. The minimum transition period among these counties is equal to 0.401s. It means that if the period of vibration is smaller than 0.401s, the maximum design spectral acceleration needs to be used. Therefore, if the period calculated by regression model in this study is less than 0.4s, it will automatically be considered as 0.4s.

Table 3-9 Transition Period (Ts) for Alabama Counties

Lauderdale	0.484	Bibb	0.505
Limestone	0.521	Shelby	0.485
Madison	0.498	Talladega	0.491
Jackson	0.438	Clay	0.521
Colbert	0.499	Randolph	0.530
Lawrence	0.521	Sumter	0.560
Morgan	0.508	Greene	0.540
Marshall	0.475	Hale	0.542
DeKalb	0.402	Perry	0.564
Franklin	0.513	Chilton	0.538
Marion	0.513	Coosa	0.543

Winston	0.502	Tallapoosa	0.558
Cullman	0.487	Chambers	0.583
Blount	0.477	Lee	0.627
Etowah	0.463	Elmore	0.598
Cherokee	0.413	Autauga	0.599
Lamar	0.519	Dallas	0.599
Fayette	0.492	Marengo	0.590
Walker	0.472	Choctaw	0.588
Jefferson	0.466	Wilcox	0.629
St. Clair	0.474	Lowndes	0.634
Calhoun	0.470	Montgomery	0.633
Cleburne	0.481	Macon	0.644
Pickens	0.520	Russell	0.662
Tuscaloosa	0.482	Min	0.401

Table 3-10 shows the results of parametric study for one span bridges. There is only one simple span supported by two abutments which were assumed to be fixed on the ground. Therefore, the parameters related with piers and soil were not included in the Table 3-10. Two algebraic expressions based on the parametric study dataset were developed for estimating the fundamental period in the longitudinal and transverse directions for one-span bridges, respectively. Figures 3-17 and 3-18 indicate that the predicted values of the fundamental period which are larger than 0.4s are within 10% of the calculated fundamental period for both the longitudinal and transverse directions.

Table 3-10 Parametric Study Results for One-Span Bridges

Observation	span_1 (ft)	Bolt	Longitudinal Period (sec)	Transverse Period (sec)
1	35	3	0.3778	0.1109
2	50	2	0.4427	0.1666
3	60	1	0.4850	0.2088
4	70	2	0.5093	0.2222
5	80	3	0.5446	0.2187
6	90	1	0.7080	0.3258
7	100	2	0.7463	0.3117
8	120	2	0.8335	0.3802
9	130	4	0.8838	0.3971
10	140	2	0.9172	0.4350

For the longitudinal direction of one-span bridges:

$$T_{Long1} = 0.161 + 0.00553 * Span\_1 \quad \text{Equation 3.6}$$

For the transverse direction of one-span bridges:

$$T_{Trans1} = 0.0132 + 0.00302 * Span\_1 \quad \text{Equation 3.7}$$

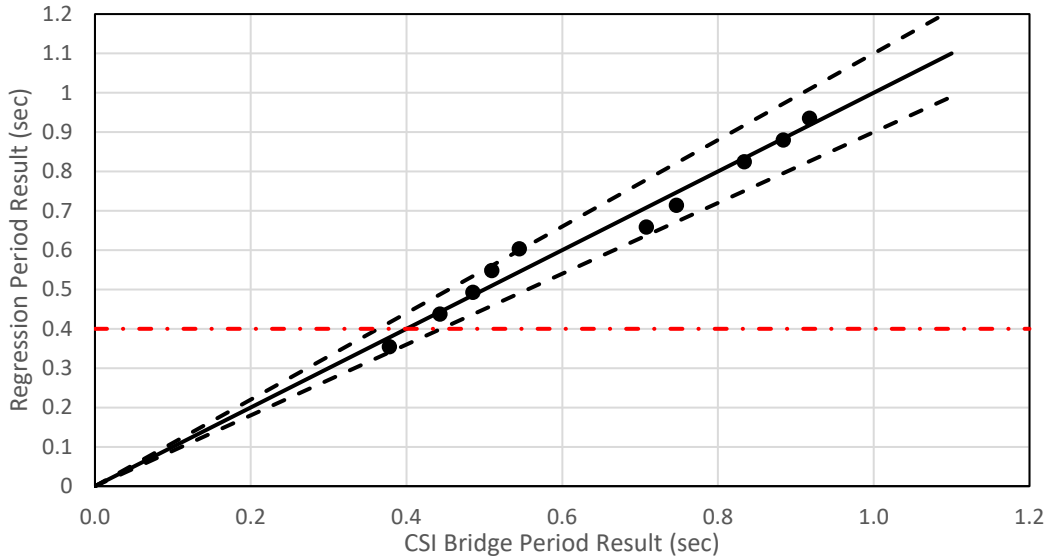

Figure 3-17 Calculated against Predicated Longitudinal Fundamental Period for One-Span Bridges

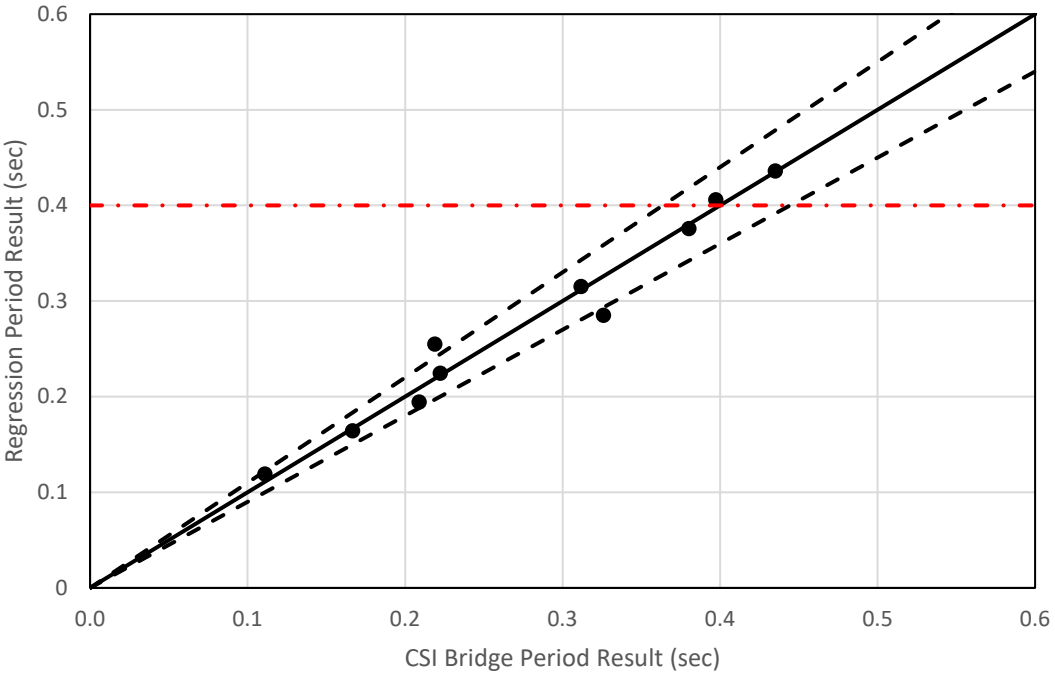

Figure 3-18 Calculated against Predicated Transverse Fundamental Period for One-Span Bridges

Table 3-11 shows the results of the parametric study for two-span bridges. Two algebraic expressions based on the parametric study dataset were developed for estimating the fundamental period in longitudinal and transverse direction for two-span bridges, respectively. Two simplified equations were also proposed by using the upper boundary of foundation rotational stiffness which is equal to 3,500,000kip-ft/rad to replace the “Soil_R2” and “Soil_R3” term in the regression model. Black dots in Figures 3-19 and 3-20 indicate that most of the predicted values of fundamental period which are larger than 0.4 s are within 10% of the calculated fundamental period for both the longitudinal and transverse directions. Grey dots which represent simplified regression model in Figures 3-19 and 3-20 indicate that the predicted values of the fundamental period are smaller than the calculated fundamental period which is conservative.

Table 3-11 Parametric Study Results for Two-Span Bridges

Observation	span_1 (ft)	span_2 (ft)	pierheight_1 (ft)	Soil_U2 (Kip/ft)	Soil_U3 (kip/ft)	Soil_R2 (kip-ft/rad)	Soil_R3 (kip-ft/rad)	Bolt	Pier_num	Pierdia_1	longitudinal Period (sec)	Transverse Period (sec)
11	35	35	38	94,389	21,851	2,321,005	1,214,246	2	1	3	0.5579	0.3915
12	35	35	17	96,644	22,084	2,132,760	2,722,171	2	2	2	0.4062	0.1488
13	35	35	10	48,746	57,037	2,694,241	3,121,063	3	2	2	0.3863	0.1205
14	35	35	12	41,380	27,613	3,253,109	2,045,885	3	1	2	0.3958	0.1428
15	40	40	28	21,600	65,377	660,995	2,819,507	4	2	2	0.5424	0.2489
16	40	40	36	94,202	1,420	3,137,139	737,434	1	1	3	0.6079	0.4064
17	40	40	8	27,361	57,933	3,475,434	2,866,599	2	1	2	0.4123	0.1530
18	50	50	18	87,991	22,059	3,117,580	2,834,130	4	2	3	0.4700	0.1607
19	50	50	45	90,800	3,720	1,746,971	2,416,310	2	1	3	0.6884	0.3379
20	55	55	9	46,336	94,516	3,259,742	2,516,307	3	2	4	0.4706	0.1613
21	55	55	54	18,380	21,660	3,174,402	1,042,370	3	2	1	0.7500	0.4937
22	70	70	37	42,340	49,653	2,392,542	2,564,847	3	2	2	0.6738	0.4132
23	70	70	47	58,732	75,013	2,361,144	1,968,770	1	2	2	0.7349	0.4026
24	75	75	19	4,617	64,521	2,661,664	25,262	2	2	3	0.5680	0.3620
25	75	75	54	61,617	2,353	2,221,075	2,565,814	4	2	2	0.7962	0.4428
26	80	80	20	92,816	59,270	3,307,857	582,016	2	2	2	0.5985	0.2864
27	80	80	49	81,488	86,532	3,296,844	1,855,876	4	1	2	0.7985	0.4959
28	90	90	47	22,027	99,965	34,533	1,489,313	4	2	3	1.1413	0.4113
29	90	90	32	45,361	76,948	1,254,285	2,297,130	4	2	4	0.8321	0.3463
30	110	110	18	56,787	52,041	37,801	1,916,707	3	1	4	1.1408	0.3560
31	110	110	34	41,874	88,109	2,190,462	1,472,100	3	1	3	0.9751	0.5286
32	115	115	26	87,187	19,757	2,723,880	546,942	3	2	3	0.8998	0.4186
33	115	115	35	63,043	76,074	2,399,929	355,534	3	2	3	0.9601	0.5608
34	120	120	10	16,776	2,499	3,051,399	610,602	2	1	4	0.9058	0.3955
35	120	120	22	95,257	36,500	1,140,596	2,753,836	1	1	1	0.9913	0.4729
36	130	130	19	6,375	85,538	1,561,108	1,386,370	2	2	4	0.9375	0.4799

37	130	130	8	92,621	92,083	1,646,251	3,343,147	2	2	2	0.9001	0.4179
38	140	140	9	62,728	61,792	2,451,047	595,750	2	1	2	0.9423	0.4295
39	140	140	48	4,869	61,304	3,252,342	2,241,692	3	1	1	1.2719	0.8252
40	140	140	21	67,923	24,837	3,422,128	2,562,959	3	1	1	1.0472	0.4857

For the longitudinal direction of two-span bridges:

$$T_{Long2} = 0.390 + 0.00561 * Span\_1 + 0.00571 * Pierheight\_1 - 5.78 * 10^{-8} * Soil\_R2 - 0.0730 * Pier\_num \quad \text{Equation 3.8}$$

For the transverse direction of two-span bridges:

$$T_{Trans2} = 0.0607 + 0.00289 * Span\_1 + 0.00616 * Pierheight\_1 - 1.38 * 10^{-8} * Soil\_R3 - 0.0429 * Pier\_num \quad \text{Equation 3.9}$$

The simplified equation for the longitudinal direction of two-span bridges:

$$T_{Long2} = 0.188 + 0.00561 * Span\_1 + 0.00571 * Pierheight\_1 - 0.0730 * Pier\_num \quad \text{Equation 3.10}$$

The simplified equation for the transverse direction of two-span bridges:

$$T_{Trans2} = 0.0125 + 0.00289 * Span\_1 + 0.00616 * Pierheight\_1 - 0.0429 * Pier\_num \quad \text{Equation 3.11}$$

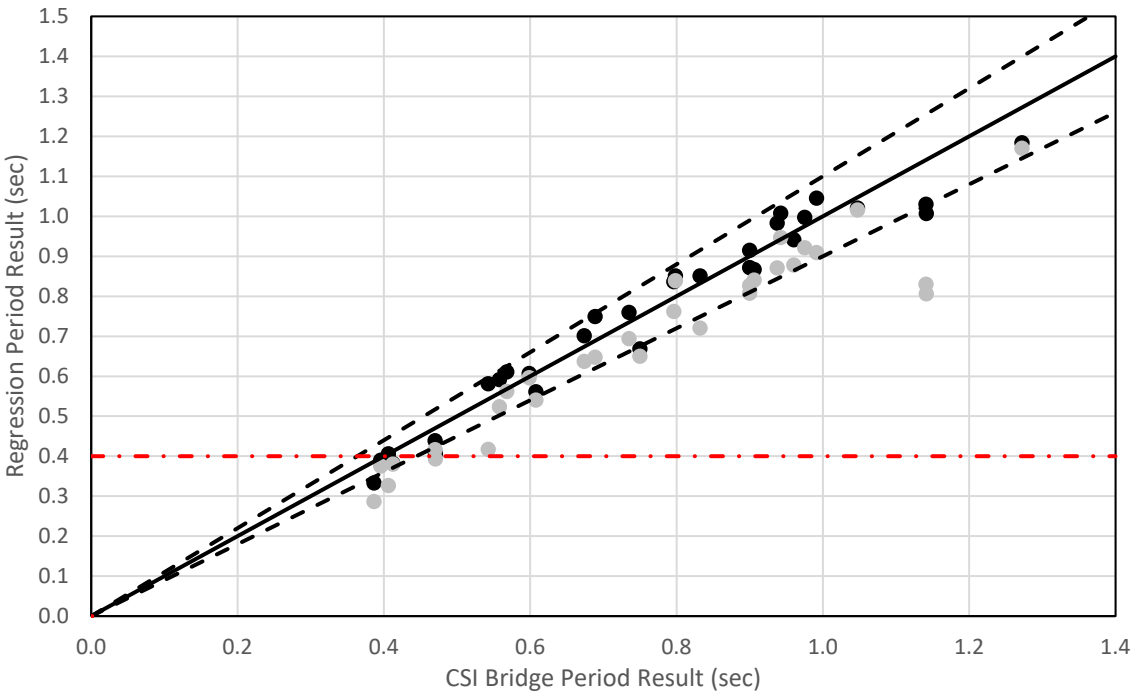

Figure 3-19 Calculated against Predicated Longitudinal Fundamental Period for Two-Span Bridges

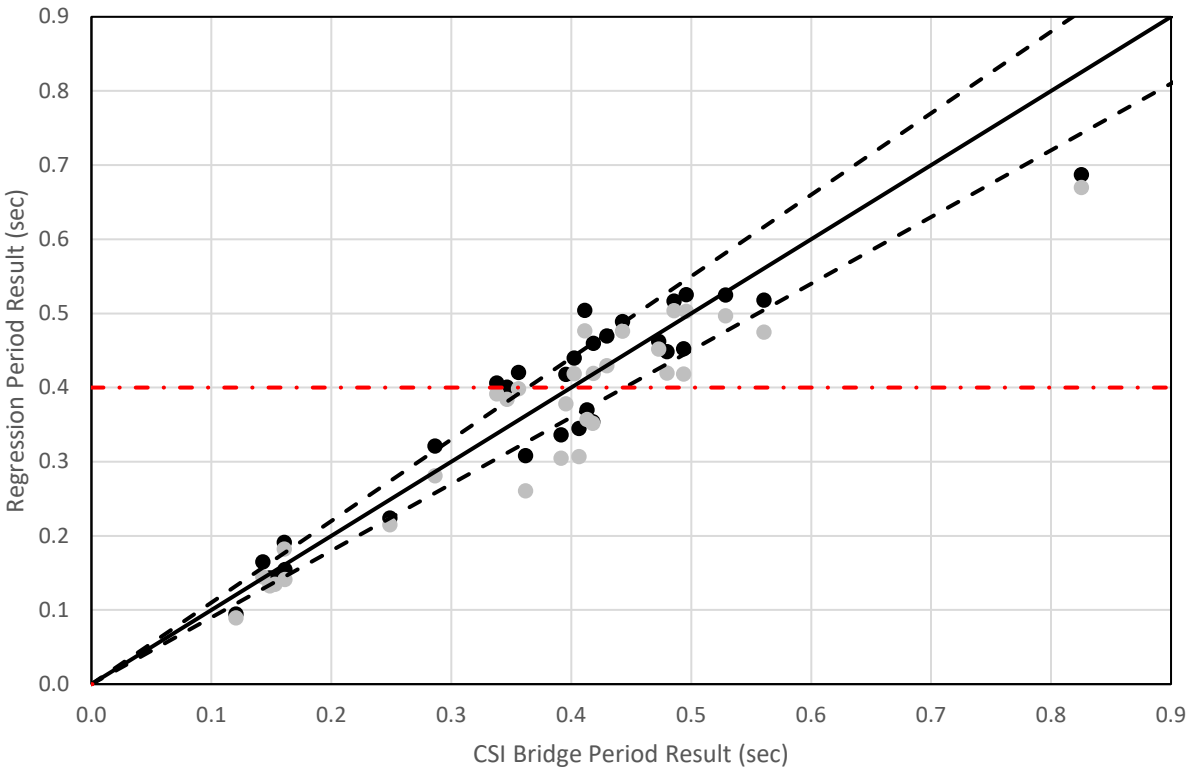

Figure 3-20 Calculated against Predicated Transverse Fundamental Period for Two-Span Bridges

Table 3-12 shows the results of the parametric study for three-span bridges. Two algebraic expressions based on the parametric study dataset were developed for estimating the fundamental period in the longitudinal and transverse direction for three-span bridges. Two simplified equations were also proposed by using the upper boundary of the foundation rotational stiffness which is equal to 3,500,000kip-ft/rad to replace the "Soil_R2" and "Soil_R3" terms in the regression model. Black dots in Figures 3-21 and 3-22 indicate that most of the predicted values of fundamental period which are larger than 0.4 s are within 10% of the calculated fundamental periods for both the longitudinal and transverse direction. Grey dots which represents simplified regression model in Figures 3-21 and 3-22 indicate that the predicted values of fundamental period are smaller than the calculated fundamental period which is conservative.

Table 3-12 Parametric Study Results for Three-Span Bridges

Observation	span_1 (ft)	span_2 (ft)	span_3 (ft)	pierheight_1 (ft)	pierheight_2 (ft)	Soil_U2 (kip/ft)	Soil_U3 (kip/ft)	Soil_R2 (kip-ft/rad)	Soil_R3 (kip-ft/rad)	Bolt	Pier_num	Pierdia_1	Pierdia_2	longitudinal Period (sec)	Transverse Period (sec)
41	35	35	35	6	26	18,309	4,117	2,683,012	647,582	2	2	3	2	0.4704	0.2491
42	35	35	35	5	50	22,032	76,328	1,677,220	1,079,333	1	1	3	4	0.6567	0.3201
43	35	35	35	7	39	64,619	88,092	1,645,299	2,437,091	4	1	3	3	0.5822	0.2993
44	40	40	40	10	46	93,526	71,554	2,965,413	2,418,229	2	2	3	3	0.6065	0.2668
45	40	40	40	18	39	53,005	10,356	2,147,896	1,119,676	2	2	2	4	0.5591	0.3149
46	40	40	40	35	53	50,768	43,169	98,821	3,011,857	1	2	2	3	1.1002	0.3334
47	50	50	50	28	19	16,334	43,454	3,143,185	2,841,292	2	1	2	1	0.5968	0.3084
48	50	50	50	31	23	59,983	28,061	388,343	2,669,031	4	2	2	2	0.7298	0.2745
49	55	55	55	11	9	2,260	56,662	170,882	748,491	2	1	2	3	0.6235	0.4184
50	55	55	55	40	30	41,403	95,449	156,914	1,071,422	1	1	2	4	1.0307	0.4755
51	60	60	60	14	37	2,019	47,817	3,396,934	2,050,752	2	1	3	3	0.6517	0.4942
52	60	60	60	45	21	9,343	59,747	2,991,658	934,071	1	1	3	1	0.7556	0.4092

53	70	70	70	41	14	81,299	32,995	3,454,422	2,356,680	1	1	1	3	0.7357	0.3768
54	70	70	70	9	50	22,689	50,595	1,163,526	192,857	2	1	3	1	0.7547	0.5347
55	85	85	85	22	5	93,632	44,338	3,489,636	1,865,464	3	1	1	1	0.6561	0.2865
56	85	85	85	5	24	50,843	4,609	444,978	1,545,029	1	2	3	2	0.7422	0.3203
57	85	85	85	16	8	28,620	12,485	1,833,430	1,934,552	3	2	1	2	0.6299	0.2543
58	90	90	90	23	52	4,975	86,992	2,221,306	385,578	3	2	2	2	1.0333	0.5069
59	90	90	90	14	32	15,840	94,684	2,534,325	754,537	1	2	3	1	0.8573	0.4584
60	90	90	90	25	34	7,419	87,732	1,155,839	3,382,431	3	1	2	3	1.0039	0.5052
61	100	100	100	42	32	58,419	28,803	1,062,171	3,057,852	3	1	4	3	1.1470	0.4403
62	105	105	105	44	21	53,704	35,215	3,136,369	1,191,130	2	1	3	1	1.0940	0.5119
63	110	110	110	15	21	49,997	28,647	3,399,977	2,531,611	4	1	3	2	0.9057	0.3752
64	110	110	110	44	31	56,488	11,637	1,464,712	2,463,079	1	2	3	3	1.1241	0.4766
65	120	120	120	40	41	36,602	41,840	1,304,647	2,863,731	1	1	2	1	1.4049	0.7097
66	120	120	120	46	37	17,536	14,299	1,312,120	2,737,674	3	2	4	2	1.2383	0.5065
67	130	130	130	48	42	20,135	67,476	1,417,597	2,214,796	3	1	3	3	1.4386	0.6134
68	130	130	130	42	11	49,842	34,160	570,737	1,716,860	2	1	4	4	1.2478	0.4552
69	130	130	130	32	54	76,775	94,059	386,756	1,509,356	3	2	1	2	1.5355	0.6378
70	135	135	135	10	9	35,554	46,740	3,401,053	2,845,588	2	1	3	1	0.9397	0.4384
71	135	135	135	50	19	52,149	30,745	1,951,818	2,913,337	4	2	3	4	1.1061	0.4584
72	140	140	140	40	35	68,443	49,371	3,194,472	2,222,452	2	1	3	1	1.3777	0.7673
73	140	140	140	29	51	80,619	76,386	196,412	2,025,493	2	1	3	1	1.7127	0.6426
74	140	140	140	38	23	74,728	74,027	3,459,901	535,408	1	2	3	1	1.1542	0.5921
75	140	140	140	10	28	30,954	34,718	1,417,109	320,657	2	1	2	2	1.1290	0.5631
76	50	35	50	55	16	63,627	40,802	2,040,314	1,654,743	2	1	1	3	0.7479	0.5149
77	60	35	60	22	9	71,654	84,919	2,861,380	1,531,881	3	1	2	2	0.5340	0.2289
78	70	35	70	44	51	8,136	19,947	1,207,412	3,099,441	2	1	3	1	0.8922	0.4510
79	35	40	35	28	26	61,905	91,667	62,358	2,840,476	2	2	3	3	0.9603	0.1993
80	50	40	50	48	49	36,857	26,551	2,660,692	3,039,708	3	2	2	2	0.8159	0.3426
81	90	40	90	36	47	34,530	64,904	2,317,609	3,134,288	2	2	3	4	0.8624	0.3441
82	40	45	40	13	50	89,777	17,363	3,490,995	2,160,527	2	1	3	3	0.6934	0.3230

83	80	45	80	32	37	4,277	83,736	187,713	2,013,197	1	1	4	2	0.9796	0.4850
84	100	45	100	45	29	50,901	65,348	1,491,901	2,407,881	3	2	3	2	0.9200	0.4195
85	40	50	40	32	7	27,295	72,794	2,051,500	2,123,979	3	2	3	3	0.5318	0.2607
86	70	50	70	20	16	66,037	61,291	2,048,093	2,679,746	3	2	3	1	0.5519	0.2176
87	110	50	110	51	47	4,430	19,459	3,098,163	386,012	2	1	1	1	1.2154	0.7847
88	40	55	40	23	8	17,099	54,636	620,540	2,505,942	1	1	2	2	0.5689	0.2773
89	80	55	80	6	25	62,355	86,747	1,997,135	1,353,841	4	2	2	3	0.5974	0.2457
90	50	60	50	30	21	27,029	5,625	3,082,756	3,411,255	4	2	3	4	0.5855	0.2607
91	80	60	80	52	40	97,826	31,508	540,168	175,003	2	2	3	2	0.9820	0.5547
92	120	60	120	29	27	41,614	66,424	3,141,222	897,728	1	2	3	2	0.9058	0.4551
93	50	65	50	25	41	53,871	29,030	1,921,803	1,442,136	3	1	4	4	0.7269	0.3209
94	120	65	120	7	16	4,508	97,584	2,914,762	2,427,961	4	2	2	1	0.7954	0.3752
95	50	70	50	44	27	8,876	25,578	2,694,193	815,488	2	2	1	2	0.7945	0.4156
96	90	75	90	17	41	35,704	55,733	2,744,615	207,851	2	1	1	4	0.8617	0.3837
97	110	75	110	36	36	31,030	58,035	2,278,343	1,436,201	3	1	2	1	1.1062	0.5596
98	130	75	130	10	12	9,922	61,480	255,267	3,352,886	4	2	2	4	0.9470	0.3764
99	40	80	40	33	39	6,296	25,522	1,741,205	2,315,278	2	2	3	1	0.8311	0.5027
100	60	80	60	38	14	55,927	31,858	529,685	278,437	3	2	1	2	0.8124	0.5083
101	120	80	120	41	18	98,398	72,385	2,647,287	1,146,533	4	1	4	4	0.9273	0.3697
102	130	80	130	14	46	69,996	29,630	2,006,045	37,437	4	2	3	2	0.9007	0.4600
103	50	85	50	33	24	82,697	81,402	3,337,376	2,675,073	4	2	3	2	0.6944	0.3174
104	90	85	90	44	47	56,308	30,850	3,227,719	448,129	3	1	3	1	1.1507	0.5436
105	100	85	100	12	36	7,686	94,265	515,797	1,394,698	2	1	2	2	0.9824	0.4772
106	130	85	130	42	40	71,215	20,053	3,083,331	673,278	4	1	2	3	1.1916	0.5636
107	45	90	45	30	6	44,620	10,209	1,741,467	1,116,396	1	1	1	4	0.8416	0.4268
108	60	90	60	39	30	3,780	29,527	652,308	2,616,953	4	1	3	3	1.0484	0.5881
109	120	90	120	42	49	89,531	18,347	748,510	1,341,716	3	2	4	3	1.2561	0.4312
110	50	100	50	51	52	26,366	28,257	168,824	1,322,910	1	2	4	3	1.3917	0.4711
111	80	100	80	10	47	43,417	12,711	1,182,402	402,579	3	1	1	2	0.9097	0.4625
112	120	100	120	44	20	5,865	28,238	542,418	2,811,310	2	2	3	3	1.1546	0.4553

113	140	100	140	34	30	93,506	24,974	1,241,125	2,833,730	3	1	2	3	1.2082	0.4919
114	40	105	40	49	8	32,541	66,063	2,233,115	1,962,627	2	1	3	2	0.9628	0.4433
115	70	105	70	24	10	45,425	95,719	292,695	3,149,729	2	2	2	1	0.8826	0.3296
116	90	105	90	47	40	63,562	77,203	2,327,377	2,734,889	2	2	2	3	1.1404	0.5063
117	110	105	110	36	10	27,111	29,195	1,244,463	13,382	2	2	2	2	0.9273	0.5960
118	40	110	40	53	38	22,878	58,928	1,131,956	2,280,121	2	2	3	3	1.1425	0.4897
119	50	110	50	50	46	19,461	36,237	2,931,148	3,075,985	3	1	3	3	1.1702	0.5163
120	90	110	90	10	50	83,586	75,778	1,687,449	2,748,705	3	2	2	3	0.9783	0.3863
121	120	110	120	26	13	60,548	54,506	2,518,074	1,983,540	3	1	2	3	0.8896	0.3862
122	130	110	130	12	50	93,858	61,106	3,252,742	1,947,926	2	2	3	3	0.9816	0.4414
123	40	115	40	7	7	41,961	90,414	345,154	3,304,241	3	2	3	4	0.8331	0.3058
124	60	115	60	51	14	73,109	46,556	1,314,909	1,021,528	4	1	3	3	1.0250	0.4532
125	70	115	70	25	19	8,224	51,192	2,849,588	1,291,316	2	2	1	4	0.8687	0.4199
126	90	115	90	22	37	8,860	21,369	1,750,270	1,949,606	1	2	2	2	0.9920	0.5087
127	120	115	120	27	11	75,408	20,886	1,073,469	2,888,350	4	2	2	4	0.9147	0.3560
128	140	115	140	11	24	93,711	42,230	912,604	2,525,301	1	1	3	2	1.0761	0.4756
129	40	120	40	26	7	7,829	45,303	1,244,753	3,479,304	2	1	2	3	0.9221	0.4625
130	60	120	60	15	10	4,076	63,476	143,249	1,236,271	2	2	4	2	0.9702	0.4381
131	80	120	80	39	30	19,755	33,336	3,012,383	2,871,549	2	1	3	3	1.0124	0.5127
132	100	120	100	28	16	54,047	95,853	1,286,182	877,318	3	2	1	4	0.9325	0.3744
133	110	120	110	23	27	87,394	69,601	1,781,307	2,782,607	3	1	1	4	1.0511	0.4443
134	130	120	130	26	24	88,412	84,128	3,134,284	327,462	4	2	4	3	0.9673	0.4491
135	60	125	60	47	42	12,736	18,637	1,816,048	3,202,908	3	1	3	3	1.2295	0.5296
136	100	125	100	27	45	49,946	7,151	1,368,580	332,888	2	1	2	2	1.2667	0.6569
137	140	125	140	40	14	69,536	84,450	2,619,561	2,950,690	2	1	3	1	1.1530	0.5206
138	70	130	70	35	48	1,500	5,210	168,277	116,412	3	2	2	1	1.5195	0.9103
139	90	130	90	53	5	89,304	25,429	105,740	360,363	4	2	4	1	1.3192	0.4396
140	105	130	105	11	42	50,338	75,363	1,113,977	2,044,736	3	1	3	1	1.0376	0.4845
141	115	130	115	32	54	39,889	95,419	1,072,219	1,961,662	4	1	4	3	1.3694	0.5397
142	120	130	120	25	45	95,898	43,834	849,215	881,734	3	1	2	4	1.3153	0.5444

143	135	130	135	10	30	73,987	24,375	3,485,354	2,644,669	2	1	3	4	0.9180	0.4339
144	140	130	140	44	20	88,255	41,482	2,896,133	1,195,879	4	1	3	3	1.2045	0.4719
145	60	140	60	43	53	30,083	76,798	2,529,124	842,339	4	2	2	3	1.2732	0.5550
146	80	140	80	19	49	66,526	20,044	2,487,492	2,781,796	4	1	2	2	1.0705	0.4964
147	90	140	90	18	8	13,556	2,645	205,331	2,612,944	3	1	3	3	1.1935	0.3788
148	100	140	100	19	16	29,790	47,833	1,943,340	727,170	3	1	3	3	0.9529	0.4121
149	120	140	120	6	18	15,299	62,831	1,518,634	16,695	2	1	3	3	0.8660	0.4214
150	130	140	130	11	51	93,672	36,554	1,012,240	282,496	3	2	4	2	1.1055	0.5384

For the longitudinal direction of three-span bridges:

$$T_{Long3} = 0.264 + 0.00205 * Span\_1 + 0.00349 * Span\_2 + 0.00703 * Pierheight\_1 + 0.00610 * Pierheight\_2 - 6.72 * 10^{-8} * Soil\_R2 - 0.0420 * Pier\_num$$

Equation 3.12

For the transverse direction of three-span bridges:

$$T_{Trans3} = 0.208 + 0.000590 * Span\_1 + 0.00137 * Span\_2 + 00304 * Pierheight\_1 + 0.00294 * Pierheight\_2 - 2.92 * 10^{-8} * Soil\_R3 - 0.0431 * Pier\_num$$

Equation 3.13

The simplified equation for the longitudinal direction of three-span bridges:

$$T_{Long3} = 0.0288 + 0.00205 * Span\_1 + 0.00349 * Span\_2 + 0.00703 * Pierheight\_1 + 0.00610 * Pierheight\_2 - 0.0420 * Pier\_num$$

Equation 3.14

The simplified equation for the transverse direction of three-span bridges:

$$T_{Trans3} = 0.106 + 0.000590 * Span\_1 + 0.00137 * Span\_2 + 00304 * Pierheight\_1 + 0.00294 * Pierheight\_2 - 0.0431 * Pier\_num$$

Equation 3.15

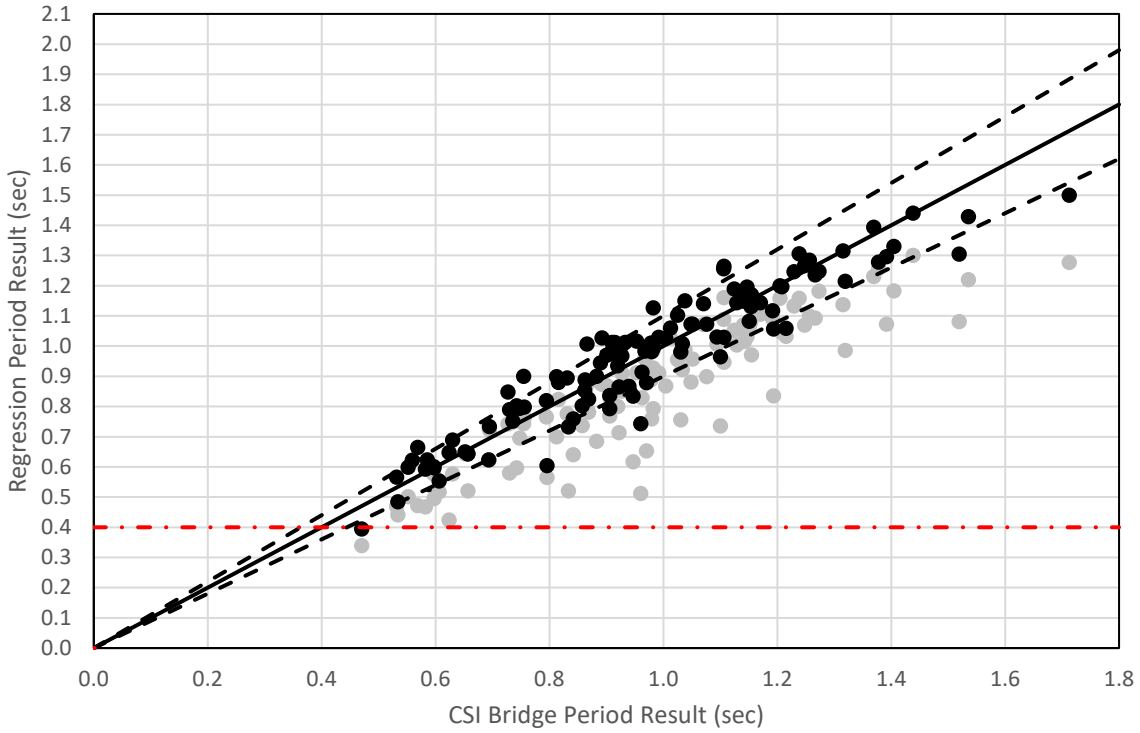

Figure 3-21 Calculated against Predicated Longitudinal Fundamental Period for Three-Span Bridges

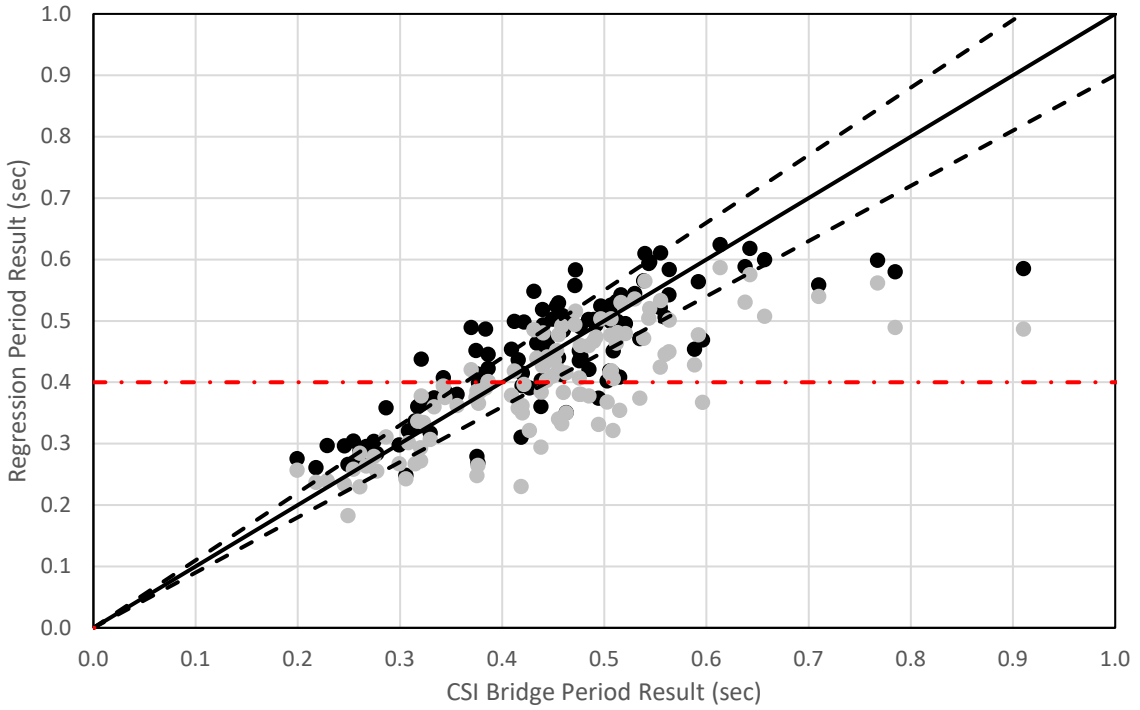

Figure 3-22 Calculated against Predicated Transverse Fundamental Period for Three-Span Bridges

Table 3-13 shows the results of the parametric study for four-span bridges. Two algebraic expressions based on the parametric study dataset were developed for estimating the fundamental period in the longitudinal and transverse directions for four-span bridges. Two simplified equations were also proposed by using the upper boundary of foundation rotational stiffness which is equal to 3,500,000kip-ft/rad to replace the "Soil_R2" and "Soil_R3" term in the regression model. Black dots in Figures 3-23 and 3-24 indicate that most of the predicted values of fundamental period which are larger than 0.4s are within 10% of the calculated fundamental period in both the longitudinal and transverse direction. Grey dots which represent simplified regression model in Figure 3-23 and 3-24 indicate that the predicted values of the fundamental period are smaller than the calculated fundamental period which is conservative.

Table 3-13 Parametric Study Results for Four-Span Bridges

Observation	span_1 (ft)	span_2 (ft)	span_3 (ft)	span_4 (ft)	Pier height_1 (ft)	Pier height_2 (ft)	Pier height_3 (ft)	Soil_U2 (kip/ft)	Soil_U3 (kip/ft)	Soil_R2 (kip-ft/rad)	Soil_R3 (kip-ft/rad)	Bolt	Pier_num	Pier dia_1	Pier dia_2	Pier dia_3	longitudinal Period (sec)	Transverse Period (sec)
151	35	35	35	35	48	28	40	75,775	65,900	1,360,334	2,696,767	2	1	3	3	1	0.7653	0.4157
152	35	35	35	35	53	22	47	48,476	27,721	1,756,273	1,826,636	1	1	2	4	2	0.7385	0.4057
153	50	50	50	50	11	16	5	20,052	8,509	3,385,145	2,316,097	4	2	2	2	3	0.4851	0.1807
154	50	50	50	50	30	32	46	83,668	98,040	1,946,817	392,052	4	1	3	4	4	0.7535	0.3895
155	50	50	50	50	33	18	22	20,923	22,955	924,155	145,896	4	1	1	4	3	0.6997	0.4605
156	60	60	60	60	36	36	18	40,149	53,875	2,585,731	3,256,801	2	1	4	2	3	0.7734	0.3973
157	60	60	60	60	45	45	8	54,836	21,336	1,791,466	3,383,970	2	1	2	2	2	0.9493	0.3847
158	80	80	80	80	9	52	10	59,598	50,520	2,994,966	2,678,543	2	1	4	3	4	0.7636	0.3615
159	80	80	80	80	42	23	24	80,249	81,418	322,499	397,055	2	1	3	1	2	1.1145	0.4547
160	100	100	100	100	41	13	41	74,064	14,197	3,474,353	2,689,321	2	1	1	4	3	1.0140	0.4478
161	100	100	100	100	13	40	18	71,057	22,265	2,891,003	3,492,924	3	2	3	3	4	0.9672	0.4383

162	100	100	100	100	14	26	20	94,528	92,783	542,633	2,820,631	2	1	2	2	2	1.0880	0.3650
163	110	110	110	110	38	22	13	41,351	51,636	1,822,885	1,005,340	2	2	2	3	3	0.9786	0.4861
164	110	110	110	110	24	26	21	31,250	51,110	2,183,742	377,091	3	2	3	2	3	0.9462	0.4271
165	130	130	130	130	30	8	50	71,290	41,376	294,769	1,092,767	4	2	2	2	1	1.1830	0.5115
166	130	130	130	130	32	9	47	49,224	28,970	2,946,663	489,808	2	2	3	2	3	1.0524	0.5547
167	130	130	130	130	34	53	52	20,444	21,029	3,126,610	3,264,745	2	2	3	4	1	1.4734	0.6031
168	140	140	140	140	41	11	44	70,566	48,266	1,817,759	752,277	2	2	1	3	3	1.1320	0.5181
169	50	35	35	50	38	19	14	1,426	99,688	2,712,493	1,578,994	1	2	3	3	3	0.5597	0.4567
170	70	35	35	70	44	38	37	46,808	64,262	1,666,356	1,509,684	3	2	3	3	3	0.7657	0.3655
171	70	35	35	70	41	25	46	98,515	84,347	2,046,376	1,412,243	2	1	1	1	4	0.8246	0.3761
172	90	35	35	90	49	33	42	7,277	50,951	2,158,133	2,134,705	4	1	3	2	1	0.9758	0.4881
173	90	35	35	90	30	26	21	75,982	31,775	3,286,891	2,804,606	3	1	2	3	4	0.7996	0.3415
174	35	40	40	35	22	38	42	86,226	96,463	1,940,248	591,244	3	1	1	4	1	0.7728	0.3994
175	60	40	40	60	21	36	30	79,001	97,882	3,468,352	365,419	3	1	1	1	2	0.7251	0.4352
176	60	40	40	60	48	38	48	17,649	79,152	2,467,632	1,960,348	2	1	2	2	1	0.9208	0.4581
177	100	40	40	100	45	34	7	68,970	9,206	651,005	2,014,373	3	1	4	3	3	0.9832	0.3476
178	40	50	50	40	39	14	9	22,836	2,765	1,131,706	1,129,850	3	2	3	2	1	0.6594	0.3092
179	40	50	50	40	36	52	31	58,365	14,459	3,300,725	1,453,701	2	2	3	2	2	0.8235	0.3955
180	80	50	50	80	31	14	29	77,568	32,102	3,443,943	9,058	2	2	3	3	4	0.6150	0.3763
181	80	50	50	80	39	16	15	96,408	19,501	2,745,233	567,813	3	1	1	3	4	0.7359	0.5529
182	110	50	50	110	50	33	43	21,076	45,224	2,098,767	1,089,558	4	2	1	2	2	1.0499	0.4527
183	50	60	60	50	22	18	51	64,679	16,248	1,328,094	1,254,138	1	1	1	1	4	0.8047	0.3690
184	50	60	60	50	19	28	33	87,053	34,654	2,083,049	1,459,411	1	1	3	3	4	0.6852	0.3484
185	80	60	60	80	12	33	16	37,470	97,812	1,443,675	853,364	2	1	1	3	2	0.6951	0.3220
186	80	60	60	80	13	27	44	44,225	97,333	91,469	2,484,282	3	2	1	2	3	1.1600	0.3024
187	120	60	60	120	48	41	41	8,616	57,095	3,201,753	2,937,471	3	1	3	4	2	1.0883	0.5060
188	120	60	60	120	49	7	25	98,521	53,303	2,715,995	2,448,603	3	2	3	3	2	0.9495	0.3941
189	45	65	65	45	38	38	28	96,639	2,321	452,745	3,029,670	2	2	1	2	3	1.0616	0.4471
190	45	65	65	45	11	13	42	75,160	79,714	2,183,687	587,935	1	1	4	4	4	0.6754	0.3225
191	70	65	65	70	19	34	23	13,948	99,286	2,103,237	2,505,097	3	1	1	1	2	0.8135	0.3979

192	90	65	65	90	18	46	52	23,562	1,602	230,879	2,960,624	3	2	1	1	2	1.7761	0.4190
193	130	65	65	130	47	44	27	57,609	87,932	623,395	2,368,901	4	1	3	2	3	1.3207	0.4481
194	130	65	65	130	7	43	37	56,669	78,990	1,063,693	1,936,920	1	2	2	1	4	0.9843	0.4713
195	35	70	70	35	34	37	53	80,967	99,994	1,425,236	1,475,358	3	1	2	2	2	1.0717	0.5329
196	40	70	70	40	38	35	10	61,186	70,324	1,602,407	1,305,537	3	2	2	3	1	0.7902	0.4051
197	40	70	70	40	20	48	27	17,403	52,461	2,852,071	2,560,455	3	1	2	4	3	0.8307	0.3861
198	90	70	70	90	44	52	51	43,198	8,343	3,072,494	703,355	4	2	3	4	1	1.1100	0.4805
199	90	70	70	90	44	42	44	96,252	56,404	2,780,755	906,794	4	2	4	4	3	0.9289	0.3418
200	40	85	85	40	18	34	22	52,891	21,374	3,398,831	2,995,653	4	1	4	1	4	0.8315	0.4655
201	40	85	85	40	34	15	31	22,992	49,655	2,756,291	971,924	3	1	1	2	2	0.7737	0.4421
202	50	85	85	50	33	55	53	49,556	20,869	1,312,437	1,250,752	2	2	2	3	4	1.1382	0.4703
203	50	85	85	50	27	52	29	22,314	38,737	3,389,506	1,094,095	1	1	4	1	2	1.0259	0.6003
204	90	85	85	90	33	53	25	34,736	84,565	220,664	769,550	1	1	2	2	1	1.5251	0.5454
205	90	85	85	90	6	9	39	26,537	38,530	243,947	2,860,338	3	2	2	2	1	0.8711	0.4130
206	115	85	85	115	48	36	49	96,001	79,653	2,522,585	1,301,797	3	1	3	2	3	1.2197	0.5591
207	115	85	85	115	38	45	10	60,155	2,925	111,704	2,133,850	4	2	4	2	4	1.4824	0.3883
208	120	85	85	120	43	32	25	10,275	43,351	83,314	3,094,398	3	1	2	3	1	1.7454	0.4795
209	120	85	85	120	17	24	15	85,103	1,109	2,313,834	1,550,272	3	2	1	2	2	0.9404	0.3288
210	60	95	95	60	31	12	39	31,254	53,359	2,699,981	1,692,523	4	1	4	2	1	0.9052	0.4849
211	60	95	95	60	49	10	48	35,513	81,422	3,275,505	3,423,569	2	2	3	2	2	0.8755	0.3840
212	90	95	95	90	7	49	25	2,313	5,635	921,269	2,654,006	2	2	2	3	3	1.0342	0.5070
213	90	95	95	90	8	23	53	70,526	28,199	257,047	524,409	1	1	2	4	3	1.3337	0.4827
214	110	95	95	110	9	30	38	85,946	10,345	901,525	1,802,289	1	1	3	2	4	1.0481	0.4693
215	110	95	95	110	36	32	34	6,264	87,873	1,637,332	826,288	4	1	4	3	4	1.1048	0.6216
216	110	95	95	110	54	26	37	9,527	70,184	997,608	328,360	4	1	3	4	3	1.2274	0.6979
217	40	105	105	40	6	22	10	44,843	65,099	2,986,639	2,308,928	4	1	3	1	1	0.8772	0.3640
218	40	105	105	40	21	30	19	71,253	42,413	2,288,139	3,345,196	4	2	3	1	3	0.9876	0.4280
219	90	105	105	90	17	38	41	15,569	57,867	432,342	261,318	4	2	3	2	3	1.3313	0.5574
220	90	105	105	90	16	54	14	74,916	99,354	3,170,278	3,361,334	4	2	1	2	2	1.0053	0.4154
221	90	105	105	90	39	23	25	7,687	19,919	2,591,300	1,479,578	2	1	2	2	3	1.0077	0.5585

222	125	105	105	125	34	27	49	37,382	39,236	1,718,651	2,258,692	1	1	3	1	3	1.2927	0.5881
223	125	105	105	125	55	11	42	35,914	22,564	1,956,209	146,360	2	2	2	3	2	1.0808	0.5409
224	70	115	115	70	16	6	50	67,483	4,371	1,111,910	3,177,411	2	2	4	1	1	0.9552	0.4224
225	70	115	115	70	21	13	10	9,660	56,221	821,413	1,805,789	3	1	3	2	3	0.8749	0.4216
226	100	115	115	100	18	42	23	13,405	23,821	2,829,514	2,198,950	3	2	2	3	3	1.0005	0.4069
227	100	115	115	100	12	35	31	97,588	53,402	3,470,606	95,945	3	1	2	4	4	0.9672	0.5369
228	130	115	115	130	20	22	29	29,389	3,919	2,139,670	1,624,663	1	2	4	1	1	1.0080	0.4840
229	130	115	115	130	21	47	32	65,330	55,172	2,728,891	2,956,968	3	1	3	4	3	1.2173	0.4609
230	80	120	120	80	31	44	15	78,517	62,127	2,566,028	3,021,556	4	2	2	3	3	1.0814	0.4098
231	80	120	120	80	52	32	6	86,800	30,962	714,706	1,364,700	4	2	1	3	3	1.1496	0.4841
232	100	120	120	100	49	26	20	96,106	24,587	1,753,079	3,187,716	3	1	2	3	2	1.1070	0.4607
233	100	120	120	100	33	22	49	92,980	57,400	741,075	651,570	1	2	2	1	3	1.2511	0.5226
234	130	120	120	130	33	42	44	23,344	83,111	2,404,968	3,186,190	4	2	3	1	3	1.3508	0.5163
235	130	120	120	130	7	30	55	29,445	4,493	260,879	2,233,500	3	1	1	2	3	1.6296	0.5159
236	100	125	125	100	20	37	24	15,671	86,614	3,151,344	3,272,323	1	2	4	3	4	0.9992	0.4943
237	100	125	125	100	17	17	27	72,243	17,778	3,262,280	1,860,710	1	1	3	2	2	0.9202	0.4302
238	120	125	125	120	11	23	26	97,529	26,529	186,556	337,155	3	1	3	1	3	1.4856	0.4613
239	140	125	125	140	11	37	38	32,438	86,442	36,120	749,942	3	2	1	3	4	2.0941	0.5173
240	140	125	125	140	31	13	24	4,276	64,320	273,668	487,081	4	1	1	3	3	1.3546	0.6077
241	60	130	130	60	28	34	14	71,906	20,758	371,279	2,886,236	1	2	3	3	2	1.3271	0.5088
242	60	130	130	60	47	43	25	86,575	57,185	2,482,679	502,464	1	1	2	2	3	1.4316	0.7041
243	100	130	130	100	10	32	53	90,810	44,002	1,801,017	2,300,845	3	1	1	4	3	1.1471	0.5008
244	120	130	130	120	43	54	45	24,132	36,015	1,952,735	413,192	4	1	4	3	4	1.5792	0.6179
245	120	130	130	120	27	28	12	12,965	16,123	3,143,901	1,339,663	2	2	2	3	4	0.9620	0.4652
246	90	140	140	90	53	16	20	72,468	99,544	1,822,213	1,765,105	4	1	4	2	3	1.0767	0.4497
247	90	140	140	90	33	38	41	24,213	10,613	1,562,192	1,121,435	2	1	4	4	2	1.4786	0.6755
248	120	140	140	120	6	47	21	82,296	59,063	1,909,918	1,274,910	3	2	2	1	2	1.0952	0.4876
249	120	140	140	120	16	55	45	40,821	27,247	132,191	1,466,806	4	1	1	3	1	2.0881	0.7505
250	130	140	140	130	25	13	17	56,361	4,575	707,866	2,554,137	3	1	1	2	1	1.2310	0.4445
251	35	35	50	50	32	9	37	32,007	86,583	1,747,894	3,333,153	4	2	3	2	3	0.6033	0.2971

252	35	35	50	50	23	39	34	6,970	68,136	1,342,014	764,705	1	2	1	3	4	0.6968	0.4412
253	35	35	60	60	25	51	51	35,468	30,594	3,098,794	886,346	3	1	2	3	2	0.9868	0.4837
254	35	35	60	60	13	39	11	34,457	11,979	974,443	1,778,647	3	1	1	3	2	0.7139	0.3284
255	35	35	80	80	43	54	23	43,732	93,139	3,329,298	545,141	3	1	1	4	1	0.9517	0.4430
256	35	35	80	80	48	11	47	73,358	88,469	3,065,849	2,091,161	3	1	3	2	2	0.8679	0.4296
257	40	40	65	65	15	32	47	37,363	98,762	2,616,282	1,591,274	2	2	4	4	2	0.8133	0.3657
258	40	40	65	65	36	42	36	65,431	4,748	3,077,542	3,417,879	3	1	4	4	4	0.8350	0.3660
259	40	40	90	90	5	45	21	87,857	47,170	227,818	1,526,014	4	2	4	4	1	1.1540	0.3337
260	40	40	90	90	17	30	50	40,198	49,023	1,750,728	1,435,713	3	1	3	1	1	1.1656	0.5740
261	50	50	70	70	30	48	26	33,914	34,200	1,756,273	3,244,574	3	1	3	3	3	0.8840	0.3623
262	50	50	70	70	34	16	53	8,103	59,762	3,338,390	1,718,851	4	1	3	2	2	0.8101	0.4641
263	50	50	70	70	42	20	37	83,615	5,478	1,235,638	3,437,075	1	2	3	1	2	0.8044	0.4048
264	50	50	70	70	10	14	38	9,546	73,401	1,364,486	3,029,251	2	1	3	3	3	0.7626	0.4027
265	50	50	115	115	40	12	13	83,990	12,305	1,713,074	263,857	2	2	1	4	2	0.8472	0.4282
266	50	50	115	115	15	20	23	90,617	71,338	913,013	3,431,012	2	2	3	3	1	0.9520	0.4039
267	60	60	120	120	47	49	25	98,010	85,771	1,831,234	1,850,825	3	2	1	3	2	1.1500	0.4399
268	60	60	120	120	35	41	38	41,235	21,585	860,668	63,996	2	2	3	3	4	1.2068	0.6002
269	60	60	120	120	24	30	47	89,482	29,326	1,478,625	1,163,747	1	2	1	3	3	1.1359	0.5013
270	65	65	115	115	52	31	33	39,452	70,000	894,915	1,277,166	2	1	2	1	4	1.2393	0.5832
271	65	65	115	115	18	51	51	86,361	72,465	949,522	647,109	2	2	2	3	2	1.2618	0.5540
272	65	65	115	115	27	43	55	90,618	25,841	2,291,316	191,738	3	1	1	3	2	1.3084	0.7141
273	65	65	115	115	15	16	50	18,170	70,115	2,063,314	726,314	4	2	3	2	3	0.9893	0.4541
274	75	75	80	80	52	44	7	15,185	57,263	2,688,546	3,324,954	3	1	2	1	2	0.9626	0.4590
275	75	75	80	80	9	33	35	32,794	78,394	1,032,210	790,847	3	2	1	1	4	0.8542	0.4172
276	75	75	115	115	40	31	43	84,286	84,022	2,803,161	1,613,428	3	2	2	1	4	1.0805	0.4681
277	75	75	115	115	33	44	21	16,195	44,402	2,742,012	2,276,923	1	2	3	2	3	0.9895	0.4585
278	80	80	60	60	13	26	22	77,447	94,016	1,204,315	1,859,052	3	2	2	3	3	0.6580	0.2666
279	80	80	60	60	11	35	32	45,458	65,823	244,664	348,680	2	1	3	3	1	1.0504	0.4713
280	80	80	60	60	43	54	23	95,888	82,489	2,553,630	1,912,290	3	2	2	3	3	0.9720	0.3920
281	80	80	60	60	46	34	22	83,022	17,062	1,259,534	2,227,779	4	1	4	3	1	0.9628	0.3729

282	80	80	60	60	12	18	13	57,910	28,935	2,199,979	3,094,154	3	1	2	3	3	0.6158	0.2418
283	80	80	120	120	30	38	50	81,734	62,986	3,299,053	521,558	3	2	3	4	3	1.1042	0.5219
284	80	80	120	120	44	32	48	71,091	3,252	2,084,650	124,510	1	2	2	1	1	1.2752	0.6785
285	80	80	120	120	41	32	46	23,036	87,799	1,772,854	3,479,268	3	2	2	3	3	1.1109	0.4490
286	80	80	120	120	46	18	23	48,759	37,454	2,865,216	2,747,799	1	2	3	2	2	1.0378	0.5512
287	85	85	55	55	13	53	44	46,475	23,849	1,903,438	2,349,765	2	1	2	4	4	0.9164	0.3779
288	85	85	55	55	52	24	10	71,016	3,240	741,934	2,010,148	4	2	3	4	3	0.9430	0.3633
289	85	85	135	135	29	11	36	83,595	29,595	1,866,092	2,553,014	3	2	2	3	1	0.9672	0.5182
290	85	85	135	135	8	35	35	97,488	2,749	279,619	1,169,972	2	1	4	3	3	1.4707	0.5659
291	90	90	115	115	26	29	27	36,686	75,131	3,334,178	340,502	4	2	4	1	1	0.9855	0.4833
292	90	90	115	115	36	48	44	73,213	55,686	1,526,892	1,579,321	2	1	2	1	3	1.5063	0.5554
293	95	95	100	100	7	37	5	86,785	72,266	973,178	782,603	3	1	1	1	2	0.8841	0.3729
294	95	95	100	100	50	37	50	45,349	11,631	1,584,490	709,474	1	1	3	2	2	1.3935	0.6248
295	110	110	75	75	46	23	41	89,344	71,731	360,632	1,123,202	3	1	2	2	2	1.3982	0.4852
296	110	110	75	75	6	32	41	40,871	53,546	3,492,813	1,395,580	2	2	4	2	2	0.9059	0.4034
297	110	110	75	75	47	7	21	69,406	25,532	1,493,818	107,396	1	1	2	4	3	0.9882	0.5727
298	110	110	90	90	14	11	29	8,978	14,320	3,096,774	2,119,613	3	2	2	1	3	0.8286	0.3724
299	110	110	90	90	12	14	21	22,737	98,020	2,229,795	3,081,587	3	2	3	1	2	0.8067	0.3247
300	120	120	110	110	11	43	37	26,494	43,849	21,369	846,074	3	1	3	1	2	2.1556	0.5937
301	120	120	110	110	16	45	33	39,381	75,274	1,245,988	2,663,634	3	2	2	4	1	1.1253	0.4491
302	120	120	135	135	12	41	32	43,786	8,395	2,466,440	2,467,636	2	1	1	1	4	1.1502	0.5053
303	120	120	135	135	32	46	20	26,857	55,129	708,785	193,890	1	2	3	3	1	1.3769	0.6202
304	130	130	95	95	35	22	22	52,984	90,722	719,268	264,541	4	1	3	3	1	1.2642	0.5600
305	130	130	95	95	14	32	45	90,698	23,292	452,291	1,977,138	3	2	2	4	1	1.2924	0.4280
306	130	130	140	140	8	40	43	11,141	31,760	394,545	196,628	3	2	3	4	2	1.3453	0.6042
307	140	140	105	105	24	11	26	57,962	76,446	2,352,815	3,391,036	3	1	2	3	2	0.9389	0.4148
308	140	140	105	105	53	10	52	99,883	51,568	585,553	1,300,525	3	2	3	1	2	1.2081	0.5335
309	140	140	120	120	18	24	37	65,628	25,230	1,407,389	836,926	2	2	2	2	1	1.1732	0.5275
310	140	140	120	120	53	54	13	43,570	61,211	1,628,380	293,656	1	1	3	1	4	1.4088	0.7782

For the longitudinal direction of four-span bridges:

$$T_{Long4} = 0.310 + 0.00253 * Span\_1 + 0.00388 * Span\_3 + 0.00296 * Pierheight\_1 + 0.00772 * Pierheight\_2 + 0.00479 * Pierheight\_3 - 1.10 * 10^{-7} * Soil\_R2 - 0.0696 * Pier\_num$$

Equation 3.16

For the transverse direction of four-span bridges:

$$T_{Trans4} = 0.214 + 0.000339 * Span\_1 + 0.00180 * Span\_3 + 0.00207 * Pierheight\_1 + 0.00169 * Pierheight\_2 + 0.00169 * Pierheight\_3 - 2.76 * 10^{-8} * Soil\_R3 - 0.0420 * Pier\_num$$

Equation 3.17

The simplified equation for the longitudinal direction of four-span bridges:

$$T_{Long4} = -0.075 + 0.00253 * Span\_1 + 0.00388 * Span\_3 + 0.00296 * Pierheight\_1 + 0.00772 * Pierheight\_2 + 0.00479 * Pierheight\_3 - 0.0696 * Pier\_num$$

Equation 3.18

The simplified equation for the transverse direction of four-span bridges:

$$T_{Trans4} = 0.117 + 0.000339 * Span\_1 + 0.00180 * Span\_3 + 0.00207 * Pierheight\_1 + 0.00169 * Pierheight\_2 + 0.00169 * Pierheight\_3 - 0.0420 * Pier\_num$$

Equation 3.19

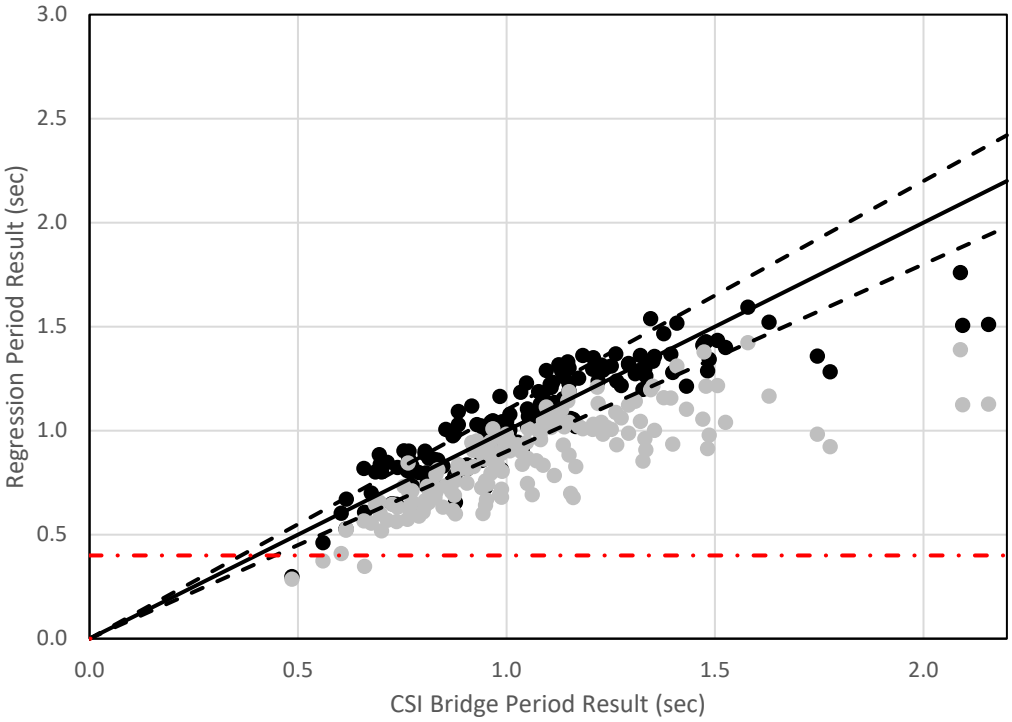

Figure 3-23 Calculated against Predicated Longitudinal Fundamental Period for Four-Span Bridges

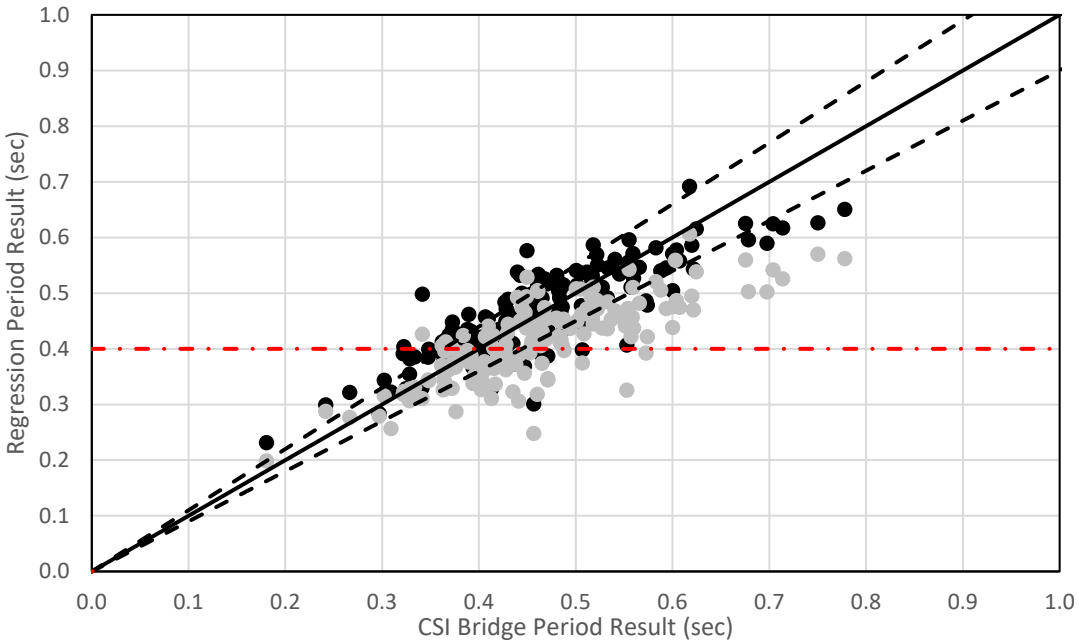

Figure 3-24 Calculated against Predicated Transverse Fundamental Period for Four-Span Bridges

Table 3-14 shows the results of the parametric study for five-span bridges. Two algebraic expressions based on the parametric study dataset were developed for estimating the fundamental period in the longitudinal and transverse directions for five-span bridges. Two simplified equations were also proposed by using the upper boundary of the foundation rotational stiffness which is equal to 3,500,000 kip-ft/rad to replace the "Soil_R2" and "Soil_R3" term in the regression model. Black dots in Figure 3-25 and 3-26 indicate that most of the predicted values of fundamental period which are larger than 0.4 s are within 10% of the calculated fundamental period for both the longitudinal and transverse directions. Grey dots which represent simplified regression model in Figures 3-25 and 3-26 indicate that the predicted values of fundamental period are smaller than the calculated fundamental period which is conservative.

Table 3-14 Parametric Study Results for Five-Span Bridges

Observation	span_1 (ft)	span_2 (ft)	span_3 (ft)	span_4 (ft)	span_5 (ft)	Pier height_1 (ft)	Pier height_2 (ft)	Pier height_3 (ft)	Pier height_4 (ft)	Soil_U2 (kip/ft)	Soil_U3 (kip/ft)	Soil_R2 (kip-ft/rad)	Soil_R3 (kip-ft/rad)	Bolt	Pier_num	Pier dia_1	Pier dia_2	Pier dia_3	Pier dia_4	Long. Period (sec)	Trans. Period (sec)
311	40	40	40	40	40	37	37	7	25	99,442	37,288	702,148	3,492,550	1	1	2	3	2	4	0.8078	0.3461
312	45	45	45	45	45	16	21	14	15	75,864	16,780	2,305,338	115,593	1	2	2	2	4	1	0.4931	0.2501
313	45	45	45	45	45	13	31	38	29	58,215	38,736	737,389	1,722,601	2	2	2	1	2	3	0.8045	0.3445
314	50	50	50	50	50	46	5	7	34	10,775	83,810	3,135,253	2,429,432	3	2	4	1	4	3	0.6131	0.2972
315	50	50	50	50	50	49	5	47	39	81,492	73,071	3,278,899	1,518,111	3	2	3	1	1	1	0.8391	0.4062
316	50	50	50	50	50	9	45	47	40	85,265	41,945	3,191,515	2,784,923	3	2	3	2	1	4	0.8974	0.3541
317	60	60	60	60	60	38	36	9	13	60,735	11,191	1,878,890	2,457,921	2	2	2	3	1	3	0.7540	0.3456
318	60	60	60	60	60	27	27	26	18	20,438	56,682	283,534	1,827,870	2	2	1	3	3	2	0.9192	0.3164
319	80	80	80	80	80	36	48	50	36	34,788	96,972	132,999	178,389	3	1	2	2	3	3	1.8051	0.6278
320	80	80	80	80	80	52	33	22	45	61,507	93,040	376,850	2,647,472	1	2	2	1	3	3	1.1592	0.4384
321	100	100	100	100	100	26	39	26	40	39,977	21,273	3,194,275	1,678,471	1	2	2	2	2	4	1.0222	0.4830
322	100	100	100	100	100	5	49	20	12	30,318	80,740	912,185	2,146,791	2	2	2	2	3	2	0.9341	0.3809
323	100	100	100	100	100	48	36	35	22	61,110	64,889	3,234,793	1,824,067	1	1	1	3	3	3	1.1101	0.5453

324	120	120	120	120	120	5	55	24	51	95,314	89,239	3,234,187	3,132,840	1	1	1	3	2	3	1.2897	0.5835
325	120	120	120	120	120	20	29	27	33	20,799	35,744	1,405,839	1,265,144	2	1	1	1	2	1	1.3118	0.6068
326	120	120	120	120	120	41	11	36	41	42,679	72,431	1,626,189	1,105,593	2	1	2	1	4	2	1.1356	0.5532
327	140	140	140	140	140	36	52	37	11	93,780	30,658	1,939,883	215,342	3	1	2	3	1	1	1.3798	0.8858
328	140	140	140	140	140	23	46	22	50	24,648	66,877	1,632,087	2,562,538	2	1	3	2	2	3	1.4566	0.6381
329	140	140	140	140	140	48	51	37	6	45,797	12,813	3,158,681	2,656,413	2	2	2	3	2	4	1.3505	0.5827
330	35	40	40	40	35	21	28	28	10	53,538	14,971	1,549,522	3,431,413	4	2	2	2	1	2	0.5973	0.2425
331	35	40	40	40	35	14	5	29	25	90,940	51,655	2,112,397	2,458,553	4	1	2	2	1	1	0.6324	0.2713
332	35	50	50	50	35	7	44	26	23	48,408	94,067	762,038	400,756	1	2	2	4	3	3	0.7574	0.3154
333	35	50	50	50	35	17	38	32	29	27,046	31,127	2,854,571	3,411,244	1	1	4	1	1	3	0.8363	0.4570
334	70	50	50	50	70	22	37	15	34	67,232	21,697	2,123,520	775,319	4	1	2	1	3	2	0.7379	0.4662
335	70	50	50	50	70	22	13	10	23	54,021	75,744	388,262	2,636,117	2	1	1	3	4	2	0.6919	0.2804
336	90	60	60	60	90	19	45	21	46	57,940	61,777	3,160,325	2,516,861	3	1	1	4	3	2	0.9024	0.3741
337	90	60	60	60	90	29	17	16	20	23,008	7,378	221,818	2,348,973	1	1	3	4	3	4	1.0072	0.3603
338	90	60	60	60	90	41	44	11	27	97,999	25,413	1,109,110	947,515	1	2	3	2	2	4	0.9439	0.3493
339	35	80	80	80	35	43	50	22	29	6,989	68,576	3,419,035	2,936,744	3	1	3	3	3	1	0.9944	0.4632
340	35	80	80	80	35	32	49	18	26	19,154	90,859	1,213,100	1,165,127	2	1	4	2	1	3	1.0129	0.4630
341	100	80	80	80	100	38	41	22	27	98,811	10,344	1,839,623	848,613	1	2	3	3	3	3	0.9404	0.4442
342	100	80	80	80	100	22	51	36	20	34,073	3,672	1,933,305	3,228,465	2	2	4	2	1	3	0.9892	0.4088
343	100	80	80	80	100	37	23	12	54	63,200	21,039	1,636,780	1,120,060	2	2	2	4	3	3	0.9277	0.4729
344	125	80	80	80	125	11	27	46	54	91,471	90,747	6,893	368,006	2	2	1	1	1	2	2.3887	0.5055
345	125	80	80	80	125	37	18	52	40	43,352	26,973	922,577	574,763	2	2	2	3	3	3	1.0949	0.5059
346	125	80	80	80	125	26	36	39	41	99,297	36,860	2,895,469	438,384	3	2	2	2	1	3	1.0611	0.5051
347	60	90	90	90	60	37	13	48	40	5,312	87,347	340,685	1,917,104	2	2	3	3	2	3	1.2488	0.4831
348	60	90	90	90	60	29	19	37	14	1,270	32,352	3,207,421	1,784,749	3	1	2	2	4	2	0.8900	0.7192
349	60	90	90	90	60	18	16	52	51	77,993	12,707	613,081	2,696,906	4	2	2	3	3	3	1.2126	0.3774
350	120	90	90	90	120	17	35	36	13	58,704	29,354	812,380	1,678,019	3	1	2	3	1	2	1.0505	0.4662
351	120	90	90	90	120	45	33	45	53	6,559	1,436	2,641,261	488,954	1	1	2	3	3	2	1.4276	0.6924
352	120	90	90	90	120	19	45	12	16	48,949	32,423	257,014	3,134,348	1	1	3	2	2	3	1.1254	0.4119
353	50	100	100	100	50	10	41	50	40	43,696	79,588	627,723	2,051,376	1	1	2	3	3	2	1.5370	0.5089

354	50	100	100	100	50	24	54	30	43	86,570	77,193	1,851,896	277,239	2	1	2	2	3	3	1.2359	0.6066
355	50	100	100	100	50	53	24	49	41	43,274	7,359	1,661,078	1,349,194	2	2	2	3	4	2	1.1617	0.4484
356	115	100	100	100	115	52	14	10	26	65,784	20,356	1,784,866	1,038,671	2	2	3	3	3	2	0.9493	0.4201
357	115	100	100	100	115	8	25	29	34	53,700	14,472	572,788	3,371,839	1	2	3	3	2	3	1.0524	0.4223
358	115	100	100	100	115	52	41	32	35	23,946	72,034	818,879	1,644,037	3	1	1	3	3	4	1.5028	0.5452
359	70	110	110	110	70	39	28	53	42	87,817	96,862	1,992,897	1,282,879	3	2	2	3	2	1	1.2552	0.5357
360	70	110	110	110	70	23	18	29	11	41,787	43,296	2,806,662	2,642,965	3	1	4	3	3	1	0.8861	0.3751
361	70	110	110	110	70	15	34	15	36	30,291	89,365	1,027,945	702,016	3	2	2	3	3	3	0.9795	0.4890
362	70	120	120	120	70	41	52	28	21	11,656	35,072	956,818	1,665,252	1	1	3	1	4	2	1.3641	0.6525
363	70	120	120	120	70	53	17	6	35	53,739	30,230	1,343,378	2,239,766	2	1	3	3	2	4	0.9746	0.4657
364	130	120	120	120	130	50	22	31	12	94,836	30,144	2,321,000	2,152,645	3	2	4	3	1	4	1.0456	0.4749
365	130	120	120	120	130	17	27	18	55	83,399	43,598	2,795,712	912,210	2	1	3	1	1	4	1.0737	0.5582
366	130	120	120	120	130	34	47	47	42	97,541	36,104	1,595,074	1,623,163	1	2	2	2	4	4	1.4421	0.5516
367	60	130	130	130	60	7	40	35	27	21,430	27,491	2,339,173	1,235,762	1	2	2	3	3	3	1.1282	0.5980
368	60	130	130	130	60	19	23	12	51	33,664	79,447	3,174,473	1,478,443	3	2	3	2	3	2	0.9871	0.4446
369	120	130	130	130	120	28	28	45	17	67,422	84,858	1,679,989	643,655	2	2	3	3	4	2	1.0908	0.4802
370	120	130	130	130	120	34	27	7	18	28,993	68,896	327,219	3,261,571	4	1	1	2	1	2	1.1883	0.4798
371	120	130	130	130	120	24	11	19	8	99,524	20,250	3,003,057	3,485,487	2	2	3	2	2	3	0.8618	0.3979
372	90	140	140	140	90	34	7	12	37	76,449	67,009	2,071,139	319,520	4	2	2	2	1	3	0.9557	0.6079
373	90	140	140	140	90	22	44	53	42	37,105	23,457	611,917	3,314,209	3	2	4	1	2	3	1.8426	0.5543
374	115	140	140	140	115	30	45	10	35	10,209	93,289	2,856,517	3,163,467	2	2	3	2	3	2	1.0907	0.5732
375	115	140	140	140	115	17	28	18	16	29,975	12,502	1,121,749	3,417,576	4	1	3	2	4	3	1.0315	0.4351

For the longitudinal direction of five-span bridges:

$$T_{Long5} = 0.229 + 0.00171 * Span\_1 + 0.00314 * Span\_2 + 0.00227 * Pierheight\_1 + 0.00548 * Pierheight\_2 + 0.00876 * Pierheight\_3 + 0.00707 * Pierheight\_4 - 1.05 * 10^{-7} * Soil\_R2 - 0.0714 * Pier\_num$$

Equation 3.20

For the transverse direction of five-span bridges:

$$T_{Trans5} = 0.251 + 0.000193 * Span\_1 + 0.00214 * Span\_2 + 0.00139 * Pierheight\_1 + 0.00193 * Pierheight\_2 + 0.00196 * Pierheight\_3 + 0.000861 * Pierheight\_4 - 3.30 * 10^{-8} * Soil\_R3 - 0.0745 * Pier\_num$$

Equation 3.21

The simplified equation for the longitudinal direction of five-span bridges:

$$T_{Long5} = -0.139 + 0.00171 * Span\_1 + 0.00314 * Span\_2 + 0.00227 * Pierheight\_1 + 0.00548 * Pierheight\_2 + 0.00876 * Pierheight\_3 + 0.00707 * Pierheight\_4 - 0.0714 * Pier\_num$$

Equation 3.22

The simplified equation for the transverse direction of five-span bridges:

$$T_{Trans5} = 0.136 + 0.000193 * Span\_1 + 0.00214 * Span\_2 + 0.00139 * Pierheight\_1 + 0.00193 * Pierheight\_2 + 0.00196 * Pierheight\_3 + 0.000861 * Pierheight\_4 - 0.0745 * Pier\_num$$

Equation 3.23

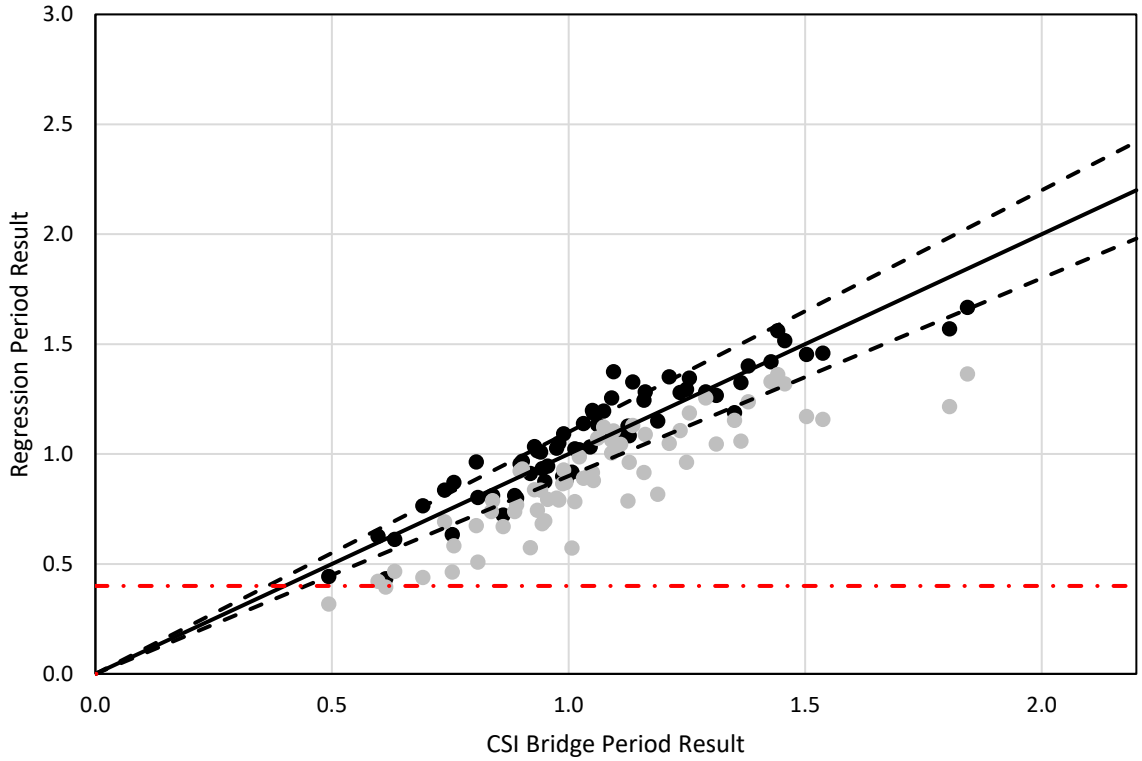

Figure 3-25 Calculated against Predicated Longitudinal Fundamental Period for Five-Span Bridges

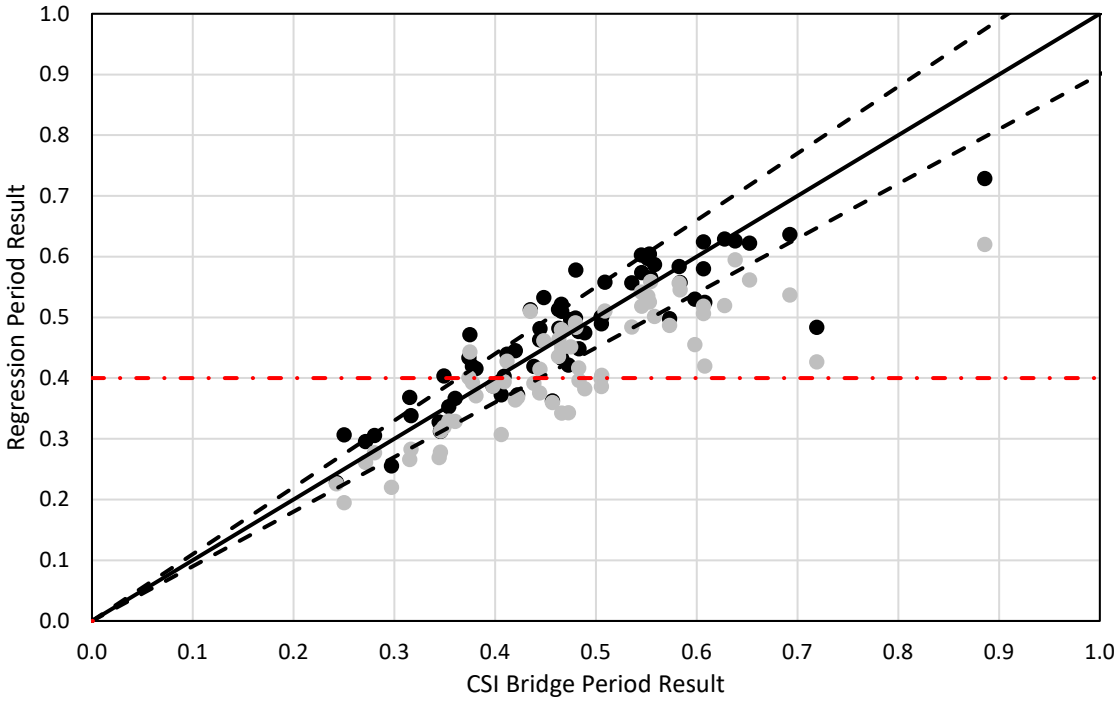

Figure 3-26 Calculated against Predicated Transervse Fundamental Period for Five-Span Bridges

3.5 Summary

The purpose of this chapter was to provide empirical equations which can be used by bridge engineers to calculate the bridge fundamental period in both the longitudinal and transverse directions without any dynamic modelling based on the primary bridge properties. First, a detailed modelling procedure of superstructure, substructure and connections of standard highway bridges was discussed. Then, both modal analysis and single-mode spectral method were used to generate the parametric study dataset of fundamental periods for three hundred and seventy-five highway bridges based on the CSIBRIDGE models. Finally, regression equations based on the parametric study were developed for one-span, two-span, three-span, four-span, and five-span bridges in both longitudinal and transverse direction, respectively.

Chapter 4. Determination of Column Ductility Capacity

4.1 Introduction

Ductility, a non-dimensional factor which is defined as the ratio of total deformation to yield deformation has become a very important term in modern seismic design practice. Ductility can be measured at different levels within a structure. One level is section ductility (curvature ductility) and another is system or member ductility (displacement ductility). Compared with the section ductility approach, the displacement ductility approach has been widely used by design companies and engineers in the seismic analysis and design of highway bridges. According to the requirements of the AASHTO guide specification (AASHTO, 2011). Ductile detailing is required to make sure that sufficient ductility is available in a bridge's structural system to safely survive an earthquake in SDC B and C. Figure 4-1 shows the expectation for damage and energy dissipation for bridges. Plastic hinges are developed in the bent columns while the bent and the foundation should remain undamaged through the full strength of the column hinging.

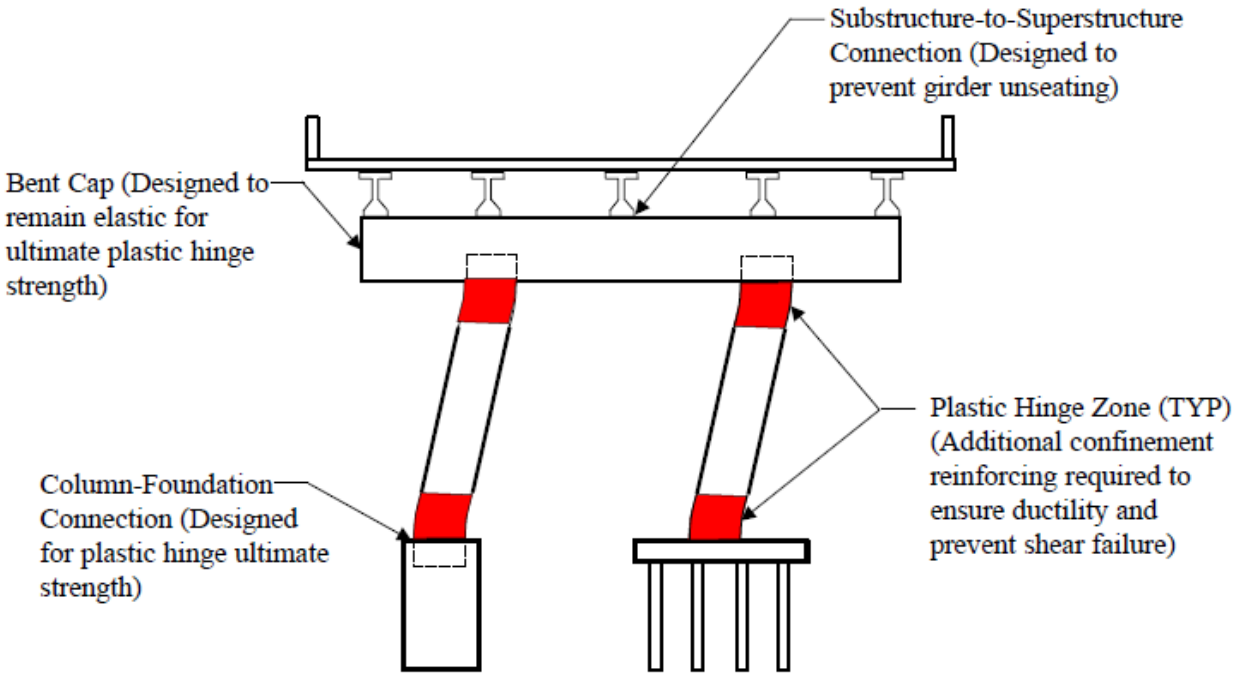

Figure 4-1 Inelastic Behavior of Bridge Elements in Design Level Seismic Event

4.2 AASHTO Local Displacement Capacity for SDCs B and C

SDC B bridge columns are targeted for a limited displacement corresponding to minor damage which can be considered as a limit state of initiation of concrete cover spalling. SDC C bridge columns are targeted for a maximum displacement corresponding to moderate damage which can be considered as an equivalent column member ductility of 3 or less. Regression analyses based on experiments and numerical analysis results have been done by Berry and Eberhard (2003) and Imbsen (2006) to determine the empirical formula for displacement capacity. A few column pushover analyses were done by Imbsen (2006) as well to estimate the column displacement capacity under different limit states. The range of column diameters is from 3 feet to 7 feet with 1% to 4% longitudinal reinforcement ratio, ρ, and the column height range is from 20 feet to 50 feet. Table 4-1 shows the column parameters in the numerical analysis. Multiple regression models were established and related to different limit states based on the numerical column pushover analysis. Figure 4-2 shows the lower bound curves which are identified for different limit states. Curve 1, labeled as C1(yield), represents drift capacity corresponding to the limit state of column yielding. Curve 2, labeled as C2(Spalling), represents drift capacity corresponding to limit state of concrete spalling. Curve 3, labeled as C3(Ductility 4), represents drift capacity corresponding to a column ductility of 4. The vertical axis is drift capacity $\frac{\Delta_C^L}{H_o}$ while the horizontal axis is a function of the slenderness ratio $x = \frac{\Lambda B_o}{H_o}$ which is $\frac{Fb}{L}$ in Figure 4-2 where:

Δ_C^L = Displacement capacity (in)

Λ = Factor for column end restraint condition, 1 for fixed-free (pinned on one end), 2 for fixed top and bottom

B_o = Column diameter or width (ft)

H_o = Clear height of column (ft)

Table 4-1 Column Parameters (Imbsen, 2006)

Column Diameter D (ft)	ρ (%)	Column Height L (ft)
3	1,2,3,4	20,
4	1,2,3,4	20,30
5	1,2,3,4	20,30,40
6	1,2,3,4	30,40,50
7	1,2,3,4	30,40,50

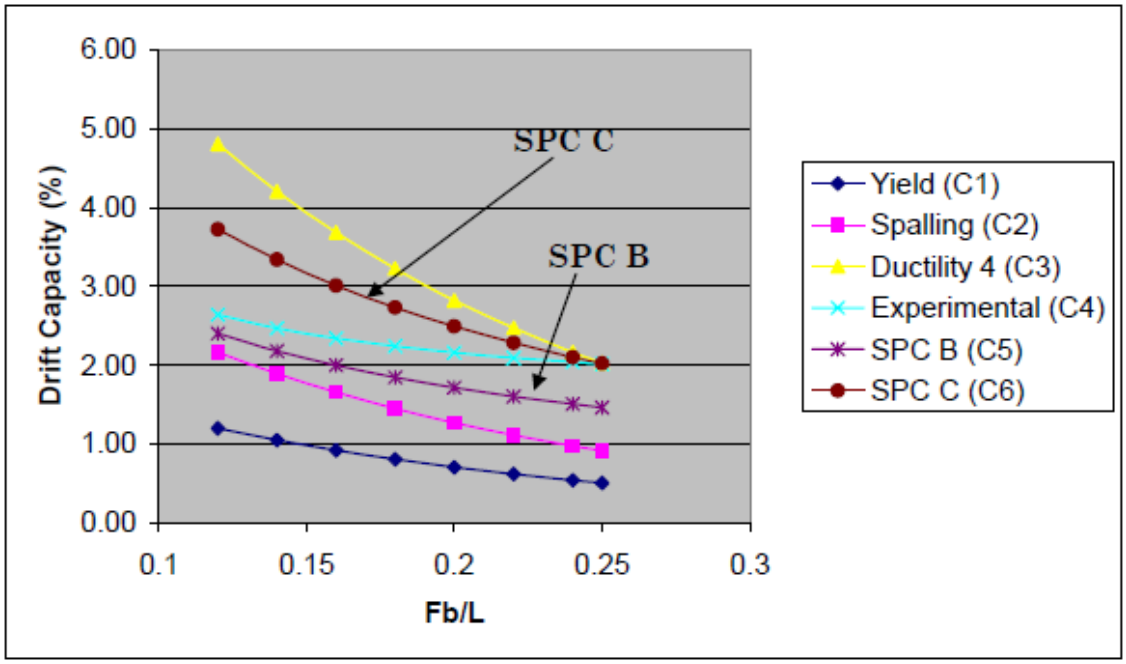

Figure 4-2 Drift Capacity for SDC B and C (Imbsen, 2006)

Curve 4, labeled as C4 (Experimental), represents the drift capacity based on the estimate of displacement at the onset of cover spalling in flexure-dominant reinforced concrete columns. This displacement estimate is recommended by Berry and Eberhard (2003) according to the UW-PEER database (UW & PEER, 2004) which contains the results of cyclic lateral load test on reinforced concrete columns which were assembled by University of Washington supported by the National Science Foundation through the Pacific Earthquake Engineering Research Center

(PEER). The proposed equation by Berry and Eberhard based on the statistical study adopted by PEER is:

$$\frac{\Delta_C^L}{H_o} = 1.6(1 - \frac{P}{A_g f_c'})(1 + \frac{1}{10(\frac{B_o}{H_o})}) \quad \text{Equation 4-1}$$

Where:

P= Axial load in the column (kips)

A_g= Column cross section area (in^2)

f_c'= Concrete compressive strength (ksi)

For simplification purposes, axial force P in the equation can be assumed as $0.1A_g f_c'$.

Curve 5, labeled as C5 (SPC B), represents the maximum drift capacity for SDC B bridges based on Curve 2 and Curve 4. The equation is shown below:

$$Curve5 = \frac{Curve2+Curve4}{2} \quad \text{Equation 4-2}$$

Curve 6, labeled as C6 (SPC C), represents the maximum drift capacity for SDC C bridges based on Curve 3 and Curve 4. The equation is shown below:

$$Curve6 = \frac{Curve3+Curve4}{2} \quad \text{Equation 4-3}$$

The two empirical equations of local displacement capacity for both SDCs B and C highway bridge columns provided by the current AASHTO guide specification (AASHTO, 2011) are modified from Curve 5 and 6, respectively. The two final approximate equations provided in the current AASHTO standard (Equations 4.8.1-1 and 4.8.1-2) are shown below:

For SDC B:

$$\Delta_C^L = 0.12H_o(-1.27\ln(x) - 0.32) \geq 0.12H_o \quad \text{Equation 4-4}$$

For SDC C:

$$\Delta_C^L = 0.12H_o(-2.32\ln(x) - 1.22) \geq 0.12H_o \qquad \text{Equation 4-5}$$

According to the AASHTO guide specification (2011), these two equations are calibrated for bridge columns that have clear heights which are greater than or equal to about 15 feet in height and where plastic hinging is anticipate above ground. However, based on past work, several case study bridge columns have fallen outside the bounds of these two equations. This chapter will use a parametric study to expand the applicable range of the equations such that nonlinear pushover analysis will not be required to determine displacement capacity for bridges in SDC B and C. Pushover analyses of bridges both within and outside the current applicable ranges will be evaluated to allow for new displacement capacity equations. The primary variables investigated in this study were the column height, column diameter and reinforcement ratio. As with the previous task, the bridges that have been utilized in previous research were used as the basis for the range of the various parameters. Additional bridge geometry or design recommendations to modify existing bridges were used to fill the parameter gaps which basically is bridge columns shorter than 15 feet. Nonlinear pushover analyses were performed both in SAP2000 V19 (CSI., 2011) and ABAQUS (2017) to compare results in advance of the final parametric study for columns less than 15 ft in height. ABAQUS models were used to do the pushover analyses used in the parametric evaluation.

4.3 ABAQUS Modelling

3D solid elements are usually not used to model reinforced concrete columns in design practice since it is much more computationally expensive than frame elements. However, there are some advantages to using 3D elements. The most important is that different failure modes can be directly captured by using solid elements instead of beam or truss elements. For example,

concrete spalling and longitudinal reinforcement buckling cannot be captured in frame elements. In this study, ABAQUS was selected to do the solid element modelling and analysis.

4.3.1 Geometry

Multiple 3D concrete columns with reinforcement bars were constructed by using the ABAQUS/CAE structural analysis modeling tool to execute a static pushover analysis. The example column geometry including the reinforcement details is shown in Figure 4-3.

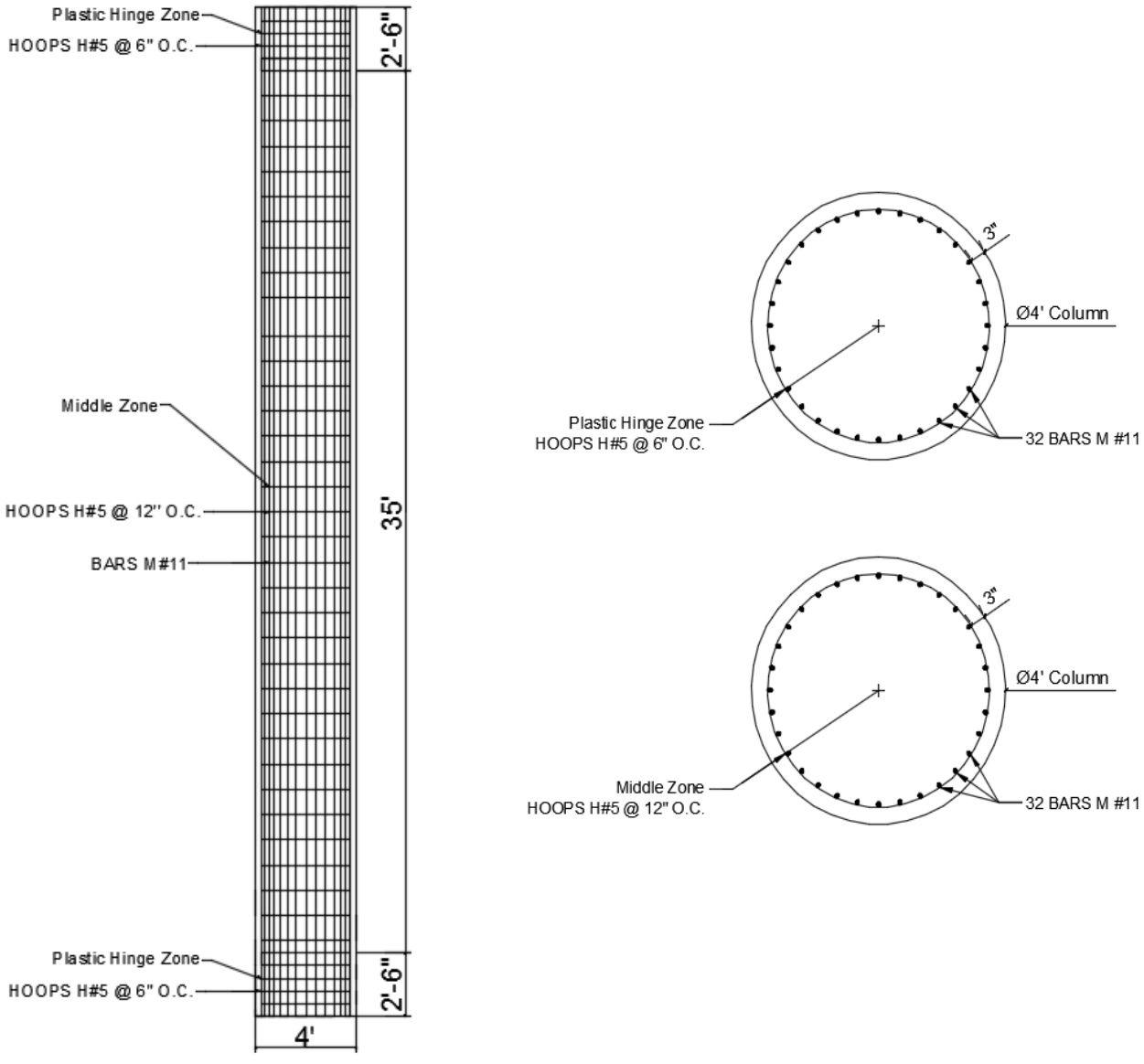

Figure 4-3 Dimensions and Reinforcement Details of Example Column

This is a 40 feet clear height circular bridge column with a 4 ft diameter. There are 32 #11 longitudinal reinforcement bars in the cross section. The thickness of concrete cover is 3 in. Two 2.5 ft plastic hinge zones were preliminarily defined on the top and bottom of the column. The plastic hinge zone length was calculated based on the AASHTO guide specification (2011):

$$L_p = 0.08L + 0.15f_{ye}d_{bl} \geq 0.3f_{ye}d_{bl} \quad \text{Equation 4-6}$$

where:

L_p= Analytical plastic hinge length (in)

L= Length of column from point of maximum moment to the point of moment contraflexure (in)

f_{ye}= Expected yield strength of longitudinal column reinforcing steel bars (ksi)

d_{bl} = Nominal diameter of longitudinal column reinforcing steel bars (in)

The remaining column length was called the middle zone. In the plastic hinge zone, #5 reinforcement bars with 6 inches spacing were applied while #5 reinforcement bars with 12 in spacing were applied in the middle zone. Most inelastic behavior expected during pushover analysis will happen in the plastic hinge zone. All the geometry and reinforcement related to the different column sections modelled in Abaqus are shown in Table 4-2. The range of the column aspect ratio is from 3.2 to 10. The reinforcing ratio range includes a lower limit (0.01), mid-range (0.025) and upper limit (0.04) longitudinal reinforcement ratio, ρ. The column height range in the parametric study is from 8 feet to 40 feet. The model name in this table contains basic column properties. For example, in A044016_612_0, A means ABAQUS model, 04 means the diameter of column is 4ft, 40 means the height of column is 4 0ft, 16 means 16 longitudinal rebars, 612 means 6 in transverse spacing in the plastic hinge zone and 12 in in the middle zone and 0 means there is no axial force on the top of column. If there is an axial force ($0.1f'_cA_g$) on the top of column, an ‘a’ will be at the end of the model name.

Table 4-2 Column Geometry and Reinforcement Details for ABAQUS Models

Model Name	Column Diameter (ft)	Column Height (ft)	Longitudinal Reinforcing Bars and Ratio	Axial Force (kip)	Plastic Hinge Zone Length(in)	Transverse Reinforcing Spacing (middle, PHZ) (in)
A044016_612_0	4	40	16 #9 [0.88%]	0	72	12, 6
A044016_612_a	4	40	16 #9 [0.88%]	724	72	12, 6
A044032_612_0	4	40	32 #9 [1.77%]	0	72	12, 6
A044032_612_a	4	40	32 #9 [1.77%]	724	72	12, 6
A044044_612_0	4	40	44 #11 [3.79%]	0	72	12, 6
A044044_612_a	4	40	44 #11 [3.79%]	724	72	12, 6
A043016_612_0	4	30	16 #9 [0.88%]	0	72	12, 6
A043016_612_a	4	30	16 #9 [0.88%]	724	72	12, 6
A043032_612_0	4	30	32 #9 [1.77%]	0	72	12, 6
A043032_612_a	4	30	32 #9 [1.77%]	724	72	12, 6
A043044_612_0	4	30	44 #11 [3.79%]	0	72	12, 6
A043044_612_a	4	30	44 #11 [3.79%]	724	72	12, 6
A2.51008_612_0	2.5	10	8 #9 [1.13%]	0	48	12, 6
A2.51008_612_a	2.5	10	8 #9 [1.13%]	283	48	12, 6
A2.51012_612_0	2.5	10	12 #11 [2.59%]	0	48	12, 6
A2.51012_612_a	2.5	10	12 #11 [2.59%]	283	48	12, 6
A2.51016_612_0	2.5	10	16 #11 [3.53%]	0	48	12, 6
A2.51016_612_a	2.5	10	16 #11 [3.53%]	283	48	12, 6
A2.51008_412_0	2.5	10	8 #9 [1.13%]	0	48	12, 4
A2.51008_412_a	2.5	10	8 #9 [1.13%]	283	48	12, 4
A2.51012_412_0	2.5	10	12 #11 [2.59%]	0	48	12, 4
A2.51012_412_a	2.5	10	12 #11 [2.59%]	283	48	12, 4
A2.51016_412_0	2.5	10	16 #11 [3.53%]	0	48	12, 4
A2.50816_412_a	2.5	10	16 #11 [3.53%]	283	48	12, 4
A2.50808_612_0	2.5	8	8 #9 [1.13%]	0	48	12, 6
A2.50808_612_a	2.5	8	8 #9 [1.13%]	283	48	12, 6
A2.50812_612_0	2.5	8	12 #11 [2.59%]	0	48	12, 6
A2.50812_612_a	2.5	8	12 #11 [2.59%]	283	48	12, 6
A2.50816_612_0	2.5	8	16 #11 [3.53%]	0	48	12, 6
A2.50816_612_a	2.5	8	16 #11 [3.53%]	283	48	12, 6
A2.50808_412_0	2.5	8	8 #9 [1.13%]	0	48	12, 4
A2.50808_412_a	2.5	8	8 #9 [1.13%]	283	48	12, 4
A2.50812_412_0	2.5	8	12 #11 [2.59%]	0	48	12, 4
A2.50812_412_a	2.5	8	12 #11 [2.59%]	283	48	12, 4
A2.50816_412_0	2.5	8	16 #11 [3.53%]	0	48	12, 4
A2.50816_412_a	2.5	8	16 #11 [3.53%]	283	48	12, 4

4.3.2 Element Type and Mesh

There are various elements which are available in the ABAQUS program library. In this pushover analysis modeling, the concrete part of the column is modelled by using C3D8R elements in Abaqus. This type of element is an eight-node solid element. Each node has three translational degrees of freedom. Hex-structured and wedge-sweep meshes are used to simulate the column concrete part. The height of element (z-direction) is important since a horizontal displacement will be imposed at the top of the column. The element height needs to be small enough to capture all the inelastic behavior. For the example column shown in Figure 4-3, a 6-inch element height was selected after the mesh size sensitivity analysis. Meanwhile, a mesh dimension of 0.69 inch was selected in the circumferential direction while 2.33 inch and 0.33 inch were selected for core concrete part and concrete cover part in radial direction, respectively. The mesh size of concrete varies among the different column models in this study. For the longitudinal and transverse reinforcement bars, 3D line (beam) element B31 was selected in this study. All the rebar elements are embedded in the 3D concrete solid element. The mesh of the reinforcement bar strictly follows the concrete mesh to make sure the nodes on the rebar match up with the nodes on the concrete solid elements. The mesh pattern of the finite element model of the example column with reinforcement bars is shown in Figure 4-4.

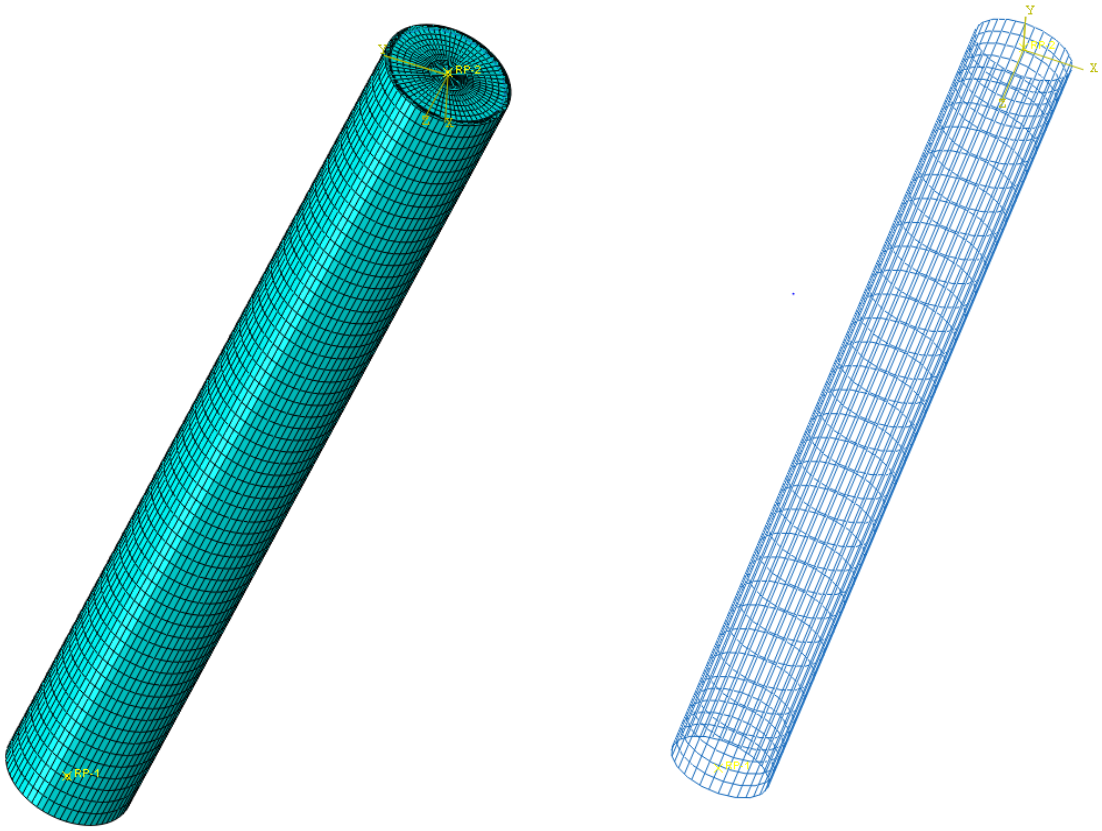

Figure 4-4 Mesh Configuration of Concrete and Configuration of rebar of the Example Column

4.3.3 Concrete Material Modeling

Linear elastic and nonlinear plastic concrete models were both considered for pushover analysis to model the deformations of the brittle concrete materials in a case where large localized deformation would be required. The linear elastic concrete model was defined by using two parameters, Young's modulus and Poisson's ratio. The Young's modulus in this study is 3,605 ksi and the Poisson's ratio is 0.2. Both parameters were selected based on the default 4,000 psi concrete material property in SAP2000 to facilitate comparisons with SAP models. The ABAQUS/CAE modelling tool was used to simulate concrete inelastic and damage behavior by using a different concrete constitutive model. There are three built-in constitutive models in

ABAQUS for concrete materials. They are the smeared crack concrete model, the concrete damage plasticity model and the brittle crack model. The concrete damage plasticity model which uses concepts of isotropic damaged elasticity in combination with isotropic tensile and compressive plasticity to represent the inelastic behavior of concrete was selected in this study to simulate the concrete material. The inelastic behavior and damage characteristics of concrete in compression and tension can be defined in the program. The concrete damage plasticity model can be used under both static and cyclic loading conditions.

4.3.3.1 Basic Plasticity Parameters

The basic plasticity parameters for the concrete damaged plasticity model were selected based on previous research (Kmiecik & Kaminski, 2011). Dilation angle and flow potential eccentricity are 36 degrees and 0.1, respectively. The ratio of the strength in the biaxial state to the strength in the uniaxial state (σ_{b0}/σ_{c0}) is equal to 1.16. In addition, the ratio of the second stress invariant on the tensile meridian (K_C) is equal to 0.667. For concrete materials, the viscosity parameter is supposed to be assigned as 0. However, for numerical converge purposes, a very small number, 0.00001, which has insignificant effect on the analysis was adopted in this study.

4.3.3.2 Concrete Compression Stress-Strain Curve

In this study, the concrete damage plasticity model was selected to simulate concrete cracking and crack propagation. Based on this constitutive model, a stress-strain relationship for concrete in compression including a post-failure stress-strain relationship in tension are required. The default 4,000 psi concrete material stress-strain curve in SAP2000 was applied for concrete compression. This uniaxial stress-strain curve was established based on the Mander concrete theory (Mander, Priestley, & Park, 1984). The unconfined Mander concrete was used in the ABAQUS model since the transverse reinforcement bars will be modelled additionally. The

theoretical Mander unconfined stress-strain curve for concrete compression portion has two parts. One is the curved part and the other one is the linear part. Figure 4-5 shows the general Mander unconfined concrete stress -strain curve.

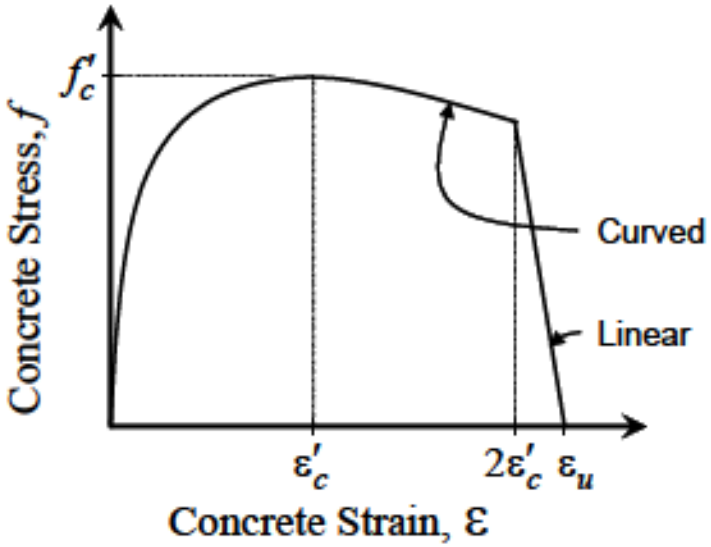

Figure 4-5 General Mander Unconfined Concrete Stress-Strain Curve (CSI., 2011)

The detailed expressions for these two parts of the concrete model are shown in Equations 4-7 and 4-8. Figure 4-6 shows the comparison between the theoretical curve, the SAP default curve and ABAQUS curve for the unconfined 4,000 psi concrete material. An ultimate strain capacity of 0.02 is assumed for the unconfined concrete material in this study. The linear portion with a small positive slope at the end of ABAQUS curve was needed for convergence purposes since only one-way pushover analyses were conducted on these models.

For $\varepsilon \leq 2\varepsilon'_c$ (Curved segment)

$$f = \frac{f'_c x r}{r - 1 + x^r} \qquad \text{Equation 4-7}$$

where

$$x = \varepsilon / \varepsilon'_c$$

$$r = \frac{E}{E - (f'_c / \varepsilon'_c)}$$

For $2\varepsilon_c' \leq \varepsilon \leq \varepsilon_u$ (Linear segment)

$$f = (\frac{2f'_c r}{r-1+2^r})(\frac{\varepsilon_u - \varepsilon}{\varepsilon_u - 2\varepsilon_c'})$$ Equation 4-8

where

ε= Concrete strain

f= Concrete stress (ksi)

E= Modulus of elasticity (ksi)

f'_c= Concrete compressive strength (ksi)

ε_c'= Concrete strain at f'_c

ε_u= Ultimate concrete strain capacity

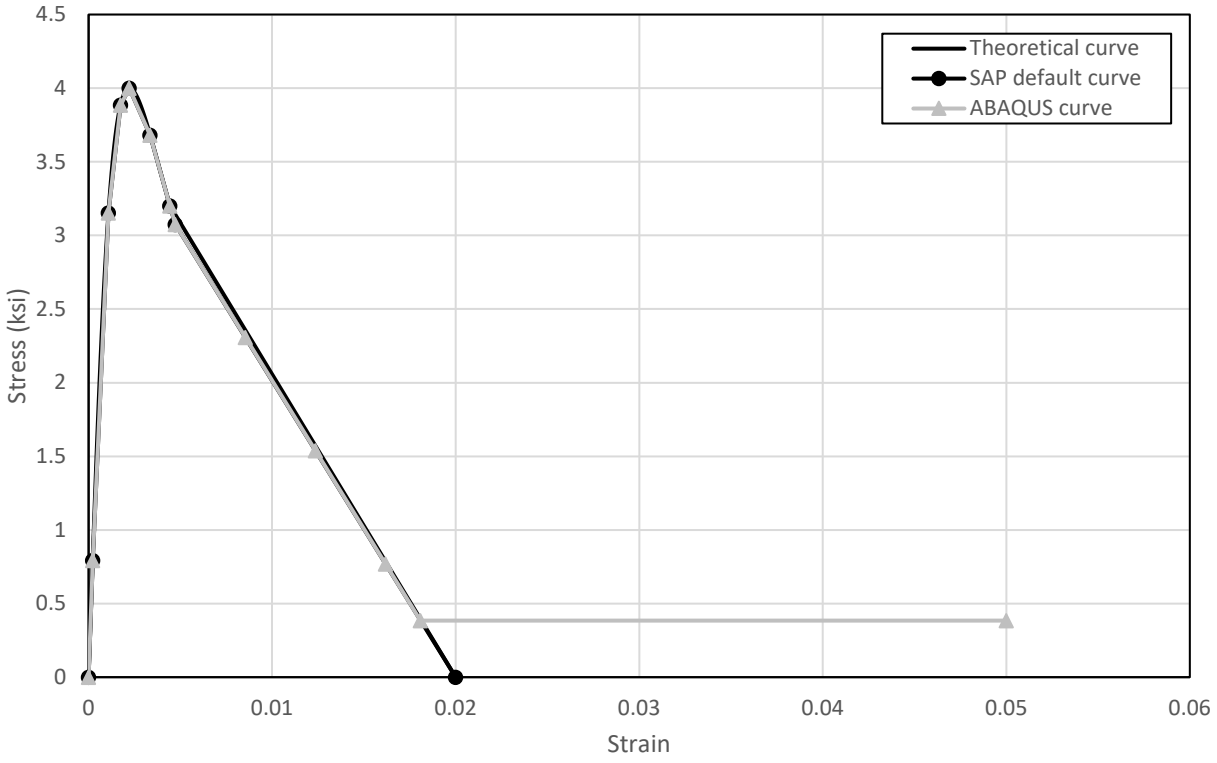

Figure 4-6 Stress-Strain Curve for 4,000 psi Unconfined Concrete in Compression

In ABAQUS, inelastic strain, $\widetilde{\varepsilon_c^{in}}$, corresponding to compressive stress, $\sigma_{c,}$ needs to be defined in the concrete damage plasticity model. Figure 4-7 shows the definition of the concrete damage plasticity model on the compression side. The compressive stress can be determined from the concrete stress-strain curve directly while inelastic strain, $\widetilde{\varepsilon_c^{in}}$, needs to be calculated by substituting the elastic strain, ε_{oc}^{el}, which corresponds to undamaged material from the total strain, ε_c. The equation is shown in Equation 4-9.

$$\widetilde{\varepsilon_c^{in}} = \varepsilon_c - \varepsilon_{oc}^{el} \qquad \text{Equation 4-9}$$

where

$$\varepsilon_{oc}^{el} = \frac{\sigma_c}{E_0}$$

E_0= Modulus of elasticity (ksi)

σ_c= Compressive stress (ksi)

ε_{oc}^{el}= Elastic strain corresponding to undamaged material in compression

ε_c= Total strain corresponding to compression stress σ_c

$\widetilde{\varepsilon_c^{in}}$= Inelastic strain corresponding to compression stress σ_c

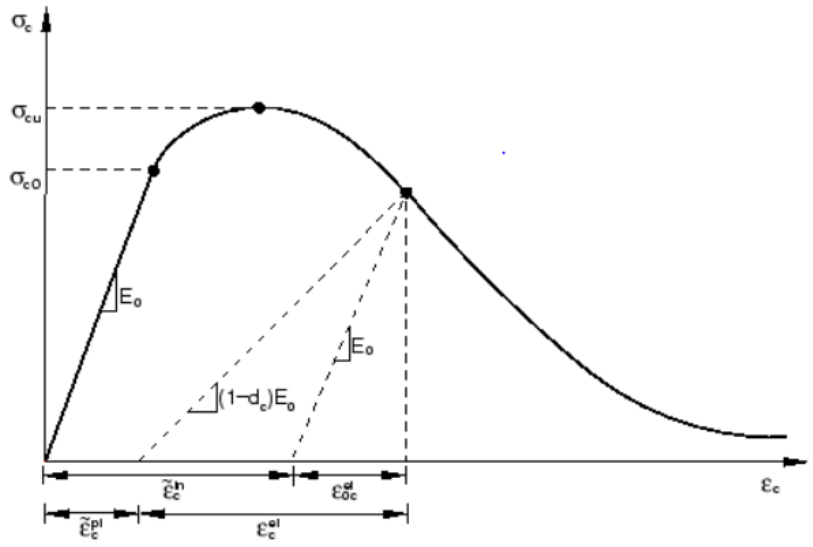

Figure 4-7 Concrete Damage Plasticity Model in Compression (ABAQUS, 2017)

4.3.3.3 Concrete Tension Stress-Strain Curve

In this study, like the concrete compression stress-strain curve, the default 4,000 psi unconfined concrete material tensile stress-strain curve in SAP2000 was applied for concrete in tension. Tensile strength of concrete was taken as approximate 10% of its compressive strength which is 0.474 ksi in this case. Based on previous research, the concrete can still carry tension even after it cracks. However, the tensile strength will decrease gradually along with the increasing tensile strain. In this study, a linear stress-strain relationship was adopted for the concrete constitutive model in tension. The stress was assumed to reduce to zero linearly at a total strain of approximately 10 times the tensile crack strain which is 0.00145 in this case. Figure 4-8 shows the comparison between SAP2000 default curve and ABAQUS curve for unconfined 4,000 psi concrete material in tension. Again, the linear portion with a small positive slope at the end of ABAQUS curve was included for convergence purposes since only one-way pushover analyses were conducted on these models.

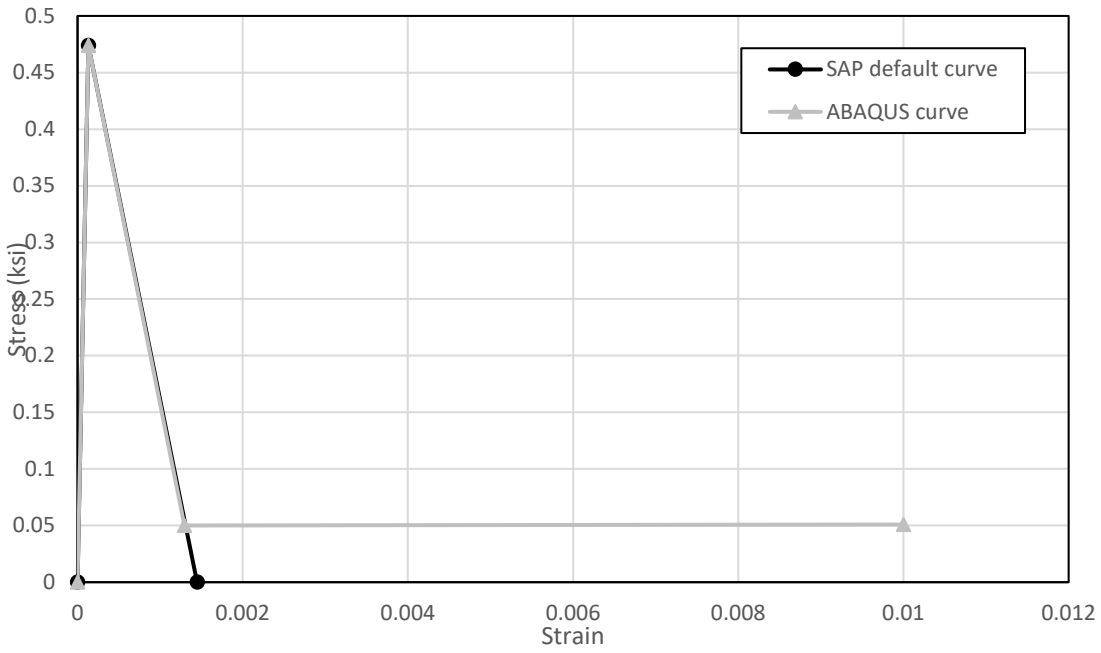

Figure 4-8 Stress-Strain Curve for 4000 psi Unconfined Concrete in Tension

In ABAQUS, cracking strain, $\widetilde{\varepsilon_t^{ck}}$, corresponding to tensile stress, σ_t, needs to be defined in the concrete damage plasticity model. Figure 4-9 shows the definition of the concrete damage plasticity model on the tension side. The tensile stress can be calculated from the concrete stress-strain curve directly while the cracking strain, $\widetilde{\varepsilon_t^{ck}}$, needs to be calculated by substituting the elastic strain, ε_{ot}^{el}, which corresponds to the undamaged material from the total strain, ε_t, as shown in Equation 4-10.

$$\widetilde{\varepsilon_t^{ck}} = \varepsilon_t - \varepsilon_{ot}^{el} \qquad \text{Equation 4-10}$$

where

$$\varepsilon_{ot}^{el} = \frac{\sigma_t}{E_0}$$

where

E_0= Modulus of elasticity (ksi)

σ_t= Tensile stress (ksi)

ε_{ot}^{el}= Elastic strain corresponding to undamaged material in tension

ε_t= Total strain corresponding to tensile stress σ_t

$\widetilde{\varepsilon_t^{ck}}$= Cracking strain corresponding to tensile stress σ_t

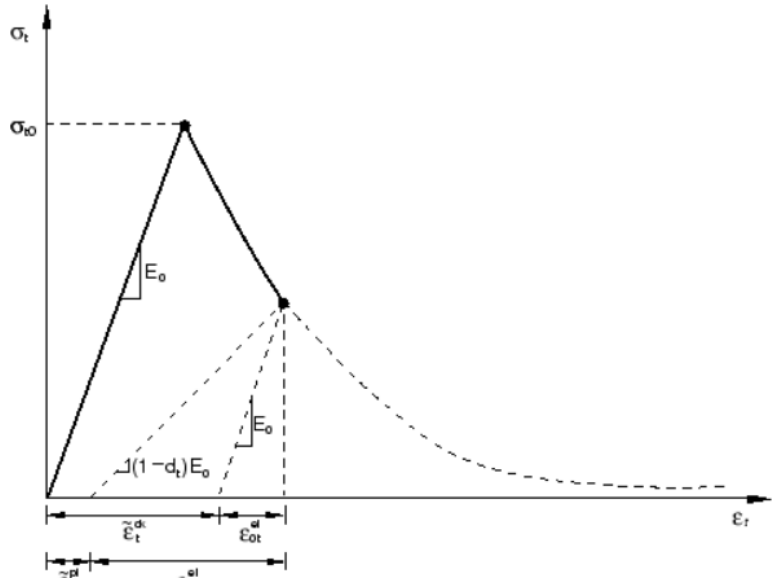

Figure 4-9 Concrete Damage Plasticity Model in Tension (ABAQUS, 2017)

4.3.3.4 Yield Function and Plastic Flow for Concrete Materials

In ABAQUS, multiple effective stress invariants are defined. Both the plastic flow potential function and the yield function are defined in term of two stress invariants of the effective stress tensor. One is the hydrostatic pressure stress, $\bar{p}$, and the other is the Mises equivalent effective stress, $\bar{q}$. The effective stress is defined as

$$\bar{\boldsymbol{\sigma}} = \boldsymbol{D_0^{el}}: (\varepsilon - \varepsilon^{pl}) \qquad \text{Equation 4-11}$$

The hydrostatic pressure stress is defined as

$$\bar{p} = -\frac{1}{3} trace(\bar{\boldsymbol{\sigma}}) \qquad \text{Equation 4-12}$$

The Mises equivalent effective stress is defined as

$$\bar{q} = \sqrt{\frac{3}{2}(\bar{\boldsymbol{S}}: \bar{\boldsymbol{S}})} \qquad \text{Equation 4-13}$$

Where

$$\bar{\boldsymbol{S}} = \bar{\boldsymbol{\sigma}} + \bar{p}\,\mathbf{I}$$

Where

$\boldsymbol{D_0^{el}}$= Elasticity tensor

ε= Total strain

ε^{pl}= Plastic strain

$\bar{\boldsymbol{S}}$= Effective stress deviator

The yield function for concrete damage plasticity model was first proposed by Lubliner et. al. (1989). Then it was modified by Lee and Fenves (1998) to account for a different evolution of strength under tension and compression. The change of the yield surface is controlled by two hardening variables, tension plastic strain, $\widetilde{\varepsilon_t^{pl}}$, and compression plastic strain, $\widetilde{\varepsilon_c^{pl}}$. Figures 4-10

and 4-11 show the yield surface in the deviatoric plane corresponding to different values of K_c and the yield surface in plane stress, respectively. The yield function is shown below:

$$F = \frac{1}{1-\alpha}\left(\bar{q} - 3\alpha\bar{q} + \beta\left(\widetilde{\varepsilon^{pl}}\right)\left(\widehat{\overline{\sigma_{max}}}\right) - \gamma\left(-\widehat{\overline{\sigma_{max}}}\right)\right) - \bar{\sigma}_c\left(\widetilde{\varepsilon_c^{pl}}\right) = 0 \qquad \text{Equation 4-14}$$

$$\alpha = \frac{\left(\frac{\sigma_{b0}}{\sigma_{c0}}\right) - 1}{2\left(\frac{\sigma_{b0}}{\sigma_{c0}}\right) - 1}$$

$$\beta = \frac{\bar{\sigma}_c\left(\widetilde{\varepsilon_c^{pl}}\right)}{\bar{\sigma}_t\left(\widetilde{\varepsilon_t^{pl}}\right)}(1-\alpha) - (1+\alpha)$$

$$\gamma = \frac{3(1-K_c)}{2K_c - 1}$$

Where

$\widehat{\overline{\sigma_{max}}}$= Maximum effective stress (ksi)
$\frac{\sigma_{b0}}{\sigma_{c0}}$= Ratio of initial equiaxial compressive yield stress to initial uniaxial compressive yield stress which is 1.16 in this study
K_c= Ratio of the second stress in variant on the tensile meridian which is 0.667 in this study
$\bar{\sigma}_c\left(\widetilde{\varepsilon_c^{pl}}\right)$= Effective compressive cohesion stress (ksi)
$\bar{\sigma}_t\left(\widetilde{\varepsilon_t^{pl}}\right)$= Effective tensile cohesion stress (ksi)

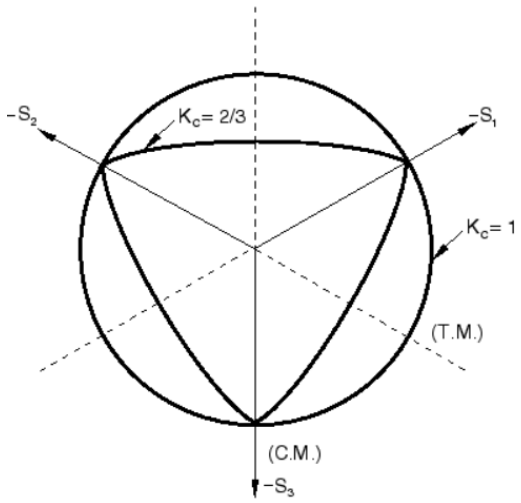

Figure 4-10 Yield Surface in the Deviatoric Plane Corresponding to Different Values of K_c (ABAQUS, 2017)

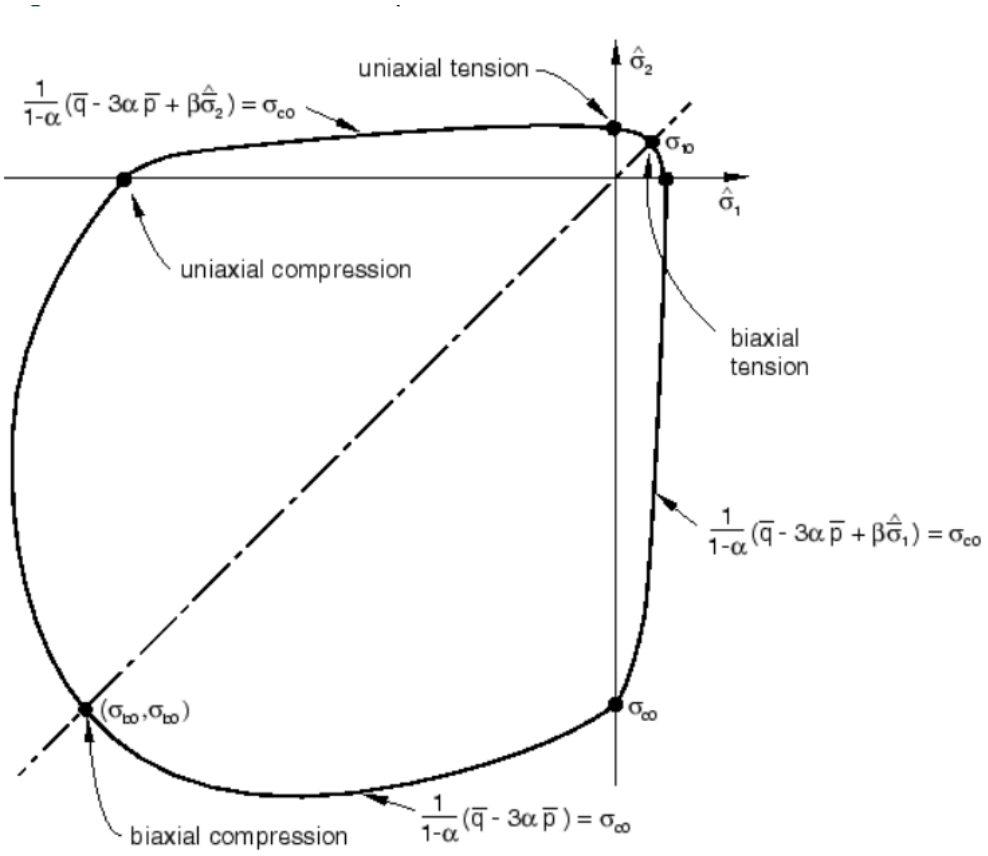

Figure 4-11 Yield Surface in Plane Stress (ABAQUS, 2017)

The non-associated potential plastic flow is assumed for the concrete damage plasticity model. The use of the concrete damage plasticity results in a nonsymmetrical material stiffness matrix since the plastic flow is non-associated. Therefore, the unsymmetrical matrix storage and solution scheme should be used. The Drucker-Prager hyperbolic function is adopted to calculate the flow potential, G, for the concrete damage plasticity model.

$$G = \sqrt{(\in \sigma_{t0} tan\varphi)^2 + \bar{q}^2} - \bar{p} tan\varphi \qquad \text{Equation 4-15}$$

Where

φ= Dilation angle measured in the p-q plane which is 36 degrees in this study

σ_{t0}=Uniaxial tensile stress at failure which is 0.474 ksi in this study

ϵ= Eccentricity parameter which defines the rate at which the function approaches the asymptote (the flow potential tends to a straight line as the eccentricity tends to zero). In this study, 0.1 was adopted.

4.3.4 Modeling of Steel Material

Like the concrete constitutive model, the linear elastic model for steel in this study was defined by using two parameters as well, Young's modulus and Poisson's ratio. The Young's Modulus in this study is 29,000 ksi and the Poisson's ratio is 0.3. Both two parameters were selected based on the default A615Gr60 steel material property in SAP2000 to correlate with SAP model. The ABAQUS/CAE modelling tool was used to simulate inelastic behavior for steel reinforcement bars by using the metal plasticity model. The metal plasticity model was applied to both longitudinal and transverse reinforcement bars in this study.

4.3.4.1 Steel Stress-Strain Curve

Steel for reinforcement bars were considered to have a linear elastic behavior at low strain levels, less than 0.0021. However, at higher strain levels, nonlinear plastic behavior is considered. The steel plastic behavior was controlled by the steel stress-strain curve which is required by ABAQUS to complete the steel constitutive model. There are four different portions to describe the stress-strain relationship curve in this study, linear elastic portion, flat yielding portion, nonlinear hardening portion and linear strength loss portion. The transition from elastic portion to inelastic potion occurs at the yield point which is (0.0021, 60) on the material stress-strain curve. The behavior of the steel prior to reaching the yield point creates only elastic strains which are fully recoverable while permanent deformation starts to occur when the steel exceeds the yield strain. Figure 4-12 shows the stress-strain curve for steel in the ABAQUS model. The

method to define the plasticity for metal plasticity model in ABAQUS is very similar to the concrete damage plasticity model.

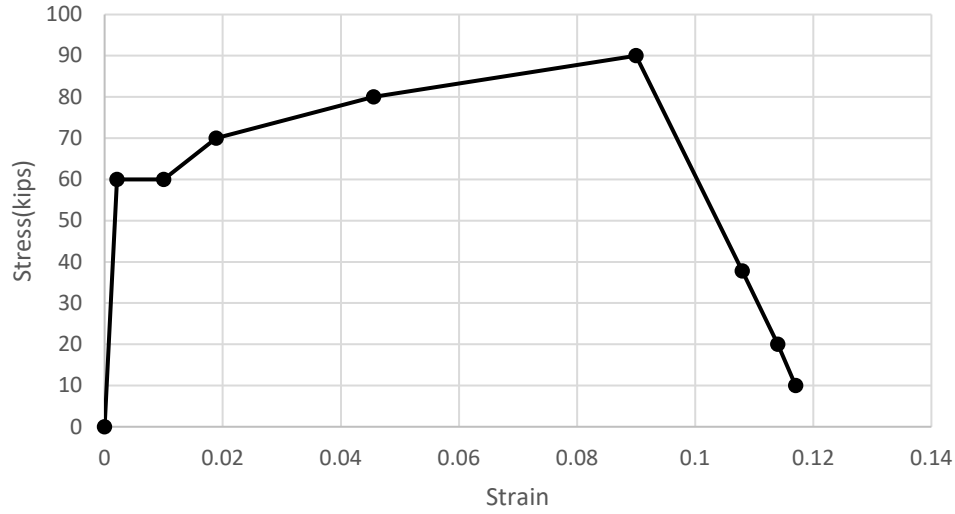

Figure 4-12 Stress-Strain Curve for Steel in Compression and Tension

4.3.4.2 Yield Function and Plastic Flow for Steel Material

Several different models were provided by ABAQUS for metal plasticity analysis. The main options are a choice between rate-independent and rate-dependent plasticity, a choice between the Mises yield surface for isotropic materials and Hill's yield surface for anisotropic materials, and for rate-independent modeling a choice between isotropic and kinematic hardening. In this study, rate-independent plasticity, Mises yield surface and isotropic hardening were chosen.

The reason for choosing rate-independent plasticity is because the pushover analysis in this study is always under the normal temperature and low strain rates condition. The rate-independent metal plasticity model uses associated plastic flow. Therefore, as the metal yields, the inelastic deformation rate is in the direction of the normal to the yield surface.

Mises yield surface theory is established based on the assumption that yielding of the metal is independent of the equivalent pressure stress. The Mises yield surface is used to define isotropic yielding. It is defined by the uniaxial stress-strain curve above. A detailed definition can be

found in (Boresi & Schmidt, 2003). Figures 4-13 and 4-14 show the yield surface in principal stress space and yield surface for biaxial stress state, respectively.

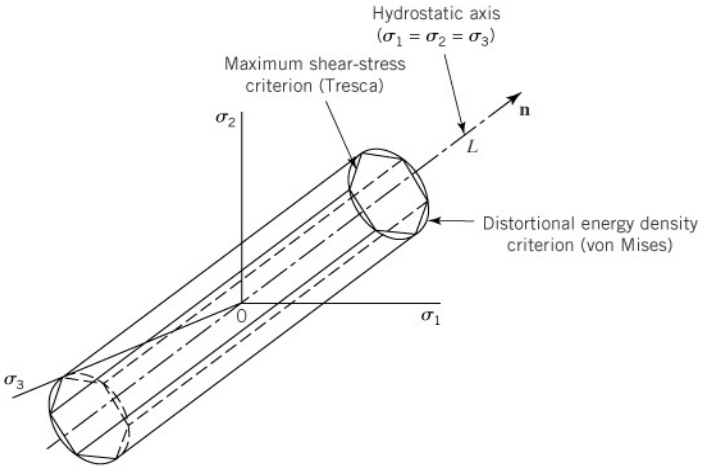

Figure 4-13 Yield Surface in Principal Stress Space (Boresi & Schmidt, 2003)

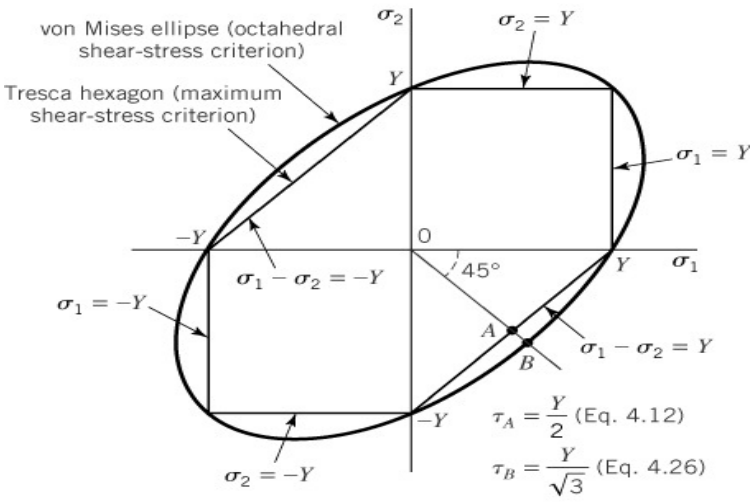

Figure 4-14 Yield Surface for Biaxial Stress State (Boresi & Schmidt, 2003)

The kinematic hardening model is usually used to do dynamic analysis for metal materials. However, in this displacement controlled pushover analysis, the displacement increments are very small which can be considered as an equivalent static analysis. Therefore, isotropic

hardening was adopted in this case. Isotropic hardening means that the yield surface changes size uniformly in all directions.

4.3.5 Loading and Boundary Condition

As shown in Figure 4.1, bridge columns are continuous at the bent cap and foundation cap (or drilled shaft transition) on both sides directly while the bent cap and foundation are free to move longitudinally and transversely with the restraint from the superstructure and piles or drilled shafts. Therefore, in the pushover analysis model, the bottom of the column is fixed for all six degrees of freedom including all translational and rotational degrees of freedom. For the top of column, the boundary condition is almost the same as at the bottom of the column except the z translational degree of freedom was released. An imposed displacement was added to the top of column in the x direction to capture the material softening behavior correctly. Since the x translational degree of freedom was fixed, a reaction force will be generated after imposing a displacement in that direction. For the highway bridge, axial load on the top of bridge column based on bridge dead load is typically less than $0.1f'_cA_g$, where f'_c is concrete compressive strength and A_g is bridge column gross area. An axial force of $0.1f'_cA_g$ is applied on the top of some models to evaluate the effect of axial force in the column pushover analysis. Although there is no axial force term in the equation on the AASHTO code to calculate the column displacement capacity based on Equations 4.4 and 4.5, it is still necessary to know how big the influence on the displacement capacity will be by adding an axial force to the column.

4.3.6 Analysis Method

Both the general static method and RIKS method are used in this study depending on the situation. The ‘NLgeom’ option was selected for both of these two methods to capture the large displacement effect. The RIKS method was also selected in this column pushover analysis

because the General static method in ABAQUS might not handle the concrete tension behavior well which might cause convergence problems. The RIKS method is generally used to predict the unstable and nonlinear collapse of an element or structure. In the RIKS method, the load or displacement increments will be applied proportionally in several steps. In each load step the equilibrium iteration is performed and the equilibrium path is tracked for each load or displacement step. This method is widely used in static analysis for concrete and proved to be a good method for nonlinear analysis, especially for the brittle, unconfined concrete. However, the RIKS method usually require more computational time and resources compared with the general static method in ABAQUS. Moreover, convergence problems are often encountered when material damage and failure are included and thus the ultimate load could not be achieved.

4.4 SAP Fiber Hinge Modelling

Besides using solid elements to model reinforced concrete columns directly, many other simplified methods have been developed and verified to do pushover analysis with second order effect for reinforcement concrete columns including fiber model which can only account normal stress and strain for the fibers in the cross section. There are two major fiber modelling strategies adopted by previous research. One is the fiber model with distributed plasticity and the other one is the fiber model with lumped plasticity. Figure 4-15 shows the analytical fiber model with distributed plasticity or lumped plasticity for pushover analysis in this study. In the fiber model with distributed plasticity, a reinforced concrete column is discretized into finite elements. The cross section is divided into fibers for each finite element. The fiber model with distributed plasticity can capture the change of stress and strain for each individual fiber throughout the cross section and along the column length (Wang, Zhang, & Hao, 2010). Although the fiber model with distributed plasticity has been proved to be a comprehensive model to do nonlinear

analysis, it still requires a large amount of computational time and resources to complete a nonlinear analysis on complicated models. Compared with the fiber model with distributed plasticity, the fiber model with lumped plasticity which is equivalent to a fiber hinge model is much simpler and more efficient to be analyzed using nonlinear analysis. In the fiber hinge model, the material nonlinear behavior is represented by two plastic hinges which are located at or near the two ends of a column or in another location where inelastic behavior is expected. The properties of these two plastic hinges are defined based on the cross section with fibers, while the length of the plastic hinge is defined by an analytical length which can be calculated by Equation 4-6. The middle portion of the column will be defined with elastic elements which means fiber cross sections are not required for this portion. The simplified model is proven to be sufficiently accurate for practical designs. In addition, it requires fewer elements compared with the fiber model with distributed plasticity and the solid model. However, shear stress limit states would not be included in the analytical model, and the yield surface is not accurate for all the fibers (Kim, Park, & Choi, 2001).

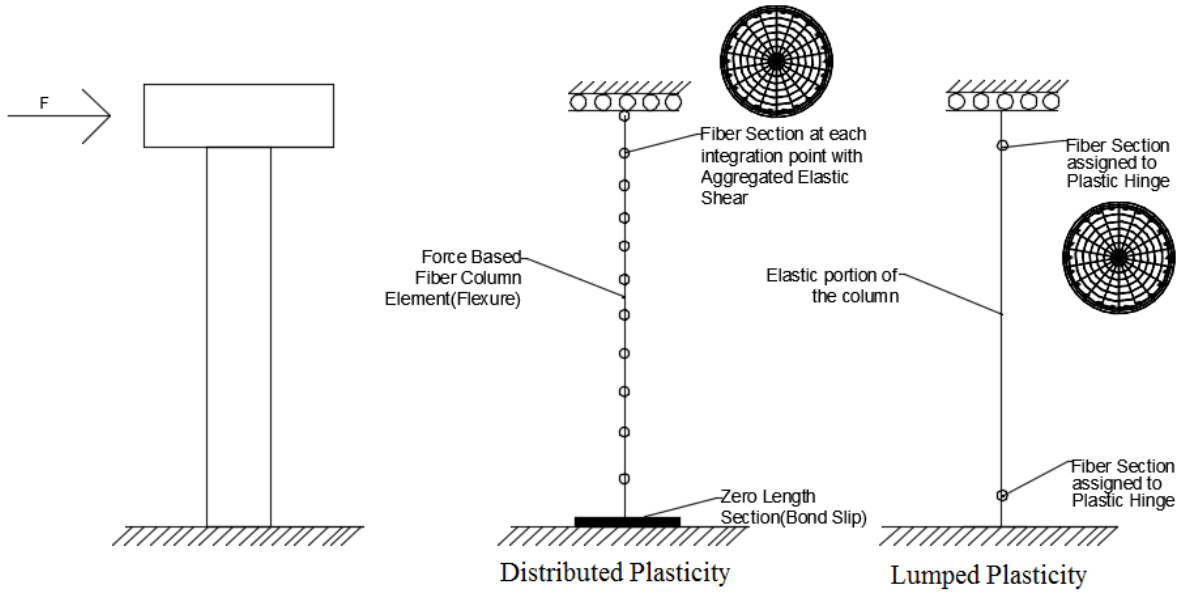

Figure 4-15 Analytical Fiber Model with Distributed Plasticity or Lumped Plasticity

Although the fiber model with distributed plasticity is more accurate, it requires more computational time and resources as well. Compared with the fiber model with distributed plasticity, the plastic hinge model is simpler with less accuracy which is still good enough to estimate the column pushover behavior. Therefore, the plastic hinge model was selected to conduct the column pushover analysis to take advantage of computational efficiency by using SAP2000 (CSI., 2011). All the geometry and reinforcement related to the columns modeled in SAP2000 are shown in Table 4-3. The model name system is similar to the ABAQUS models, where "A" was replaced by "S" to represent SAP model.

Table 4-3 Column Geometry and reinforcement details information for SAP2000 Model

Model Name	Column Diameter (ft)	Column Height (ft)	Longitudinal Reinforcing Bars and Ratio	Axial Force (kip)	Plastic Hinge Zone Length(in)	Transverse Reinforcing Spacing (middle, PHZ) (in)
S044016_612_0	4	40	16 #9 [0.88%]	0	29.35	12, 6
S044016_612_a	4	40	16 #9 [0.88%]	724	29.35	12, 6
S044032_612_0	4	40	32 #9 [1.77%]	0	29.35	12, 6
S044032_612_a	4	40	32 #9 [1.77%]	724	29.35	12, 6
S044044_612_0	4	40	44 #11 [3.79%]	0	31.89	12, 6
S044044_612_a	4	40	44 #11 [3.79%]	724	31.89	12, 6
S043016_612_0	4	30	16 #9 [0.88%]	0	24.55	12, 6
S043016_612_a	4	30	16 #9 [0.88%]	724	24.55	12, 6
S043032_612_0	4	30	32 #9 [1.77%]	0	24.55	12, 6
S043032_612_a	4	30	32 #9 [1.77%]	724	24.55	12, 6
S043044_612_0	4	30	44 #11 [3.79%]	0	27.09	12, 6
S043044_612_a	4	30	44 #11 [3.79%]	724	27.09	12, 6
S2.51008_612_0	2.5	10	8 #9 [1.13%]	0	14.95	12, 6
S2.51008_612_a	2.5	10	8 #9 [1.13%]	283	14.95	12, 6
S2.51012_612_0	2.5	10	12 #11 [2.59%]	0	17.49	12, 6
S2.51012_612_a	2.5	10	12 #11 [2.59%]	283	17.49	12, 6
S2.51016_612_0	2.5	10	16 #11 [3.53%]	0	17.49	12, 6
S2.51016_612_a	2.5	10	16 #11 [3.53%]	283	17.49	12, 6
S2.51008_412_0	2.5	10	8 #9 [1.13%]	0	14.95	12, 4
S2.51008_412_a	2.5	10	8 #9 [1.13%]	283	14.95	12, 4
S2.51012_412_0	2.5	10	12 #11 [2.59%]	0	17.49	12, 4
S2.51012_412_a	2.5	10	12 #11 [2.59%]	283	17.49	12, 4

S2.51016_412_0	2.5	10	16 #11 [3.53%]	0	17.49	12, 4
S2.50816_412_a	2.5	10	16 #11 [3.53%]	283	17.49	12, 4
S2.50808_612_0	2.5	8	8 #9 [1.13%]	0	13.99	12, 6
S2.50808_612_a	2.5	8	8 #9 [1.13%]	283	13.99	12, 6
S2.50812_612_0	2.5	8	12 #11 [2.59%]	0	16.53	12, 6
S2.50812_612_a	2.5	8	12 #11 [2.59%]	283	16.53	12, 6
S2.50816_612_0	2.5	8	16 #11 [3.53%]	0	16.53	12, 6
S2.50816_612_a	2.5	8	16 #11 [3.53%]	283	16.53	12, 6
S2.50808_412_0	2.5	8	8 #9 [1.13%]	0	13.99	12, 4
S2.50808_412_a	2.5	8	8 #9 [1.13%]	283	13.99	12, 4
S2.50812_412_0	2.5	8	12 #11 [2.59%]	0	16.53	12, 4
S2.50812_412_a	2.5	8	12 #11 [2.59%]	283	16.53	12, 4
S2.50816_412_0	2.5	8	16 #11 [3.53%]	0	16.53	12, 4
S2.50816_412_a	2.5	8	16 #11 [3.53%]	283	16.53	12, 4

4.4.1 Element Type and Mesh

According to previous research, the fiber hinge model has proven to be a reliable numerical simulation method for nonlinear analysis. Figure 4-15 shows that it is developed by using a linear elastic beam system including two plastic fiber hinges which contain material uniaxial constitutive models. SAP2000 was selected to conduct the bridge column pushover analysis since it can introduce the fiber plastic hinge model into the analysis by using a “Fiber PMM Hinge”. For the linear elastic beam element which is the middle portion of column, beam elements with correct column cross section properties were used while the mesh of these beam elements was automatically done by SAP2000. For the plastic fiber hinge portion which represents two plastic hinge zones on the column, the ductile “Fiber PMM Hinge” based on the fiber cross section was used in this study. The detailed cross section including concrete and longitudinal reinforcement was modelled through the section designer in SAP2000. The detailed cross sections were divided into multiple fibers which are enough to reasonably match with the cross section exact integration curve. Figure 4-16 shows a typical bridge column fiber cross section.

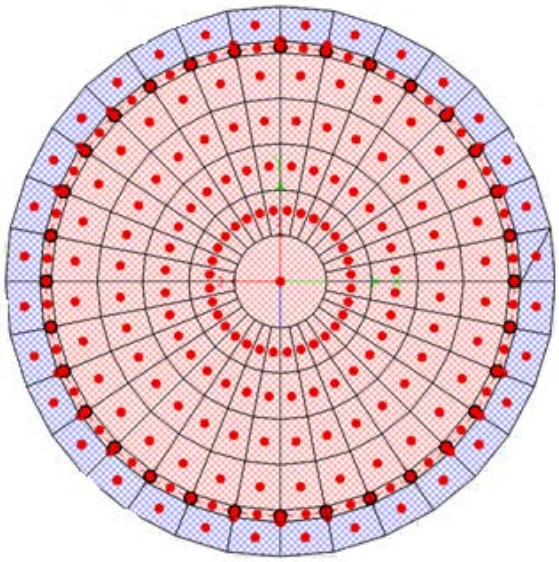

Figure 4-16 Bridge Column Fiber Cross Section

There are three aspects that need careful attention to do fiber modelling: cross section division, fiber hinge length and material constitutive model. Cylindrical coordinates were used to divide the cross section into fibers. For the example column cross section, there are 32 fibers in the tangential direction and 6 fibers in the radial direction. Each red point in the cross section represents an integration point of an individual fiber. Each longitudinal reinforcement bar is one individual fiber. The purple part of cross section is the unconfined concrete which is also known as concrete cover. The red part of cross section is the confined concrete which was defined using the Mander concrete model with confinement. Transverse reinforcement bars are not included in the fiber hinge model directly since the Mander concrete model can include the confinement effect caused by transverse reinforcement bars indirectly. The mechanical response of each fiber is characterized by a uniaxial stress-strain relationship of concrete and steel while the deformation coordination between the fibers is described by the plane section assumption. Therefore, the exact integration and fiber model moment curvature can be calculated. Figure 4-

17 shows the exact integration and fiber model moment curvature for the example bridge column.

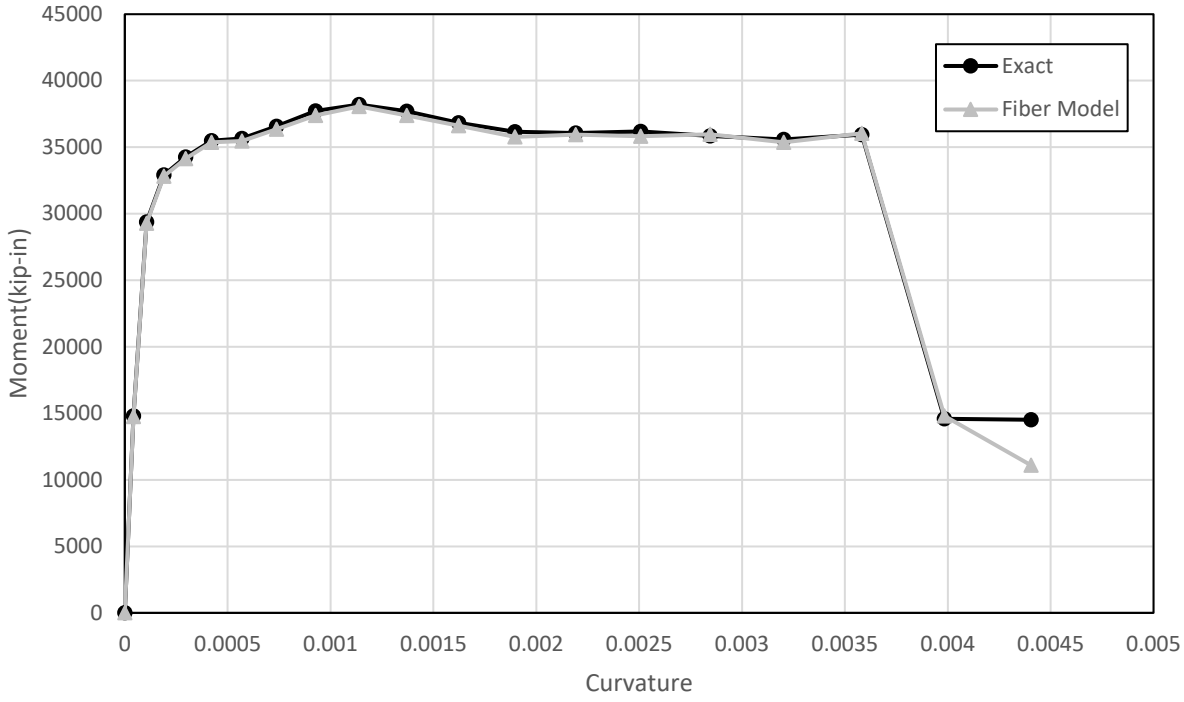

Figure 4-17 Exact Integration and Fiber Model Moment Curvature for Example Bridge Column

4.4.2 Modelling of Concrete Material

Like the ABAQUS concrete constitutive model, both linear elastic and nonlinear plastic concrete models are considered for pushover analysis. The linear elastic model of concrete was the same as the elastic material property in ABAQUS. The Young's modulus in this study is 3,605 ksi and the Poisson's ratio is 0.2. For concrete inelastic behavior, the SAP2000 modelling tool was used to define the concrete stress-strain curve. However, the Drucker-Prager parameter including friction angle and dilation angle cannot be considered in the fiber hinge model since the fibers in the bridge column cross section are all axial fibers which cannot account for the shear stress and strain during the coupled axial and biaxial bending behavior in frame elements.

4.4.2.1 Concrete Stress-Strain Curve

In this study, the uniaxial stress-strain curve was also established based on the Mander concrete theory (Mander, Priestley, & Park, 1984). For the unconfined concrete, the uniaxial stress-strain curve in tension and compression is exactly same as in the ABAQUS model based on Figures 4-6 and 4-8. However, for the confined concrete, the uniaxial stress-strain curve in tension is same as the unconfined concrete while the effect of transverse reinforcement needs to be considered in the compressive uniaxial stress-strain curve since the transverse rebar are not modeled directly in the fiber hinge model. Figure 4-18 shows the Mander confined concrete stress-strain curve. The Mander confined concrete stress-strain curve is defined by the following equations:

$$f = \frac{f'_{cc} x r}{r - 1 + x^r} \qquad \text{Equation 4-16}$$

Where

$$\varepsilon'_{cc} = \{5\left(\frac{f'_{cc}}{f'_c} - 1\right) + 1\}\varepsilon'_c$$

$$x = \varepsilon / \varepsilon'_{cc}$$

$$E_{sec} = \frac{f'_{cc}}{\varepsilon'_{cc}}$$

$$r = \frac{E}{E - (f'_c / \varepsilon'_c)}$$

Where

ε= Concrete strain

f= Concrete stress (ksi)

E= Modulus of elasticity (ksi)

E_{sec}= Secant modulus of elasticity (ksi)

f'_c= Concrete compressive strength of unconfined concrete (ksi)

f'_{cc}= Compressive strength of confined concrete which is dependent on the confinement steel provided in the section (ksi)

ε'_c= Concrete strain at f'_c

ε_u= Ultimate concrete strain capacity for unconfined concrete and concrete spalling strain for confined concrete

ε'_{cc}= Concrete strain at f'_{cc}

ε_{cu}= Ultimate concrete strain capacity for confined concrete which is dependent on the confined steel provided in the section

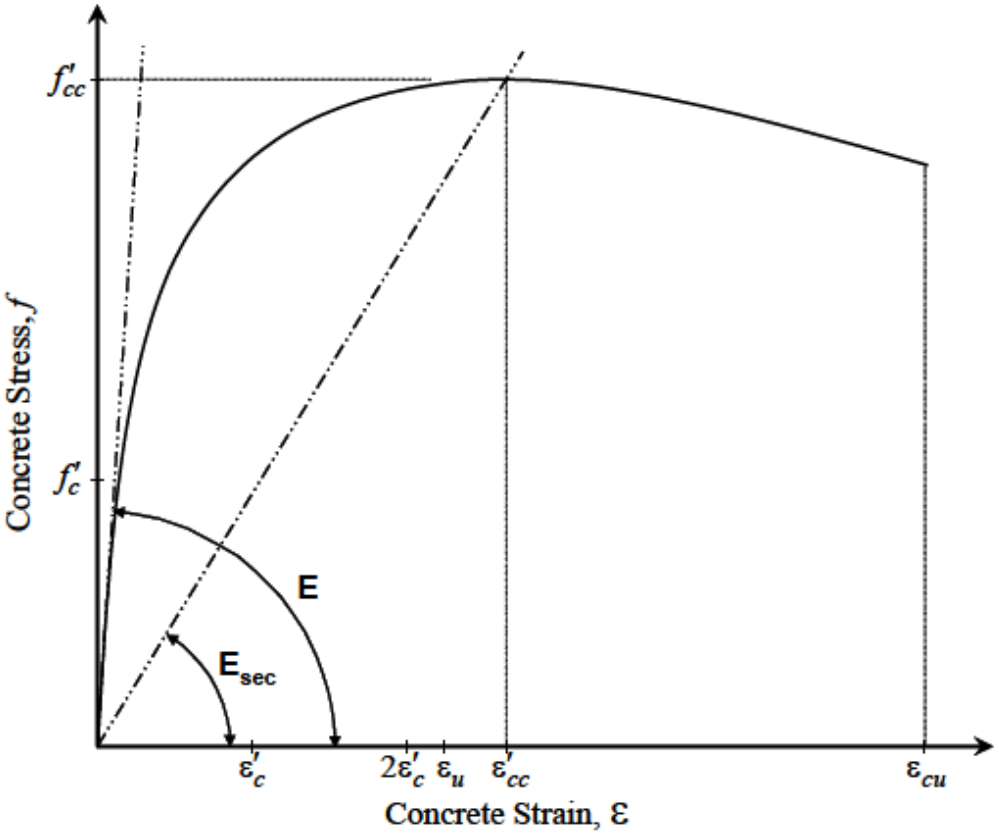

Figure 4-18 General Confined Concrete Stress-Strain Curve (CSI., 2011)

Figure 4-19 shows the comparison between the unconfined and confined stress-strain curves in compression for the example bridge column.

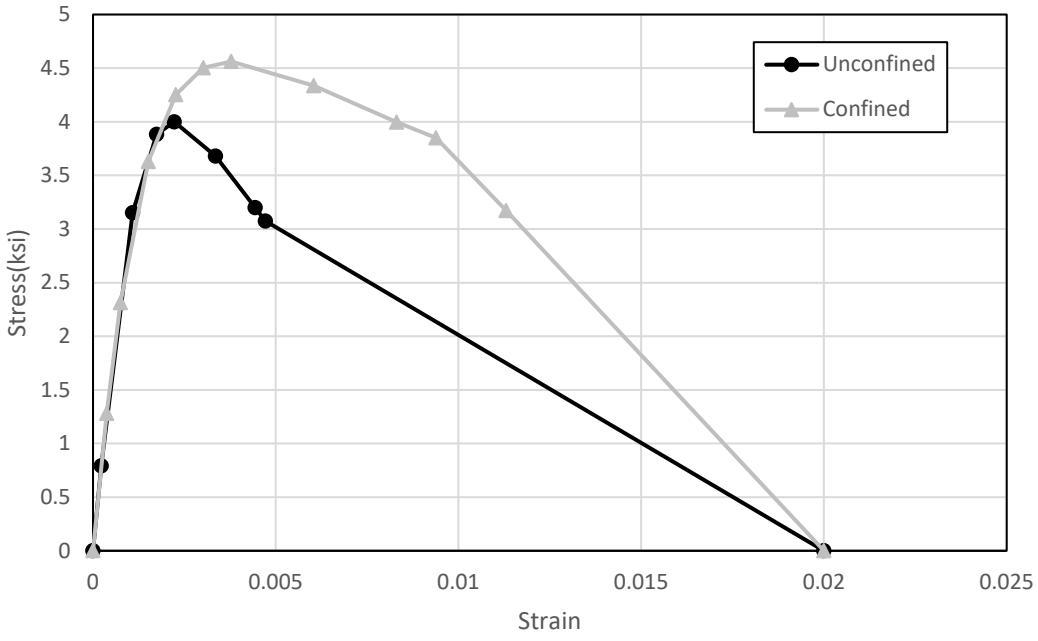

Figure 4-19 Comparison between Unconfined and Confined Stress-Strain Curve in Compression

4.4.3 Modelling of Steel Material

Like the ABAQUS steel constitutive model, the linear elastic model for steel in this study was defined by using two parameters as well, Young's modulus and Poisson's ratio. The Young's modulus in this study is 29,000 ksi and the Poisson's ratio is 0.3. For steel inelastic behavior, the SAP2000 modelling tool was used to define the steel stress-strain curve which is exactly the same as that in ABAQUS according to Figure 4-12.

4.4.4 Interaction Surface

Since all the fibers in the cross section are axial fibers which are one dimensional fibers, a material yield surface is not required in the fiber hinge model. All the fibers' stress-strain behavior will strictly follow the trace of the predefined material stress-strain curves. For the column which will have a flexural yielding in pushover analysis, a column interaction surface

which combines axial force and bending moment is the best way to describe the column capacity. Figure 4-20 and 4-21 show the 2D column interaction curve and 3D column interaction surface for an example bridge column, respectively. The purple line in the 3D interaction surface represents one of the 2D interaction curves.

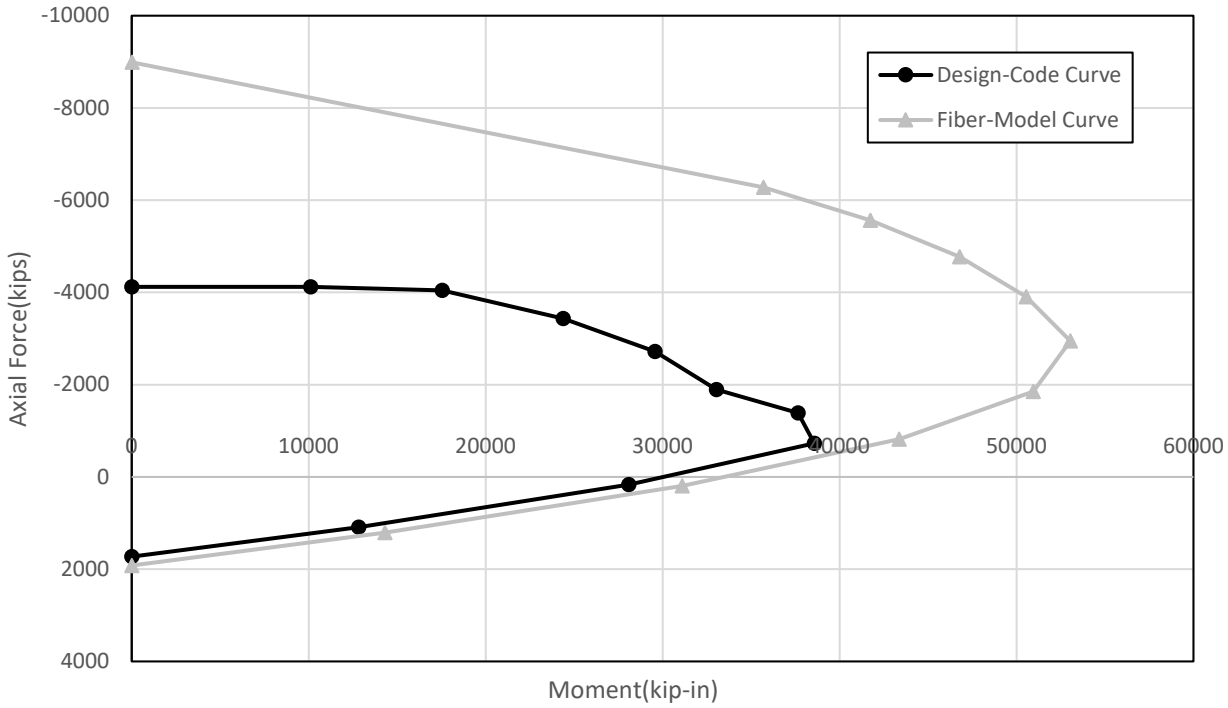

Figure 4-20 2D Column Interaction Curve

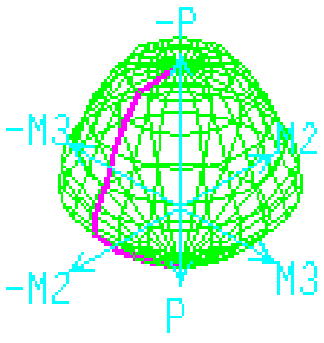

Figure 4-21 3D Column Interaction Surface

4.4.5 Loading and Boundary Condition

Since the force-based pushover analysis instead of displacement based pushover analysis was applied in the SAP model, the boundary conditions in the SAP model were not the same as those in ABAQUS model. The SAP model is restrained in all six degrees of freedom including all translational and rotational degrees of freedom on the bottom of columns while it is only rotationally restrained on the top of column. All the nodes on the top of the column can move translationally in the x, y and z direction without any restraint. A lateral force was added to the top of column to capture the column pushover behavior to compare the results from ABAQUS. An axial force of $0.1f'_cA_g$ is also applied on the top of some models to evaluate the effect of axial force in the column pushover analysis.

4.5 Local Displacement Capacity from Pushover Curve for SDCs B and C

Significant efforts have been completed in the past years to develop the methodology of displacement-based seismic design. Based on the AASHTO guide specifications (AASHTO, 2011), the maximum local member displacement ductility is 2 for SDC B and 3 for SDC C, respectively. Therefore, the local displacement capacity for the columns in displacement-based seismic design is related to the estimates of yield displacement from pushover analysis. This section introduces a simple method to estimate the effective yield displacement for normal strength circular reinforced concrete bridge columns based on the moment curvature analyses of the column sections in the plastic hinge zone and pushover analyses of the whole column. This method will be used to find the yield displacement of circular reinforced concrete columns in the parametric study. In this study, the yield displacement is directly related with the cross section yield curvature. When the top or bottom cross section of the bridge column reaches its yield curvature, the corresponding displacement in the pushover curve will be considered as the yield

displacement. There are different definitions of yield curvature which can be found based on previous research. In seismic design practice for columns, effective yield curvature is more important than true yield curvature (Priestley, Ranzo, Benzoni, & Kowalsky, 1996). In Priestley et. al (1996), the effective yield curvature, ϕ_y, is calculated by extrapolating the first yield curvature, ϕ_y', to the nominal strength, M_n. The first yield curvature in this study is defined as the point when the first longitudinal rebar in the column reaches steel yield strain which is 0.002. Figure 4-22 shows the definition of the yield curvature for the example bridge column.

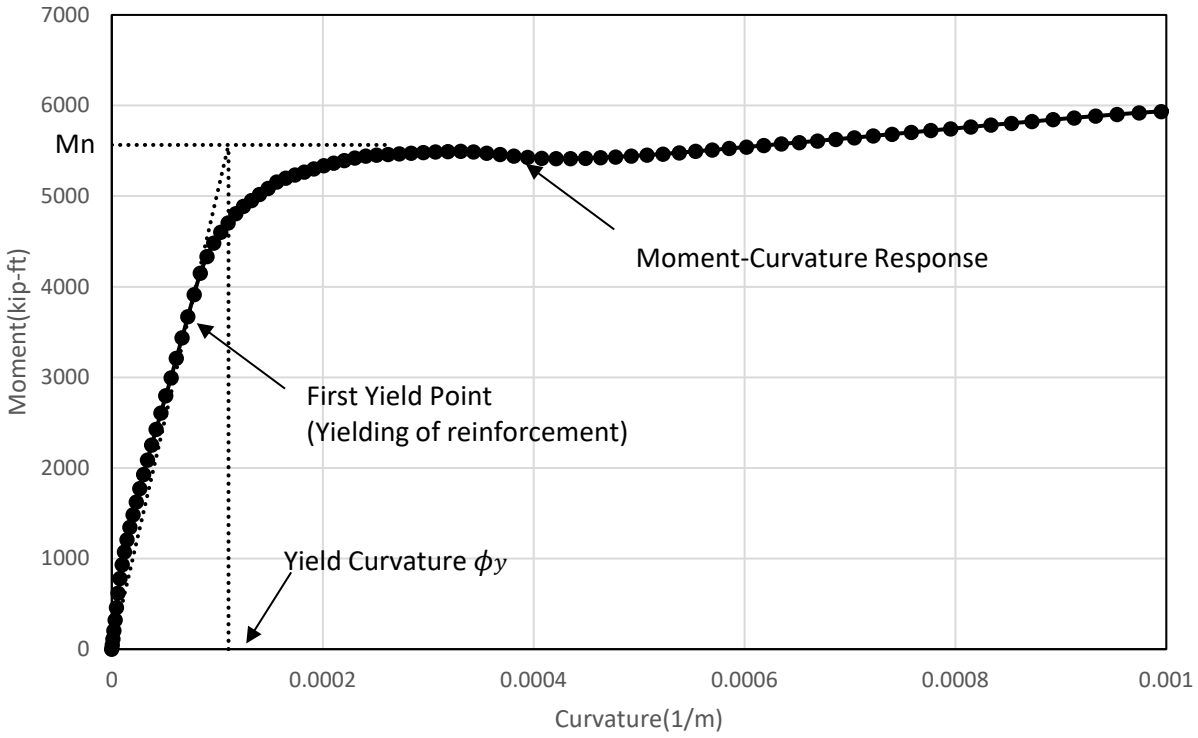

Figure 4-22 Definition of yield curvature for circular bridge column

Based on the definition of yield curvature for a circular bridge column, yield curvature can be calculated by using the moment-curvature response. In addition, a parametric study has been done on more than 200 columns, algebraic expressions have been developed below for estimating effective yield curvature (Sheikh, Tsang, McCarthy, & Lam, 2010).

$$\phi_y = 2.0 \times \frac{\varepsilon_{ys}}{D^{1.1}} \times MF(f_c') \times MF(n) \times MF(\rho) \qquad \text{Equation 4-17}$$

$$MF(f_c') = 1.25 \times f_c'^{-0.07}$$

$$MF(n) = 1 + (0.041 \times f_c' - 0.26) \times n - (0.043 \times f_c' + 0.85) \times n^2$$

$$MF(\rho) = \rho^{0.16}$$

ϕ_y= Yield Curvature (1/m)

ε_{ys}= Steel Yield Strain

D= Bridge Column Cross Section Diameter (m)

f_c'= Concrete Compressive Strength (Mpa)

n=Axial force ratio

ρ= Longitudinal Reinforcement Ratio

The yield curvature in these equations above are directly related with the column cross section diameter, steel yield strain, concrete compressive strength, axial force ratio and longitudinal reinforcement ratio. All this information can be found using the bridge column properties. Figure 4-23 shows the comparison between the calculated yield curvature and predicted yield curvature from the equations.

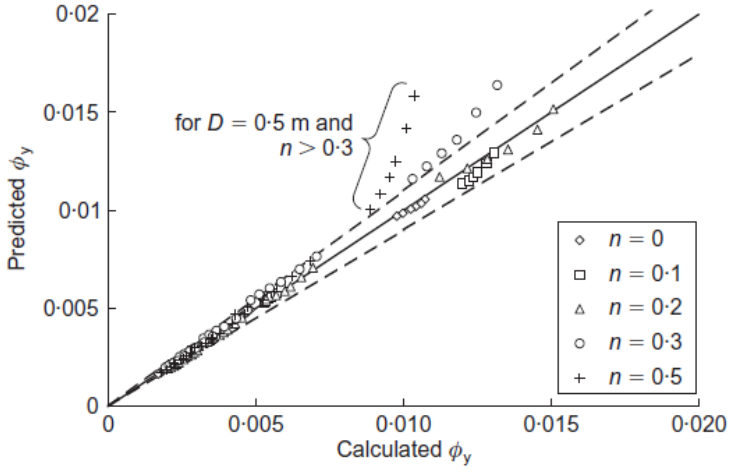

Figure 4-23 Comparison Between Calculated and Predicted Yield Curvature (Sheikh, Tsang, McCarthy, & Lam, 2010)

Figure 4-23 shows that the difference between the predicted values and calculated values of effective yield curvatures are within 10%. There are some special cases for the predicted values are significantly different from the calculated values. All the special cases are for 0.5 m diameter columns with axial load ratios between 0.3 and 0.5. However, in bridge design practice, a column which has diameter less than 2ft with an axial load ratio of 0.3 or more is not common and not applicable to this research.

After determining the yield curvature, the corresponding yield moment can be found according to the moment-curvature relationship. Then, the shear force at top and bottom of column corresponding with yield moment can be calculated by the formula below since the bridge columns are fixed at bottom while they are rotationally fixed on the top.

$$V_{yield} = \frac{M_{yield}}{H/2} \qquad \text{Equation 4-18}$$

V_{yield}= Yield Shear Force (kips)

M_{yield}=Yield Moment (kip-ft)

H= Bridge Column Height (ft)

In the end, the corresponding yield displacement can be read from the column pushover curve since the yield shear force has been calculated based on the yield moment which comes from the section moment curvature curve. The displacement capacity for SDC B and C can be calculated by the equations 4-19 and 4-20.

For SDC B:

$$\Delta_C^L = 2 \times \Delta_{yield} \qquad \text{Equation 4-19}$$

For SDC C:

$$\Delta_C^L = 3 \times \Delta_{yield} \qquad \text{Equation 4-20}$$

Based on Equations 4-4 and 4-5, the displacement capacity for SDC B and C is not related with the axial force and longitudinal reinforcement ratio which is not always true according to the method mentioned above. Therefore, a comparison between the specification value and ABAQUS model value of displacement capacity was conducted in this project to select the more accurate case to represent the model displacement capacity value for SDC B and C. Figures 4-24, 25 and 26 show the SAP and ABAQUS pushover curve with the Guide Specification (code) and ABAQUS model displacement capacity for a column which has a 4 ft diameter and a 40 ft height with lower limit, mid-range, and upper limit longitudinal reinforcement ratio, respectively. Lower limit reinforcement ratio means the ratio is close to the minimum reinforcement limitation (0.01) while upper limit reinforcement ratio means it is close to the maximum reinforcement limitation (0.04).

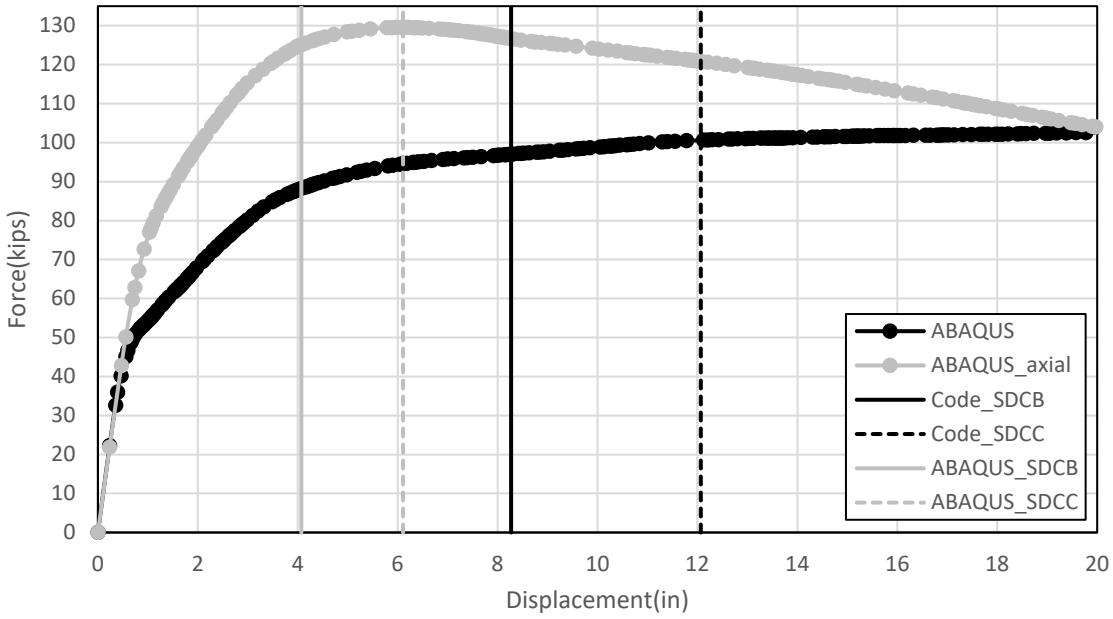

Figure 4-24 Pushover Curve for 4 ft Diameter and 40 ft Height Column with Lower Limit Reinforcement Ratio

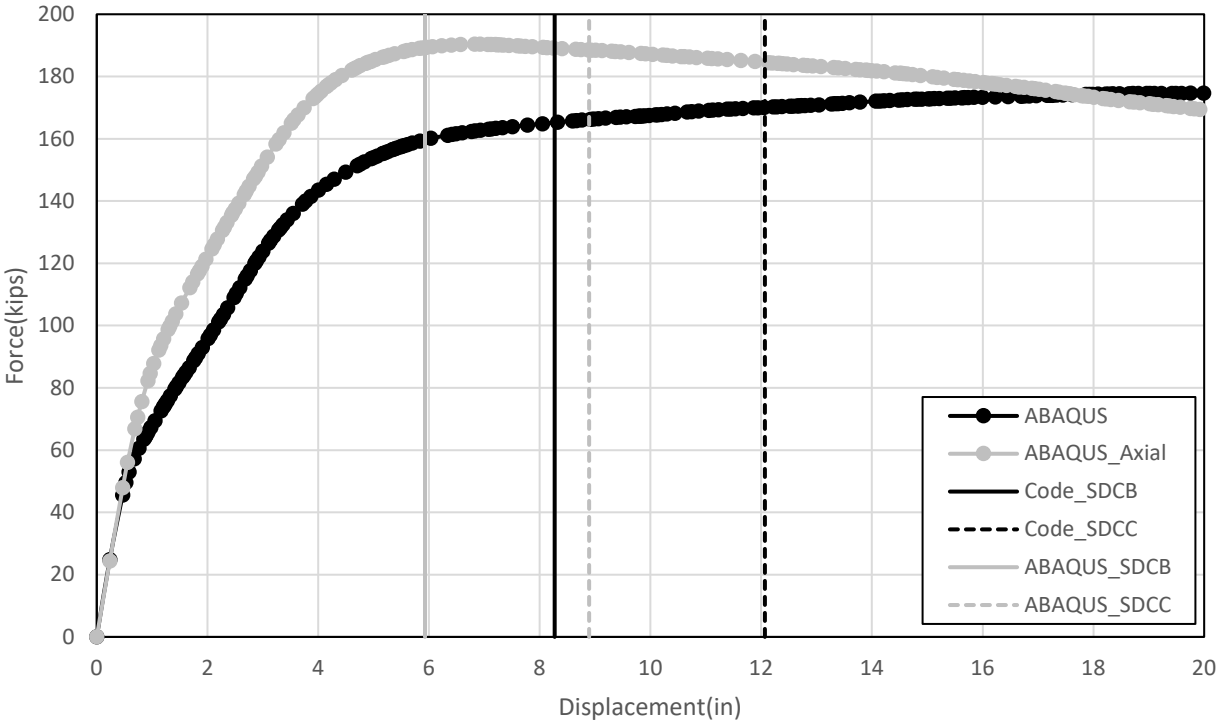

Figure 4-25 Pushover Curve for 4 ft Diameter and 40 ft Height Column with Mid-range Reinforcement Ratio

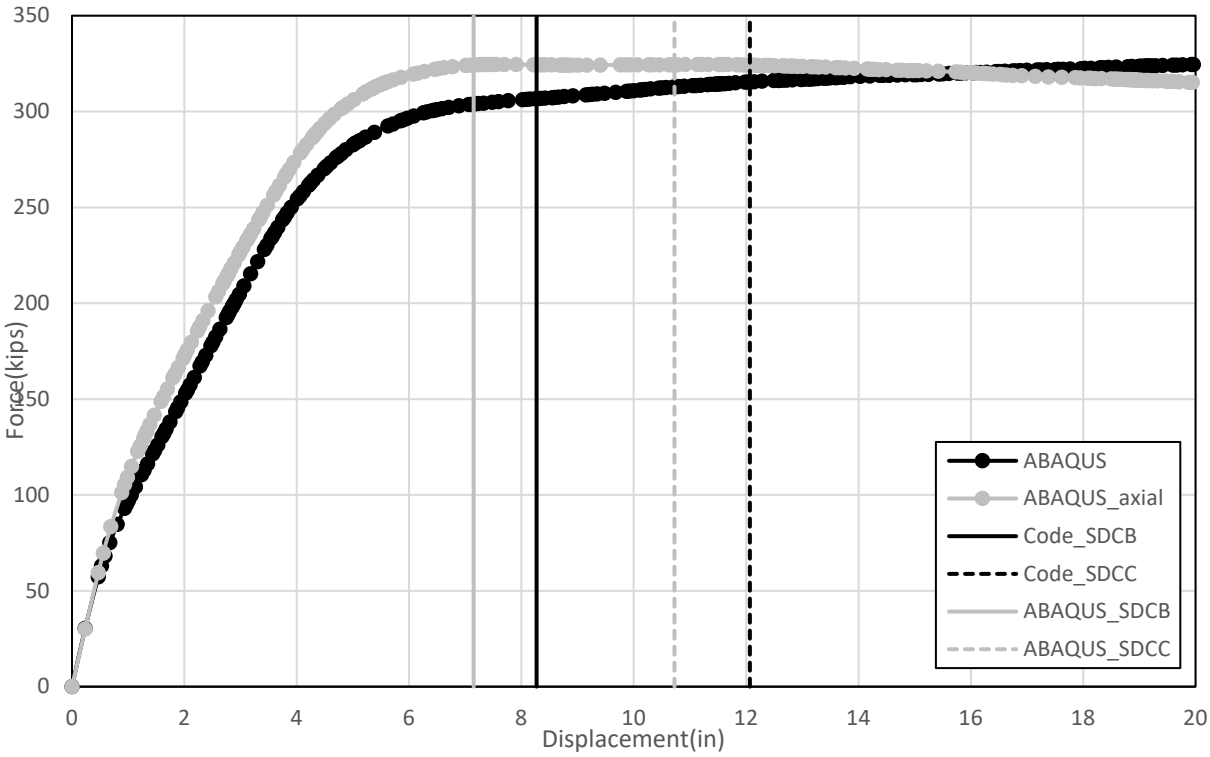

Figure 4-26 Pushover Curve for 4 ft Diameter and 40 ft Height Column with Upper Limit Reinforcement Ratio

According to the figures above, the black lines with round markers represent ABAQUS pushover curve without axial loading while the grey lines with round markers represent the ABAQUS pushover curve with axial loading ($0.1f'_cA_g$). The grey vertical solid lines and dashed lines represent the column displacement capacity for SDC B and C based on the ABAQUS pushover curve, respectively. The black vertical solid line and dashed line represent the column displacement capacity for SDC B and C based on AASHTO guide specification (AASHTO, 2011)(Equation 5.4 and 5.5). It can be found that the displacement capacity of a column with the large reinforcement ratio which is calculated by using ABAQUS pushover curve is closest to the displacement capacity calculated based on the AASHTO guide specification. Another comparison with a column which has a 4 ft diameter and 30 ft height with lower limit, mid-range, upper limit longitudinal reinforcement ratio has been done in this study. The results are shown in appendix A which indicates the same conclusion compared with the column which has 4 ft diameter and 40 ft height. Therefore, the displacement capacity of a column with the upper limit reinforcement ratio would represent the displacement capacity of all the columns which have the same cross section diameter and column height.

4.6 ABAQUS and SAP Model Comparison and Discussion

To compare the ABAQUS and SAP results, the bridge column pushover analysis curves conducted by these two programs are plotted in the same figures one by one. All the ABAQUS models were compared with the corresponding SAP models. For instance, the pushover curve of the A044016_612_0 model in this study is compared to the pushover curve of S044016_612_0 model which means the black line with round markers and grey line with round markers need to be compared with each other to represent the comparison between A044016_612_0 model and S044016_612_0 model. Figure 4-27 shows the program comparison of pushover curves for 2.5ft

diameter and 10ft height columns with the upper limit reinforcement ratio. The remaining pushover comparison curves can be found in Appendix A.

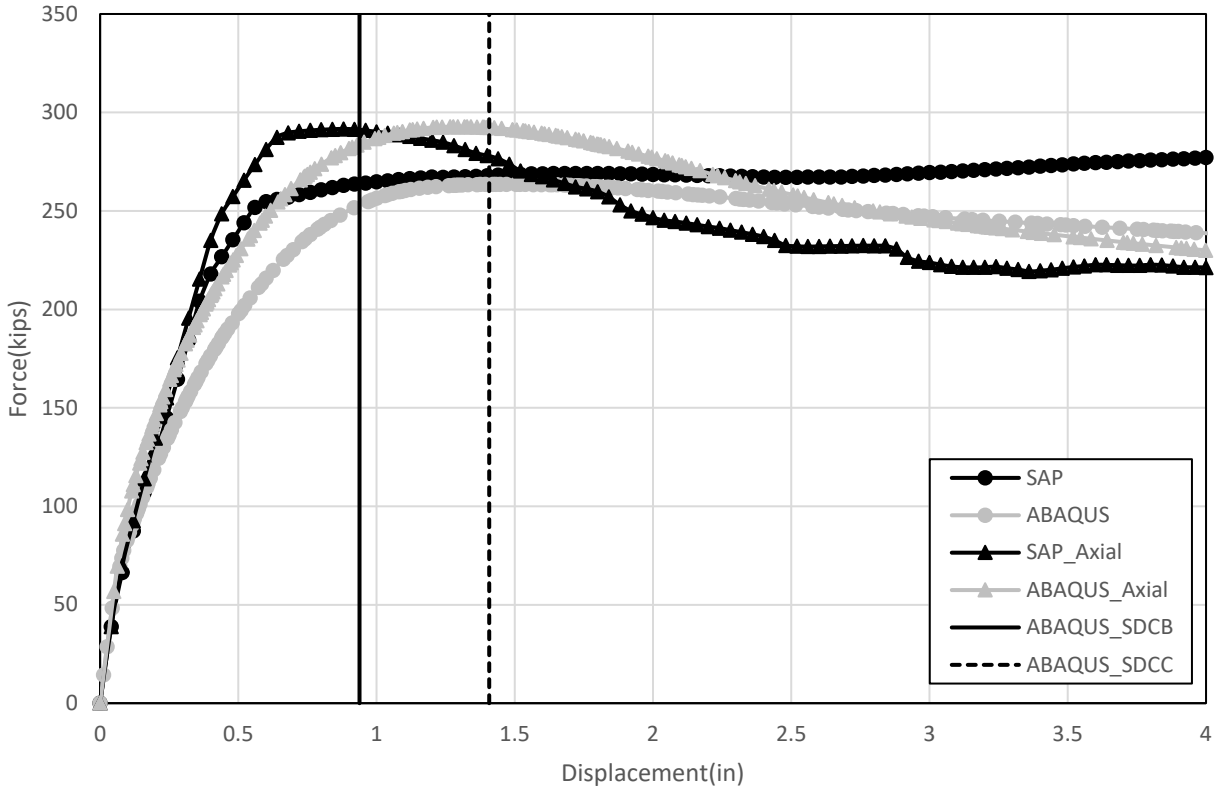

Figure 4-27 Pushover Curve for 2.5 ft Diameter and 10 ft Height Column with Upper Limit Reinforcement Ratio

In Figure 4-27, the black line with round markers which represents model S2.51016_612_0 which needs to be compared with the grey line with round markers which represents model A2.51016_612_0. The black line with triangular markers represents model S2.51016_612_a and needs to be compared with the grey line with triangular markers which represents A2.51016_612_a. These two comparisons look close enough to conclude that the SAP model and ABAQUS model correlate well with each other for this column's pushover analysis in the range of interest which is around the column displacement capacity for SDC B and C which are represented by vertical solid and dashed lines. In addition, a quantitative method to compare the difference between these two programs for the same pushover analysis was introduced in this

study which compares the difference of the shear strength at the column displacement capacity for SDC B and C defined by the columns with the upper limit reinforcement ratio. Table 4-4 shows the comparison in column shear strength at the displacement capacity point for SDC B and C. The difference in this table for SDC B and C is calculated by using the shear strength from the ABAQUS model divided by the shear strength in SAP model. Only columns which have aspect ratios larger than 4 were included in this table.

Table 4-4 Comparison of Column Shear Strength at Displacement Capacity Point for SDC B and C

Model	Shear Strength for SDC B (kips)	Shear Strength for SDC C (kips)	Model	Shear Strength for SDC B (kips)	Shear Strength for SDC C (kips)	Shear Strength Ratio for SDC B	Shear Strength Ratio for SDC C
S044016_612_0	87.00	94.20	A044016_612_0	95.92	99.60	1.10	1.06
S044016_612_a	121.29	118.47	A044016_612_a	128.80	122.90	1.06	1.04
S044032_612_0	158.57	168.45	A044032_612_0	163.27	168.63	1.03	1.00
S044032_612_a	185.05	182.29	A044032_612_a	190.28	186.20	1.03	1.02
S044044_612_0	295.57	307.68	A044044_612_0	303.91	312.81	1.03	1.02
S044044_612_a	314.56	313.92	A044044_612_a	324.32	324.46	1.03	1.03
S043016_612_0	115.61	124.73	A043016_612_0	132.21	136.31	1.14	1.09
S043016_612_a	168.60	168.17	A043016_612_a	153.42	154.08	0.91	0.92
S043032_612_0	211.68	223.89	A043032_612_0	211.32	226.70	1.00	1.01
S043032_612_a	254.30	254.10	A043032_612_a	265.27	262.14	1.04	1.03
S043044_612_0	396.35	411.59	A043044_612_0	401.30	411.42	1.01	1.00
S043044_612_a	429.99	431.01	A043044_612_a	443.71	453.57	1.03	1.05
S2.51008_612_0	105.32	109.33	A2.51008_612_0	119.53	119.63	1.13	1.09
S2.51008_612_a	161.92	158.52	A2.51008_612_a	161.99	161.20	1.00	1.02
S2.51012_612_0	217.81	222.00	A2.51012_612_0	214.81	222.12	0.99	1.00
S2.51012_612_a	251.22	250.80	A2.51012_612_a	252.00	257.51	1.00	1.03
S2.51016_612_0	263.78	267.89	A2.51016_612_0	253.65	263.44	0.96	0.98
S2.51016_612_a	291.00	277.88	A2.51016_612_a	284.52	292.22	0.98	1.05
S2.51008_412_0	105.22	109.32	A2.51008_412_0	119.43	120.20	1.14	1.10
S2.51008_412_a	162.33	159.73	A2.51008_412_a	162.83	161.78	1.00	1.01
S2.51012_412_0	218.01	222.22	A2.51012_412_0	214.80	222.15	0.99	1.00
S2.51012_412_a	251.71	251.94	A2.51012_412_a	253.99	260.41	1.01	1.03
S2.51016_412_0	264.12	296.11	A2.51016_412_0	257.83	269.44	0.98	0.91
S2.50816_412_a	294.33	290.33	A2.50816_412_a	290.01	300.75	0.99	1.04

Based on Table 4-4, all the differences of column shear strength at the displacement capacity point for SDC B and C between the SAP and ABAQUS models were less than 15%. What's more, most of the differences between these two programs are less 10% which means the SAP model and ABAQUS model are well correlated with each other in this study for the pushover analysis.

There are three different failure types in the column pushover analysis experimentally and numerically. They are flexural failure, flexure-shear failure and shear failure. Preventing brittle column failure is necessary to ensure structural safety since columns are always critical in the structure load path. Column failure will always affect the adjacent structural members which might cause progressive collapse of the entire structure. Column shear failures, in particular, should be prevented since it is a type of failure which is sudden and brittle failure, occurring with very little warning. Based on the UW-PEER database (UW & PEER, 2004), column failure type is highly related with the column aspect ratio, longitudinal reinforcement ratio and axial force ratio. The axial force ratio in this project is always less than 0.1 which are not common cases in the UW-PEER database. What's more, the axial force ratio is not included in the column displacement capacity equations in the AASHTO guide specification (AASHTO, 2011). Therefore, the axial force ratio would not be considered in the column failure type analysis and column parametric study later. However, axial force ratio, aspect ratio and longitudinal reinforcement ratio all have a significant influence on the column failure mechanism. It shows that columns which have higher aspect ratio with smaller longitudinal reinforcement ratio are most likely to have flexural failure while those which have lower aspect ratio with larger longitudinal reinforcement ratio are most likely to have shear failure in the column pushover analysis. The flexural shear failure is the middle failure type between the flexural failure and

shear failure. All the columns which have aspect ratio 3 or larger have flexural shear behavior in this database. Therefore, pushover analyses of columns which have aspect ratio 3.2 with various reinforcement ratio and columns which have aspect ratio 4 with various reinforcement ratio have been conducted in this study to find the marginal aspect ratio with various reinforcement ratios to ensure column failure mechanisms are flexural in the range of interest for the pushover analyses. Figure 4-28 shows the pushover curve for a 2.5 ft diameter and 10 ft height column with an upper limit reinforcement ratio.

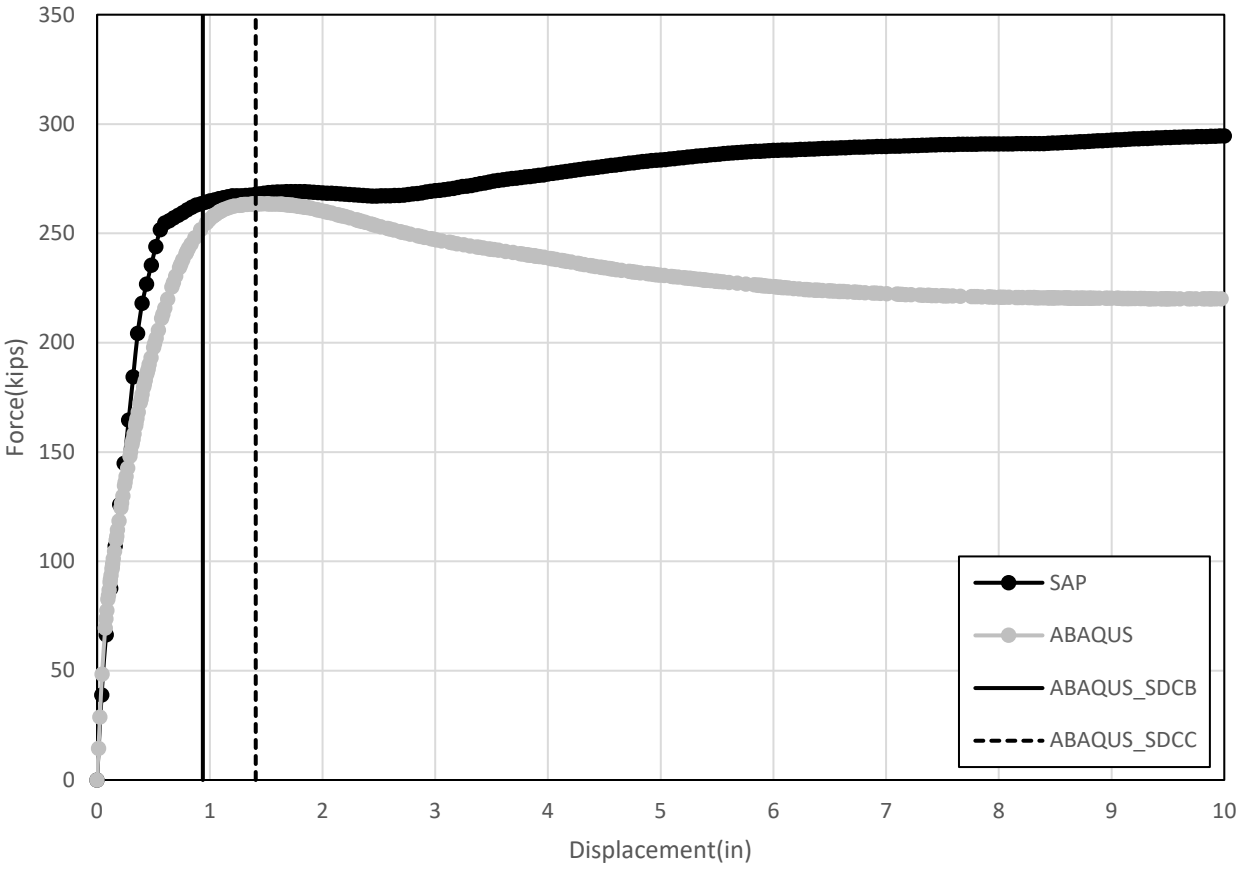

Figure 4-28 Pushover Curve for 2.5 ft Diameter and 10 ft Height Column with Upper Limit Reinforcement Ratio

Based on the figures above, the black line with round markers represents the SAP pushover curve without axial loading while the grey line with round markers represents the ABAQUS pushover curve without axial loading. These two pushover curves match up with each other in

the displacement range of interest (around vertical black solid and dashed lines) in this project. However, the shear strength in the SAP model had a positive post-yield behavior while the shear strength in ABAQUS model started to decrease after 2-inches of displacement. The reason for the difference is because the SAP model cannot account for the column shear behavior and the growth of the plastic hinge zone when the displacement became larger and larger. Figures 4-29 and 4-30 show the equivalent plastic strain contour (PEEQ) for 2.5ft diameter and 10ft height column with upper limit reinforcement ratio when displacement is equal to 1.41 in which is the SDC C displacement capacity for this column and 3 in which is beyond the range of interest in this project, respectively.

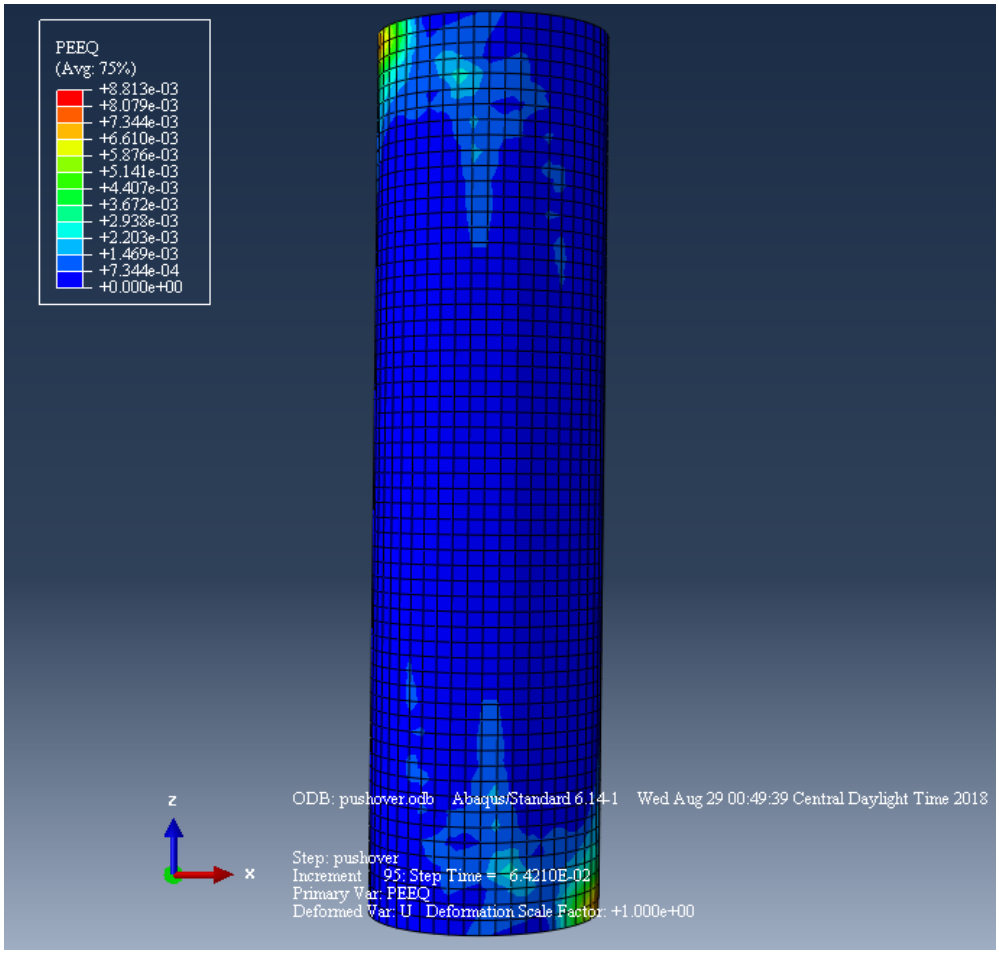

Figure 4-29 PEEQ for 2.5 ft Diameter and 10 ft Height Column with Upper Limit Reinforcement Ratio at 1.41 in of Displacement

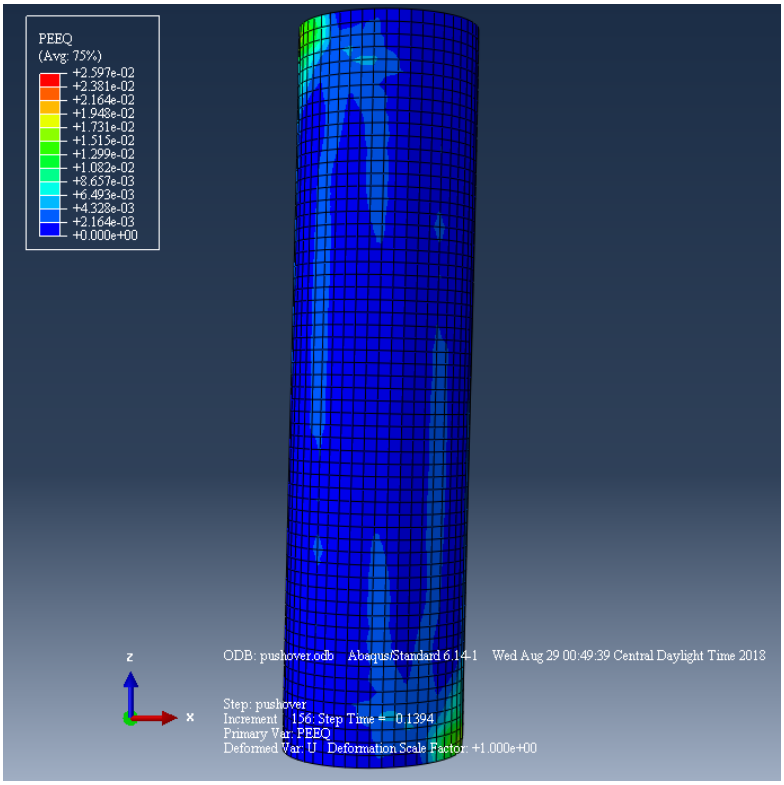

Figure 4-30 PEEQ for 2.5 ft Diameter and 10 ft Height Column with Upper Limit Reinforcement Ratio in 3 in of Displacement

According to Figure 4-29, flexural behavior was dominating the column pushover behavior. Two plastic hinges were formed in the top and bottom of the column. However, based on Figure 4-30, some shear failure behavior starts to occur in the pushover analysis. Large plastic strain was found along with the column height which means shear failure behavior might occur to this column which has aspect ratio equal to 4 when the displacement became larger than the range of interest. A pushover analysis for this column with a smaller transverse reinforcement spacing which is equal to 4 in was conducted in this study as well to find the possibility of improving the column pushover behavior. Figures 4-31 and 4-32 show the comparison of the pushover curve between a 2.5 ft diameter and 10 ft height column with upper limit reinforcement ratio with regular transverse reinforcement spacing (6 in) and smaller transverse reinforcement spacing (4 in) in SAP and ABAQUS, respectively.

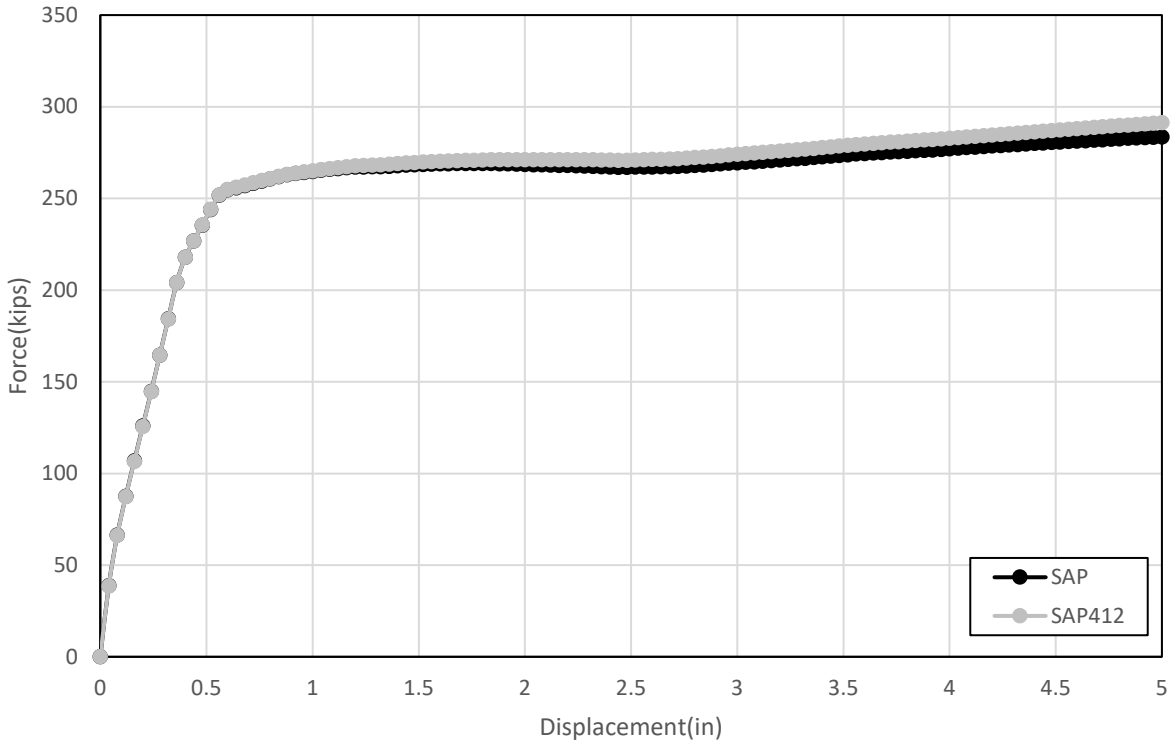

Figure 4-31 Comparison of Pushover Curve between Column with Regular Transverse Reinforcement Spacing and Smaller Spacing in SAP Model

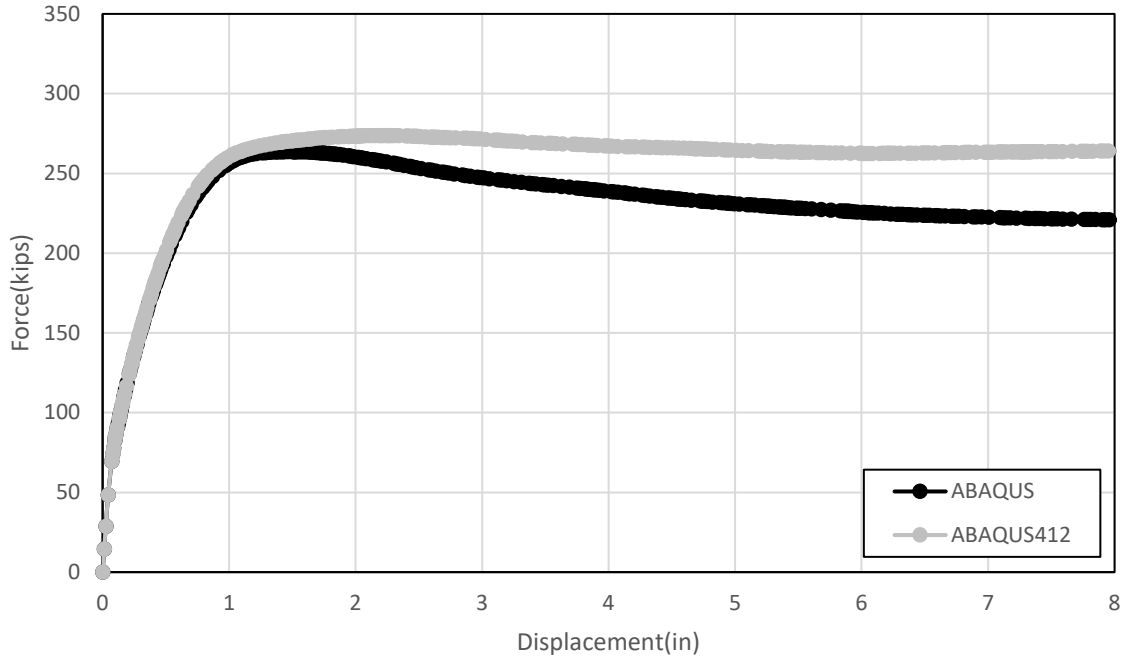

Figure 4-32 Comparison of Pushover Curve between Column with Regular Transverse Reinforcement Spacing and Smaller Spacing in ABAQUS Model

Based on Figures 4-31 and 4-32, a smaller transverse reinforcement spacing has a significant effect on increasing the shear strength during the pushover analysis. However, it cannot change the column failure type completely. Since SAP models cannot account for the shear behavior and the plastic hinge zone growth, the difference between the black line with round markers which represents 6 in transverse reinforcement spacing and the grey line with round markers which represents 4 in transverse reinforcement spacing is not significant based on Figure 4-32. Pushover analyses of columns which have an aspect ratio of 3.2 with various reinforcement ratios were conducted in this study as well. Figure 4-33 shows the pushover curve for a column with 2.5 ft diameter and 8 ft height with an upper limit reinforcement ratio.

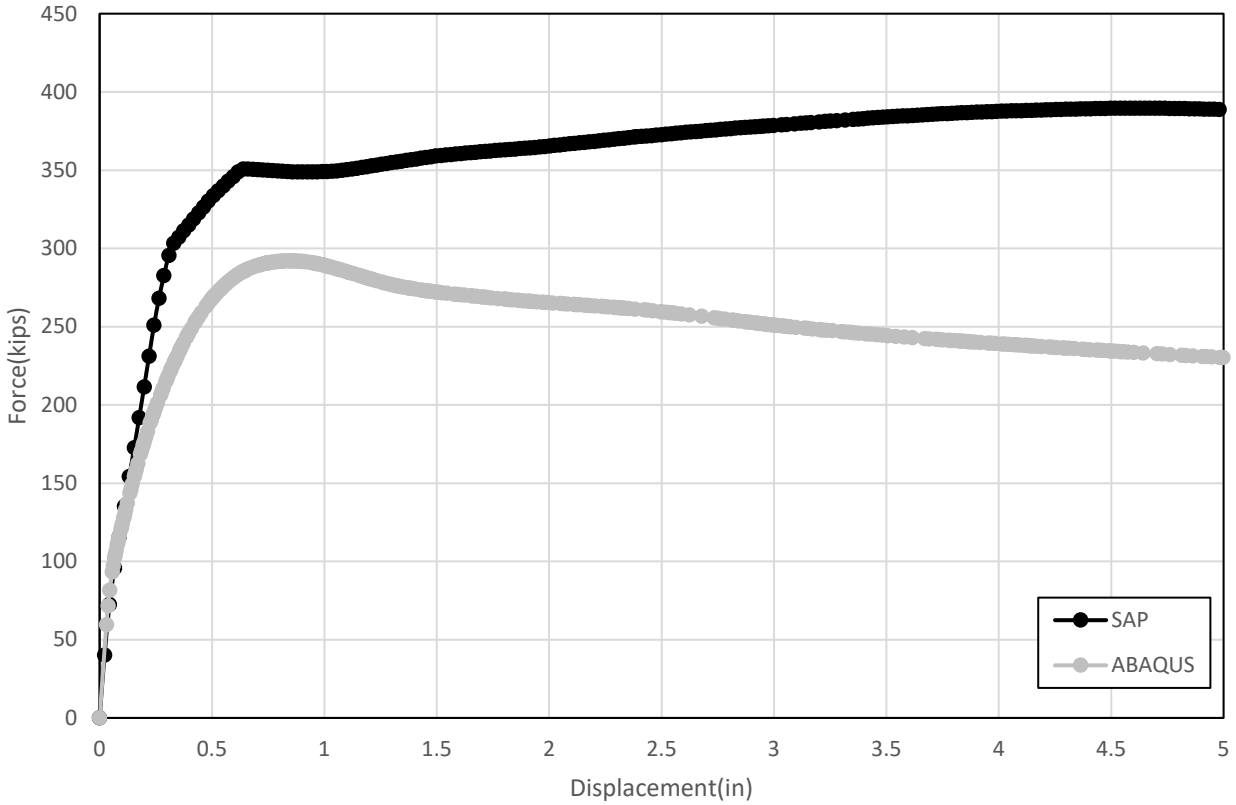

Figure 4-33 Pushover Curve for 2.5 ft Diameter and 8 ft Height Column with Upper Limit Reinforcement Ratio

Based on Figure 4-33, the black line with round markers represents the SAP pushover curve without axial loading while the grey line with round markers represents the ABAQUS pushover curve without axial loading. Different from the pushover curve of columns with aspect ratio 4, these two pushover curves cannot match up with each other in the displacement range of interest. The shear strength of the column in the ABAQUS model does not reach the shear strength in the SAP model since the shear failure of the column cannot be captured. The results indicate that the shear failure behavior started to occur at the early stages of the column pushover analysis. In addition, similar to a column with an aspect ratio greater than 4, the shear strength in the SAP model had positive post-yield behavior while the shear strength in the ABAQUS model started to decrease after 0.9 in of displacement. Figure 4-34 shows the equivalent plastic strain contour(PEEQ) for 2.5 ft diameter and 8 ft tall column with upper limit reinforcement ratio when displacement is equal to 1.41 in which is the range of interest in this project.

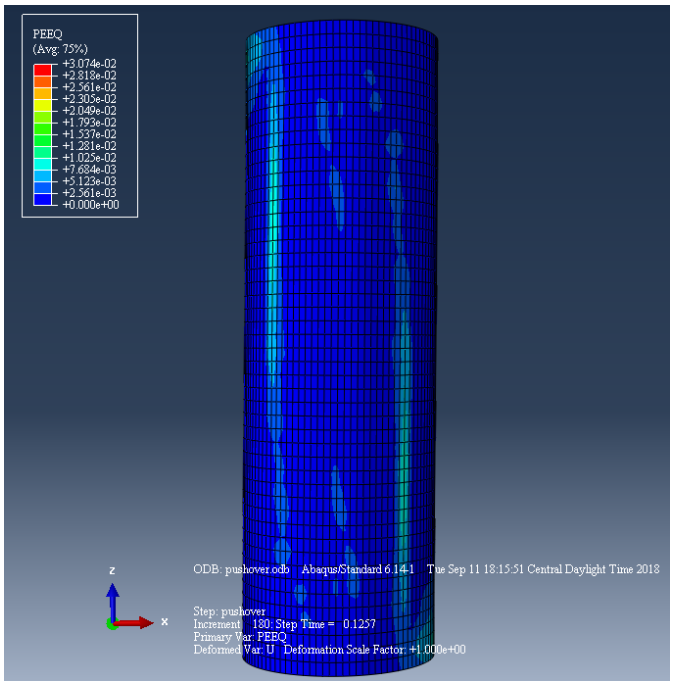

Figure 4-34 PEEQ for 2.5 ft Diameter and 8 ft Height Column with Upper Limit Reinforcement Ratio at 1.41 in of Displacement

Based on Figure 4-34, some shear failure behavior starts to occur during the pushover analysis. Large plastic strain was found along the column height which means shear failure behavior might occur in this column which has an aspect ratio equal to 3.2 when the displacement is still within the interest range.

In conclusion, the failure type analysis indicates that an aspect ratio of 4 is the marginal aspect ratio to have the flexural behavior in the range of interest range for the bridge column pushover analysis. Therefore, columns which have aspect ratio less than 4 are not recommended to be used in seismic design.

4.7 Parametric Study Using ABAQUS Model

The goal of this chapter is to use a parametric study to expand the applicable range of the AASHTO Guide Specification equations for column displacement capacity such that nonlinear pushover analysis will not be required. According to the previous discussion in this chapter, the displacement capacity of columns with the upper limit reinforcement ratio which is calculated by using an ABAQUS pushover curve is closest to the displacement capacity calculated based on the AASHTO guide specification. Therefore, a parametric study based on pushover analyses using an ABAQUS model was created in this project. Table 4-5 shows detailed information and results of the parametric study for the column pushover analysis. The basic variables in the parametric study are the column height and column diameter which are same as the displacement capacity equations in the AASHTO Guide Specification. The secondary variables including slenderness, x, and ln(x) are also used in the parametric study. The aspect ratios of all the columns in this parametric study were between 4 and 10 since column shear failure needs to be prevented and the slender columns need to be avoided because of column buckling and p-delta effects. If a column has aspect ratio greater than 10, struts in the middle of column are

recommended to avoid these potential problems. There are 26 columns in this parametric study including 16 columns less than 15ft which are currently not suitable to use the AASHTO Guide Specification equations, since they have a clear height less than 15 ft, to calculate the displacement capacity and 10 columns which are within the suitable range provided by the AASHTO guide specification.

Table 4-5 Detailed Information and Results of the Parametric Study for Column Displacement Capacity

Number	Column Diameter (ft)	Column Height (ft)	x	ln(x)	Displacement Capacity for SDC B (in)	Displacement Capacity for SDC C (in)
Column1	2	8	0.50	-0.69	0.73	1.10
Column2	2	9	0.44	-0.81	0.87	1.31
Column3	2	10	0.40	-0.92	1.02	1.54
Column4	2	11	0.36	-1.01	1.20	1.79
Column5	2	12	0.33	-1.10	1.37	2.06
Column6	2	13	0.31	-1.18	1.56	2.34
Column7	2	14	0.29	-1.25	1.77	2.66
Column8	2.5	10	0.50	-0.69	0.98	1.47
Column9	2.5	11	0.45	-0.79	1.12	1.67
Column10	2.5	12	0.42	-0.88	1.26	1.89
Column11	2.5	13	0.38	-0.96	1.42	2.14
Column12	2.5	14	0.36	-1.03	1.58	2.37
Column13	3	12	0.50	-0.69	1.20	1.80
Column14	3	13	0.46	-0.77	1.32	1.98
Column15	3	14	0.43	-0.85	1.46	2.19
Column16	3.5	14	0.50	-0.69	1.39	2.09
Column17	2	16	0.25	-1.39	2.24	3.36
Column18	2	18	0.22	-1.50	2.76	4.14
Column19	3	16	0.38	-0.98	1.77	2.65
Column20	3	24	0.25	-1.39	3.40	5.10
Column21	3	27	0.22	-1.50	4.18	6.27
Column22	3.5	18	0.39	-0.94	1.96	2.94
Column23	3.5	25	0.28	-1.27	3.26	4.89
Column24	3.5	35	0.20	-1.61	5.86	8.78
Column25	4	30	0.27	-1.32	4.14	6.21
Column26	4	40	0.20	-1.61	7.15	10.72

After conducting a parametric study, regression analysis was applied to the column pushover analysis dataset to find the relationship between column displacement capacity and column diameter and height that applies to the columns that are not currently covered in the specification. A new variable called standardized displacement capacity was created to help complete the regression analysis. The equation to calculate the standardized displacement capacity is shown below:

$$Standardized\ Displacement\ Capacity = \frac{Displacement\ capacity}{0.12 \times Column\ Height} \qquad \text{Equation 4-21}$$

Figures 4-35 and 4-36 show the standardized displacement capacity calculated by ABAQUS for SDC B and C. The vertical axis represents the standardized displacement capacity while the horizontal axis represents the expression ln(x) which is directly related with column slenderness, x.

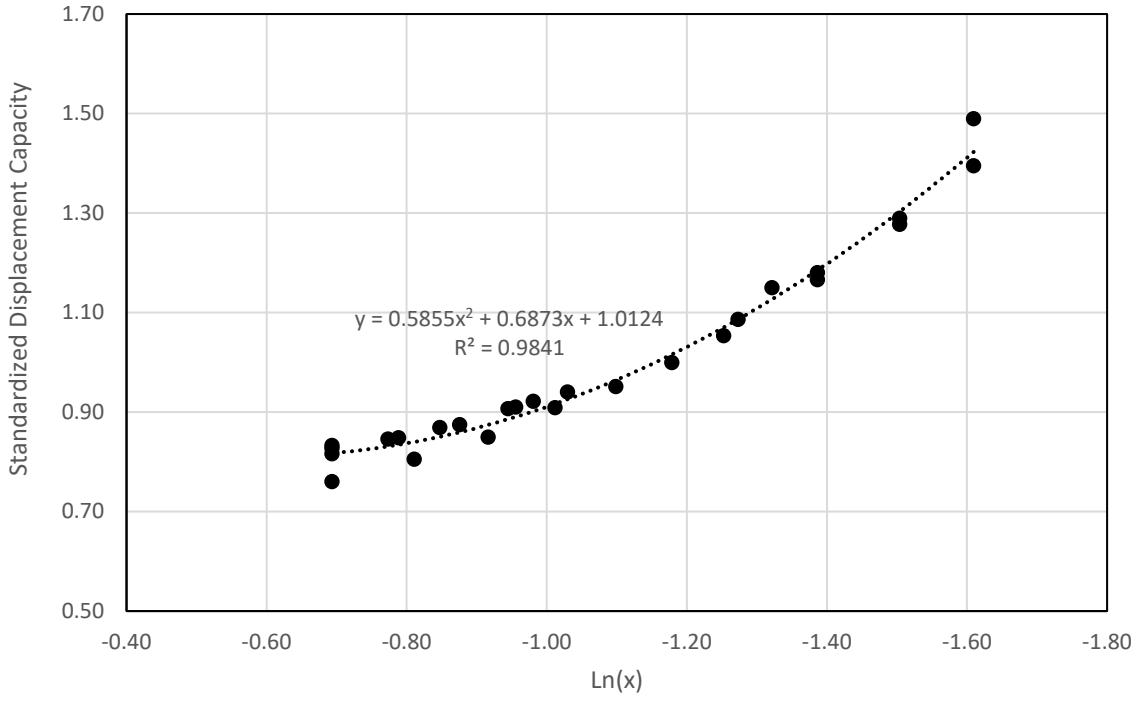

Figure 4-35 Standardized Displacement Capacity for SDC B

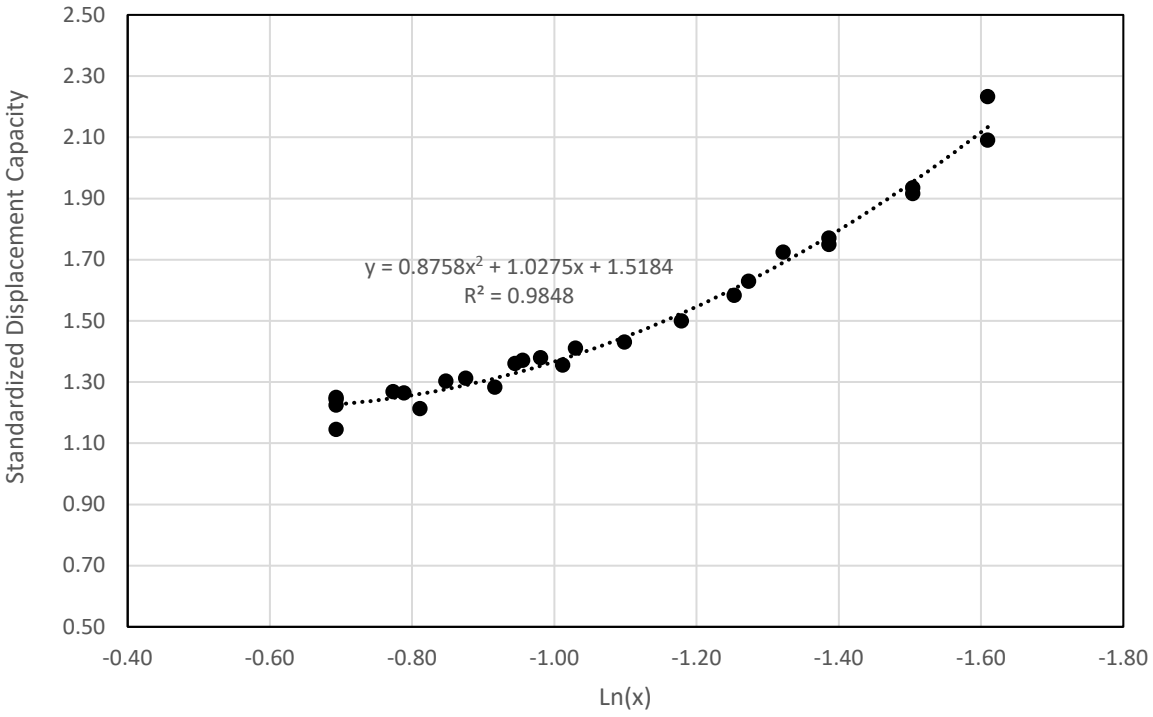

Figure 4-36 Standardized Displacement Capacity for SDC C

Therefore, two algebraic expressions based on the parametric study dataset were developed for estimating the displacement capacity of bridge columns which are less than 15ft in heights for SDC B and C. Figures 4-37 and 4-38 indicate that the predicted values of displacement capacity are within 10% of the calculated displacement capacity for SDC B and C.

For SDC B:

$$\Delta_C^L = 0.12H_o(0.59\ln(x)^2 + 0.69\ln(x) + 1.01) \qquad \text{Equation 4-22}$$

For SDC C:

$$\Delta_C^L = 0.12H_o(0.88\ln(x)^2 + 1.03\ln(x) + 1.52) \qquad \text{Equation 4-23}$$

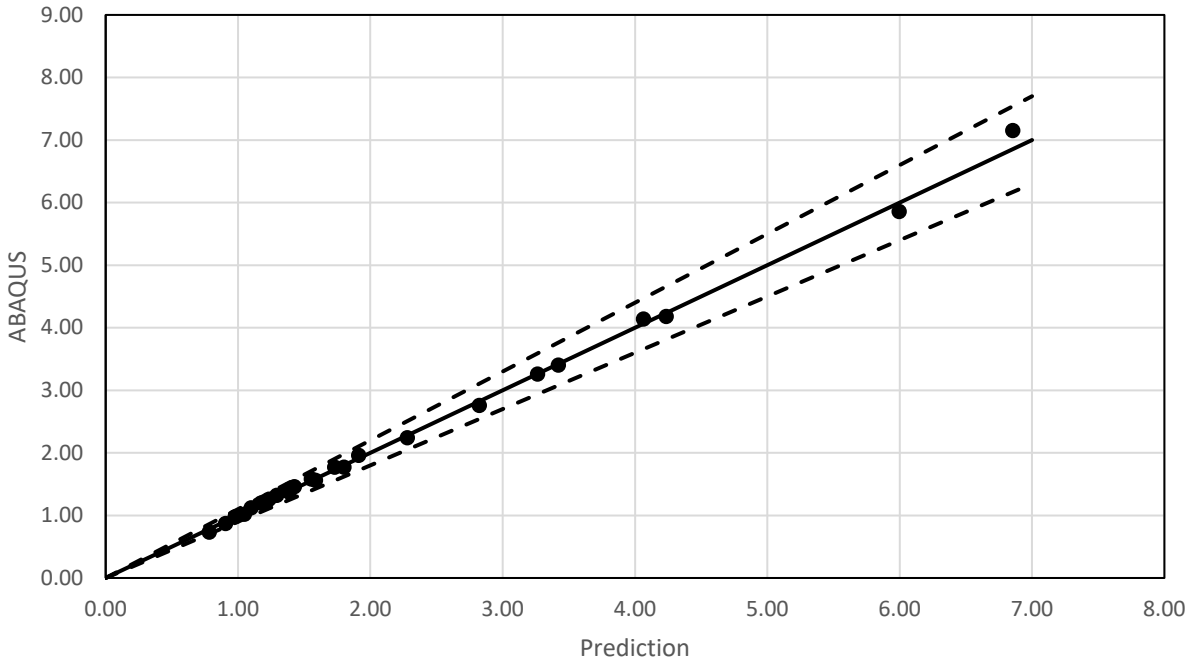

Figure 4-37 Calculated against Predicated Displacement Capacity for SDC B

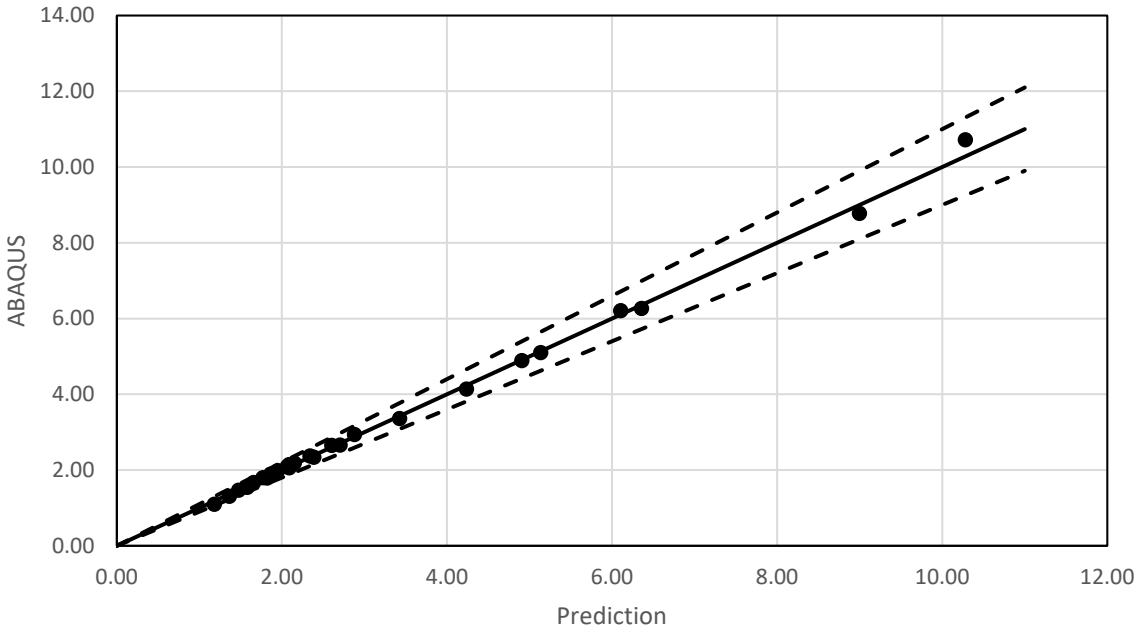

Figure 4-38 Calculated against Predicated Displacement Capacity for SDC C

A comparison between the AASHTO Guide Specification equations and the new displacement capacity equations have been done. Figures 4-39 and 4-40 show the comparison of column standardized displacement capacity between AASHTO guide specification and regression analysis result for SDC B and C.

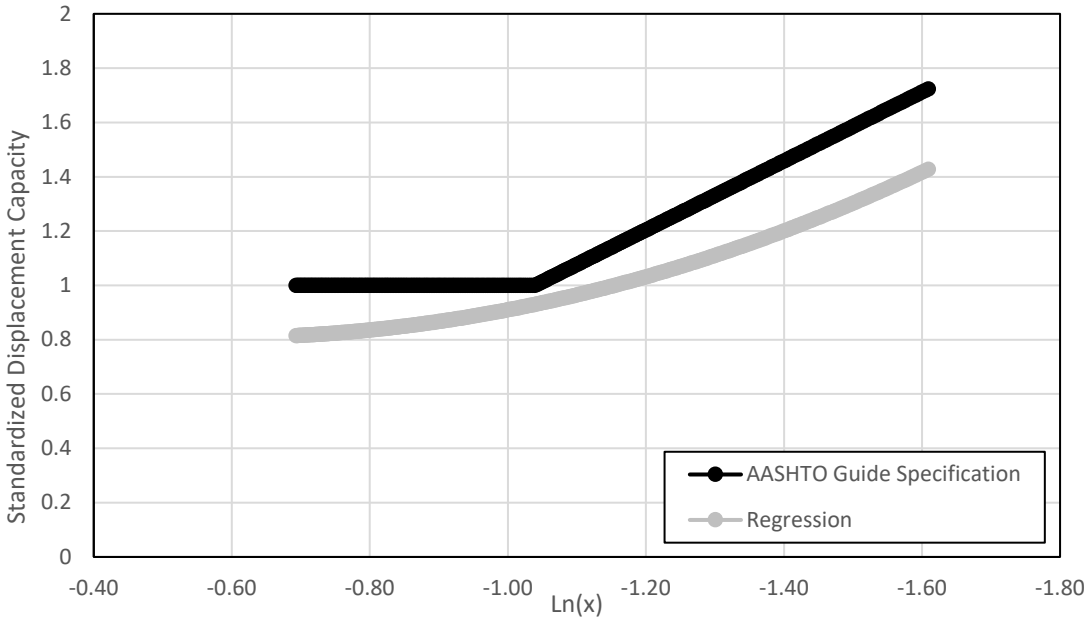

Figure 4-39 Comparison of Column Standardized Displacement Capacity for SDC B

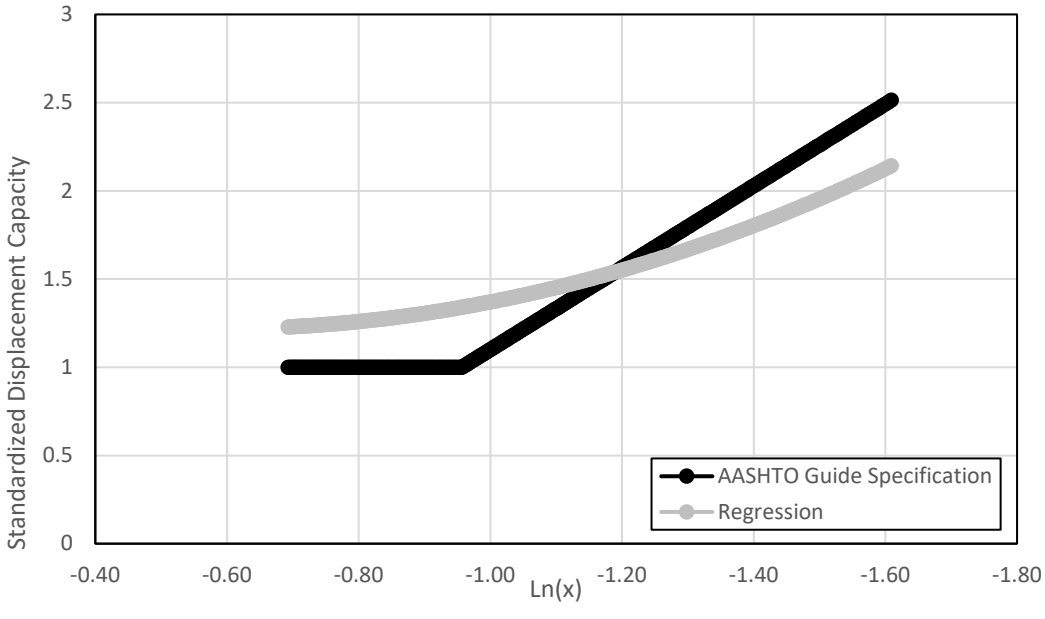

Figure 4-40 Comparison of Column Standardized Displacement Capacity for SDC C

Based on these two figures above, the black line represents the standardized displacement capacity calculated by the AASHTO guide specification while the grey line represents standardized displacement capacity calculated by regression equations. For SDC B, standardized displacement capacity calculated by regression model for all the columns which have aspect ratio between 4 and 10 is smaller than that calculated by AASHTO guide specification. However, for SDC C, standardized displacement capacity calculated by regression model for all the columns which have aspect ratio between 6.6 and 10 is smaller than that calculated by AASHTO guide specification while it is opposite for the columns which have aspect ratio between 4 and 6.6. For conservative purposes, the lower boundary of the displacement capacity between the AASHTO Guide Specification method and the regression method was selected for this project. Therefore, the final recommended displacement capacity of columns which are less than 15ft for SDC B and C were shown below

For SDC B:

$$\Delta_C^L = 0.12H_o(0.59\ln(x)^2 + 0.69\ln(x) + 1.01) \quad 0.2 \le x \le 0.5 \qquad \text{Equation 4-24}$$

For SDC C:

$$\Delta_C^L = \begin{cases} 0.12H_o(0.88\ln(x)^2 + 1.03\ln(x) + 1.52) & 0.2 \le x \le 0.3 \\ 0.12H_o(-2.32\ln(x) - 1.22) \ge 0.12H_o & 0.3 < x \le 0.5 \end{cases} \qquad \text{Equation 4-25}$$

The remaining columns which are longer than 15ft should still follow Equations 4-4 and 4-5 which are adopted by the current AASHTO Guide Specification.

4.8 Summary

The purpose of this chapter was to build a tool for bridge engineers to calculate the displacement capacity for the columns which are not covered by the current AASHTO guide specification. First, two modelling procedures by using two different software which are SAP 2000 and

ABAQUS were discussed. Then, a comparison between the pushover analysis of these two different kinds of models were performed to correlate with each other. In addition, a parametric study of column displacement capacity has also been done through the analysis results from ABAQUS models which include bridges both within and outside the current applicable ranges of applicability. Finally, two regression equations were developed for the columns which are shorter than 15 ft and fall within SDC B and C.

Chapter 5. Construction Details for Ductile RC Columns

5.1 Introduction

Bridges are not typically designed to allow the substructure to remain elastic during a design level seismic event because doing so would be uneconomical. The large inertial loads induced by the earthquake are too large to resist elastically. Thus, plastic hinges are formed from these large forces within the concrete column. Engineers design the region that develops the plastic hinge to have high ductility in order to dissipate the energy that is imparted to the structure from the earthquake (Mander J. B., 1983). Ductile elements are defined as, "Parts of the structure that are expected to absorb energy and undergo significant inelastic deformations while maintaining their strength and stability" (AASHTO, 2011). To allow the plastic hinge zones to behave in a ductile fashion, there are special detailing requirements for the reinforcement within this zone. While the requirements mainly apply to the transverse reinforcement, some requirements are placed on the longitudinal reinforcement as well. This chapter will discuss the requirements of the plastic hinge zone and will present a set of standard drawings in order to concisely display the detailing requirements in the plastic hinge zone.

5.2 Plastic Hinge Zone Requirements

The first requirement for the plastic hinge zone is the length of the hinge zone. The AASHTO Guide Specifications (2011) indicate that the length of the zone is the largest of:

- 1.5 times the largest column cross-sectional dimension
- The region of the column where the moment demand exceeds 75% of the maximum moment
- The analytical plastic hinge length, L_p

The analytical plastic hinge length is defined in the AASHTO Guide Specifications (2011) 4.11.6 as Equation 5.1 below.

$$L_p = 0.08 * L + 0.15 * f_{ye} * d_{bl} \geq 0.3 * f_{ye} * d_{bl} \qquad \text{Equation 5.1}$$

Where

L_p = Analytical plastic hinge length (in.)

L = Height of column (in.)

f_{ye} = Yield stress of longitudinal reinforcement (ksi)

d_{bl} = Diameter of longitudinal reinforcement (in.)

The next requirement for the plastic hinge zone is that longitudinal bars cannot be spliced within the zone. While this is only a requirement for SDC C and D, the commentary of the specifications recommends applying this to SDC B as well (AASHTO, 2011). One result from this requirement is that if a column has an aspect ratio (ratio of length to width) of less than 3.0, it can be difficult to have an area long enough within the column to splice the reinforcement. Thus, it is recommended that a minimum aspect ratio of 4.0 be used.

There are several requirements for the transverse reinforcement within the plastic hinge zone. First, the maximum spacing of transverse reinforcement in the zone is the smallest of:

- 1/5 the smallest dimension of the column cross-section
- 6 times the diameter of the longitudinal reinforcement
- 6 inches

If number 9 or smaller longitudinal reinforcement is used, the transverse reinforcement must be number 4 bars. If the longitudinal reinforcement is larger than number 9, the transverse reinforcement must be number 5 bars. There are also minimum reinforcement ratios (ρ_t) depending on if the transverse reinforcement is spiral or rectangular. If it is spiral reinforcement,

ρ_t must be at least 0.003 in SDC B or 0.005 in SDCs C and D. If the transverse reinforcement is rectangular, ρ_t must be at least 0.002 in SDC B or 0.004 in SDCs C and D. The transverse reinforcement also must be fully enclosed and developed in order to provide shear strength and confining pressure to the core concrete in the plastic hinge zone (AASHTO, 2011).

There is also a requirement for the plastic hinge zone to be extended into the bent cap or foundation for a certain length. This extends the plastic hinge zone spacing of transverse reinforcement into the foundation and cap beam. This extension ensures that strain penetration into the connecting elements is accounted for and that the transverse reinforcement will not fail in their anchorage. This extension is only required for SDCs C and D, but the commentary recommends applying it to SDC B as well. The extension is required to be the largest of (AASHTO, 2011):

- One-half the maximum column dimension
- 15 inches

While not a requirement of the specifications it is highly recommended that there be a change in diameter between the bridge column and a drilled shaft foundation. The primary reason for this is to generate greater certainty in the location of the inelastic action. Due to the complexity of the soil-structure interaction at the ground surface the maximum moment location could have significant variability in location. If a diameter transition is put at our near the ground surface, this would result in a plastic hinge location with more certainty and would make the rebar detailing simpler. The location of the transition could be at the ground surface or below the surface in order to increase the aspect ratio of the columns if the aspect ratio of the column is close to 4.0. The minimum recommended diameter change is 6 in as is shown in the drawings.

5.3 Plastic Hinge Zone Standard Drawings

Based on the above requirements, a set of standard drawings was developed to illustrate the requirements in a concise manner. These drawings were developed in Autodesk Revit 2018 and a reduced version is shown below (Autodesk, 2018). The full version is presented on an 11x17 drawing sheet.

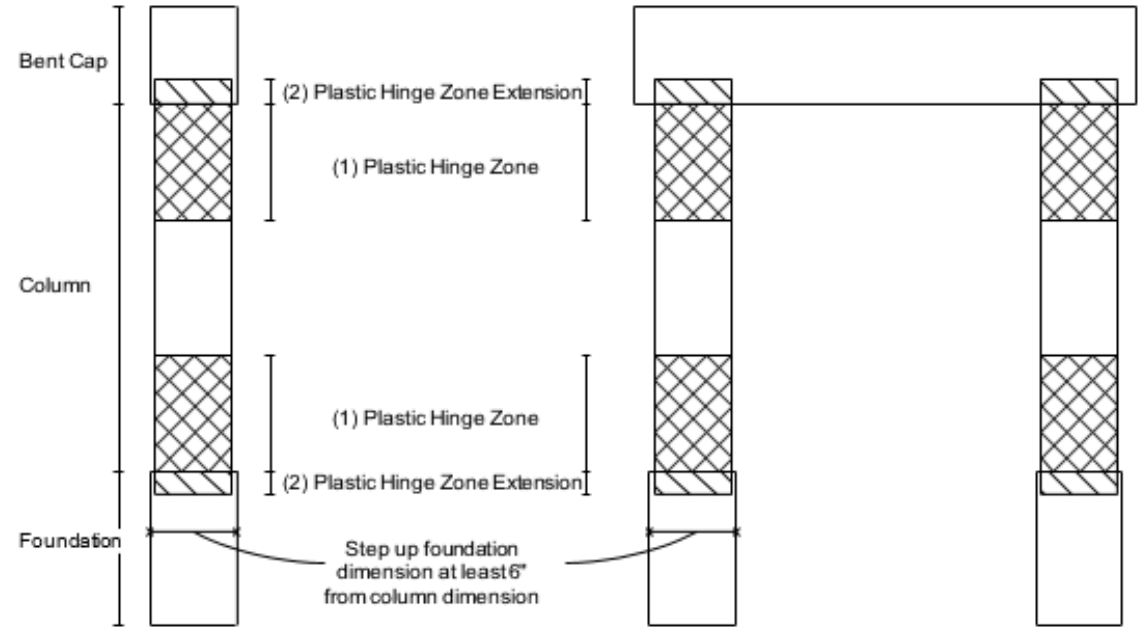

(1) Plastic Hinge Zone: *
- (A) Plastic Hinge Length largest of:
  - (i) 1.5 times largest column cross-sectional dimension
  - (ii) Region of column where the moment demand exceeds 75% of the maximum plastic moment
  - (iii) $L_P = 0.08*L + 0.15*f_{ye}*d_{bl} >= 0.3*f_{ye}*d_{bl}$
- (B) Cannot splice longitudinal bars within Plastic Hinge Zone (For SDC C and D) **
- (C) Maximum spacing of transverse reinforcement in Plastic Hinge Zone is least of:
  - (i) 1/5 the least dimension of the column cross-section
  - (ii) $6*d_{bl}$
  - (iii) 6 inches
- (D) #4 transverse reinforcement required if longitudinal reinforcement is #9 or smaller; #5 transverse reinforcement required otherwise
- (E) p_t must be at least 0.003 for spiral reinforcement in SDC B or 0.005 in SDCs C and D and 0.002 for rectangular reinforcement in SDC B or 0.004 in SDCs C and D

(2) Plastic Hinge Zone Extension:
- (A) Continue the Plastic Hinge Zone spacing of transverse reinforcement into the foundation and cap beam (For SDC C and D) **
- (B) Extension dimension largest of:
  - (i) 1/2 largest column dimension
  - (ii) 15 inches

* If S_{D1} is less than 0.10g, columns do not need to meet these requirements

** Requirements are only for SDC C and D; however, specification commentary recommends applying these requirements to SDC B as well

L = Column length (must be in.)

f_{ye} = Yield stress of longitudinal bars (must be ksi)

d_{bl} = Diameter of longitudinal bars (must be in.)

p_t = Transverse reinforcement ratio

S_{D1} = One-Second Period Design Spectral Acceleration

Figure 5-1 Plastic Hinge Zone Standard Drawings

5.4 Summary

This chapter discussed the method that slab-on-girder bridges use to dissipate seismic energy—a ductile plastic hinge within the substructure. Standard drawings were created to aid in the design of the plastic hinge zone within the reinforced concrete columns. The plastic hinge zone has multiple requirements that must be met in order to ensure that a ductile response is established within the superstructure. A ductile response will allow the bridge to avoid collapse and remain open for emergency vehicles after a seismic event. Thus, accuracy and attention to detail when designing the plastic hinge zone is paramount.

Chapter 6. Support Length

6.1 Introduction

During a seismic event, there can be large amounts of movement for a bridge span, which makes it necessary to design for certain limit states. One of these limit states is the unseating of bridge spans, therefore determining how much support length is required at each support is necessary. Providing enough support length will ensure that the bridge spans can “ride out” a seismic event without becoming unseated. This is especially important for the current method of design in Alabama because there is no longitudinal restraint of the bridge spans, thus, they are at risk of becoming unseated due to ground motions. The purpose of this chapter is to determine which procedure to calculate the support length is recommended.

6.2 Definitions

AASHTO Guide Specifications (2011) define the support length, N, as “the length of overlap between the girder and the seat.” Figure 6-1 gives a visual representation of what the support length is. In this chapter, a displacement limit will be placed on bridge spans that is assumed to be the limit state at which a bridge span will be at risk of becoming unseated. Unseating of a bridge span happens when the girders fall off the edge of the support and the span collapses. The displacement that is assumed to cause this is when the location of the girders that is aligned with the centerline of the bearing connection is displaced to the edge of the bent cap. This displacement limit is shown in Figure 6-1. This is a more conservative assumption than allowing the girder to displace the full support length. This limit was chosen because it was assumed that the demand placed on the girders and bearing pad after this limit is reached may become too large.

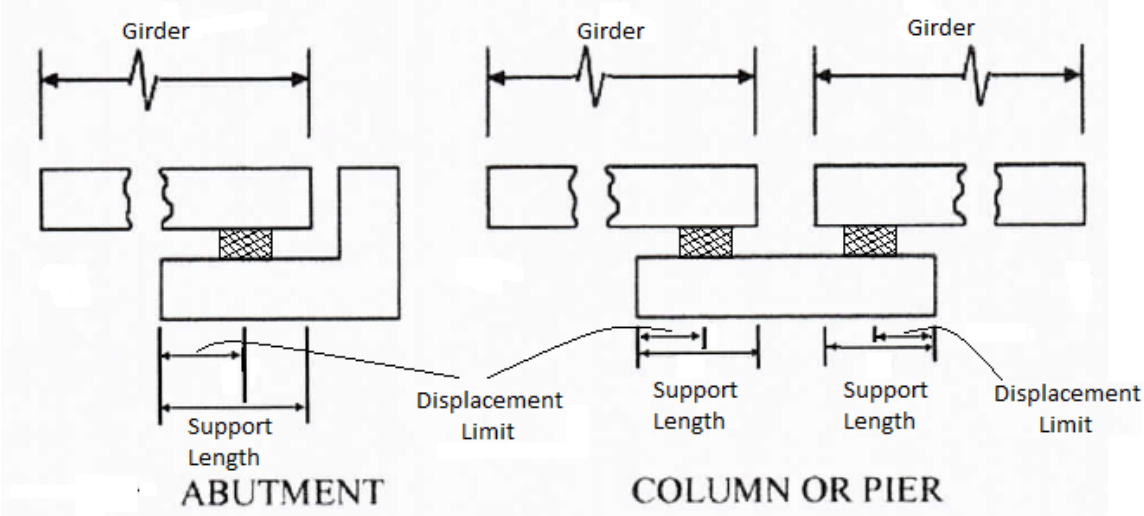

Figure 6-1 Support Length and Displacement Limit Definitions

6.3 Procedure

Two methods were used to calculate the required support length. The first method was the equation given by AASHTO Guide Specifications (2011) Article 4.12.2 in Equation 6-1. This equation is a function of the span length (L), the column height (H), and the angle of skew (S). This equation is only applicable to SDCs A, B, and C while SDC D has its own equation which is not investigated in this report. This equation is then increased by a percentage based on the SDC. For SDC B, it is increased by 150%.

$$N = (8 + 0.02L + 0.08H)(1 + 0.000125S^2) \qquad \text{Equation 6-1}$$

Where

N = Support length (in)

L = Span length (ft)

H = Column height (ft)

S = Angle of skew (degrees)

The Applied Technology Council (ATC) and the Multidisciplinary Center for Earthquake Engineering Research (MCEER) proposed the second method that was used (ATC/MCEER Joint

Venture, 2003). Equation 6-2 was developed by the ATC/MCEER Joint Venture in 2003 and differed from the above AASHTO equation by including the S_{D1} coefficient in the calculation instead of multiplying the equation by a flat percentage. This allowed the support length calculation to be tailored to the seismic demand of the site.

$$N = \left(4 + 0.02L + 0.08H + 1.09\sqrt{H}\sqrt{1 + \left(2\frac{B}{L}\right)^2}\right) * \left(\frac{1+1.25S_{D1}}{\cos\propto}\right) \qquad \text{Equation 6-2}$$

Where B = Width of superstructure (ft)

S_{D1} = One second period design spectral acceleration (g)

α = Angle of skew (degree)

Because of this, Law (2013) recommended to ALDOT that they use this equation instead of the AASHTO equation and use the highest S_{D1} that SDC B can have of 0.30g. By using this equation and this value of S_{D1}, the ATC/MCEER equation was more conservative than the AASHTO equation, but ALDOT decided that they did not want to use an equation that was not in the specifications. Law (2013) also suggested an improvement to the superstructure-to-substructure connection that would apply a positive load resistance mechanism in the longitudinal direction because ALDOT's connection provided no longitudinal resistance other than the friction between the bearing pad and the girder. ALDOT also declined to use this recommendation and instead wanted only to provide sufficient seat length to allow the superstructure to withstand any ground motions in the longitudinal direction. Thus, the goal of this chapter is to discover whether the span displacements analyzed by Panzer (2013) exceeded the support length capacity calculated with Equation 6-1, or if this equation is adequate in determining the support length for the state of Alabama.

Three concrete girder bridges were used to investigate whether Equation 6-1 is adequate. These bridges will be labeled as Little Bear Creek, Oseligee Creek, and Scarham Creek. Law (2013)

and Panzer (2013) investigated different aspects of the support length for all three bridges previously. Law (2013) investigated the differences between methods of calculating the support length while Panzer (2013) investigated the presence of span unseating during different ground motions. It is important to note that the investigations completed by these theses were only conducted on prestressed concrete girder bridges with simple spans. These findings may not be directly transferrable to steel girder bridges with continuous spans.

Law's (2013) calculations of the support length using both equations were recorded for all bents of each bridge, then the structural drawings of these bridges were used to determine the actual provided seat length. Panzer (2013) ran several different analyses for each bridge while changing four main parameters for each analysis. The first analysis was run with a lower limit friction coefficient for the bearing pads of 0.20. The second analysis was run with an upper limit friction coefficient of 0.40. The next two analyses were with the same differing friction coefficients but with an MCE-level ground motion instead of a design ground motion. Span displacements were calculated from each of these analyses for each bridge, and these values were recorded from Panzer's (2013) thesis. The structural drawings of each bridge were then used to determine the displacement limit as defined in Section 6.2.

6.4 Result

Table 6-1 shows the calculated support length from both equations and the actual provided seat length from the construction drawings. In all cases except for Oseligee Creek bent 2, the provided support length was greater than or equal to the required support length calculated from Equation 6-1. In all cases except for Oseligee Creek bents 2 and 3, the provided support length was greater than or equal to the required support length calculated from Equation 6-2.

Table 6-1 Support Lengths

	Little Bear Creek Bent 2	Little Bear Creek Bent 3	Oseligee Creek Bent 2	Oseligee Creek Bent 3	Scarham Creek Bent 2	Scarham Creek Bent 3	Scarham Creek Bent 4
Equation 6-1 (in.)	17.3	17.9	16.5	17.5	20.0	23.0	19.8
Equation 6-2 (in.)	16.6	18.3	17.6	20.1	23.1	29.1	22.6
Provided Support Length (in.)	22.5	22.5	16.5	16.5	27.0	33.0	27.0

Although Table 6-1 may seem to show that Equation 6-1 is adequate for most cases, the values that need to be compared to determine if that is true are the displacement limit values. Table 6-2 shows the displacement limit and the maximum span displacements. The displacement limit exceeds the maximum span displacements in all cases. Because the displacement limit is greater than the maximum span displacements that Panzer (2013) calculated, Equation 6-1 is adequate in calculating the required support length.

Table 6-2 Displacement Limit and Maximum Span Displacements

		Max Span Displacements (in.)			
	Displacement Limit (in.)	Lower limit friction	Upper limit friction	MCE Lower limit friction	MCE Upper limit friction
Little Bear Creek Bent 2	10.5	2.35	2.75	3.05	2.85
Little Bear Creek Bent 3	10.5	2.35	2.75	3.05	2.85
Oseligee Creek Bent 2	9.00	3.28	3.21	4.44	4.77
Oseligee Creek Bent 3	9.00	3.28	3.21	4.44	4.77
Scarham Creek Bent 2	15.0	3.68	3.95	3.82	3.81
Scarham Creek Bent 3	21.0	3.68	3.95	3.82	3.81

6.5 Summary

The goal of this chapter was to determine whether the AASHTO Guide Specification's method of calculating the required support length is sufficiently conservative to provide enough support length with only friction due to gravity loads resisting any longitudinal ground motions. After comparing not only the provided support length to the required support length, but also the displacement limit to the calculated maximum span displacements, it was determined that Equation 6-1 provides sufficient support length. Therefore, it is recommended that ALDOT use the specification equation to determine the required support length, which will provide sufficient safety against span unseating without changing the connection configuration. It is important to note, however, that the research conducted by Law (2013) and Panzer (2013) was limited to prestressed concrete girders with simply supported spans. These findings may not be directly transferrable to steel girder bridges with continuous spans, although the only support length that is important in a continuous-span-steel-girder bridge are those at the abutments. Unseating is not possible for continuous spans without significant damage occurring before the unseating occurs.

Chapter 7. Super Superstructure-to-Substructure Connection for Steel Girder Bridges

7.1 Introduction

Alabama's most common type of bridge is the slab-on-girder bridge configuration which makes up a system that is split into two main components, the superstructure and the substructure. The superstructure consists of the deck, the roadway, and the girders, while the substructure consists of a reinforced concrete beam (referred to here as a "bent cap") that the girders rest on, columns that support the bent cap, and finally, the foundation which connects to the columns and completes the load path into the ground. One critical part of this system is the connection between the superstructure and the substructure. This chapter will investigate the connection between the superstructure and substructure of slab-on-girder steel bridges to determine whether the current connection that ALDOT uses for steel girder bridges is adequate in terms of load path and strength. A complete load path between the superstructure and substructure is critical to enable the ductile substructure to be effective. Thus, every part of the connection must be able to resist the lateral loads in each direction and transfer them to the ductile substructure.

Previous research by Law (2013) investigated the connection for prestressed girder bridges but this report will specifically look at the bearing connections for steel girder bridges. This chapter reports the investigation of whether the superstructure-to-substructure connection provides an adequate load path for the structure and whether it provides adequate strength to resist Alabama's moderate seismic loads. This chapter will provide details on the procedure taken to design the connection.

7.2 ALDOT's Connection and Load Path

ALDOT uses elastomeric bearing pads for this connection which "are designed to support the vertical compressive loads from bridge beams and to allow horizontal movement of beams due to thermal expansion and contraction, traffic loads, elastic shortening, beam end rotations, and time-dependent changes in concrete" (Yazdani, Eddy, & Cai, 2000). A varying number of layers of neoprene and steel shims are alternated to form the elastomeric bearing pad connection that allows relative movement between the top and bottom of the pad (Yazdani, Eddy, & Cai, 2000). ALDOT's current bearing connection consists of four main components: the elastomeric bearing pad, a bearing plate fixed to the top of the bearing pad, a sole plate resting on the bearing plate, and anchor bolts connecting the sole plate to the bent cap. This connection is shown in Figure 7-1, and a plan view of the sole plate is shown in Figure 7-2.

The purpose of the bearing pad is explained above. The purpose of the bearing plate is to provide a sliding surface for the sole plate to slide along. The purpose of the sole plate is to both connect to the steel girder through welds and to connect to the bent cap through the anchor bolts. This system allows for a complete load path in the transverse direction (left and right in Figure 7-1) between the superstructure and the substructure. Shear force is transferred from the girders to the sole plate through welds and to the bent cap through the sole plate and anchor bolts. Although the load path is complete for the transverse direction, observation of the sole plate shows that because of the long-slotted holes, there is no complete load path in the longitudinal direction (in and out of the page on Figure 7-1). The girders are free to slide in the longitudinal direction, so it is necessary to provide enough support length to allow the spans to "ride out" the ground motion without becoming unseated. This was discussed in further detail in Chapter 6 of this report. While this sole plate configuration is most common for the internal supports, ALDOT does

sometimes provide a different configuration at the abutments that does not have long-slotted holes. While this connection would provide some longitudinal restraint, it was assumed that this restraint would not have adequate strength to resist the movement of continuous span steel girder bridges. This assumption will be confirmed with the study done in this chapter.

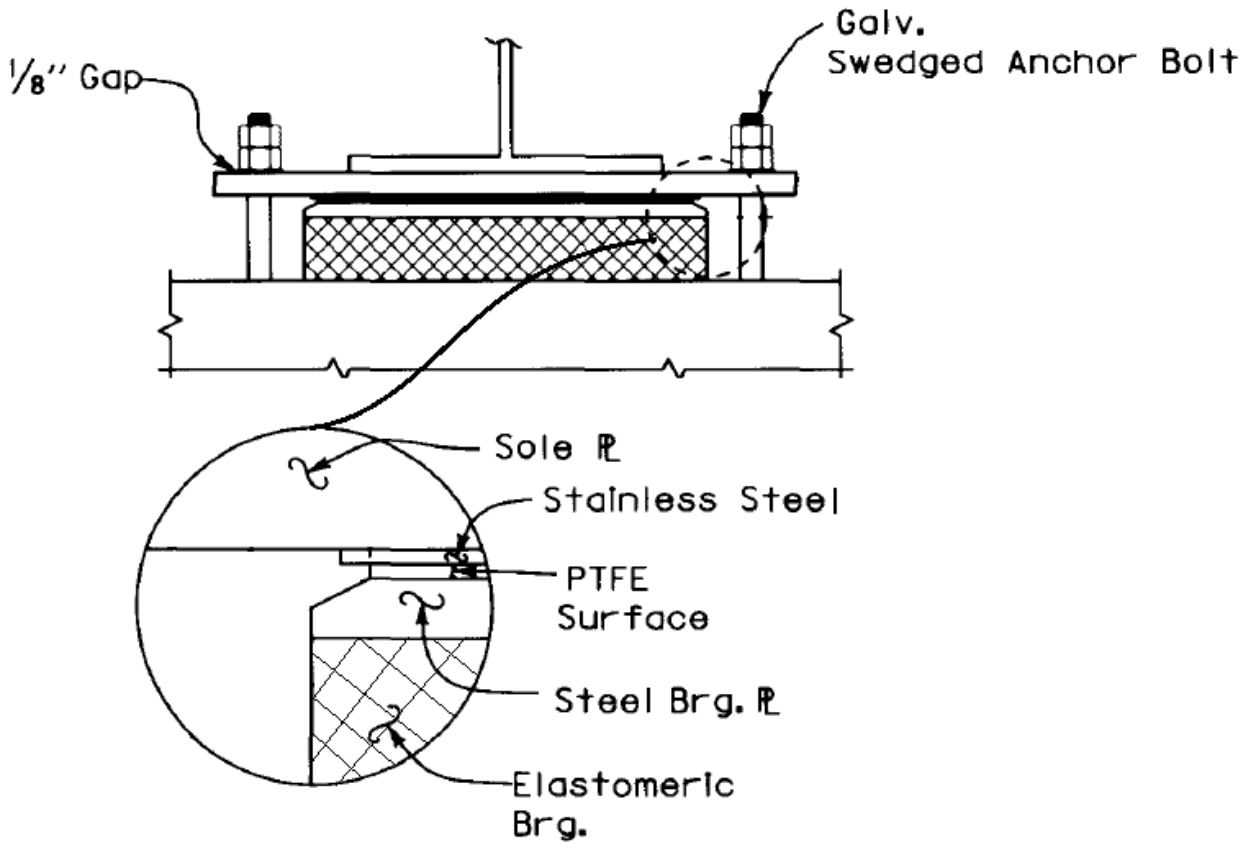

Figure 7-1 Superstructure-to-substructure connection

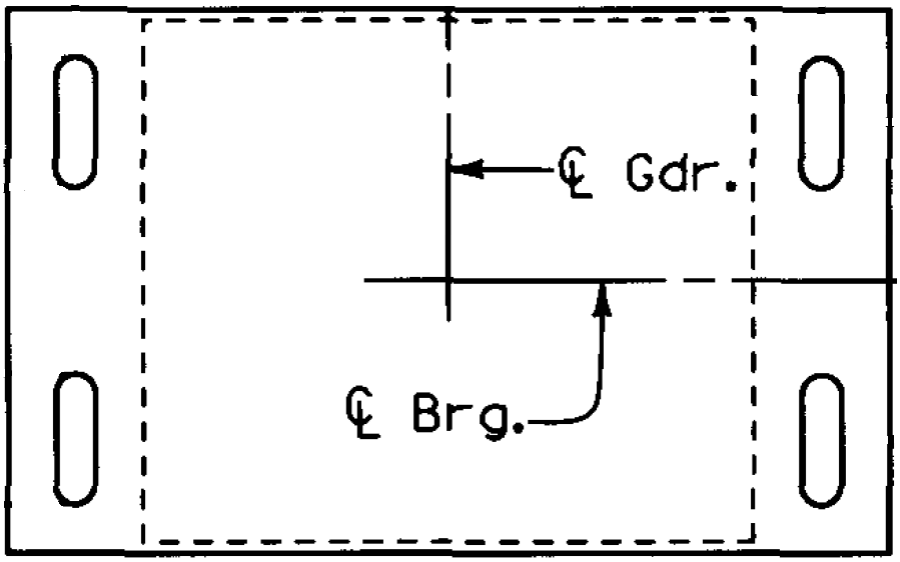

Figure 7-2 Sole Plate Plan View

7.3 Bridge Selection and Overview

The three bridges that were analyzed were from Walker County, Limestone County, and Montgomery County. Limestone County is at the very northern edge of Alabama, Walker County is north central, and Montgomery is in central Alabama. This selection of bridges allowed for the analysis to represent a good sample of the seismic hazard in Alabama. The Walker County bridge consisted of four continuous steel girder spans and one simply supported prestressed girder span ranging between a 100-foot length and a 210-foot length for an overall length of 862 feet. The first four spans contained six steel girders with 8.5-foot web depths while the last span consisted of six Type BT-72 prestressed concrete girders. The construction project consisted of two bridges—one westbound bridge and one eastbound. The two bridges were nearly identical, only varying in small details such as elevations, and thus only one was considered for design in this thesis. The deck was a constant 58.75-foot width and 7.5-inch thickness. Each bent contained three circular columns ranging in height from 40 feet to 90 feet and in diameter from 5 feet to 7.5 feet. Each bent used between one to two struts and either

drilled shafts, spread footings, or battered pile foundations. While the prestressed girder span was included in the analytical model described below, the bearing connections between the prestressed girders and substructure were not considered for design.

The Limestone County bridge consisted of three continuous spans with two equal spans of 71 feet and one span of 158 feet for an overall length of 300 feet. The three spans contained eight steel girders with 5-foot web depths. The deck was a constant 56.75-foot width and 6.5-inch thickness. Each bent contained three circular columns with heights around 21 feet, diameters of 3.25 feet, and battered pile foundations.

The Montgomery County bridge consisted of nine spans with six prestressed concrete girder simple span lengths of 113 feet and three 200-foot steel girder continuous spans for an overall length of 1,275 feet. The prestressed girder spans contained five Type BT-1830 girders while the last three spans contained five steel girders with 7-foot web depths. The deck was a constant 42-foot width and 7.0-inch thickness. Each bent contained a single oval column that ranged from 12 feet by 5 feet to 15 feet by 6 feet with heights ranging from 50 feet to 65 feet. The bents used battered piles as their foundation. This bridge also contained a horizontal curve that started with the first steel girder span. The radius of the horizontal curve was 1,000 feet and ended at the end abutment. Because this bridge had a horizontal curve, the Equivalent Static Analysis method that was described in Chapter 2 does not fit well as an analysis method for this bridge. However, this method was still used because ALDOT places great importance on the simplification of analyses. Precaution should be taken if the ESA method is used in the design of an actual curved bridge and measures should be taken to address the inaccuracies of the model.

7.4 Connection Design Validation

The construction drawings of three steel girder bridges were provided by ALDOT for the investigation of the superstructure-to-substructure connection design. The first step taken was to determine the seismic hazard of each of the bridges in order to determine the loads that were applied. Analytical models were created for all three bridges using CSIBRIDGE V15, which is a structural analysis and design program specifically for modeling bridge structures (CSI., 2011). Special attention was placed on the method for modeling the superstructure-to-substructure connection which will be discussed in Section 7.4.3. After the models were complete, the structural analysis was run to determine the forces in each element. Finally, the strength of the connection was determined and compared to the demand. The following sections will detail each of these steps.

7.4.1 Seismic Hazard and Load Determination

In order to determine the demand on each element in the structure, the seismic hazard for each site must be determined. The process for determining the SDC and other hazard variables is described in Chapter 2 of this report. The essential variables that describe the seismic hazard are shown in Table 7-1. After recording these values, the seismic forces required for design were calculated using the Equivalent Static Analysis (ESA) uniform load method described in the AASHTO Guide Specifications (AASHTO, 2011).

Table 7-1 Seismic Hazard Values

Bridge	A_S	S_{DS}	S_{D1}	SDC
Walker County	0.139g	0.293g	0.155g	B
Limestone County	0.132g	0.316g	0.177g	B
Montgomery County	0.067g	0.154g	0.104g	A

The first step in the ESA method is to determine the fundamental period of the bridge by running a modal analysis on the bridge models. A modal analysis will give the period for both the longitudinal and the transverse direction. As a note, the parametric study of prestressed concrete girder bridges to determine a simplified method of estimating the period of vibration was reported in Chapter 3. However, because steel bridges are much more variable in their parameters, this parametric study was not extended to include them. Thus, a modal analysis using a computer model, or calculations in accordance with AASHTO Guide Specifications (2011), need to be completed for steel bridges. After determining the period, the design spectral acceleration (S_a) can be calculated from AASHTO Guide Specifications (2011) section 3.4.1. Next, the weight of the bridge can be determined by calculation. These values, along with the length of the bridge, were used in Equation 7-1 below to calculate the uniformly distributed load that is applied to the bridge. A distributed load is calculated both for the longitudinal direction and the transverse direction. This load represents the equivalent static forces that a seismic event would create on the bridge through dynamic inertial forces. The fundamental period, S_a, and the uniform load for each of the three bridges is shown in Table 7-2 below.

$$P_e = \frac{S_a * W}{L} \qquad \text{Equation 7-1}$$

Where

P_e = Equivalent static uniform load (kip/ft)

S_a = Design spectral acceleration coefficient

W = Weight of bridge (kip)

L = Length of bridge (ft)

Table 7-2 Equivalent Static Loads

Bridge	Longitudinal Period (sec)	Transverse Period (sec)	Longitudinal S_a (g)	Transverse S_a (g)	Longitudinal Uniform Load (k/ft)	Transverse Uniform Load (k/ft)
Walker County	1.33	0.626	0.117	0.248	1.58	3.35
Limestone County	0.724	0.682	0.244	0.259	2.49	2.64
Montgomery County	1.30	0.672	0.080	0.154	0.844	1.62

In lieu of calculating a period of vibration, the maximum spectral acceleration for determining the seismic forces, S_{DS}, can be used in the calculation of P_e, instead of the S_a value which is based on the period. With this method, the same uniform load will be applied in both directions. This allows the designer to transition directly from determining the seismic hazard to determining the equivalent static forces. The percent increases in load from the simplified S_{DS} selection as opposed to calculation of the period of vibration are shown in Table 6.3. It can be seen that the load does not increase at all for the transverse load of the Montgomery County bridge, but it increases by 158% for the longitudinal load of the Walker County bridge. All the other cases show an increase between these two values that vary from around 20% up to 92%. It should be noted that the increases are more significant for the bridges in the higher seismic zones.

Table 7-3 Simplified Uniform Loads

	Walker County	Limestone County	Montgomery County
Uniform Load from S_{DS} (kip/ft)	3.97	3.21	1.62
Longitudinal Uniform Load (k/ft)	1.58	2.49	0.844
Longitudinal Percent Increase (%)	158	29.3	91.7
Transverse Uniform Load (k/ft)	3.35	2.64	1.62
Transverse Percent Increase (%)	21.4	21.8	0

7.4.2 Analytical Bridge Models

It is important to get a general understanding of how the three-dimensional model was created in order to be more familiar with the overall analysis. The three bridges were modeled in CSIBRDGE from the information given by the construction drawings, which allowed the overall geometry of the bridge to be specified. Details were input to define the overall layout, deck, girders, diaphragms, bearing connections, abutments, bents and bent caps, spans, and foundations.

The deck was modeled as an “area object model” which uses two-dimensional (shell) elements to represent the stiffness and strength of the deck. Frame elements were used to represent the girders’ cross-sectional properties and material properties and were modeled in the same plane as the area elements of the deck. The diaphragms also used frame elements to represent the actual truss members and the chords and diagonals tied into nodes at the top and bottom of the girders. Because the girders were modeled within the plane of the deck, rigid link elements were used to represent the depth of the girders and were connected to the top and bottom nodes into which the diaphragms were framed.

Next, the bearing connections used link elements to represent the stiffness of the connection and were specified to link the bottom of the girders to the top of the bent cap. More details on this connection are provided in section 7.4.3. The substructure used frame elements for both the bent cap and the columns, and a moment connection was provided between the two. For all frame elements in the model, four-foot sections of the members were used to provide more precise results. Lastly, the foundation elements were represented as fixed connections at the bottom of the bents and abutments.

After creating a model of the structure, the equivalent seismic loads were applied to the deck. For the Walker County and Limestone County bridges, the longitudinal uniform load was placed at the center of the deck and loaded the entire bridge length. The transverse uniform load was placed on the edge of the deck perpendicular to the longitudinal axis and loaded the entire bridge length. However, because the Montgomery County bridge was curved, a different method of applying loads was used. Area loads were used instead of uniform loads, and these loads were applied to every area element within the deck. The loads were defined in the local axis directions of the area elements to ensure that the longitudinal loads remained parallel to the longitudinal axis and the transverse loads remained perpendicular to the longitudinal axis. The value of the area loads was calculated by dividing the uniform load values by the width of the deck. Figure 7-3 presents an example of the models with a cross section of the Walker County bridge at one of the bents. All of the structural elements discussed here can be seen in Figure 7-3. One note about Figure 7-3 is that the girders frame in and out of the page which makes the girders and other nodal points within the deck look similar. However, the girders are only located above the rigid link elements. Figure 7-4 shows how the transverse seismic uniform loads were applied to the bridge deck.

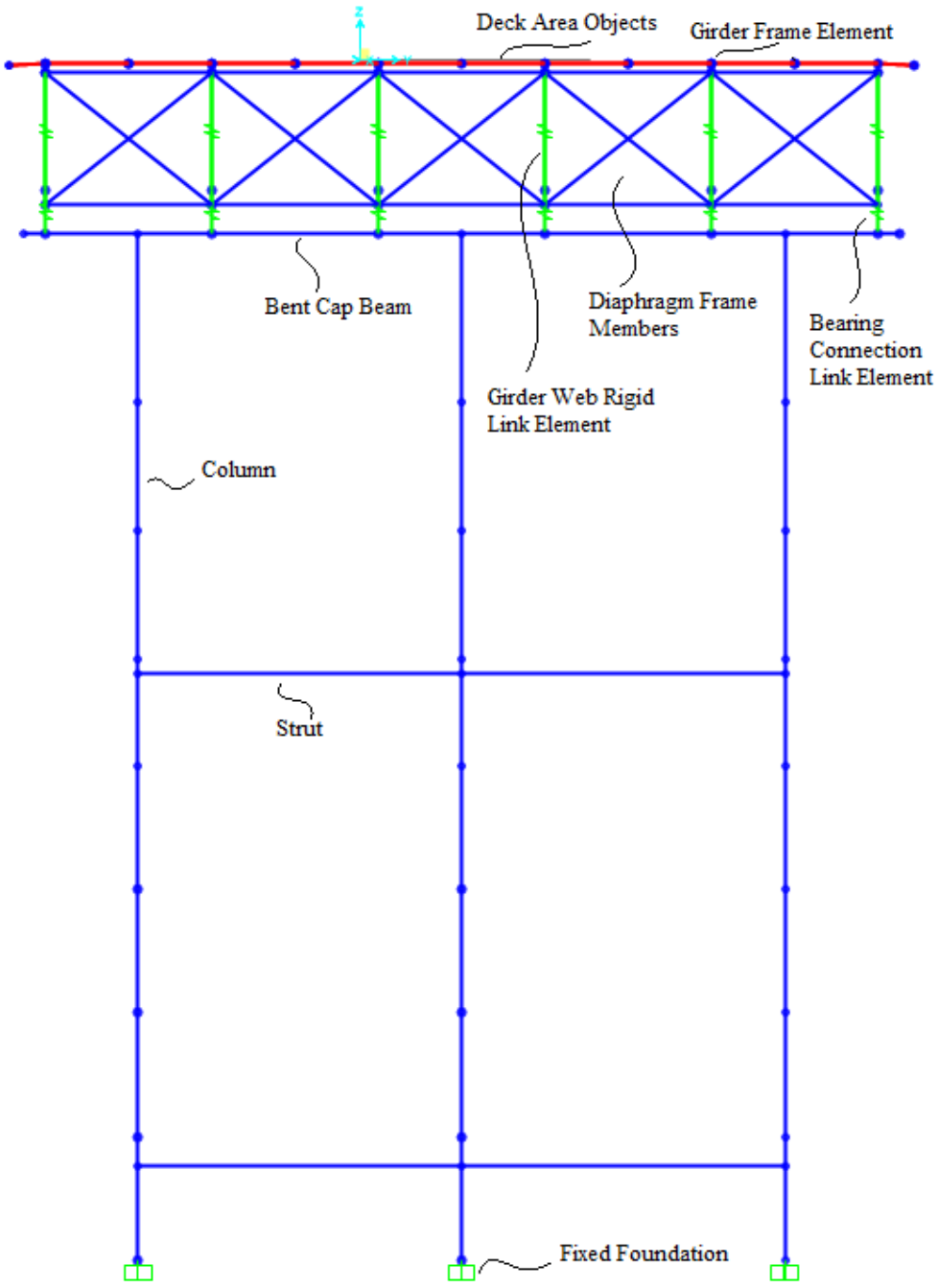

Figure 7-3 Walker County Bridge Cross Section

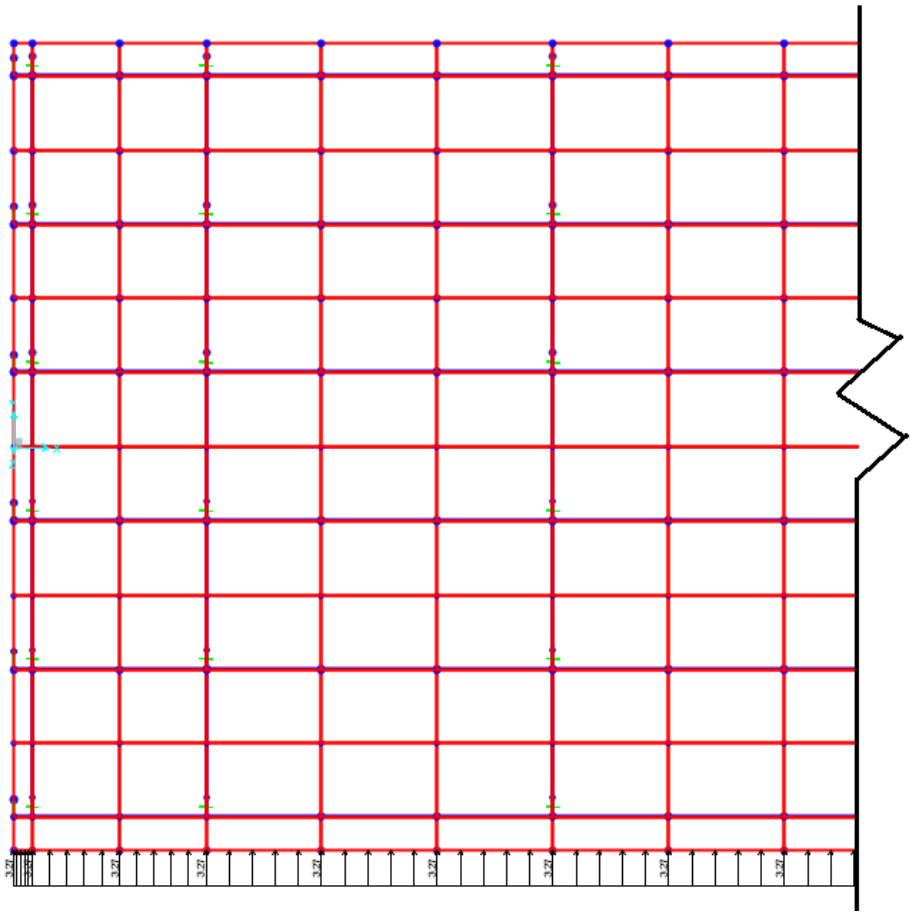

Figure 7-4 Transverse Seismic Loads

7.4.3 Analytical Bridge Models

To model the elastomeric bearing connection, it was important to be as accurate as possible in representing the stiffness of the connections. In order to calculate the stiffness of the connection in each direction, Equations 7-2 and 7-3 were used. Equation 7-2 represents the stiffness of the bearing pad alone, while Equation 7-3 represents the stiffness of the anchor bolts alone. The only component providing resistance in the longitudinal direction was the bearing pad, therefore only Equation 7-2 was used to calculate the longitudinal stiffness. The anchor bolts provide resistance in the transverse direction along with the bearing pad, therefore the stiffness for the transverse direction was the sum of both equations. The stiffness of the anchor bolts was calculated from the stiffness of combined shear and flexural cantilever bending. The anchor bolts extend past the

bent cap and span a gap between the bent cap and the sole plate. Therefore, it was determined that the anchor bolts would behave as a cantilever element. A value of 135 psi was used for the shear modulus (G) of the bearing pads based on a Caltrans (1994) design memo. All other values in the equations were recorded from the design drawings provided by ALDOT. The calculated stiffness for each bearing pad is provided in Table 7-4. Note that the Limestone County bridge has the same stiffness for the longitudinal direction as the transverse direction. This is because the connections for this bridge had no anchor bolts. This was an old connection from 1984 that ALDOT used, and they have since moved to the connection shown in Figure 7-1 that includes anchor bolts. To model the stiffness of all the connections, a link element was defined with partial fixity in the longitudinal and transverse directions. The value for the partial fixity was the stiffness calculated using Equations 7-2 and 7-3. The connection stiffness for all the bridge models are shown in Table 7-4.

$$k_{bearing} = \frac{G*A}{t} \qquad \text{Equation 6.2}$$

Where $k_{bearing}$ = Stiffness of bearing pad (kip/in)

G = Shear modulus of elasticity of bearing pad (ksi)

A = Plan area of bearing pad (in^2)

T = Thickness of bearing pad (in)

$$k_{bolt} = \frac{3*E*I}{L^3} * N_b \qquad \text{Equation 6.3}$$

Where k_{bolt} = Stiffness of anchor bolt (kip/in)

E = Modulus of elasticity of anchor bolt (ksi)

I = Moment of inertia of anchor bolt (in^4)

L = Length of anchor bolt (in)

N_b = Number of anchor bolts

Table 7-4 Stiffness of Elastomeric Bearings

Bridge	Connection Location	Longitudinal Stiffness (k/in)	Transverse Stiffness (k/in)
Walker County	Abutment 1	14.4	128
	Bent 2	24.5	401
	Bent 3	63.4	1880
	Bent 4	24.5	401
	Bent 5	14.4	128
	Abutment 6	14.4	128
Limestone County	Abutment 1	19.9	19.9
	Bent 2	18.5	18.5
	Bent 3	18.5	18.5
	Abutment 4	19.9	19.9
Montgomery County	Abutment 1	22.6	834
	Bents 2-6	13.2	236
	Bent 7	17.6	246
	Bents 8-9	40.5	852
	Abutment 10	22.6	834

7.4.4 Superstructure to-Substructure Connection Design

After determining the equivalent uniform load, it was applied to the bridge model, and the structural analysis was run for both the longitudinal and transverse loads. CSIBRIDGE was used to determine the shear force induced by the uniform loads in the link elements that represented the elastomeric bearing connection. The shear force created by the dead load was also recorded and factored loads were calculated based on AASHTO LRFD Specifications Table 4.3.1-1 and 4.3.1-2 (AASHTO, 2014). These values were calculated for each of the bents along each bridge, and the worst-case connection at each bent was chosen for design. The factored loads for both the longitudinal and transverse directions for every bent are shown in Table 7-5.

Table 7-5 Factored Connection Loads

Bridge	Connection Location	Factored Longitudinal Shear Force (k)	Factored Transverse Shear Force (k)
Walker County	Abutment 1	41.6	-41.9
	Bent 2	50.0	-117
	Bent 3	50.8	-180
	Bent 4	13.3	-85.1
	Bent 5	24.2	-74.8
Limestone County	Abutment 1	30.1	-25.3
	Bent 2	17.4	-24.8
	Bent 3	18.9	-24.8
	Abutment 4	30.1	-25.3
Montgomery County	Bent 7	12.7	-42.1
	Bent 8	31.2	-76.2
	Bent 9	30.9	-60.8
	Abutment 10	49.2	-28.6

Once the factored loads were determined, the strength of the welds connecting the girder to the sole plate was calculated. Different values such as the length of the weld, the weld size, the weld yield strength, and sole plate thickness were obtained from the design drawings. Three limit states were checked to determine the overall strength of the welded connection: base metal yielding on the gross section and rupture on the net section (AASHTO, 2014, p. 6-235), base metal shear failure (AASHTO, 2014, p. 6-235), and weld metal shear rupture (AASHTO, 2014, p. 6-232). The equations used to calculate these are shown as Equations 7-4, 7-5 and 7-6, respectively. The limit state that gave the lowest resistance was recorded as the capacity of the welded connection. This capacity was then compared to the factored shear demand from Table 7-5. These values are shown below in Table 7-6.

$$\phi R_n = \phi_y F_y A_g \leq \phi_u F_u R_p A_n U$$ Equation 7-4

Where

ϕR_n = Nominal resistance of base metal in tension (kip)

ϕ_y = Resistance factor for yielding of tension members

F_y = Base metal yield stress (ksi)

A_g = Gross connection area (in^2)

ϕ_u = Resistance factor for fracture of tension members

F_u = Base metal minimum tensile strength (ksi)

R_p = Reduction factor for holes

A_n = Net connection area (in^2)

U = Shear lag factor

$$\phi R_n = 0.58\phi_v F_y A_g$$ Equation 7-5

Where

ϕR_n = Nominal resistance of base metal in shear (kip)

ϕ_v = Resistance factor for base metal shear (ksi)

$$\phi R_n = 0.6\phi_{e2} F_{exx} A$$ Equation 7-6

Where

ϕR_n = Nominal resistance of weld shear rupture (kip)

ϕ_{e2} = Resistance factor for weld metal shear rupture

F_{exx} = Yield stress of weld (ksi)

A = Connection area (in^2)

Table 7-6 Connection Weld Capacities

Bridge	Connection Location	Weld Capacity (k)	Adequate Capacity?
Walker County	Abutment 1	143	Yes
	Bent 2	261	Yes
	Bent 3	261	Yes
	Bent 4	261	Yes
	Bent 5	143	Yes
Limestone County	Abutment 1	91.6	Yes
	Bent 2	91.6	Yes
	Bent 3	91.6	Yes
	Abutment 4	91.6	Yes
Montgomery County	Bent 7	238	Yes
	Bent 8	356	Yes
	Bent 9	356	Yes
	Abutment 10	238	Yes

The other part of the superstructure-to-substructure connection that needed to have its capacity calculated was the anchor bolts. Before calculating the capacity though, it was determined that the anchor bolts would be subjected to flexural demand as well as shear demand. This is because the anchor bolts extend from the bent cap through the bolt holes in the sole plate. The nut that is placed on the anchor bolts is not tightened to the sole plate completely, so there is a 1/8 in. gap between the nut and the sole plate. This will cause the bolt to bend as a cantilever element and be subjected to significant flexural demand. Additionally, the AASHTO Guide Specifications explicitly state, “The anchor bolts shall be designed for the combined effect of bending and shear for seismic loads” (AASHTO, 2011).

To determine the flexural demand of the anchor bolts, the behavior of the bending needed to be investigated. While the stiffness and the initial behavior was based on a cantilever element, it

was determined that eventually the top of the anchor bolt would come into contact with the sole plate and cause moment to be developed there. Therefore, the first step in determining the flexural demand was to calculate the required shear force that would cause the anchor bolt to deflect 0.25 in at the top. The distance of 0.25 in. represents the difference between the width of the slotted holes and the diameter of the anchor bolt. This value could vary, but the examples given by ALDOT were consistent with a 0.25 in. gap. After deflecting 0.25 in., the anchor bolt would contact the sole plate.

After determining the amount of shear force that would cause the anchor bolt to deflect 0.25 in., this force was compared to the total shear force at the bearing connection. If the total shear force was less than the calculated force, then the anchor bolt would not come into contact with the sole plate and would behave as a cantilever element completely. However, if the total shear force was more than the calculated force, then the calculated force would cause moment at the base of the anchor bolt equal to the calculated force multiplied by the length of the anchor bolt as defined above. The remaining shear force at the bearing connection would then continue to bend the anchor bolt similar to having a fixed-fixed connection. Therefore, the rest of the moment developed at the base of the anchor bolt could be calculated by multiplying the remaining force by half the length of the anchor bolt. It is important to note that the length of the anchor bolts ranged anywhere from around three inches to over seven inches which caused significant bending moments to be developed in the anchor bolt. These moments can be seen in Table 7-7. As previously stated, the Limestone County bridge did not have anchor bolts as part of the connection so there were no bending moments developed.

Table 7-7 Anchor Bolt Bending Moments

Bridge	Connection Location	Anchor Bolt Bending Moment (kip*in)
Walker County	Abutment 1	-304
	Bent 2	-715
	Bent 3	-651
	Bent 4	-521
	Bent 5	-542
Limestone County	Abutment 1	N/A
	Bent 2	N/A
	Bent 3	N/A
	Abutment 4	N/A
Montgomery County	Bent 7	-303
	Bent 8	-362
	Bent 9	-289
	Abutment 10	-136

After determining the flexural demand, the flexural and shear capacities of the anchor bolts were calculated. An interaction equation for the combination of flexure and shear loading was sought, but after considerable research, a sufficient equation was not able to be found. Thus, the flexural and shear capacities were calculated separately. The flexural capacity was calculated using Equation 7-7, which was based on flexural yielding alone because lateral torsional buckling does not apply to solid round bars (AASHTO, 2014, p. 6-212). The elastic section modulus and the plastic section modulus had to be calculated for the anchor bolts, and Equations 7-8 and 7-9 show the method for these calculations. Finally, the shear strength was calculated with Equation 7-10, and all capacities were compared to the corresponding flexural and shear demand from Tables 7-4 and 7-6. The capacities are shown in Table 7-8 below.

$$\phi M_n = \phi_f F_y Z \leq \phi 1.6 F_y S \quad \text{Equation 7-7}$$

Where

ϕM_n = Nominal moment resistance (kip-in)

ϕ_f = Resistance factor for flexural bending

F_y = Yield stress of anchor bolt (ksi)

Z = Plastic section modulus (in^3)

S = Elastic section modulus (in^3)

$$Z = \frac{D^3}{6} \quad \text{Equation 7-8}$$

$$S = \frac{\pi D^3}{32} \quad \text{Equation 7-9}$$

Where

D = Diameter of anchor bolt (in)

$$\phi R_n = 0.48 A_b F_{ub} N_s \quad \text{Equation 7-10}$$

Where

A_b = Area of anchor bolt (in^2)

F_{ub} = Minimum tensile strength of anchor bolt (ksi)

N_s = Number of shear planes per anchor bolt

Table 7-8 Flexural and Shear Capacities of Anchor Bolts

Bridge	Connection Location	Flexural Capacity (kip*in)	Adequate Capacity?	Shear Capacity (kip)	Adequate Capacity?
Walker County	Abutment 1	63.6	No	76.3	Yes
	Bent 2	127	No	153	Yes
	Bent 3	127	No	153	No
	Bent 4	127	No	153	Yes
	Bent 5	127	No	76.3	Yes
Limestone County	Abutment 1	N/A	N/A	N/A	N/A
	Bent 2	N/A	N/A	N/A	N/A
	Bent 3	N/A	N/A	N/A	N/A
	Abutment 4	N/A	N/A	N/A	N/A
Montgomery County	Bent 7	127	No	204	Yes
	Bent 8	127	No	204	Yes
	Bent 9	127	No	204	Yes
	Abutment 10	63.6	No	102	Yes

7.5 Discussion

After investigating the welded connection, it was determined that all welds had adequate capacity to resist the shear force being transferred. The connection with the highest shear demand was Bent 3 in the Walker County bridge, but the weld's capacity exceeded the demand by over 80 kips. The anchor bolts also performed well in shear resistance with all but one bolt containing enough capacity. Bent 3 for the Walker County bridge had its capacity exceeded by 29 kips, resulting in the anchor bolts failing. However, this is not necessarily a problem with the design of the connection itself, rather, it means that extra care needs to be given to the selection of bolt sizes. Increasing the anchor bolts' diameter by only a quarter of an inch would provide enough capacity to resist the shear demand. It should be noted, however, that the elastomeric bearing pad most likely will absorb some of the shear force as well instead of the full force being applied to the anchor bolts. Still, AASHTO Guide Specifications (2011) state that elements

resisting force through friction should not be considered to provide beneficial resistance in design. Thus, the anchor bolts were considered to resist the full shear force.

While the connection performs well in resisting shear, the anchor bolts do not have nearly enough flexural capacity. The flexural demand exceeded the capacity from anywhere between 73 kip-in. to 588 kip-in. The simplest solution to this would be to increase the bolt's diameter. However, to achieve enough strength to resist the demand of the Walker County bridge, the anchor bolts would need to be 3.25 inches at the worst case bent. It may be unrealistic to provide anchor bolts of this size so another solution was investigated.

7.6 Recommendation

As previously stated, clear guidance for the design of combined shear and flexural loads in anchor bolts was not found; therefore, an alternate design was investigated to resist the transverse movement of the superstructure. Shear blocks, or girder stops, were chosen for this design and, although anchor bolts are still required for the design of elastomeric bearing connections (AASHTO, 2014), they will act as redundant resistance to the transverse forces if the anchor bolts fail. Shear blocks are short blocks of reinforced concrete that are cast monolithically to the top of the bent cap between two girders. The Federal Highway Administration (FHWA, 2011) provided the following guidance for girder stops:

> The girder stop will act as secondary restraint members. The girder stops should not participate under service or the design seismic load conditions. A girder stop should exist between each girder line. A gap should be provided between the load plate of the bearing assembly and the girder stop equal to design displacement in the transverse direction. It is common to design each girder stop for a force equal to the total bearing shear demands at a pier. This is because the girder stops don't always engage simultaneously. Under this

condition, the girder stop contacted first could be overloaded and fail before the other girder stops are engaged. This could lead to an "unbuttoning" effect of the girder stops. The "unbuttoning" effect described here is the consecutive failure of each shear block caused by the superstructure contacting only one block at a time. This conservatively assumes that the entire base shear of the bent will be resisted by one block. Based on this guidance, a design example was created for abutment 10 of the Montgomery County bridge. This section will detail the procedure for design of shear blocks.

7.6.1 Shear Block Design Procedure

To ensure that the design and construction of the shear blocks is as simplified as possible, it is recommended that only one shear block be used between two of the girders near the center of the bent. The dimensions of the shear block can usually be determined outright—or at least a close estimation can be made. The height (h) of the shear block can be determined by adding the concrete cover length to the distance between the top of the sole plate and the top of the bent cap. The length (l_v) of the shear block can be assumed to be the width of the bent cap. Finally, the width (w) of the sole plate can be estimated by the clear distance of adjacent girder sole plates minus a gap determined by the designer. The recommendation from the FHWA (2011) was to make the gap as large as the design displacement in the transverse direction. Figure 6.5 shows what the different dimensions of the shear block represent. The length of the shear block is not shown in Figure 7-5 because it is in and out of the page.

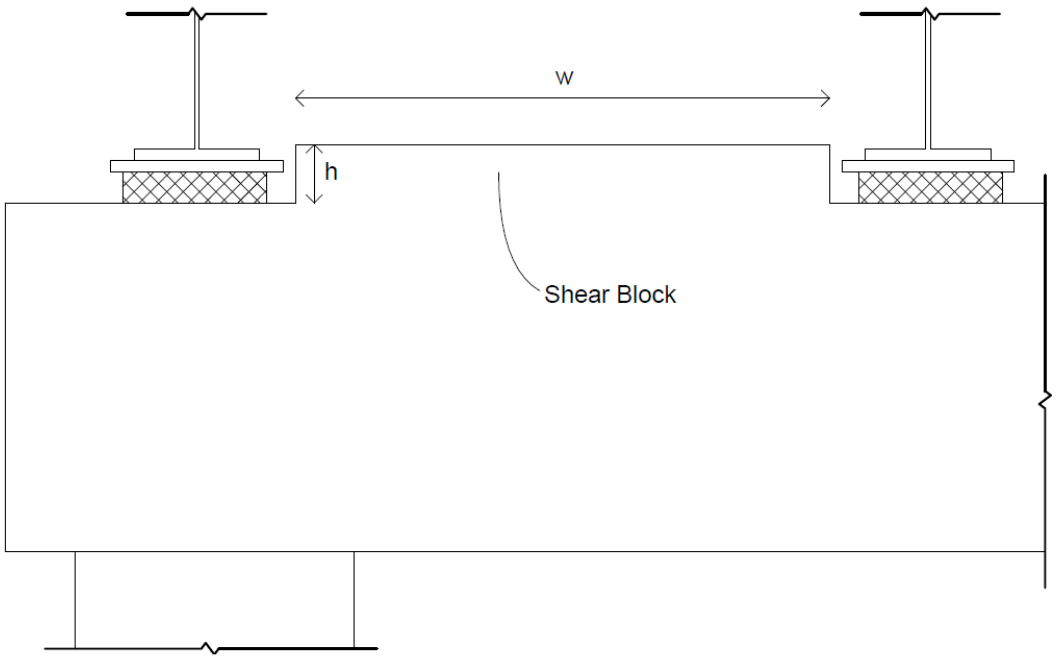

Figure 7-5 Shear Block

In order to ensure the shear block has adequate strength and is able to transfer the shear into the bent cap, shear friction reinforcement was provided at the interface between the shear block and the bent cap. LRFD Specifications (2014) state that shear friction reinforcement must be provided across a given plane at:

- An existing or potential crack
- An interface between dissimilar materials
- An interface between two concretes cast at different times
- The interface between different elements of the cross section

The shear resistance for the plane between the shear block and bent cap can be determined using Equation 7-11. Upon investigation of this equation, the shear resistance provided by the concrete is very large because the plan dimensions of the shear block are very large. According to the calculation, the concrete was able to resist the base shear at abutment 10 of the

Montgomery County bridge without any shear friction reinforcement. However, a minimum amount of reinforcement is required based on Equation 7-12. After determining the minimum amount of reinforcement required, the total shear resistance was calculated again using Equation 7-11. This resistance was then compared to two design checks shown in Equations 7-13 and 7-14. One interesting note is that if the shear strength was calculated only using the resistance of the minimum required shear friction reinforcement in Equation 7-11, the resistance of the reinforcement alone would be adequate to resist the base shear at abutment 10.

$$\phi_{shear} V_n = \phi_{shear} c A_{cv} + \mu A_{vf} f_y \qquad \text{Equation 7-11}$$

Where

ϕ_{shear} = Resistance factor for shear

V_n = Nominal shear resistance (kip)

c = Cohesion factor

c = 0.4 ksi for concrete cast monolithically

A_{cv} = Area of concrete considered to be engaged in interface shear transfer (in^2)

μ = Friction factor

μ = 1.4 for concrete cast monolithically

A_{vf} = Area of shear friction reinforcement (in^2)

f_y = Yield stress of shear friction reinforcement (ksi)

$$A_{vf,min} \geq \frac{0.05 A_{cv}}{f_y} \qquad \text{Equation 7-12}$$

Variables previously defined.

$$V_n \leq K_1 f'_c A_{cv} \qquad \text{Equation 7-13}$$

Where

K_1 = Fraction of concrete available to resist interface shear

K_1 = 0.25 for concrete cast monolithically

f'_c = Compressive strength of concrete (ksi)

$$V_n \leq K_2 A_{cv} \qquad \text{Equation 7-14}$$

Where

K_2 = Limiting interface shear resistance

K_2 = 1.5 ksi for concrete cast monolithically

The shear friction reinforcement was provided in two rows along the edges of the shear block (left and right sides in Figure 7-5). In order to aid in constructability and to control cracking, two transverse reinforcement tie layers were provided within the shear block. The shear friction reinforcement was also specified to be hooked within the shear block to ensure adequate development. The details for the design of the shear block are provided in Table 7-9.

Table 7-9 Shear Block Design Details

Length (in)	60
Width (in)	78
Height (in)	10
Shear Demand (kip)	281
Interface Shear Capacity (kip)	2200
Number of Shear Friction Bars	14 (7 each side)
Size of Shear Friction Bars	#5
Shear Reinforcement Spacing (in)	9

It can be seen from this table that the shear block's capacity is far greater than the demand. This is because the shear block is designed with large dimensions but is only lightly reinforced. In order to save materials, the designer could design two smaller shear blocks that are more heavily reinforced that would be placed on the interior side of two adjacent girders. However, because ALDOT desires simplification, it is recommended that the design method with a single shear block as described above be followed.

7.7 Summary

The purpose of this task was to verify whether the current steel girder superstructure-to-substructure connection that ALDOT uses is adequate to resist seismic loads. The strength and demand were calculated for both the welded part of the connection and the anchor bolt part of the connection. While the welded connection had adequate capacity, the anchor bolt connection was greatly under-designed for flexural resistance. Thus, a recommendation was made to provide shear blocks at the bents between girders. These shear blocks provide a secondary resistance to

transverse movement of the superstructure if the anchor bolts fail during ground motions. An example design from abutment 10 of the Montgomery County bridge was provided to show the design process of the shear keys. Overall, if the guidance in this section is followed, the superstructure-to-substructure connection will provide adequate resistance for seismic events.

Chapter 8. End Diaphragm of Steel Girder Bridges

8.1 Introduction

Another critical element of steel girder bridges is the diaphragms, or cross frames, that are spaced throughout each span and at the supports. These are typically made up of a truss system that resists loads axially, but they can also be made of a beam element that will resist loads in flexural bending. The truss system type is the most common and will be studied in this report as ALDOT only provided examples of this type of diaphragm. The diaphragms span between the bridge girders with a top and bottom chord located near the top and bottom flanges of the girder and diagonal bracing between the chords.

The main purpose of diaphragms is to prevent twisting of the bridge girders which are heavily susceptible to lateral-torsional buckling (Helwig & Wang, 2003). The truss configuration of the diaphragms allows the elements in the truss to resist twisting of the bridge girders through axial loads in those elements. Depending on whether the diaphragm is located at the support (referred to here as “end diaphragms”) or between the supports (referred to here as “intermediate diaphragms”), the main cause of this movement has different sources. Intermediate diaphragms mainly resist movement caused by truck live loads as they move along the bridge (Helwig & Wang, 2003). Conversely, end diaphragms mainly resist movement caused by lateral loads on the bridge structure (Zahrai & Bruneau, 1998). Consequently, end diaphragms generally resist much larger loads than intermediate diaphragms, and they will be the focus of this study.

8.2 ALDOT's End Diaphrams

ALDOT does not have a standard system that they use for an end diaphragm because steel girder bridges vary widely in their parameters. However, the diaphragms from the three bridges studied have many similarities and are shown below in Figures 8-1, 8-2 and 8-3. The Walker County diaphragm uses a single angle as the top chord and an X-brace as the configuration for the diagonals. It uses gusset plates to connect all truss members to the bearing stiffeners. The Limestone and Montgomery County diaphragms are similar—both using a channel section for the top chord and single angles for the bottom chord and diagonals. They both also use a chevron type configuration for the diagonals. The main difference between the Limestone and Montgomery diaphragms is that the Limestone County diaphragm connects all truss members directly to the bearing stiffeners whereas the Montgomery County diaphragm uses gusset plates to attach the diagonals and bottom chord to the transverse stiffeners and girder.

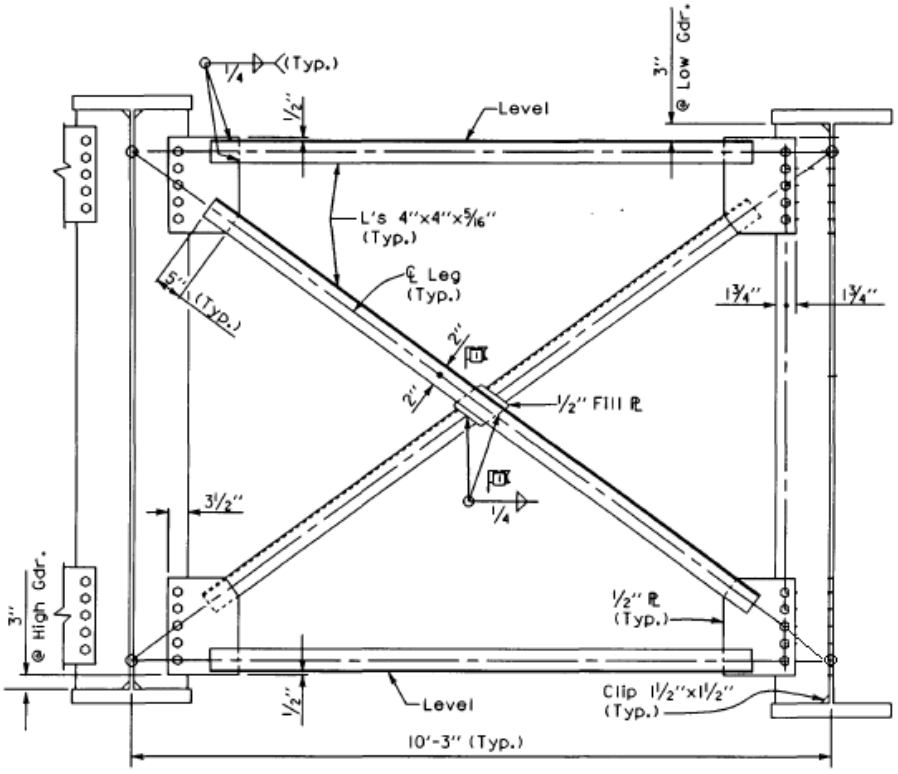

Figure 8-1 Walker County End Diaphragm

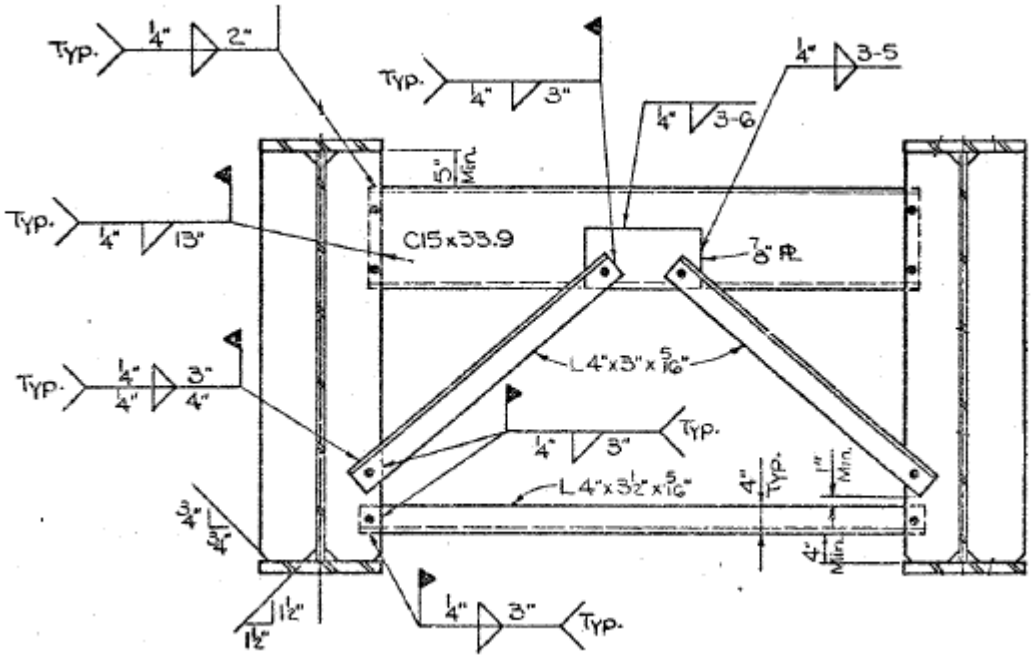

Figure 8-2 Limestone County End Diaphragm

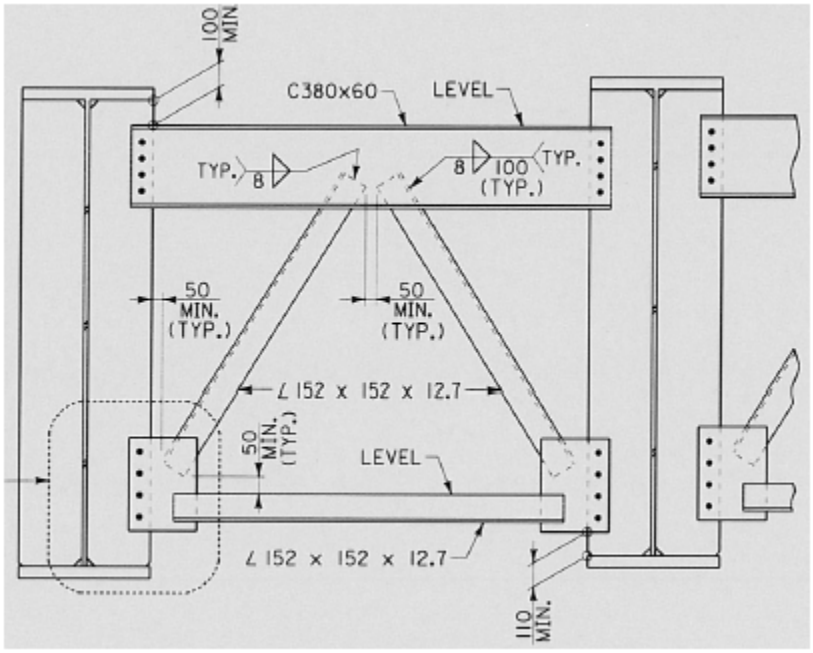

Figure 8-3 Montgomery County End Diaphragm (metric units)

8.3 End Diaphragm Model

The analytical diaphragm model within CSIBRIDGE was created using the diaphragm tool in the software. This tool creates frame elements to represent the truss members and ties the chords and diagonals into nodes at the top and bottom of the girders. Because the girders were modeled within the plane of the deck, rigid link elements were used to represent the depth of the girders and connected the top and bottom nodes into which the diaphragms were framed. The size of the truss elements was recorded from Figures 8-1, 8-2, 8-3 and specified within the model. The same bridge models as described in Chapter 7 of this report were used along with the same seismic forces. Figure 8-4 presents an example of one set of diaphragms from the Walker County bridge that displays the internal axial forces of the truss members. This figure shows the diagonals that were over capacity as described in the next section.

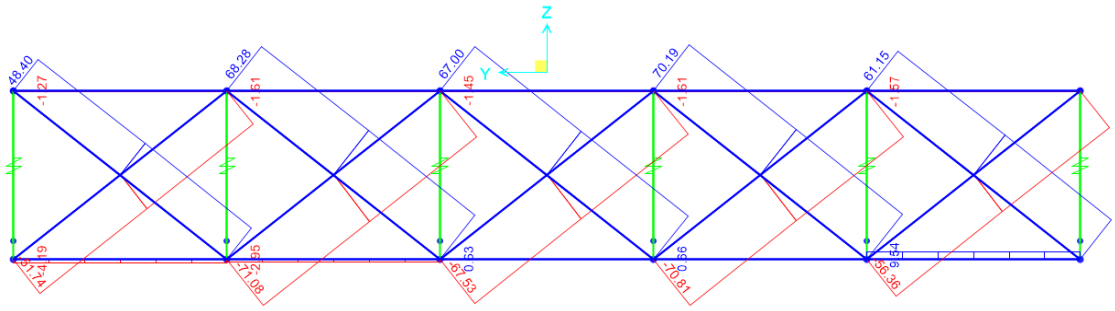

Figure 8-4 Walker County Diaphragm Axial Forces

8.4 End Diaphragm Design

After the analysis, the maximum compressive force and maximum tensile force was recorded for the top chord, the bottom chord, and the diagonals. These forces were used to design each member as a compression member and a tension member. The tension members were designed for yielding on the gross section, fracture on the net section, and block shear failure whereas compression members were designed for flexural buckling and/or flexural torsional buckling. The equations for yielding on the gross section and rupture on the net section are shown in Equation 7-4. The equation for block shear failure is shown in Equation 8-1. The overall tensile strength of the truss member was taken as the lowest value calculated from these equations.

$$\phi R_n = \phi_{bs} R_p (0.58 F_u A_{vn} + U_{bs} F_u A_{tn}) \leq \phi_{bs} R_p (0.58 F_y A_{vg} + U_{bs} F_u A_{tn}) \quad \text{Equation 8-1}$$

Where ϕ_{bs} = Resistance factor for block shear failure

R_p = Reduction factor for bolt holes

F_u = Minimum tensile strength (ksi)

A_{vn} = Net area along the plane resisting shear stress (in^2)

U_{bs} = Reduction factor for block shear rupture resistance

A_{tn} = Net area along the plane resisting tension stress (in^2)

F_y = Minimum yield strength (ksi)

A_{vg} = Gross area along the plane of resisting shear stress (in^2)

The method of designing the members for compression was dependent on whether the member was a single angle or a channel section. For a channel section, the equations for singly symmetric open-section members for flexural buckling and flexural torsional buckling apply (AASHTO, 2014, p. 6-86). The first step in calculating the capacity of a channel section is to ensure that the cross section is not slender. The first slenderness limit is specified as 120 and is compared to the ratio between the unbraced length (L_b) and the radius of gyration of the y-axis. The second slenderness limit is shown in Equation 8-2 below. If this limit is not met, then the slender element reduction factor (Q) must be calculated; but if it is met, then Q is taken as 1.0 (AASHTO, 2014, p. 6-92). After determining the slenderness of the section, the elastic critical buckling resistance (P_e) of the member can be calculated using Equation 8-3 below. This equation uses several variables that require their own calculation, so the equations for those variables follow Equation 8-3. Finally, the compressive capacity of the member can be calculated using Equation 8-8. This equation is only used when the ratio between the equivalent nominal yield resistance (P_0) to P_e is lower than 0.44; otherwise, Equation 8-9 is used.

$$\frac{b}{t} \leq k\sqrt{\frac{E}{F_y}} \qquad \text{Equation 8-2}$$

Where

b = Distance specified in Table 6.9.4.2.1-1 of the LRFD Specifications (2014) (in)

t = Thickness of flange, web, or leg (in)

k = Constant specified in Table 6.9.4.2.1-1 of the LRFD Specifications (2014)

$$P_e = \left(\frac{P_{ey}+P_{ez}}{2H}\right)\left(1 - \sqrt{1 - \frac{4P_{ey}P_{ez}H}{\left(P_{ey}+P_{ez}\right)^2}}\right)$$ Equation 8-3

Where

P_e = Elastic critical buckling resistance (kip)

$$P_{ey} = \frac{\pi^2 E}{\left(\frac{K_y l_y}{r_y}\right)^2} A_g$$ Equation 8-4

Where

P_{ey} = Elastic critical buckling resistance of y-axis (kip)

$K_y l_y$ = Effective length factor of y-axis (in)

r_y = Radius of gyration about the y-axis (in)

$$P_{ez} = \left(\frac{\pi^2 E C_w}{(K_z l_z)^2} + GJ\right)\frac{1}{{r_0}^2}$$ Equation 8-5

Where

P_{ez} = Elastic critical buckling resistance of y-axis (kip)

C_W = Warping torsional constant (in^6)

$K_z l_z$ = Effective length for torsional buckling (in)

G = Shear modulus of elasticity (ksi)

J = St. Venant torsional constant (in^4)

$$r_0{}^2 = y_0{}^2 + \frac{I_x + I_y}{A_g}$$ Equation 8-6

Where

r_0 = Polar radius of gyration about the shear center (in^4)

y_0 = Distance along the y-axis between the shear center and centroid (in)

I_x = Moment of inertia about the x-axis (in^4)

I_y = Moment of inertia about the y-axis (in^4)

$$H = 1 - \frac{y_0{}^2}{r_0{}^2}$$ Equation 8-7

Variables previously defined

$$\phi P_n = \phi_c 0.877 P_e$$ Equation 8-8

Where

ϕP_n = Factored nominal compressive resistance (kip)

ϕ_c = Resistance factor for flexural buckling

$$\phi P_n = \phi_c \left(0.658^{\left(\frac{P_0}{P_e}\right)}\right) P_0$$ Equation 8-9

Variables previously defined

For the single angle sections, the LRFD Specifications (2014) provide an approximate calculation in which there is no requirement to check flexural torsional buckling; only flexural buckling applies. This approximation can be used when the single angles meet certain criteria (AASHTO, 2014, p. 6-96):

- End connections are to a single leg of the angle and are welded or use a minimum of two bolts;
- The angle is loaded at the ends in compression through the same leg;
- The angle is not subjected to any intermediate transverse loads;
- If used as web members in trusses, all adjacent web members are attached to the same side of the gusset plate or chord.

The commentary of section 6.9.4.4 in the LRFD Specifications mentions that this approximation generally applies to all single angles in diaphragms in a bridge system (AASHTO, 2014, p. 6-96). When observing the above diaphragm drawings, it can be seen that they meet all of the requirements to use the approximate method.

The first steps in designing a single angle for compression follows the same process as the channel sections above—the slenderness limits and slenderness reduction factor must be checked and determined. After these are determined, the P_e can be calculated using Equation 8-10, then the factored nominal compressive resistance can be calculated with Equations 8-8 and 8-9. Essentially, the difference in this method is that only flexural buckling is being calculated using an alternative effective slenderness ratio. After calculating the resistance for the channels and single angles, the design of the diaphragm was complete. All compressive and tensile demand forces and capacities for each type of truss member for each bridge are shown in Table 8-1.

$$P_e = \frac{\pi^2 E}{\left(\frac{Kl}{r}\right)_{eff}} A_g \qquad \text{Equation 8-10}$$

Where

$$\left(\frac{Kl}{r}\right)_{eff} = (32 + 1.25\frac{K_x l_x}{r_x}) \text{ if } \frac{K_x l_x}{r_x} > 80 \qquad \text{Equation 8-11}$$

$$\text{or } \left(\frac{Kl}{r}\right)_{eff} = (72 + .75\frac{K_x l_x}{r_x}) \text{ if } \frac{K_x l_x}{r_x} \leq 80 \qquad \text{Equation 8-12}$$

$K_x l_x$ = Effective length factor of x-axis (in)

r_x = Radius of gyration about the x-axis (in)

Table 8-1 Diaphragm Members Demand and Capacity

Bridge	Truss Member	Max Compressive Force (kip)	Compressive Capacity (kip)	Max Tensile Force (kip)	Tensile Capacity (kip)	Adequate Capacity?
Walker County	Top Chord	2.20	81.2	1.00	66.8	Yes
	Bottom Chord	12.6	81.2	14.5	66.8	Yes
	Diagonal	71.1	81.2	70.2	66.8	No
Limestone County	Top Chord	16.7	316	15.7	285	Yes
	Bottom Chord	5.00	76.3	6.10	62.6	Yes
	Diagonal	19.8	76.3	20.0	62.6	Yes
Montgomery County	Top Chord	9.50	326	1.40	150	Yes
	Bottom Chord	9.20	196	10.1	161	Yes
	Diagonal	45.5	196	48.1	161	Yes

8.5 Summary

The purpose of this task was to ensure that the end diaphragms used in ALDOT's bridges were adequate to resist seismic loads. Three different diaphragms were considered and modeled to analyze the force demand in the truss members. After calculating the capacities of each member, it was determined that all but one of the members that make up the truss diaphragms had adequate capacity. One of the diagonal members in the Walker County bridge failed in tension

by 3.4 kips. This does not mean that the overall design of the diaphragms is inadequate. It means that a larger member was needed for the diagonals of that truss so that it would remain elastic. Comparison of the rest of the members shows that most of them had a much larger capacity than was needed. Besides the diagonals of the Walker County bridge, the largest demand to capacity ratio was 0.32. Although the strength of the diaphragms was in general much higher than needed, the stiffness of the diaphragms could have been the controlling factor in their design. If torsional deformations were too large, a stiffer diaphragm could have been needed to prevent the girders from twisting. Whether this is true or not is difficult to determine in a post-design analysis, so it was not investigated further. In summary, the same method of designing diaphragms can continue to be used with the only change being considering the seismic demands in the end diaphragms. Based on the examples cited, the differences in diaphragm design will be minimal.

Chapter 9. Summary, Conclusions, and Recommendations

9.1 Summary

The objective of this project was to provide new and investigate current design details and procedures for the seismic design of standard bridges in the state of Alabama. Because of the low to moderate seismic hazard in the state, it was desired to reduce the time required to meet the seismic design requirements of the AASHTO Guide Specifications and AASHTO LRFD Specifications. Seven main topics were discussed in this study with the first topic being the development of seismic hazard maps for the state of Alabama by county. These maps will enable designers to quickly determine the level of seismic detailing needed for a bridge. The second topic was to build a tool which can be used by bridge engineers to quickly calculate the bridge fundamental period for typical, precast concrete girder bridges without any dynamic modelling based on the primary bridge properties. In this project, regression equations based on 375 bridge models were developed for one-span, two-span, three-span, four-span and five-span bridges in both the longitudinal and transverse direction, respectively. The third topic discussed was to determine ductility capacity of columns which is not currently included in the AASHTO Guide Specification for SDC B and C bridges. Two empirical equations of displacement capacity of column which was shorter than 15 ft were developed for SDC B and C bridges based on column pushover analyses, respectively. The fourth topic discussed was the development of standard drawings for the plastic hinge zones in reinforced concrete columns. Standard drawings will aid in the efficiency of the designer's work by quickly presenting the requirements of the reinforcement inside the plastic hinge zone. The fifth topic covered was determining the calculations required for support length. After investigating whether the bridges studied were in danger of becoming unseated, it was determined that using the AASHTO Guide Specifications

for calculating seat length is adequate. The sixth topic studied was the validation of ALDOT's current superstructure-to-substructure connection. Analytical models were created, and a static analysis was conducted to determine the demand on the connection. The load path of the connection was evaluated to determine if it was complete in the transfer of forces between the superstructure and substructure. Finally, validation of the end diaphragms of steel girder bridges was made by determining the forces within each truss element and designing each element as a compression and tension member.

9.2 Conclusions

Based on the analysis performed in this project, the following conclusions can be made about the simplification and standardization of seismic design procedures:

- Alabama's seismic hazard is noticeably higher nearer the northern part of the state due to the New Madrid and Eastern Tennessee Seismic Zones.
- The longitudinal and transverse fundamental periods of standard highway bridge are significantly related with bridge span length, height of bridge column, number of bridge columns and corresponding foundation rotational stiffness. For the purpose of conservatism and simplification, the foundation rotational stiffness can be replaced by the upper boundary of foundation rotational stiffness which is 3,500,000 kip-ft/rad in this study. However, including the actual foundation rotational stiffness will provide a longer bridge fundamental period which can be beneficial for the bridge seismic design.
- A minimum aspect ratio (ratio of length to maximum width) of 4.0 needs to be used in SDC B or greater for the reinforced concrete columns of bridges to ensure the bridge columns can have pure flexure behavior during a small or moderate earthquake and adequate space can be provided for splicing reinforcement outside the plastic hinge zone.

- A transition between the columns and drilled shaft foundations of 6 inches should be provided in order to ensure that the plastic hinge will occur at or near the ground surface to minimize the uncertainty in where the inelastic behavior will occur to prevent shear failure.
- Two regression equations were developed in this study to calculate the displacement capacity of bridge columns which are not included in AASHTO Guide Speciation can also be used for the columns which are included in AASHTO Guide Specification. In this case, the regression equations will provide a slightly smaller displacement capacity of bridge columns which means they are more conservative compared with AASHTO Guide Specification.
- The equation in the AASHTO Guide Specification for support length provides adequate support length for the hazard that is present in Alabama. The support length will allow the superstructure to “ride out” the ground motions and prevent the girders from becoming unseated which was a risk because the superstructure-to-substructure connection does not have a complete load path in the longitudinal direction.
- The anchor bolts in the superstructure-to-substructure connection of steel bridge girders do not provide adequate strength to resist transverse seismic loads due to the clear length of the bolts between the bearing and sole plates causing combined shear and flexural demands. A shear block is a simple and economical secondary resistance method to resist transverse shear forces at the top of the pier bent.
- Most of the members in the end diaphragms of the three bridges studied provide enough capacity; however, one member did fail in tension. End diaphragms provide resistance to lateral loads and therefore need to be designed for seismic loads. Because most of the

members in the truss are over-designed, including seismic loads in the analysis should not significantly change the sizes of most of the truss members.

9.3 Recommendations

Based on the conclusions above and the analysis done in this project, the following recommendations can be made to improve the seismic design process for ALDOT:

- ALDOT should use the equations developed in chapter 2 to estimate the fundamental period for the standard highway bridges. Foundation system can be excluded for simplified purpose in the bridge fundamental period analysis. However, including the stiffness of foundation can be beneficial for the bridge seismic design.
- ALDOT should use the equations developed in chapter 3 to estimate the displacement capacity for the columns of standard highway bridges. A minimum aspect ratio (ratio of length to maximum width) of 4.0 is recommended in SDC B or greater for reinforced concrete columns to ensure column flexure behavior and enough space for splicing of reinforcement.
- ALDOT should use the equation for support length from the AASHTO Guide Specifications to calculate the support length required for a bridge span.
- A shear block should be provided at abutments and bents between two interior girders. This will provide resistance to transverse movement of the superstructure in case the anchor bolts fail.
- Because shear blocks are being recommended to resist transverse motion, the anchor bolts in the superstructure-to-substructure can be limited to the design for other loads besides seismic.

- End diaphragms need to be designed for seismic loads, and in order to achieve material and financial savings, a more optimized design of the end diaphragms is suggested.

9.4 Further Research

Certain parts of this project could benefit greatly from additional research. First, the regression equations were developed based on the results of 375 CSIBRIDGE models. More bridge models are recommended to build to get more accurate regression models. Second, for the pushover analysis in chapter 4, the ABAQUS models which were used for parametric study were only correlated with the corresponding SAP models. It would be good to put additional effort to validate the ABAQUS models by comparing the numerical pushover results with the experimental results in the literature. Third, the determination that the equation for support length in the AASHTO Guide Specifications is adequate was based on research that only studied prestressed concrete girder bridges with simple spans. To extend this recommendation to steel bridges, analyses similar to Law (2013) and Panzer (2013) should be conducted for steel girder bridges. In addition, the assumption was made that the bearing connections become ineffective when half the bearing pad extends past the edge of the bent cap. Research should be conducted to find the point that the bearing pad actually becomes ineffective. What's more, the design of anchor bolts under combined shear and flexural loading is largely unstudied. Further research should be funded to understand how these anchor bolts behave under lateral loads. Finally, the axial forces within the end diaphragm trusses reported in this report were only determined based off factored dead and seismic load. Live load created by trucks and vehicles could have significant impact on the demand of these members. While AASHTO LRFD Specifications do not explicitly require the combined effects of live load and seismic loads, the commentary suggests using 50% of the live load if the designer deems it necessary. Thus, a study that

included this live load would be beneficial to determine if any more of the members are over capacity.

References

AASHTO. (2011). *AASHTO Guide Specifications for LRFD Seismic Bridge Design 2nd Edition.* Washington, DC: American Association of State Highway and Transportation Officials.

AASHTO. (2014). *LRFD Bridge Design Specifications* (4th ed.). Washington DC: American Association of State Highway and Transportation Officials.

ABAQUS. (2017). *Abaqus Analysis User's Guide.* Palo Alto, CA: ABAQUS Inc.

Alabama DOT. (2012, November 30). *ALDOT Standard Details.* Alabama Department of Transportation.

ALDOT. (2012). *ALDOT Standard Details.* Montgomery, AL: Alabama Department of Transportation.

ATC/MCEER Joint Venture. (2003). *Recommended LRFD Guidelines for the Seismic Design of Highway Briges.* Federal Highway Administration.

Autodesk. (2018). *Autodesk Revit 2018 [computer software]*.

Aviram, A., Mackie, K. R., & Stojadinović, B. (2008). *Guidelines for Nonlinear Analysis of Bridge Structures in California.* Berkeley, CA: Pacific Earthquake Engineering Research Center.

Berry, M., & Eberhard, M. (2003). *Performance Models for Flexural Damage in Reinforced Concrete Columns.* Berkeley, California: Pacific Earthquake Engineering Research Center.

Boresi, A. P., & Schmidt, R. J. (2003). *Advanced Mechanics of Materials.* Hoboken: John Wiley & Sons. Inc.

Caltrans. (1994). *Bridge Bearings. Memo to designers.* Los Angles, CA: California Department of Transportation.

Caltrans. (2015). *BRIDGE DESIGN PRACTICE.* Los Angeles, CA: California Department of Transformation.

CSI. (2011). *CSI Analysis Reference Manual for SAP2000®, ETABS®, SAFE® and CSiBridge®.* Berkely, CA: Computers and Structures Inc.

Ewins, D. J. (2000). *Modal testing: Theory and practice.* Hertfordshire, U.K: Research Studies Press Ltd.

FHWA. (2011). *LRFD Seismic Analysis and Design of Bridges Design Examples.* New York.

GOOGLE. (2018). *Google Maps.* [Graph illustration of United States map]. Retrieved from https://www.google.com/maps.

Helwig, T. A., & Wang, L. (2003). *Cross-Frame and Diaphragm Behavior for Steel Bridges with Skewed Supports.* Houston, Texas: University of Houston.

Imbsen. (2006). *Task 6 Report for Updating "Recommended LRFD Guidelines for the Seismic Design of Highway Bridges",NCHRP 20-07/Task 193.* Washington, DC: Transportation Research Board, National Research Council.

Juang, J. N. (1994). *Applied system identification.* Englewood Cliffs. N.J.: Prentice-Hall.

Kane, K. M. (2013). *Response of Deep Foundations to Seismic Loads in Alabama.* Auburn, AL: Auburn University.

Kavazanjian, E. J. (2011). *Geotechnical Engineering Circular No. 3 – LRFD Seismic Analysis and Design of Transportation Geotechnical Features and Structural Foundations – Reference Manual. Report No. FHWA-NHI-11-032.* Washington D.C: Federal Highway Administration.

Kim, S. E., Park, M. H., & Choi, S. H. (2001). Direct design of three-dimensional frames using practical advanced analysis. *Engineering Structures, 23*, 1491-1502.

Kmiecik, P., & Kaminski, M. (2011). Modelling of reinforced concrete structures and composite structures with concrete strength degradation taken into consideration. *Arch. Civ. Mech. Eng., 11(3)*, 623-636.

Kotsoglu, A., & Pantazopoulou, S. (2006). Modeling of Embankment Flexibility and Soil-structure Interaction in Integral Bridges. *Proceedings of First European Conference on Earthquake Engineering and Seismology.* Geneva, Switzerland.

Law, J. (2013). *Update of Bridge Design Standards in Alabama for AASHTO LRFD Seismic Design Requirements.* Auburn, AL: Auburn University.

Lee, J., & Fenves, G. L. (1998). Plastic-Damage Model for Cyclic Loading of Concrete Structures. *Journal of Engineering Mechanics, vol. 124, no.8*, 892–900.

Lubliner, J., J. Oliver, S. O., & Oñate, E. (1989). A Plastic-Damage Model for Concrete. *International Journal of Solids and Structures, vol. 25*, 299–329.

Maia, N. M., & Silva, J. M. (1997). *Theoretical and experimental modal analysis.* Hertfordshire, UK: Research Studies Press Ltd.

Mander, J. B. (1983). *Seismic Design of Bridge Piers.* Christchurch, New Zealand: University of Canterbury.

Mander, J., Priestley, M., & Park, R. (1984). Theoretical Stress-Strain Model for Confined Concrete. *Journal of Structural Engineering. ASCE. 114(3).*, 1804-1826.

Mapchart. (2018). *State of Alabama Map.* [Graph illustration of State of Alabama map]. Retrieved from https://mapchart.net/usa-counties.html.

Martin, G., & Lam, I. (1986). *Seismic Design of Highway Bridge Foundations.* U.S. Dept. of Transportation, Federal Highway Administration, Research, Development, and Technology.

Panzer, J. (2013). *Evaluation of Critical and Essential Concrete Highway Bridges in a Moderate Seismic Hazard.* Auburn, AL: Auburn University.

Priestley, M., Ranzo, J., Benzoni, G., & Kowalsky, M. (1996). Yield displacement of circular bridge columns. *Proceedings of the 4th Caltrans Research Workshop.* Sacramento: California Department of Transportation.

Priestley, Seible, & Calvi. (1996). *Seismic Design and Retrofit of Bridges.* New York, NY: John Wiley & Sons, Inc.

Sheikh, M. N., Tsang, H. H., McCarthy, T. J., & Lam, N. T. (2010). Yield curvature for seismic design of circular reinforced concrete columns. *Magazine of Concrete Research*, 741-748.

United States Geological Survey. (2018). *U.S. Seismic Design Maps.* [Graph illustration of Seismic Design Maps July, 2018]. Retrieved from https://earthquake.usgs.gov/designmaps/us/application.php?

UW, & PEER. (2004, January). UW-PEER STRUCTURAL PERFORMANCE DATABASE. Berkeley, California, United States. Retrieved from http://depts.washington.edu/columdat/main.htm.

Wang, L. K., Zhang, J. F., & Hao, J. P. (2010). Research of plastic-zone models for advanced analysis of space steel frames. *Steel Construction, 91*, 1-4.

Wu, H., Marshall, J., & Broderick, J. (2018). *Simplified and Standardized Seismic Design and Detailing for Alabama Bridges.* Auburn, Alabama: Auburn University.

Yazdani, N., Eddy, S., & Cai, C. S. (2000). Effect of Bearing Pads on Precast Prestressed Concrete Bridges. *Journal of Bridge Engineering*, 224-232.
Zahrai, S. M., & Bruneau, M. (1998). Impact of Diaphragms on Seismic Response of Straight Slab-on-Girder Steel Bridges. *Journal of Structural Engineering*, 938-947.

Appendix A. Result of Column Pushover Analysis

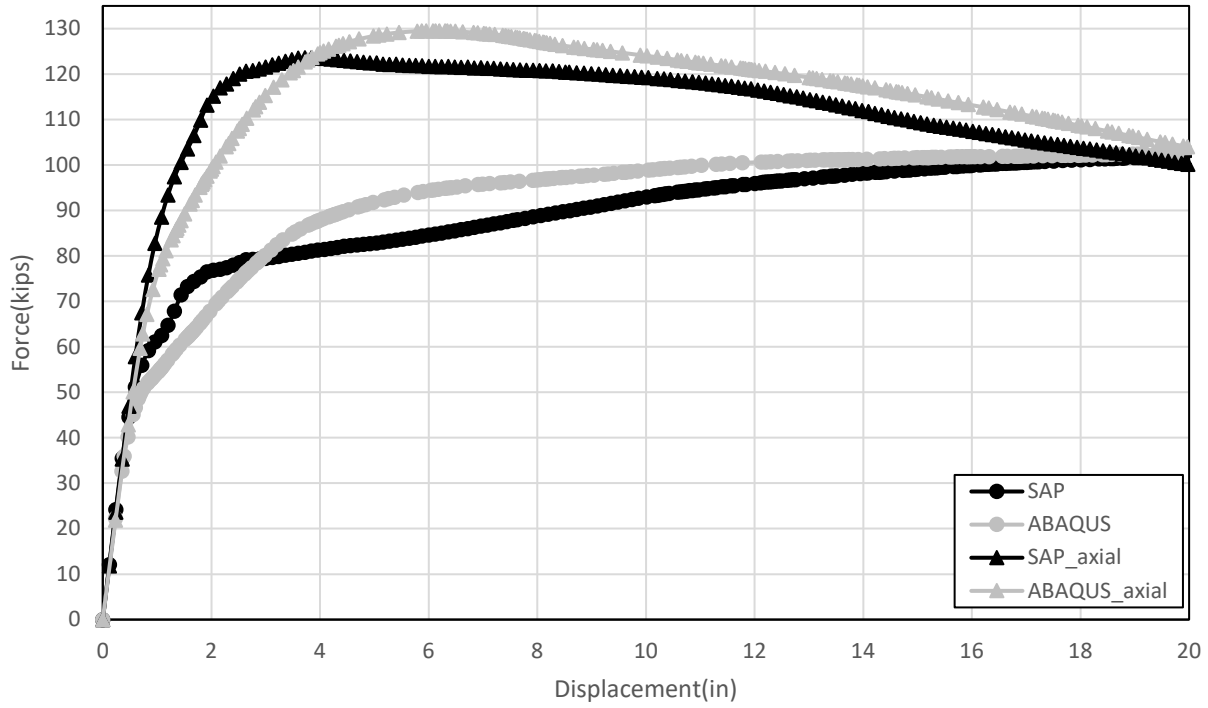

Figure A-1 Pushover Curve for 4ft Diameter and 40ft Height Column with Lower Limit Reinforcement Ratio

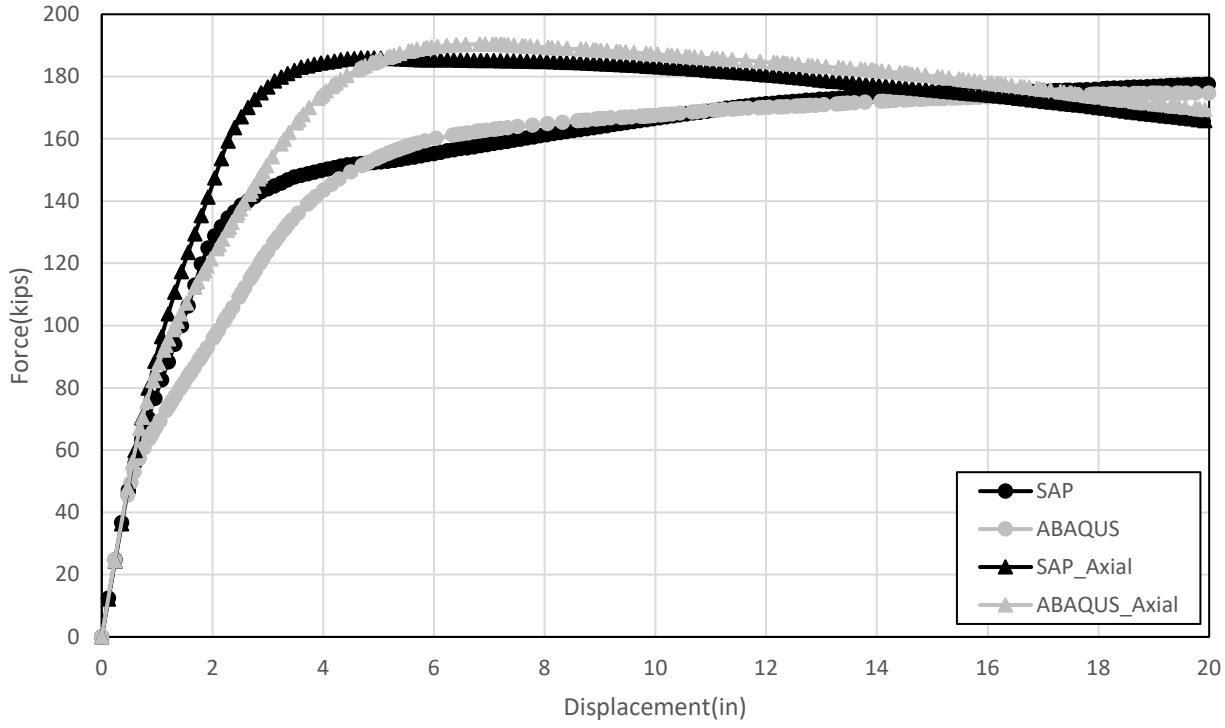

Figure A-2 Pushover Curve for 4ft Diameter and 40ft Height Column with Mid-Range Reinforcement Ratio

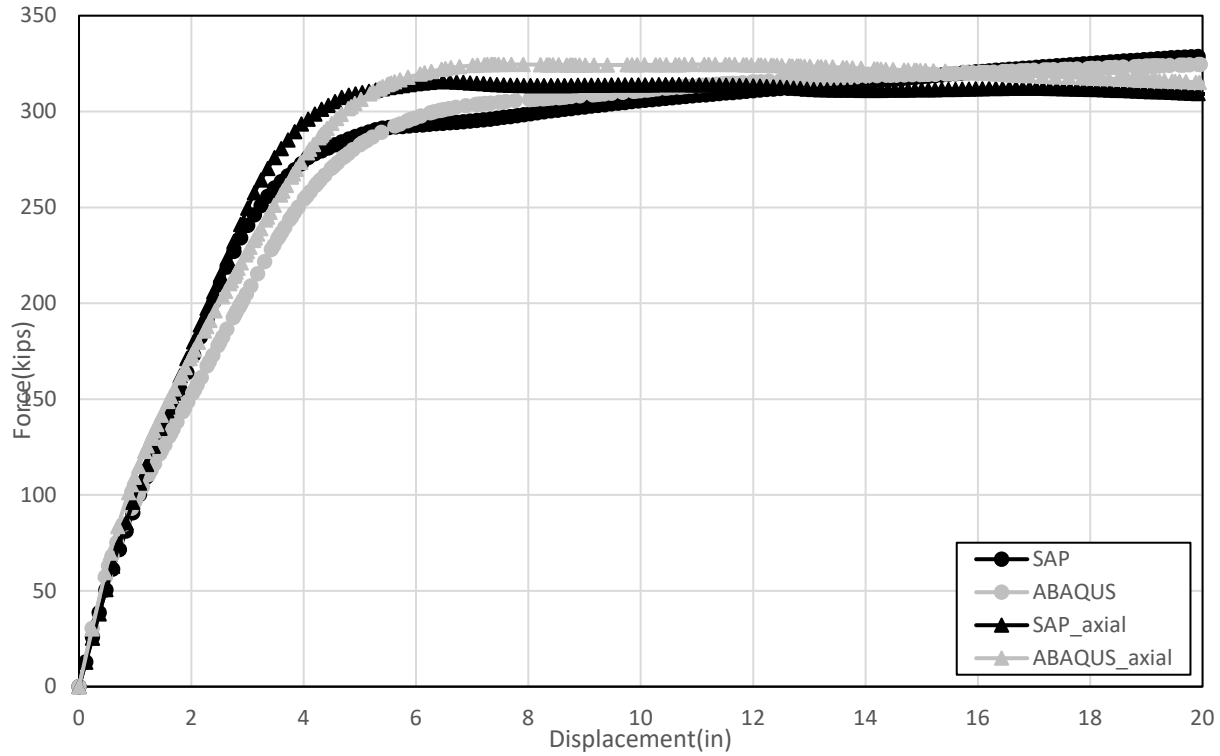

Figure A-3 Pushover Curve for 4ft Diameter and 40ft Height Column with Upper Limit Reinforcement Ratio

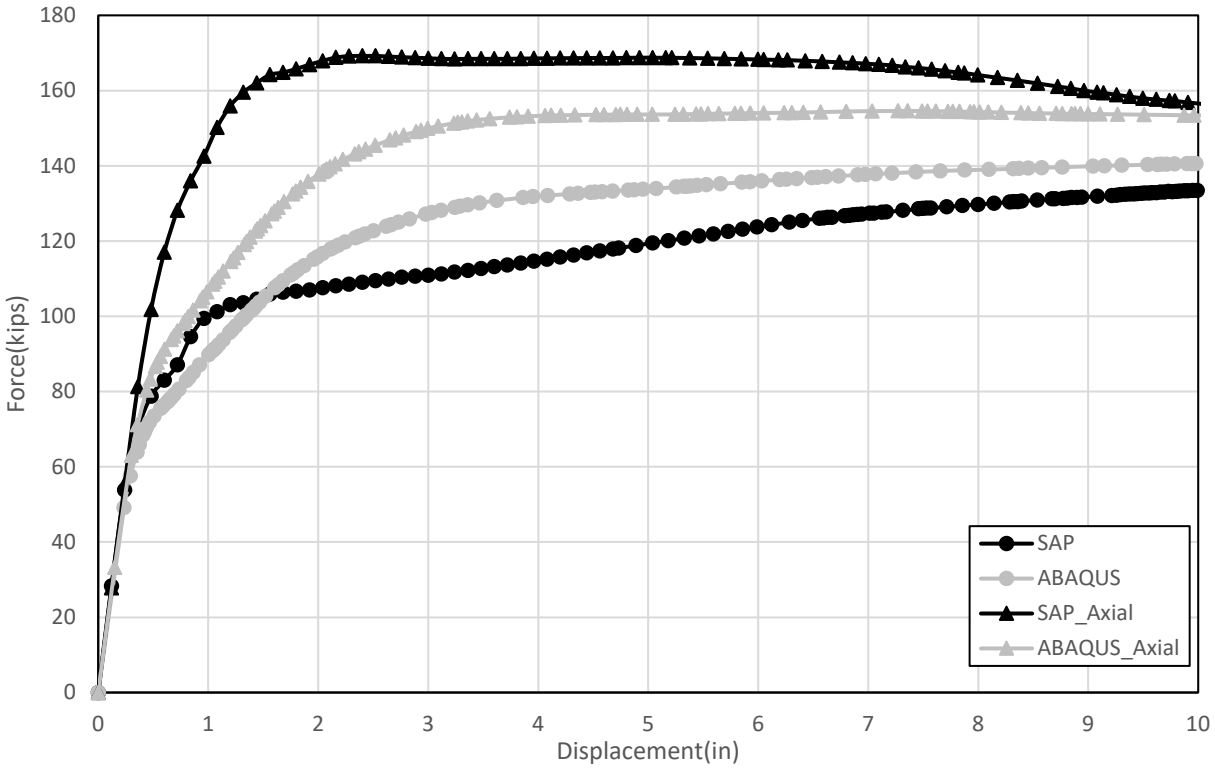

Figure A-4 Pushover Curve for 4ft Diameter and 30ft Height Column with Lower Limit Reinforcement Ratio

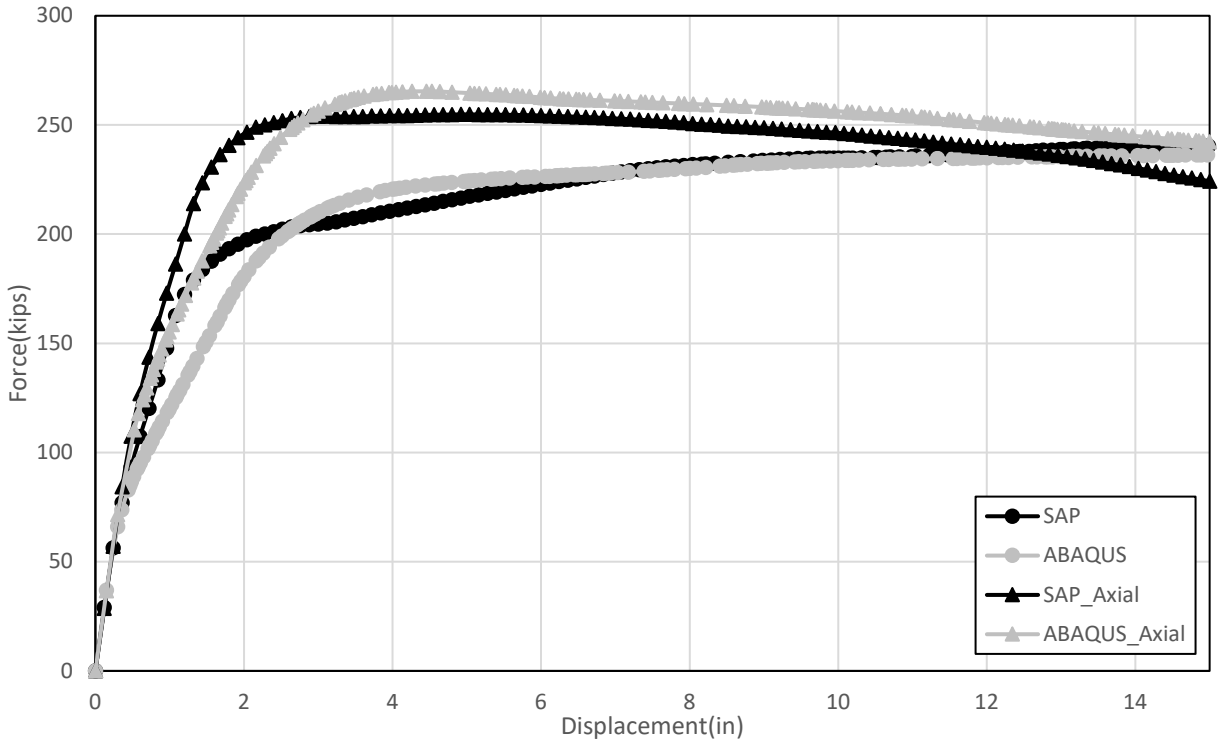

Figure A-5 Pushover Curve for 4ft Diameter and 30ft Height Column with Mid-Range Reinforcement Ratio

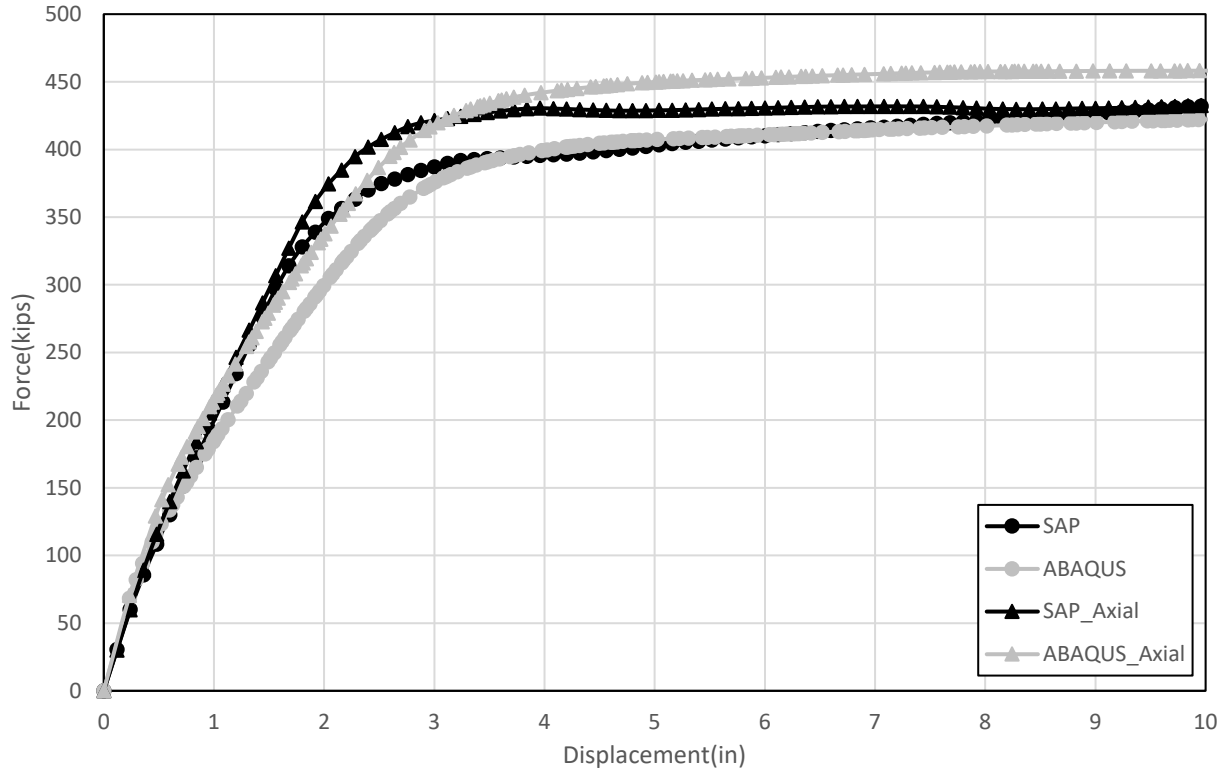

Figure A-6 Pushover Curve for 4ft Diameter and 30ft Height Column with Upper Limit Reinforcement Ratio

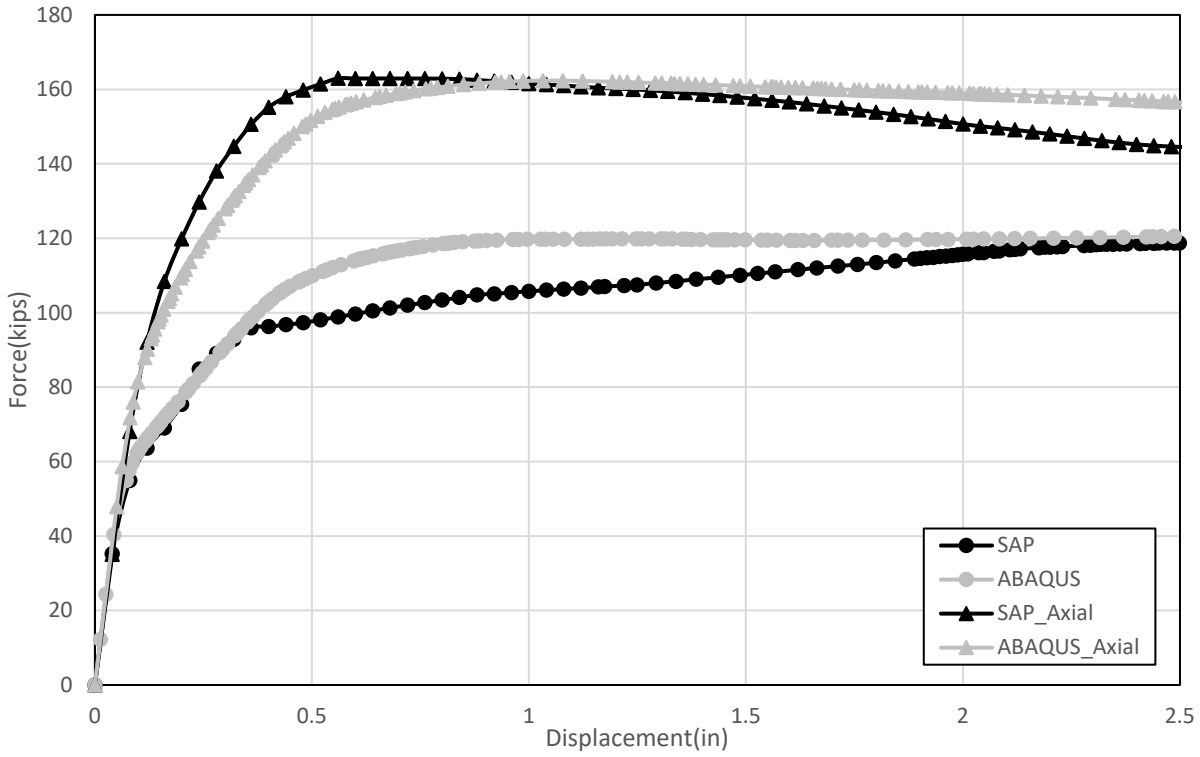

Figure A-7 Pushover Curve for 2.5ft Diameter and 10ft Height Column with Lower Limit Reinforcement Ratio

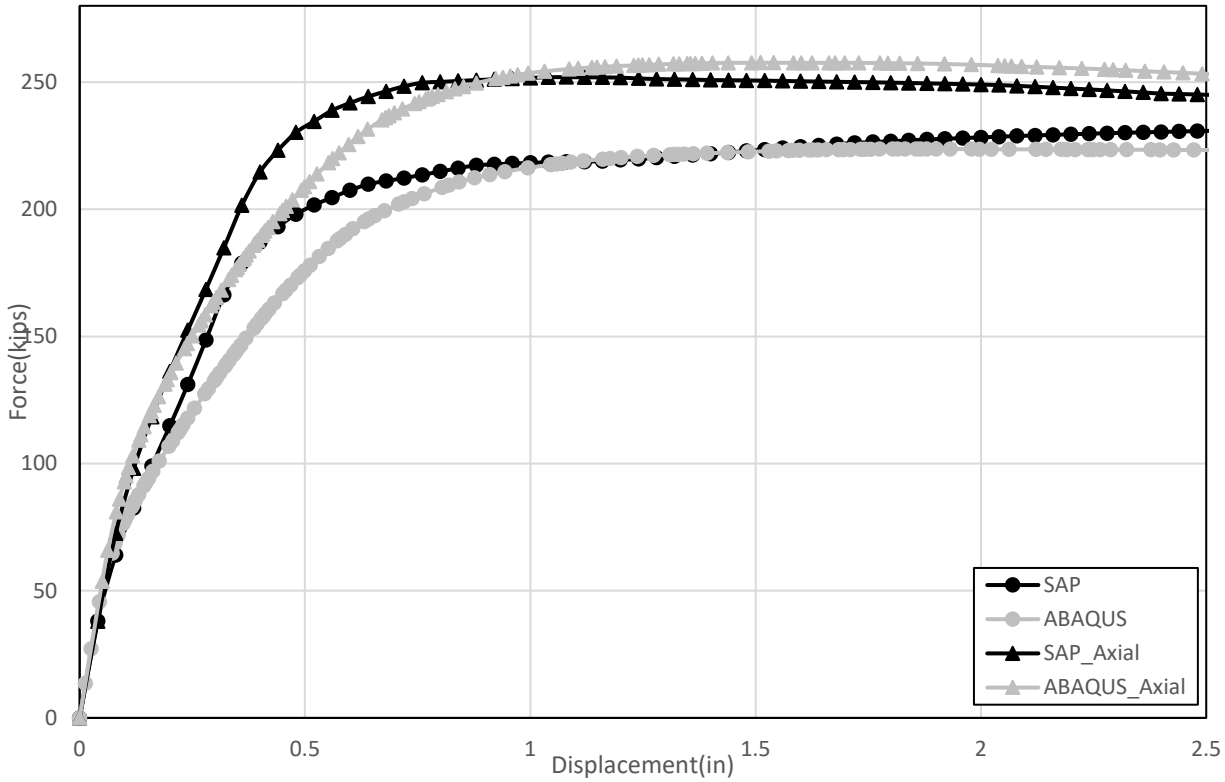

Figure A-8 Pushover Curve for 2.5ft Diameter and 10ft Height Column with Mid-Range Reinforcement Ratio

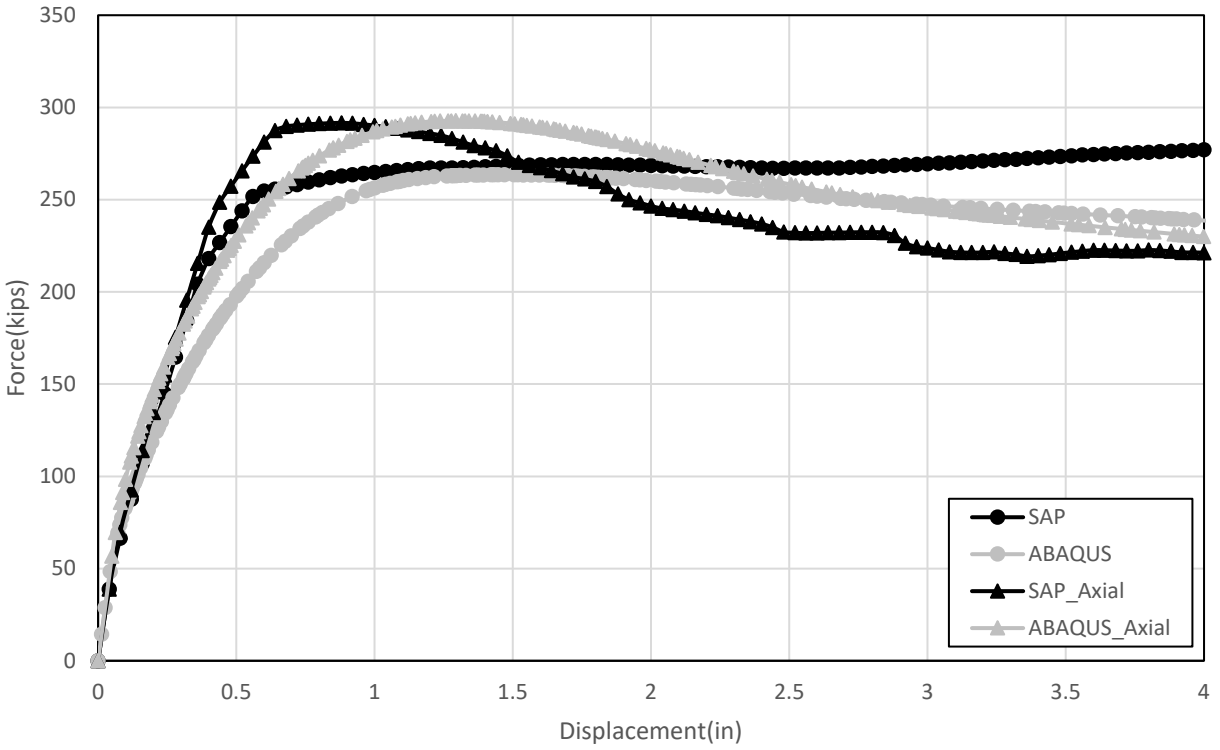

Figure A-9 Pushover Curve for 2.5ft Diameter and 10ft Height Column with Upper Limit Reinforcement Ratio

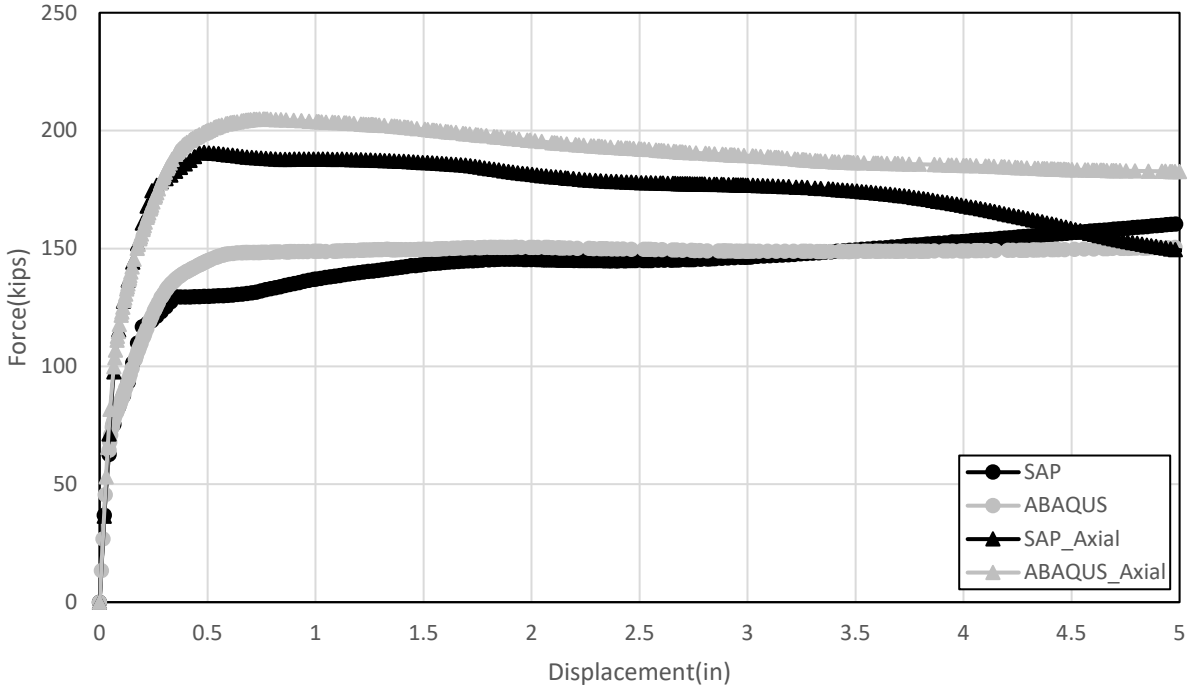

Figure A-10 Pushover Curve for 2.5ft Diameter and 8ft Height Column with lower Limit Reinforcement Ratio

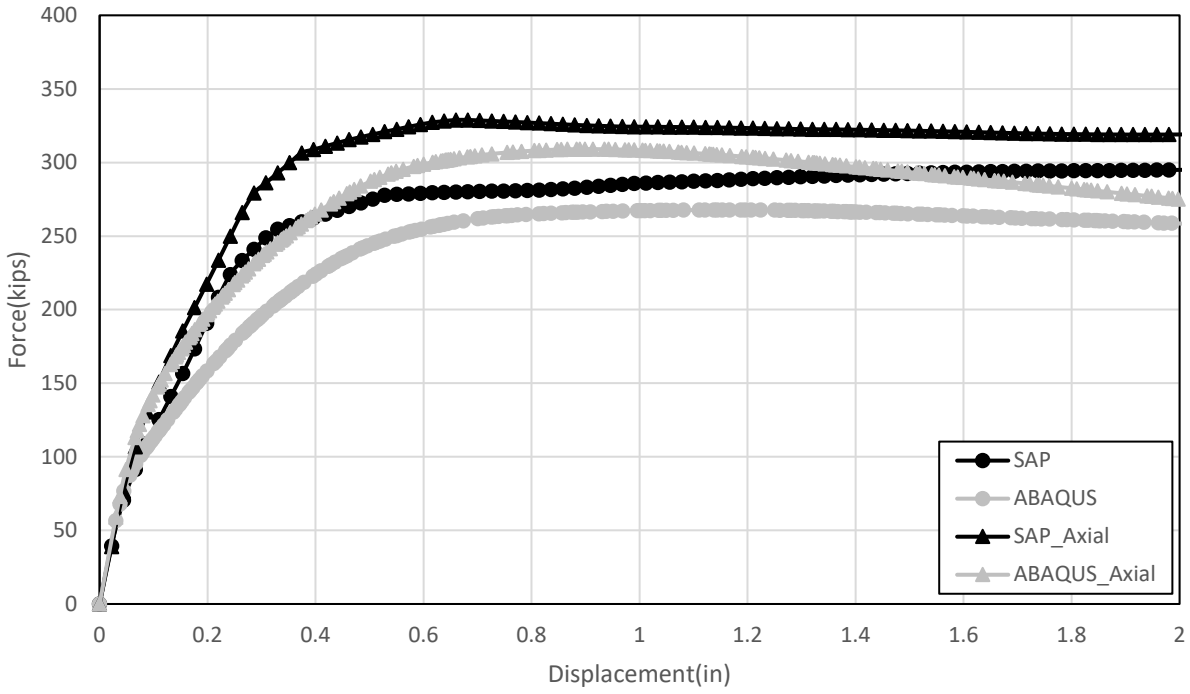

Figure A-11 Pushover Curve for 2.5ft Diameter and 8ft Height Column with Mid-Range Reinforcement Ratio

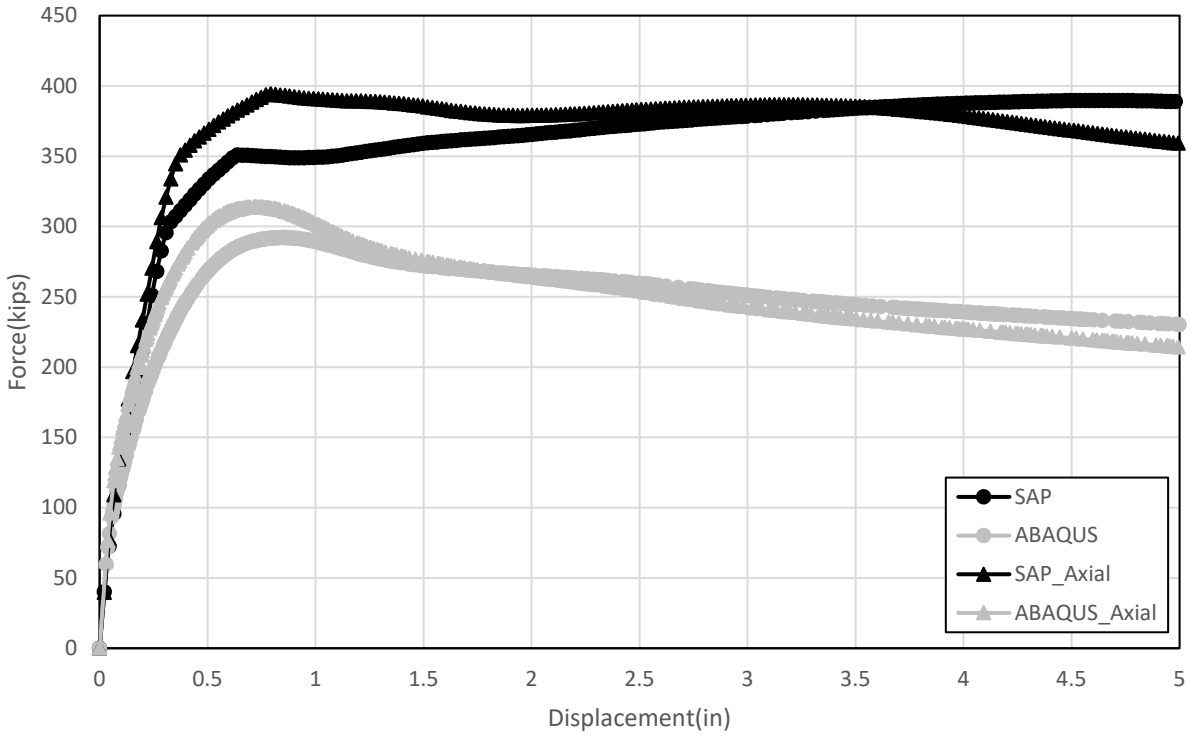

Figure A-12 Pushover Curve for 2.5ft Diameter and 8ft Height Column with Upper Limit Reinforcement Ratio

Appendix B. Sample Calculation

Montgomery County Bridge Design

$Weight := 13384.79\,kip$ From model vertical base reactions

$T_{long} := 1.29533$ From analytical model 1st Modal period

$T_{tranv} := 0.67212$ From analytical model 2nd Modal period

$Length := 1273.66\,ft$ From drawings

Geological Report not provided. Assume Site Class D

$N_{worst} := 50$

$$SiteClass := \left[\begin{array}{ll} \text{"C"} & \text{if } N_{worst} > 50 \\ \text{"D"} & \text{if } \left(15 < N_{worst}\right) \le 50 \\ \text{"F"} & \text{otherwise} \end{array} \right] = \text{"D"}$$

Guide Table 3.4.2.1-1

$S_{D1} := .104$ From county acceleration maps

$S_{DS} := .154$ From county acceleration maps

$$SDC := \left| \begin{array}{ll} \text{"A"} & \text{if } S_{D1} < 0.15 \\ \text{"B"} & \text{if } 0.15 \le S_{D1} < 0.30 \\ \text{"C"} & \text{if } 0.30 \le S_{D1} < 0.50 \\ \text{"D"} & \text{otherwise} \end{array} \right. = \text{"A"}$$

Guide Table 3.5-1

$$T_s := \frac{S_{D1}}{S_{DS}} = 0.675$$

Guide EQ 3.4.1-6

$T_{star} := 1.25 T_s = 0.844$ Guide EQ 4.3.3-3

$T_0 := 0.2 \cdot T_s = 0.135$ Guide EQ 3.4.1-5

$\mu_D := 1$ Guide 4.3.3
μ.D not specified
for SDC A

$A_s := 0.067$ From county acceleration maps

$$S_{a\_long} := \begin{cases} \left[\left(S_{DS} - A_s\right) \cdot \frac{T_{long}}{T_0} + A_s\right] & \text{if } T_{long} < T_0 = 0.08 \quad \text{Guide EQ 3.4.1-4} \\ S_{DS} & \text{if } T_0 < T_{long} < T_s \quad \text{Guide EQ 3.4.1-7} \\ \frac{S_{D1}}{T_{long}} & \text{otherwise} \quad \text{Guide EQ 3.4.1-8} \end{cases}$$

$$S_{a\_tranv} := \begin{cases} \left[\left(S_{DS} - A_s\right) \cdot \frac{T_{tranv}}{T_0} + A_s\right] & \text{if } T_{tranv} < T_0 = 0.154 \quad \text{Guide EQ 3.4.1-4} \\ S_{DS} & \text{if } T_0 < T_{tranv} < T_s \quad \text{Guide EQ 3.4.1-7} \\ \frac{S_{D1}}{T_{tranv}} & \text{otherwise} \quad \text{Guide EQ 3.4.1-8} \end{cases}$$

$p_{e\_long} := \frac{S_{a\_long} \cdot Weight}{Length} = 0.844 \cdot \frac{kip}{ft}$ Guide EQ C5.4.2-4

$p_{e\_tranv} := \frac{S_{a\_tranv} \cdot Weight}{Length} = 1.618 \cdot \frac{kip}{ft}$ Guide EQ C5.4.2-4

$$CapacityCheck(demand, capacity) := \begin{cases} \text{"OK"} & \text{if } demand < capacity \\ \text{"Capacity exceeded"} & \text{otherwise} \end{cases}$$

$$RequirementCheck(requirement, calculation) := \begin{cases} \text{"OK"} & \text{if } calculation < requirement \\ \text{"NOT OK"} & \text{otherwise} \end{cases}$$

Connection Design Check

Transverse Shear

Earthquake Loads

$v_{TEQ7} := -2.01kip + -35.91kip$ Transverse EQ shear in critical bearing connection at Bent 7

$v_{TEQ8} := 3.72kip + -77.58kip$ Transverse EQ shear in critical bearing connection at Bent 8

$v_{TEQ9} := 4.01kip + -59.5kip$ Transverse EQ shear in critical bearing connection at Bent 9

$v_{TEQ10} := -32.31kip + 2.59kip$ Transverse EQ shear in critical bearing connection at Abut 10

Dead Loads

$v_{TDL7} := -3.31kip$ Transverse DL shear in critical bearing connection at Bent 7

$v_{TDL8} := -1.83kip$ Transverse DL shear in critical bearing connection at Bent 8

$v_{TDL9} := -4.27kip$ Transverse DL shear in critical bearing connection at Bent 9

$v_{TDL10} := 0.93kip$ Transverse DL shear in critical bearing connection at Abut 10

Factored Loads

$v_{bent7connec} := 1.25 \cdot v_{TDL7} + v_{TEQ7} = -42.057 \cdot kip$ LRFD Table 4.3.1-1 abd 4.3.1-2

$v_{bent8connec} := 1.25 \cdot v_{TDL8} + v_{TEQ8} = -76.147 \cdot kip$

$v_{bent9connec} := 1.25 \cdot v_{TDL9} + v_{TEQ9} = -60.827 \cdot kip$

$v_{abut10connec} := 1.25 \cdot v_{TDL10} + v_{TEQ10} = -28.558 \cdot kip$

Weld Design

$F_{exx} := 70ksi$ Yield strength of weld metal

$t_{soleplate} := \frac{40}{25.4}in = 1.575 \cdot in$ Thickness of sole palte

$F_{yplate} := 36ksi$ Yield stress of sole plate

$F_{uplate} := 58ksi$ Ultimate tensile stress of sole plate

$L_{weldbent7} := 20in$ Weld length at bent 7

$L_{weldbent8} := 30in$ Weld length at bent 8

$L_{weldbent9} := 30in$ Weld length at bent 9

$L_{weldabut10} := 20in$ Weld length at abutment 10

$Number_{welds} := 2$ Number of welds for connection

$weld_{size} := \frac{5}{16}in$ Fillet weld throat size

Base Metal Tension LRFD 6.13.5.2

$\phi_y := 0.95$ Resistance factor for yielding on gross section

$\phi_u := 0.80$ Resistance factor for rupture on net section

$U := 1$ Shear lag factor for welded members in tension

$A_{plate7} := L_{weldbent7} \cdot t_{soleplate} = 31.496 \cdot in^2$

$A_{plate8} := L_{weldbent8} \cdot t_{soleplate} = 47.244 \cdot in^2$

$A_{plate9} := L_{weldbent9} \cdot t_{soleplate} = 47.244 \cdot in^2$

$A_{plate10} := L_{weldabut10} \cdot t_{soleplate} = 31.496 \cdot in^2$

$\phi R_{baserupture7} := \min(\phi_y \cdot F_{yplate} \cdot A_{plate7}, \phi_u \cdot F_{uplate} \cdot A_{plate7} \cdot U) = 1077.165 \cdot kip$

$\phi R_{baserupture8} := \min\left(\phi_y \cdot F_{yplate} \cdot A_{plate8}, \phi_u \cdot F_{uplate} \cdot A_{plate8} \cdot U\right) = 1615.748 \cdot kip$

$\phi R_{baserupture9} := \min\left(\phi_y \cdot F_{yplate} \cdot A_{plate9}, \phi_u \cdot F_{uplate} \cdot A_{plate9} \cdot U\right) = 1615.748 \cdot kip$

$\phi R_{baserupture10} := \min\left(\phi_y \cdot F_{yplate} \cdot A_{plate10}, \phi_u \cdot F_{uplate} \cdot A_{plate10} \cdot U\right) = 1077.165 \cdot kip$

Base Metal Shear LRFD 6.13.5.3

$\phi_v := 1.0$ Resistance factor for base metal shear

$\phi R_{baseshear7} := \phi_v \cdot 0.58 \cdot F_{yplate} \cdot A_{plate7} = 657.638 \cdot kip$

$\phi R_{baseshear8} := \phi_v \cdot 0.58 \cdot F_{yplate} \cdot A_{plate8} = 986.457 \cdot kip$

$\phi R_{baseshear9} := \phi_v \cdot 0.58 \cdot F_{yplate} \cdot A_{plate9} = 986.457 \cdot kip$

$\phi R_{baseshear10} := \phi_v \cdot 0.58 \cdot F_{yplate} \cdot A_{plate10} = 657.638 \cdot kip$

Weld Metal Shear Rupture LRFD 6.13.3.2.3

$\phi_{e2} := 0.80$ Resistance factor for base metal shear rupture

$R_{rShear} := 0.6 \cdot \phi_{e2} \cdot F_{exx}$ Factored Resistance LRFD 6.13.3.2.4b-1

$A_{effbent7} := .707 \cdot weld_{size} \cdot L_{weldbent7} \cdot Number_{welds} = 8.837 \cdot in^2$ Effective weld area LRFD 6.13.3.3

$A_{effbent8} := .707 \cdot weld_{size} \cdot L_{weldbent8} \cdot Number_{welds} = 13.256 \cdot in^2$

$A_{effbent9} := .707 \cdot weld_{size} \cdot L_{weldbent9} \cdot Number_{welds} = 13.256 \cdot in^2$

$A_{effabut10} := .707 \cdot weld_{size} \cdot L_{weldabut10} \cdot Number_{welds} = 8.837 \cdot in^2$

$\phi R_{weld7} := \phi_{e2} \cdot A_{effbent7} \cdot R_{rShear} = 237.552 \cdot kip$

$\phi R_{weld8} := \phi_{e2} \cdot A_{effbent8} \cdot R_{rShear} = 356.328 \cdot kip$

$\phi R_{weld9} := \phi_{e2} \cdot A_{effbent9} \cdot R_{rShear} = 356.328 \cdot kip$

$\phi R_{weld10} := \phi_{e2} \cdot A_{effabut10} \cdot R_{rShear} = 237.552 \cdot kip$

Weld Capacity

$\phi Weld_{bent7} := \min(\phi R_{baserupture7}, \phi R_{baseshear7}, \phi R_{weld7}) = 237.552 \cdot kip$

$\phi Weld_{bent8} := \min(\phi R_{baserupture8}, \phi R_{baseshear8}, \phi R_{weld8}) = 356.328 \cdot kip$

$\phi Weld_{bent9} := \min(\phi R_{baserupture9}, \phi R_{baseshear9}, \phi R_{weld9}) = 356.328 \cdot kip$

$\phi Weld_{abut10} := \min(\phi R_{baserupture10}, \phi R_{baseshear10}, \phi R_{weld10}) = 237.552 \cdot kip$

$CapacityCheck(|v_{bent7connec}|, \phi Weld_{bent7}) = "OK"$

$CapacityCheck(|v_{bent8connec}|, \phi Weld_{bent8}) = "OK"$

$CapacityCheck(|v_{bent9connec}|, \phi Weld_{bent9}) = "OK"$

$CapacityCheck(|v_{abut10connec}|, \phi Weld_{abut10}) = "OK"$

Anchor Bolt Design

Flexural Demand

$Dia := 1.5in$ Diameter of anchor bolts

$E := 29000ksi$

$slotwidth := \frac{45}{25.4}in = 1.772 \cdot in$ Width of bolt slot

$t_{soleplate} = 1.575 \cdot in$ Thickness of sole plate

$L_{anchorbent7} := 7.2in$ Length of anchor bolt at bent 7

$L_{anchorbent8} := 4.75in$ Length of anchor bolt at bent 8

$L_{anchorbent9} := 4.75in$ Length of anchor bolt at bent 9

$L_{anchorabut10} := 4.75in$ Length of anchor bolt at abutment 10

$I_{anchor} := \frac{\pi}{4} \cdot \left(\frac{Dia}{2}\right)^4 = 0.249 \cdot in^4$ Moment of inertia of anchor bolt

Calculate the force required to deflect the anchor bolt till it comes into contact with the sole plate.
This force creates bending moment as a cantilever element ("cant")

$$P_{bent7cant} := \frac{(slotwidth - Dia) \cdot 3 \cdot E \cdot I_{anchor}}{\left(L_{anchorbent7} - \frac{t_{soleplate}}{2}\right)^3} = 22.272 \cdot kip$$

$$P_{bent7cant} := \begin{cases} P_{bent7cant} & \text{if } P_{bent7cant} < |v_{bent7connec}| \\ |v_{bent7connec}| & \text{otherwise} \end{cases} = 22.272 \cdot kip$$

Cantilever force can't be greater than actual shear force from model

$$P_{bent8cant} := \frac{(slotwidth - Dia) \cdot 3 \cdot E \cdot I_{anchor}}{\left(L_{anchorbent8} - \frac{t_{soleplate}}{2}\right)^3} = 94.391 \cdot kip$$

$$P_{bent8cant} := \begin{cases} P_{bent8cant} & \text{if } P_{bent8cant} < |v_{bent8connec}| \\ |v_{bent8connec}| & \text{otherwise} \end{cases} = 76.147 \cdot kip$$

$$P_{bent9cant} := \frac{(slotwidth - Dia) \cdot 3 \cdot E \cdot I_{anchor}}{\left(L_{anchorbent9} - \frac{t_{soleplate}}{2}\right)^3} = 94.391 \cdot kip$$

$$P_{bent9cant} := \begin{cases} P_{bent9cant} \text{ if } P_{bent9cant} < \left|v_{bent9connec}\right| \\ \left|v_{bent9connec}\right| \text{ otherwise} \end{cases} = 60.827 \cdot kip$$

$$P_{abut10cant} := \frac{(slotwidth - Dia) \cdot 3 \cdot E \cdot I_{anchor}}{\left(L_{anchorabut10} - \frac{t_{soleplate}}{2}\right)^3} = 94.391 \cdot kip$$

$$P_{abut10cant} := \begin{cases} P_{abut10cant} \text{ if } P_{abut10cant} < \left|v_{abut10connec}\right| \\ \left|v_{abut10connec}\right| \text{ otherwise} \end{cases} = 28.558 \cdot kip$$

After the anchor bends as a cantilever element, it will contact the sole plate and behave as a fixed-fixed connection. The difference between the actual shear force and the cantilever force is the remaining force left to bend the anchor bolt as a fixed-fixed element

$$P_{bent7fixed} := \begin{cases} \left(\left|v_{bent7connec}\right| - P_{bent7cant}\right) \text{ if } \left(\left|v_{bent7connec}\right| - P_{bent7cant}\right) > 0 \\ 0 \text{ otherwise} \end{cases} = 19.785 \cdot kip$$

$$P_{bent8fixed} := \begin{cases} \left(\left|v_{bent8connec}\right| - P_{bent8cant}\right) \text{ if } \left(\left|v_{bent8connec}\right| - P_{bent8cant}\right) > 0 \\ 0 \text{ otherwise} \end{cases} = 0 \cdot kip$$

$$P_{bent9fixed} := \begin{cases} \left(\left|v_{bent9connec}\right| - P_{bent9cant}\right) \text{ if } \left(\left|v_{bent9connec}\right| - P_{bent9cant}\right) > 0 \\ 0 \text{ otherwise} \end{cases} = 0 \cdot kip$$

$$P_{abut10fixed} := \begin{cases} \left(\left|v_{abut10connec}\right| - P_{abut10cant}\right) \text{ if } \left(\left|v_{abut10connec}\right| - P_{abut10cant}\right) > 0 \\ 0 \text{ otherwise} \end{cases} = 0 \cdot kip$$

Flexural demand is the total from the cantilever and fixed-fixed bending

$$M_{bent7connec} := P_{bent7cant} \cdot \left(L_{anchorbent7} - \frac{t_{soleplate}}{2}\right) + 0.5 \cdot P_{bent7fixed} \cdot \left(L_{anchorbent7} - \frac{t_{soleplate}}{2}\right)$$

$$M_{bent7connec} = 206.261 \cdot kip \cdot in$$

$$M_{bent8connec} := P_{bent8cant}\cdot\left(L_{anchorbent8} - \frac{t_{soleplate}}{2}\right) + 0.5P_{bent8fixed}\cdot\left(L_{anchorbent8} - \frac{t_{soleplate}}{2}\right)$$

$$M_{bent8connec} = 301.742\cdot kip\cdot in$$

$$M_{bent9connec} := P_{bent9cant}\cdot\left(L_{anchorbent9} - \frac{t_{soleplate}}{2}\right) + 0.5P_{bent9fixed}\cdot\left(L_{anchorbent9} - \frac{t_{soleplate}}{2}\right)$$

$$M_{bent9connec} = 241.035\cdot kip\cdot in$$

$$M_{abut10connec} := P_{abut10cant}\cdot\left(L_{anchorabut10} - \frac{t_{soleplate}}{2}\right) + 0.5P_{abut10fixed}\cdot\left(L_{anchorabut10} - \frac{t_{solep}}{2}\right.$$

$$M_{abut10connec} = 113.162\cdot kip\cdot in$$

Flexural Strength

$F_y := 60ksi$ Yield strength of anchor bolt

$\phi_f := 1.0$ Flexural resistance factor

$A_{bolt} := \frac{\pi}{4}\cdot Dia^2 = 1.767\cdot in^2$ Area of bolt

$Z := \frac{1}{2}\cdot A_{bolt}\cdot\frac{4\cdot\frac{Dia}{2}}{3\pi}\cdot 2 = 0.562\cdot in^3$ Plastic section modulus

$S := \frac{\pi\cdot\left(\frac{Dia}{2}\right)^3}{4} = 0.331\cdot in^3$ Elastic section modulus

$N_{bolts7} := 4$ Number of bolts at bent 7

$M_{nbent7} := \min\left(F_y\cdot Z, 1.6\cdot F_y\cdot S\right)\cdot N_{bolts7} = 127.235\cdot kip\cdot in$ LRFD EQ 6.12.2.2.7-1

$\phi_f\cdot M_{nbent7} = 127.235\cdot kip\cdot in$

$N_{bolts8} := 4$

$M_{nbent8} := \min(F_y \cdot Z, 1.6 \cdot F_y \cdot S) \cdot N_{bolts8} = 127.235 \cdot kip \cdot in$

$\phi_f \cdot M_{nbent8} = 127.235 \cdot kip \cdot in$

$N_{bolts9} := 4$

$M_{nbent9} := \min(F_y \cdot Z, 1.6 \cdot F_y \cdot S) \cdot N_{bolts9} = 127.235 \cdot kip \cdot in$

$\phi_f \cdot M_{nbent9} = 127.235 \cdot kip \cdot in$

$N_{bolts10} := 2$

$M_{nabut10} := \min(F_y \cdot Z, 1.6 \cdot F_y \cdot S) \cdot N_{bolts10} = 63.617 \cdot kip \cdot in$

$\phi_f \cdot M_{nabut10} = 63.617 \cdot kip \cdot in$

$CapacityCheck(|M_{bent7connec}|, \phi_f \cdot M_{nbent7}) = \text{"Capacity exceeded"}$

$CapacityCheck(|M_{bent8connec}|, \phi_f \cdot M_{nbent8}) = \text{"Capacity exceeded"}$

$CapacityCheck(|M_{bent9connec}|, \phi_f \cdot M_{nbent9}) = \text{"Capacity exceeded"}$

$CapacityCheck(|M_{abut10connec}|, \phi_f \cdot M_{nabut10}) = \text{"Capacity exceeded"}$

Shear Strength LRFD 6.13.2.12

$F_{ub} := 60ksi$ Ultimate tensile strength of bolts

$N_{splanes} := 1$ Number of shear planes per bolt

$\phi_s := .75$ Resistance factor for shear of anchor bolts

$R_{nbent7} := .48 \cdot A_{bolt} \cdot F_{ub} \cdot N_{splanes} \cdot N_{bolts7} = 203.575 \cdot kip$

$\phi_s \cdot R_{nbent7} = 152.681 \cdot kip$

$R_{nbent8} := .48 \cdot A_{bolt} \cdot F_{ub} \cdot N_{splanes} \cdot N_{bolts8} = 203.575 \cdot kip$

$\phi_s \cdot R_{nbent8} = 152.681 \cdot kip$

$R_{nbent9} := .48 \cdot A_{bolt} \cdot F_{ub} \cdot N_{splanes} \cdot N_{bolts9} = 203.575 \cdot kip$

$\phi_s \cdot R_{nbent9} = 152.681 \cdot kip$

$R_{nabut10} := .48 \cdot A_{bolt} \cdot F_{ub} \cdot N_{splanes} \cdot N_{bolts10} = 101.788 \cdot kip$

$\phi_s \cdot R_{nabut10} = 76.341 \cdot kip$

$CapacityCheck\left(\left|v_{bent7connec}\right|, \phi_s \cdot R_{nbent7}\right) = \text{"OK"}$

$CapacityCheck\left(\left|v_{bent8connec}\right|, \phi_s \cdot R_{nbent8}\right) = \text{"OK"}$

$CapacityCheck\left(\left|v_{bent9connec}\right|, \phi_s \cdot R_{nbent9}\right) = \text{"OK"}$

$CapacityCheck\left(\left|v_{abut10connec}\right|, \phi_s \cdot R_{nabut10}\right) = \text{"OK"}$

Shear Block Design

$\phi_{shear} := 0.9$ LRFD 5.5.4.2

$\phi_{tension} := 0.9$ LRFD 5.5.4.2

$\phi_{compression} := 0.75$ LRFD 5.5.4.2

$f_{cprime} := 6.5$

$f_y := 60ksi$

Note: Because Mathcad has difficulty when units are placed under a square root, dimensions are left off of the compressive strength. Any time this variable is used, the units must be added in somewhere--usually to a constant.

$V_{bent} := 281.13kip$ Bent base shear

Assume l_v is width of bent

$l_v := 60in$ Length of shear block

$a_v := L_{anchorbent7} - \frac{t_{soleplate}}{2} = 6.413 \cdot in$

Height from surface of bent cap that shear force will be applied to Shear Block. Bent 7 was chosen as it is the longest

Assume concrete cover $d_c := 3in$

$h := a_v + d_c + 0.5in = 9.913 \cdot in$

$h := 10in$

Height of the shear block will be a_v plus the cover, plus the diameter of the transverse reinforcement. Here it is assumed that No. 4 reinforcing will be used for the transverse reinforcement.

Shear design

This spreadsheet is set up for an iterative design process. The width of the shear block (w), the shear reinforcement (A_v), and the spacing of transverse reinforcement (s) will be the three changing variables until all of the design checks are met.

Estimate $w := 78in$

Full width of the shear block. This can be estimated by the distance between adjacent girder sole plates minus a gap between the sole plate and the shear block determined by the designer.

$c := 0.4ksi$ LRFD 5.8.4.3

$\mu := 1.4$ LRFD 5.8.4.3

$A_{cv} := w \cdot l_v = 4680 \cdot in^2$

$$A_{vf.min} := \frac{0.05 \frac{kip}{in^2} \cdot A_{cv}}{f_y} = 3.9 \cdot in^2$$ LRFD 5.8.4.4

$\frac{kip}{in^2}$ applied for dimensional consistency

$V_n := c \cdot A_{cv} + \mu \cdot A_{vf.min} \cdot f_y = 2199.6 \cdot kip$ LRFD 5.8.4.1-3

$K_1 := .25$ LRFD 5.8.4.3

$K_2 := 1.5ksi$ LRFD 5.8.4.3

$V_{nmax1} := K_1 \cdot f_{cprime} \cdot A_{cv} \cdot 1ksi = 7605 \cdot kip$ LRFD 5.8.4.1-4

$V_{nmax2} := K_2 \cdot A_{cv} = 7020 \cdot kip$ LRFD 5.8.4.1-5

$\phi V_n := \min\left(\phi_{shear} \cdot V_n, V_{nmax1}, V_{nmax2}\right) = 1979.64 \cdot kip$

$CapacityCheck\left(V_{bent}, \phi V_n\right) = "OK"$

Longitudinal Shear

Earthquake Loads

$v_{LEQ7} := 14.2kip + -.99kip$ Longitudinal EQ shear in critical bearing connection at Bent 7

$v_{LEQ8} := 29.65kip + .16kip$ Longitudinal EQ shear in critical bearing connection at Bent 8

$v_{LEQ9} := 27.65kip + 3.74kip$ Longitudinal EQ shear in critical bearing connection at Bent 9

$v_{LEQ10} := 39.56kip + 3.6kip$ Longitudinal EQ shear in critical bearing connection at Abut 10

Dead Loads

$v_{LDL7} := -.38kip$ Longitudinal DL shear in critical bearing connection at Bent 7

$v_{LDL8} := 1.13kip$ Longitudinal DL shear in critical bearing connection at Bent 8

$v_{LDL9} := -.37kip$ Longitudinal DL shear in critical bearing connection at Bent 9

$v_{LDL10} := 4.85kip$ Longitudinal DL shear in critical bearing connection at Abut 10

Factored Loads:

$v_{Lbent7connec} := 1.25 \cdot v_{LDL7} + v_{LEQ7} = 12.735 \cdot kip$

$v_{Lbent8connec} := 1.25 \cdot v_{LDL8} + v_{LEQ8} = 31.223 \cdot kip$

$v_{Lbent9connec} := 1.25 \cdot v_{LDL9} + v_{LEQ9} = 30.927 \cdot kip$

$v_{Labut10connec} := 1.25 \cdot v_{LDL10} + v_{LEQ10} = 49.223 \cdot kip$

Weld Strength

$\phi Weld_{bent7} = 237.552 \cdot kip$ Weld strength is same as above

$\phi Weld_{bent8} = 356.328 \cdot kip$

$\phi Weld_{bent9} = 356.328 \cdot kip$

$\phi Weld_{abut10} = 237.552 \cdot kip$

$CapacityCheck\left(\left|v_{Lbent7connec}\right|, \phi Weld_{bent7}\right) = "OK"$

$CapacityCheck\left(\left|v_{Lbent8connec}\right|, \phi Weld_{bent8}\right) = "OK"$

$CapacityCheck\left(\left|v_{Lbent9connec}\right|, \phi Weld_{bent9}\right) = "OK"$

$CapacityCheck\left(\left|v_{Labut10connec}\right|, \phi Weld_{abut10}\right) = "OK"$

End Diaphragm Design

$\phi_{tu} := 0.80$ Tension, fracture on the net section

$\phi_{ty} := 0.95$ Tension, yielding in gross section LRFD 6.5.4.2

$\phi_{bs} := 0.80$ Block shear failure

$\phi_c := 0.95$ Axial compression

$E := 29000ksi$ $F_{yw} := 36ksi$ $F_u := 58ksi$ $G := .385 \cdot E = 11165 \cdot ksi$

Top Chord C15x40

$MaxComp := .998kip$

$MaxTen := 1.06kip$

$L_b := 8.6ft$

$A_g := 11.8in^2$ $r_x := 5.43in$ $r_y := 0.883in$ $J := 1.45in^4$ $I_x := 348in^4$

$C_w := 410in^6$ $H := .927$ $r_0 := 5.71in$ $I_y := 9.17in^4$ $t_w := 0.52in$

Tension Member Design

Check slenderness ratio

$slenderness_{limit} := 140$ LRFD 6.8.4

$slenderness_{ratio} := \frac{L_b}{r_x} = 19.006$

$RequirementCheck(slenderness_{limit}, slenderness_{ratio}) = "OK"$

Yielding on gross section

$P_{r1} := \phi_y \cdot F_y \cdot A_g = 403.56 \cdot kip$ LRFD EQ 6.8.2.1-1

Fracture on net section

$R_p := 0.9$ Assume holes are punched

$U := 1 - \frac{.5}{8}$ Shear lag factor

$Dia_{hole} := 1in$

$Num_{holes} := 4$

$A_n := A_g - \left(Dia_{hole} + \frac{1}{16}in\right) \cdot t_w \cdot Num_{holes} = 9.59 \cdot in^2$

$P_{r2} := \phi_u \cdot F_u \cdot A_n \cdot R_p \cdot U = 375.449 \cdot kip$ LRFD EQ 6.8.2.1-2

$P_r := \min(P_{r1}, P_{r2}) = 375.449 \cdot kip$

Block shear LRFD 6.13.4

$A_{tn} := 4in \cdot t_w = 2.08 \cdot in^2$

$A_{vg} := 8in \cdot t_w = 4.16 \cdot in^2$

$A_{vn} := A_{vg} - \left(Dia_{hole} + \frac{1}{16}in\right) \cdot t_w$

$U_{bs} := 1.0$

$R_r := \min\left[\phi_{bs} \cdot R_p \cdot \left(.58 \cdot F_u \cdot A_{vn} + U_{bs} \cdot F_u \cdot A_{tn}\right), \phi_{bs} \cdot R_p \cdot \left(.58 \cdot F_y \cdot A_{vg} + U_{bs} \cdot F_u \cdot A_{tn}\right)\right] = 149.401 \cdot kip$

$TopChordCapacity := \min(P_r, R_r) = 149.401 \cdot kip$

$CapacityCheck(MaxTen, TopChordCapacity) = "OK"$

Compression Member Design

Check slenderness

$slenderness_{limit} := 120$ LRFD 6.9.3

$slenderness_{ratio} := \frac{L_b}{r_y} = 116.874$

$RequirementCheck(slenderness_{limit}, slenderness_{ratio}) = "OK"$

$k := 1.49$

$b_f := 3.52in$ $t_f := 0.65in$

$slenderness_{ratio} := \frac{b_f}{t_f} = 5.415$ LRFD 6.9.4.2

$slenderness_{limit} := k \cdot \sqrt{\frac{E}{F_y}} = 42.29$

$RequirementCheck(slenderness_{limit}, slenderness_{ratio}) = "OK"$ $Q := 1.0$

Calculate Capacity

$P_{ey} := \frac{\pi^2 \cdot E}{\frac{L_b}{r_y}} \cdot A_g = 28897.532 \cdot kip$ LRFD 6.9.4.1.2-1

$P_{ez} := \left(\frac{\pi^2 \cdot E \cdot C_w}{L_b^2} + G \cdot J \right) \cdot \frac{1}{r_0^2} = 834.488 \cdot kip$ LRFD 6.9.4.1.3-5

$P_{e.elastic} := P_{ey}$

$P_{e.FTB} := \frac{(P_{ey} + P_{ez})}{2 \cdot H} \cdot \left[1 - \sqrt{1 - \frac{4 \cdot P_{ey} \cdot P_{ez} \cdot H}{(P_{ey} + P_{ez})^2}} \right] = 832.685 \cdot kip$ LRFD 6.9.4.1.3-2

$P_e := \min(P_{e.elastic}, P_{e.FTB}) = 832.685 \cdot kip$

$P_o := Q \cdot F_y \cdot A_g = 424.8 \cdot kip$ LRFD 6.9.4.1.1

$P_n := \begin{cases} (.877 \cdot P_e) & \text{if } \frac{P_e}{P_o} < 0.44 \\ \left[\left(.658^{\frac{P_o}{P_e}} \right) \cdot P_o \right] & \text{otherwise} \end{cases} = 343.124 \cdot kip$ LRFD 6.9.4.1.1-2 / LRFD 6.9.4.1.1-1

$\phi_c \cdot P_n = 325.968 \cdot kip$

$CapacityCheck(MaxComp, \phi_c \cdot P_n) = "OK"$

Bot Chord L6x6x1/2

$MaxComp := 3.38kip$

$MaxTen := 3.55kip$

$L_b := 8.6ft$

$A_g := 5.77in^2$ $r_x := 1.86in$ $r_y := 1.86in$ $J := .501in^4$ $I_x := 19.9in^4$

$C_w := 1.32in^6$ $r_0 := 3.31in$ $I_y := 19.9in^4$

Tension Member Design

Check slenderness ratio

$slenderness_{limit} := 140$ LRFD 6.8.4

$slenderness_{ratio} := \frac{L_b}{r_x} = 55.484$

$RequirementCheck(slenderness_{limit}, slenderness_{ratio}) = "OK"$

Yielding on gross section

$P_{r1} := \phi_y \cdot F_y \cdot A_g = 197.334 \cdot kip$ LRFD EQ 6.8.2.1-1

Fracture on net section

$R_p := 1.0$ No holes

$U := 0.60$ Shear lag factor

$A_n := A_g$ No area taken out of gross section because x-section is welded

$P_{r2} := \phi_u \cdot F_u \cdot A_n \cdot R_p \cdot U = 160.637 \cdot kip$ LRFD EQ 6.8.2.1-2

$P_r := \min(P_{r1}, P_{r2}) = 160.637 \cdot kip$

Block shear LRFD 6.13.4

$A_{tn} := 2 \cdot 6in \cdot \frac{5}{16}in = 3.75 \cdot in^2$

$A_{vg} := 6in \cdot \frac{5}{16}in = 1.875 \cdot in^2$

$A_{vn} := A_{vg}$

$U_{bs} := 1.0$

$R_r := \min\left[\phi_{bs} \cdot R_p \cdot \left(.58 \cdot F_u \cdot A_{vn} + U_{bs} \cdot F_u \cdot A_{tn}\right), \phi_{bs} \cdot R_p \cdot \left(.58 \cdot F_y \cdot A_{vg} + U_{bs} \cdot F_u \cdot A_{tn}\right)\right] = 205.32 \cdot kip$

$TopChordCapacity := \min\left(P_r, R_r\right) = 160.637 \cdot kip$

$CapacityCheck(MaxTen, TopChordCapacity) = \text{"OK"}$

Compression Member Design

Check slenderness

$slenderness_{limit} := 120$ LRFD 6.9.3

$slenderness_{ratio} := \frac{L_b}{r_y} = 55.484$

$RequirementCheck\left(slenderness_{limit}, slenderness_{ratio}\right) = \text{"OK"}$

$k := .45$

$b_f := 6in$ $t_f := .50in$

$slenderness_{ratio} := \frac{b_f}{t_f} = 12$ LRFD 6.9.4.2

$slenderness_{limit} := k \cdot \sqrt{\frac{E}{F_y}} = 12.772$

$RequirementCheck\left(slenderness_{limit}, slenderness_{ratio}\right) = \text{"OK"}$

USE Q=1.0 if "OK",
Otherwise use below EQ
for Q

$$Q := \begin{cases} \left(1.34 - .76 \cdot \frac{b_f}{t_f} \cdot \sqrt{\frac{F_y}{E}}\right) & \text{if } .45\sqrt{\frac{E}{F_y}} < \frac{b_f}{t_f} \le .91\sqrt{\frac{E}{F_y}} = 1 \\ \frac{.53 \cdot E}{F_y \cdot \left(\frac{b_f}{t_f}\right)^2} & \text{if } \frac{b_f}{t_f} > .91 \cdot \sqrt{\frac{E}{F_y}} \\ 1.0 & \text{otherwise} \end{cases}$$

LRFD EQ 6.9.4.2.2-5

LRFD EQ 6.9.4.2.2-6

Calculate $(KL/r)_{eff}$

$$EffSlendernessRatio := \begin{cases} \left(32 + 1.25 \cdot \frac{L_b}{r_x}\right) & \text{if } \frac{L_b}{r_x} > 80 \quad = 113.613 \\ \left(72 + .75 \cdot \frac{L_b}{r_x}\right) & \text{otherwise} \end{cases}$$

LRFD EQ 6.9.4.4-2

LRFD EQ 6.9.4.4-1

Calculate Capacity

$$P_e := \frac{\pi^2 \cdot E}{EffSlendernessRatio} \cdot A_g = 14536.033 \cdot kip$$

LRFD 6.9.4.1.2-1

$$P_o := Q \cdot F_y \cdot A_g = 207.72 \cdot kip$$

LRFD 6.9.4.1.1

$$P_n := \begin{cases} (.877 \cdot P_e) & \text{if } \frac{P_e}{P_o} < 0.44 \quad = 206.481 \cdot kip \\ \left[\left(.658^{\frac{P_o}{P_e}}\right) \cdot P_o\right] & \text{otherwise} \end{cases}$$

LRFD 6.9.4.1.1-2

LRFD 6.9.4.1.1-1

$\phi_c \cdot P_n = 196.157 \cdot kip$

$CapacityCheck(MaxComp, \phi_c \cdot P_n) = \text{"OK"}$

Diagonal L6x6x1/2

$MaxComp := 13.41kip$

$MaxTen := 13.49kip$

$L_{bx} := 11.1ft$

$A_g := 5.77in^2$ $r_x := 1.86in$ $r_y := 1.86in$ $J := .501in^4$ $I_x := 19.9in^4$

$C_w := 1.32in^6$ $r_0 := 3.31in$ $I_y := 19.9in^4$

Tension Member Design

Check slenderness ratio

$slenderness_{limit} := 140$ LRFD 6.8.4

$slenderness_{ratio} := \frac{L_b}{r_x} = 71.613$

$RequirementCheck(slenderness_{limit}, slenderness_{ratio}) = "OK"$

Yielding on gross section

$P_{r1} := \phi_y \cdot F_y \cdot A_g = 197.334 \cdot kip$ LRFD EQ 6.8.2.1-1

Fracture on net section

$R_p := 1.0$ No holes

$U := 0.60$ Shear lag factor

$A_n := A_g$ No area taken out of gross section because x-section is welded

$P_{r2} := \phi_u \cdot F_u \cdot A_n \cdot R_p \cdot U = 160.637 \cdot kip$ LRFD EQ 6.8.2.1-2

$P_r := \min(P_{r1}, P_{r2}) = 160.637 \cdot kip$

Block shear LRFD 6.13.4

$A_{nt} := 2 \cdot 6in \cdot \frac{5}{16}in = 3.75 \cdot in^2$

$A_{nvg} := 6in \cdot \frac{5}{16}in = 1.875 \cdot in^2$

$A_{nvn} := A_{vg}$

$U_{bs} := 1.0$

$R_r := \min\left[\phi_{bs} \cdot R_p \cdot \left(.58 \cdot F_u \cdot A_{vn} + U_{bs} \cdot F_u \cdot A_{tn}\right), \phi_{bs} \cdot R_p \cdot \left(.58 \cdot F_y \cdot A_{vg} + U_{bs} \cdot F_u \cdot A_{tn}\right)\right] = 205.32 \cdot kip$

$TopChordCapacity := \min\left(P_r, R_r\right) = 160.637 \cdot kip$

$CapacityCheck(MaxTen, TopChordCapacity) = \text{"OK"}$

Compression Member Design

Check slenderness

$slenderness_{limit} := 120$ LRFD 6.9.3

$slenderness_{ratio} := \frac{L_b}{r_y} = 71.613$

$RequirementCheck\left(slenderness_{limit}, slenderness_{ratio}\right) = \text{"OK"}$

$k := .45$

$b_f := 6in \qquad t_f := .50in$

$slenderness_{ratio} := \frac{b_f}{t_f} = 12$ LRFD 6.9.4.2

$slenderness_{limit} := k \cdot \sqrt{\frac{E}{F_y}} = 12.772$

$RequirementCheck\left(slenderness_{limit}, slenderness_{ratio}\right) = \text{"OK"}$

USE Q=1.0 if "OK", Otherwise use below EQ for Q

$$Q := \begin{cases} \left(1.34 - .76 \cdot \frac{b_f}{t_f} \cdot \sqrt{\frac{F_y}{E}}\right) & \text{if } .45\sqrt{\frac{E}{F_y}} < \frac{b_f}{t_f} \le .91\sqrt{\frac{E}{F_y}} = 1 \quad \text{LRFD EQ 6.9.4.2.2-5} \\ \frac{.53 \cdot E}{F_y \cdot \left(\frac{b_f}{t_f}\right)^2} & \text{if } \frac{b_f}{t_f} > .91 \cdot \sqrt{\frac{E}{F_y}} \quad \text{LRFD EQ 6.9.4.2.2-6} \\ 1.0 & \text{otherwise} \end{cases}$$

Calculate $(KL/r)_{ef}$

$$EffSlendernessRatio := \begin{cases} \left(32 + 1.25 \cdot \frac{L_b}{r_x}\right) & \text{if } \frac{L_b}{r_x} > 80 \quad = 125.71 \qquad \text{LRFD EQ 6.9.4.4-2} \\ \left(72 + .75 \cdot \frac{L_b}{r_x}\right) & \text{otherwise} \qquad \text{LRFD EQ 6.9.4.4-1} \end{cases}$$

Calculate Capacity

$$P_{ey} := \frac{\pi^2 \cdot E}{EffSlendernessRatio} \cdot A_g = 13137.261 \cdot kip \qquad \text{LRFD 6.9.4.1.2-1}$$

$$P_{oy} := Q \cdot F_y \cdot A_g = 207.72 \cdot kip \qquad \text{LRFD 6.9.4.1.1}$$

$$P_{ny} := \begin{cases} (.877 \cdot P_e) & \text{if } \frac{P_e}{P_o} < 0.44 \quad = 206.35 \cdot kip \qquad \text{LRFD 6.9.4.1.1-2} \\ \left[\left(.658^{\left(\frac{P_o}{P_e}\right)}\right) \cdot P_o\right] & \text{otherwise} \qquad \text{LRFD 6.9.4.1.1-1} \end{cases}$$

$\phi_c \cdot P_n = 196.032 \cdot kip$

$CapacityCheck(MaxComp, \phi_c \cdot P_n) = \text{"OK"}$